Palaeozoic and Mesozoic tectono-metamorphic development and geochronology of the Orobic chain (Southern Alps, Lombardy, Italy)

vorgelegt von
Dipl.-Geol. Jurriaan Feijth

von der Fakultät VI
-Bauingenieurwesen und Angewandte Geowissenschaften-
der **Technische Universität Berlin**

zur Erlangung des akademischen Grades

Doktor der Naturwissenschaften
-Dr. rer. nat.-

GENEHMIGTE DISSERTATION

Berlin 2002

D 83

Eidesstattliche Versicherung

Ich erkläre an Eides statt:

Dass ich die vorliegende Dissertationsschrift selbständig und nur unter Zuhilfenahme der angegebenen Hilfsmittel verfasst habe.

Prof. Franz Neubauer und Prof. Friedrich Finger von der Universität Salzburg mich lediglich bei Analytik und Interpretation der geochronologischen Altersdatierungen unterstützt haben, nicht jedoch bei der Interpretation meines gesamten Datensatzes.

Dass meine Ergebnisse weder teilweise noch in ihrer Gesamtheit als Grundlage für andere Dissertationen benutzt wurden.

Dass ich eine frühere oder gleichzeitige Anmeldung der Promotionsabsicht gemäß §4 der Promotionsordnung oder ein Promotionsverfahren bei einer anderen Hochschule oder bei einem anderen Fachbereich nicht beantragt habe, und mir die geltende Promotionsordnung bekannt ist.

Berlin, 30. Januar 2002

Abstract

The Orobic metamorphic basement and the Early Permian 'Collio Orobico basin' are discussed in this Ph.D.-thesis. The main goal of the investigations was the establishment of a Variscan-Permian P-T-d-t path and to reconstruct the processes that played a role in the tectonic unroofing and exhumation, that finally lead to the formation of the Permian Collio basin. Important aspects of the pre-Variscan and Mesozoic tectono-thermal development were also revealed.

The results of the investigations include:

An almost monoclinic east-west striking 'Orobic fold nappe' overlying a parautochton has been identified. It is interpreted as a Variscan structure, forms the greater part of the exposed basement and consists of two sequences.

The lower sequence, which contains schists and metabasites of volcanic origin, was affected by the Early to Middle Ordovician 'Sardic' metamorphic- and folding phase and contains slightly peraluminious granodioritic augengneisses which protoliths are Late 'Sardic'.

The upper sequence, a Middle- to Late Ordovician volcano-sedimentary complex with rhyoliths, was deposited in an active marginal basin, on 'Sardic' metamorphic basement of the lower sequence.

The following metamorphic phase, the main phase, jointly affected both sequences. The combination of monazite-xenotime thermochronometry, other geothermobarometer and phase petrographic relationships constrained maximum P at $\leq$ 1.3 Gpa, T around 750 °C and the time of peak metamorphism at 330 to 320 Ma.

The formation of the 'Orobic fold nappe' has started at Variscan peak metamorphic conditions. Melting of the hydrous phases white mica and biotite took place and caused the buoyant rise of an elongate diapir. Superimposed dextral transpression, made this diapiric ridge extrude from a rootzone and develop into a nappe-fold, spreading over the parautochton.

By far the majority of Variscan tectonic structures that formed during the formation of the nappe fold have an extensional component and/or served as adjustment minimising the potential energy in the gravity field. Although this phase occurred in an orogenic zone deforming under transpression, this phase contributed to crustal thinning, retrogression and exhumation. The P- and T conditions during the culmination of ductile-brittle deformation related to this nappe folding are ~600 °C at ~1.0 Gpa. At 325-305 Ma the 'Orobic fold-cooled down to the closure temperature of white mica, as the plateaux in the $^{40}Ar/^{39}Ar$ apparent age-spectra indicate.

$^{40}Ar/^{39}Ar$-multigrain step heating-results of all biotite and only some white mica samples indicate: (1) A Middle Permian hydrothermal phase, related to late volcanic activity of the Collio basin. (2) A Mesozoic hydrothermal phase, related to a combination of Ladinian magmatic activity and Ladinian to Liassic rifting. The latter phase has re-equilibrated the U-Th-Pb system of monazite at ~322 °C, as revealed by monazite-xenotime thermometry on samples of 'Gneiss Chiari'.

Isotopic $^{40}Ar/^{39}Ar$-dating of single detrital white mica grains from the very low-grade metamorphic volcanoclastic sequence of the 'Collio Orobico' basin indicated: (1) The source areas of the identified populations of detrital white mica grains are predominantly the Orobic basement units (2) Middle- to Late Permian hydrothermal activity (~270-255 Ma) and Mesozoic hydrothermal overprint (~250-180 Ma). (3) A contractional geodynamic setting during deposition, respectively in a molasse basin for the basal conglomerates and an intramontane basin for the 'basal conglomerates' and the 'Collio Orobica' formation, as indicated and confirmed by the Lag-times of these detrital white mica grains.

Zusammenfassung

Das Orobische metamorphe Grundgebirge und das unter-Permische ‚Collio Orobico Becken' sind das Thema in der vorliegenden Dissertation. Das wichtigste Ziel der Untersuchungen war die Ausarbeitung eines P-T-d-t-Pfades und die Rekonstruktion der Prozesse, die eine Rolle gespielt haben in der tektonischen ‚unroofing' und Exhumierung, und welche schließlich zur Bildung des Collio-Beckens geführt haben. Einige Aspekte der pre-variszischen- und mesozoischen tektono-thermischen Entwicklung wurden ebenfalls erkannt.

Die Ergebnisse der Untersuchungen sind folgende:

Eine fast monoklinale Ost-West streichende ‚Orobischen Deckenfalte' wurde im Hangenden eines Parautochtons erkannt. Diese wurde als variszische Struktur interpretiert, formt die Mehrheit des aufgeschlossenen Grundgebirges und besteht aus zwei Sequenzen.

Die untere Sequenz, welche aus Schiefern und Metabasiten vulkanischen Ursprungs besteht, wurde von einer früh- bis mittel-ordovizischen ‚sardischen' metamorphen und Faltungsphase überprägt und enthält peraluminische granodioritische Augengneisse deren Protolithe spät-‚sardisch' sind.

Die obere Sequenz, eine vulkano-sedimentäre Folge mit Rhyolithen, wurde in einem aktiven marginalen Becken, auf ‚sardisch' metamorphem Grundgebirge der unteren Sequenz abgelagert.

Die folgende metamorphe Phase, die Hauptphase, hat beide Sequenzen überprägt. Mittels der Kombination von Monazit-Xenotim Thermochronometrie, andere Geothermobarometer und phasenpetrologischen Beziehungen wurden Peak-P und -T, $\leq$ 1.3 GPa bei ~750 °C, und der Zeitpunkt der Peak-Bedingungen, 330-320 Ma, bestimmt.

Die Bildung der ‚Orobischen Deckenfalte' hat während den maximalen varizischen metamorphen Bedingungen angefangen. Dehydrations Schmelzen der wasserführenden Phasen Hellglimmer und Biotit fand statt und dadurch die Bildung eines diapirischen Rückens. Bei gleichzeitiger dextraler Transpression extrudierte der Rücken aus einer Wurzelzone. Es bildete sich die Deckenfalte, die gravitativ über das Parautochton spreizte.

Ein Großteil der variszischen tektonischen Strukturen, die sich während der Bildung dieser Deckenfalte bildeten, hat eine Extensionskomponente und/oder trat als Ausgleich zur Minimalisierung der potentiellen Energie der Schwerkraft auf. Obwohl diese Phase in einer unter Transpression deformierenden Zone stattfand hat sie zur krustalen Ausdünnung, retrograden Metamorphose und Exhumierung beigetragen. Die P- und T-Bedingungen während der Kulmination der duktil-spröden Deformation in Zusammenhang mit der Deckenfaltung lagen bei ~600 °C bei ~1.0 GPa. Die ‚Orobische Deckenfalte' erreichte Temperaturen unter der Schließungstemperatur des $^{40}Ar/^{39}Ar$-Isotopensystems von Hellglimmer um 325-305 Ma, wie Plateaus der ‚multigrain step heating'-Analysen zeigen.

Ergebnisse der $^{40}Ar/^{39}Ar$-‚multigrain step heating' aller Biotit- und nur einiger Hellglimmerproben zeigen: (1) Eine mittel-permische hydrothermale Phase die zusammenhängt mit später vulkanischer Aktivität des Collio Beckens. (2) Eine mesozoische hydrothermale Phase, zusammenhängend mit sowohl ladinischer magmatischer Aktivität als auch ladinisch, bis liassischem ‚Rifting'. Während der mesozoischen Phase wurde das U-Th-Pb-system von Monazit bei ~322 °C re-equilibriert, wie Monazit-Xenotim-Thermometrie an Proben der ‚Gneiss Chiari' gezeigt hat.

Isotopische $^{40}Ar/^{39}Ar$-Datierung einzelner detritischer Körner von Hellglimmer von der sehr niedriggradigen vulkano-sedimentären Sequenz des ‚Collio-Orobico Beckens' ergab folgende Einsichten: (1) Die orobischen Grundgebirgseinheiten sind vorwiegend die Liefergebiete der identifizierten Populationen detritischer Hellglimmer. (2) eine mittel- bis spät-permische hydrothermale Aktivität (~270-255 Ma), und mesozoische hydrothermale Überprägung (~250-180 Ma). (3) Die Ablagerung fand in einem konvergenten ‚setting' statt, respektive in ein Molasse- und ein intramontanes Becken für die ‚Basalconglomerate' und beziehungsweise die ‚Collio orobica' Formation, wie die ‚Lag-times' der detritischen Hellglimmer zeigen und bestätigen.

Riassunto

Il basamento metamorfico Orobico e il bacino Collio-Orobico sono oggetti d'interesse in questa tesi di laurea. L'obiettivo priciple delle ricerche era la reconstruzione dell'evoluzione P-T-d-t e delle processe che hanno fatto una parte importante in l'unroofing tettoniche e l'esumazione, e finalmente hanno condutto alla formazione del bacino Permiano di Collio.

Qualche aspetti della svilupo tettono-thermiche si erano mostrato anche.

I risultati delle ricerce sono seguente:

La majorità del basamento esposato si composto di un di falda qui se costituto di una piega sdraiata quasi monoclinale, la 'falda Orobica' qui se trova sull'parautoctono. Questa falda consiste di due sequenze, separato di una discordanza.

Gli scisti della sequenza inferiore, que includono di rocche metabasiche d'origine volcaniche, erano deformato per la fase 'Sarda' di piegamento e metamorfosi Ordoviziano Inferiore e -Media e seguente intrudo degli protoliti di gneiss occhiadini granodioritiche peralumini 'Sardi'-tardi.

Posteriore, in l'Ordivizio, in un 'setting' tettonico uguale, una sequenza volcanico-sedimentario con rioliti era deposito in un bacino attivo marginale e sul basamento della sequenza inferiore.

La succedente fase metamorfico principale ha influenzato le due sequenze insieme. Per mezzo della combinazione di termochronometria monazite-xenotime, altri geotermobarmetri, e relazione di phase petrologiche erano determinato i condizione massimale di questa fase a $\leq$ 1.3 GPa e ~750 °C al tempo di 330 a 320 Ma.

La formazione della 'falda Orobica' e comincato durante gli condizioni metamorfiche massime varisico. La fondatura di deidrazione delle fasi idriche mica chiaro e biotite ha causato la formazione d'un dosso diapirico. Tettonica trascorrente destrale simulatneo, parallelo alla zona radice, ha causato estrusione del dosso diapirico di questa zona e finalmente svilupo di quella strutura in la 'falda Orobica'.

La piuparte delle strutture formato durante la formazione della 'falda Orobica' ha un elemento d'estensione e/o sono formato come addatamento per minimare l'energia potenziale della gravitazione. Questa fase ha contributo a sottilerazione crostale ed eshumazione sebbene questa fase è stata luogo in una zona orogenesi di transpressione. Gli condizione P e T durante il culminazione di deformazione dutile-secco conetto a questo fase di piegamento della falda erano a ~ 600 °C e ~1.0 GPa

A 325-305 Ma e rinfrescamento la 'falda Orobica' sotto la temperatura di chiusura della systema isotopiche ^{40}Ar/^{39}Ar di mica chiaro, come indicato per i plateau degli analisi del 'multigrain stepheating'.

Risultate di '^{40}Ar/^{39}Ar-multigrain step heating' di tutte prove di biotite- e soltanto qualche prove di mica chiaro indicano: (1) Una fase idrotermale Permiano Medio relato al volcanismo tardo del bacino Collio basin. (2) Una fase idrotermale Mesozoico, relato ad una combinazione d'attività magmatismo Ladinico e 'rifting' Ladinico a Liassico. L'ultima ha re-equilibrato il systema U-Th-Pb di monazite a ~322 °C, come si erano mostrato per geotermometria monazite-xenotime su prove di 'Gneiss Chiari'.

Datazione ^{40}Ar/^{39}Ar di grane detritici di mica chiaro singoli del bacino 'Collio Orobico' ha indicato: (1) Gli unità tectoniche del basamento cristallino Orobiche representano prevalamente le zone di sorgente delle populazione di mica chiaro identificato. (2) Attività idrotermale Permiano Medio- a Superiore (~270-255 Ma) e una fase idrotermale Mesozoico (~250-180 Ma). (3) Una setting geodynamica di contrazione durante la deposizione, ripettativamente in tipi di bacini molasse e intramontano per il conglomerato basale e la formazione di 'Collio-Orobica', come indicato e confermato per gli 'lag times' di grane di mica chiaro detritico.

Table of Contents

Palaeozoic structure and evolution of the Orobic chain
(Southern Alpine Basement, Lombardy, Italy)

P-T Conditions of Variscan and Mesozoic phases in the Orobic chain
(Southern Alps, Italy)

Geochronology of the Orobic Alps (Lombardy, Italy):
(I) Evolution of the basement, constrained by U-Th-Pb-ages of monazite and ^{40}Ar/^{39}Ar-ages of biotite and muscovite

Geochronology of the Orobic Alps (Lombardy, Italy):
(II) ^{40}Ar/^{39}Ar-ages of detrital muscovite from the Collio basin, constraining tectono-thermal development

Introduction

The Orobic chain, situated in the Central Southern Alps, was chosen to investigate the Variscan-Permian tectono-metamorphic development. The choice of the study area has been made on various grounds:

The relative low-grade Alpine and Mesozoic metamorphic overprint.

The complete Variscan-Permian tectono-thermal, igneous and volcanic development can potentially be identified, because the Permian 'Collio Orobico basin' is preserved.

Although partly remote and poorly accessible, all units affected by Variscan tectono-metamorphic imprint and the Permian sequences are well exposed.

The results of this study additionally contribute to the general regional understanding of the Southern Alps in its pre-Mesozoic context with the Austroalpine. This pre-Mesozoic development includes imprint of an Ordovician orogeny, which has also affected a sequence of the Orobic basement. Pre-Variscan phases had not been identified as such in the field before.

This identification of pre-Variscan imprint in one of the sequences of the Orobic basement required the establishment of an evolutionary model for the Palaeozoic structural and metamorphic development. Therefore an analysis of Palaeozoic phase-relationships had to be included in this thesis, in order to explain how Variscan and pre-Variscan phases can be distinquished.

This Ph.D.-thesis, which represents an intermediate stage in the investigations, consists of four chapters* (1 to 4), each concentrating on a different thematic aspect:

A reconstruction of the Palaeozoic structure and evolution, which includes the pre-Variscan development.

Geothermobarometric and petrographic analysis, revealing the Variscan P- and T development and some aspects of Mesozoic overprint.

A presentation and interpretation of the geochronological results, U-Th-Pb-ages of monazite and ^{40}Ar/^{39}Ar-ages of biotite and muscovite, which constrain the tectono-thermal evolution of the basement.

^{40}Ar/^{39}Ar-isotopic dating of single detrital white mica grains from the Permian 'Collio Orobico basin' supplying information on: (a) source areas, (b) tectono-thermal characteristics of the exhumation history and (c) the geodynamic setting of basin formation.

During the course of the investigations it has been recognised that kinematic development and metamorphism are strongly interrelated. A proper interpretation of the kinematic development requires incorporation of both these aspects in the model. This model, to be published in the near future, assesses the kinematic conditions that lead to the structural configuration found in the field. Some of the results of this analysis are summarised and referred to in this thesis.

Also a paper on Alpine ^{40}Ar/^{39}Ar-isotopic ages of detrital mica grains, an interesting additional result of the study presented in chapter 4, will be published soon.

In the chapters 1 to 4 reference is made to these publications, which will be submitted for publication in the near future.

* Each of these chapters represents a publication, to be submitted for publication in a journal, and is listed as such in the references of this thesis.

Chapter 1

Palaeozoic structure and evolution of the Orobic chain (Southern Alps, Lombardy, Italy)

Abstract

By analysis of structural, stratigraphic and petrographic data from the Orobic basement its Palaeozoic polyphase evolution was reconstructed. The majority of the exposed basement constitutes of an almost monoclinic recumbent fold overlying a parautochton. This 'Orobic fold nappe', consists of two tectonic units, which sequences have a different origin, age, structural and petrographic development, and which are separated by a tectonically activated unconformity. The schists of the lower metasedimentary sequence of the fold nappe contain meta-amphibolites, deposited as tephra and subaqueous welded ash flows and containing meta-amphibolite sills. These are discontinuously exposed at a specific stratigraphic level. Before deposition of the upper sequence the Early- to Middle Ordovician 'Sardic' metamorphic- and folding phase affected the lower sequence. Late 'Sardic' igneous rocks, the protoliths of slightly peraluminious granodioritic augengneisses, the 'Gneiss Occhiadini Orobico-Valtellinese' ('GOOV') were emplaced in this sequence at shallow crustal levels. Also in the Ordovician, still in the same tectonic setting, a volcano-sedimentary complex was deposited in an active marginal basin and on 'Sardic' metamorphic basement of the lower sequence. The rhyolites are the protoliths of the 'Gneiss Chiari' and the meta-graywackes, -psammites and - pelites form the 'Gneiss di Morbegno'. The following deformation- and metamorphic phase of uppermost amphibolite facies grade, that jointly affected both sequences, is related to orogenic phases at the southern margin of the Variscan belt. The 'Orobic fold nappe' formed during and after peak conditions by gravitational spreading of a diapiric ridge over the parautochton. The initial structural stage of this diapiric ridge, formed by buoyancy and diapirism, was caused by dehydration melting of particularly the hydrous phases biotite and white mica. Superposed tectonic strain caused further extrusion. Dextral wrenching of the resulting structure of the 'Orobic fold nappe' occurred along the rootzone and has caused oblique internal structures. Late orogenic tonalites, granites, quartz-diorites and gabbro-diorites of the Val Biandino plutonic complex were emplaced in the parautochton during the waning stages of the main nappe-folding event. These igneous rocks are largely unaffected by Variscan nappe folding related brittle-ductile deformation and are quasi sealing the late-Variscan structure before development of the late-orogenic Permian 'Collio-Orobico basin' along the detachment between the parautochton and the 'Orobic fold nappe'. The 'Scisti di Edolo' of greenschist metamorphic grade, that overly the 'Orobic fold nappe', correlate with the Austroalpine 'quartzphyllites', which are also in tectonic contact with a higher grade metamorphic substrate. The metasedimentary protoliths of the parautochton might correlate with the 'Brixen quartzphyllites', the Late Cambrian to Early Tremadocian 'Agordo phyllites' and basement in similar structural position below the 'Collio Trumplino basin'.

1 Introduction

The aim of this paper and accompanying geological map (Appendix A of this thesis) is to interpret and give an overview of the Palaeozoic structural and metamorphic development of a portion of the southern margin of the Variscan belt, the 'Orobic chain'. The metamorphic and deformational relationships were extracted from field, microstructural and petrographic data in order to unravel the geodynamic setting. Also the so far unknown depositional age and nature of the protoliths is interpreted. The result is a model of Palaeozoic depositional, tectono-metamorphic and structural development, which includes the identification of pre-Variscan phases and the recognition of Palaeozoic relationships between the Austroalpine and Southern Alps. The formation of a recumbent fold nappe, of which the major part of the exposed Orobic basement consists, was the event that has determined the present configuration of the Orobic basement. The following collapse and tectonic unroofing lead to the development of the Permian 'Collio Orobico basin'. It is proposed, based on the structural sequence and metamorphic development and timing, that extrusional fold nappe-development and its gravitational collapse contributed to the exhumation process and decompression of uppermost amphibolite facies (Feijth & Franz, in prep.) assemblages and metamorphic fabrics.

Geological investigation in the Southern Alps, of which the Orobic Alps forms part of (Fig. 1), provides extra information on the Palaeozoic plate-tectonic development, which is not extractable from the Central Alps. This is due to two important aspects of the plate-tectonic and metamorphic history since the Palaeozoic:

(1) The east-west trending steeply north-dipping 'Tonale line', a segment of the 'Insubric lineament' (Fig. 1a), was an important part of the boundary between the Adriatic and European continental plates during the Oligo-Miocene and, as follows from the conclusions from data presented below and in Feijth (in prep. a), was also a major zone of transcurrent shearing during the Palaeozoic. In addition to major right-lateral Alpine strike-slip movements (Laubscher, 1971; Ahrendt, 1980; Gansser, 1968) this fault zone accommodated considerable Alpine dip-slip displacements (Schmid et al., 1989; Gansser, 1968). Evidence for this large amount of dip-slip displacement is juxtaposition of North verging Austroalpine and Penninic nappes of the Central Alps of greenschist to amphibolite facies to the South verging Southern Alps (Fig. 2), deformed under lowermost grade Alpine metamorphic conditions (Ahrendt, 1980; Crespi et al., 1981; 1982). K-Ar and Rb-Sr isotopic ages differ across the 'Insubric lineament' near 'Mello' and are Alpine to the north and pre-Variscan to the south (Ahrendt, 1980; Wiedenbeck, 1986). The lower grade overprint south of the 'Tonale line' is thus relatively weak compared to the Palaeozoic metamorphic development and additionally areas of Mesozoic overprint and faulting are avoidable, a desirable circumstance for Palaeozoic study.

(2) A second reason which makes the Southern Alps particularly well suited for studies of Palaeozoic tectono-metamorphic development is that south of the 'Insubric lineament' additional Palaeozoic plate-tectonic units might be present, which are possibly not exposed in the Central Alps.

The still rather poorly defined early-middle Palaeozoic plate-tectonic situation is the starting point of this study. This is because the youngest sedimentary protoliths of the Orobic basement are of late Ordovician to Silurian age (Gansser & Pantić, 1988) and the depositional
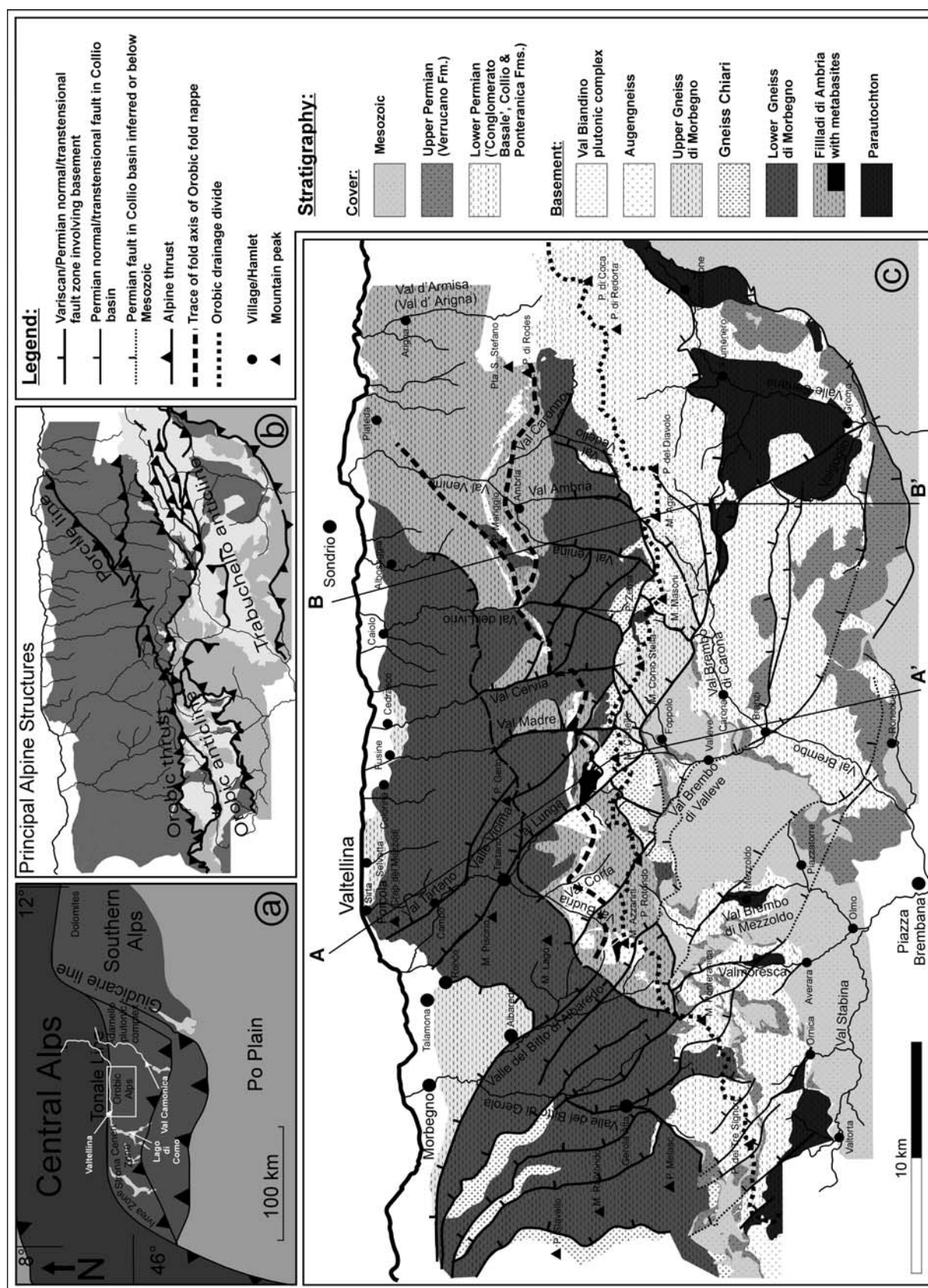
Fig. 1. Location map (a) and a map with the principal Alpine structures, including their names, indicated (b) of the investigated area in the Orobic Alps. The Variscan-Permian structures and the location of the cross-sections of Fig. 2 are shown in the geological map (c).
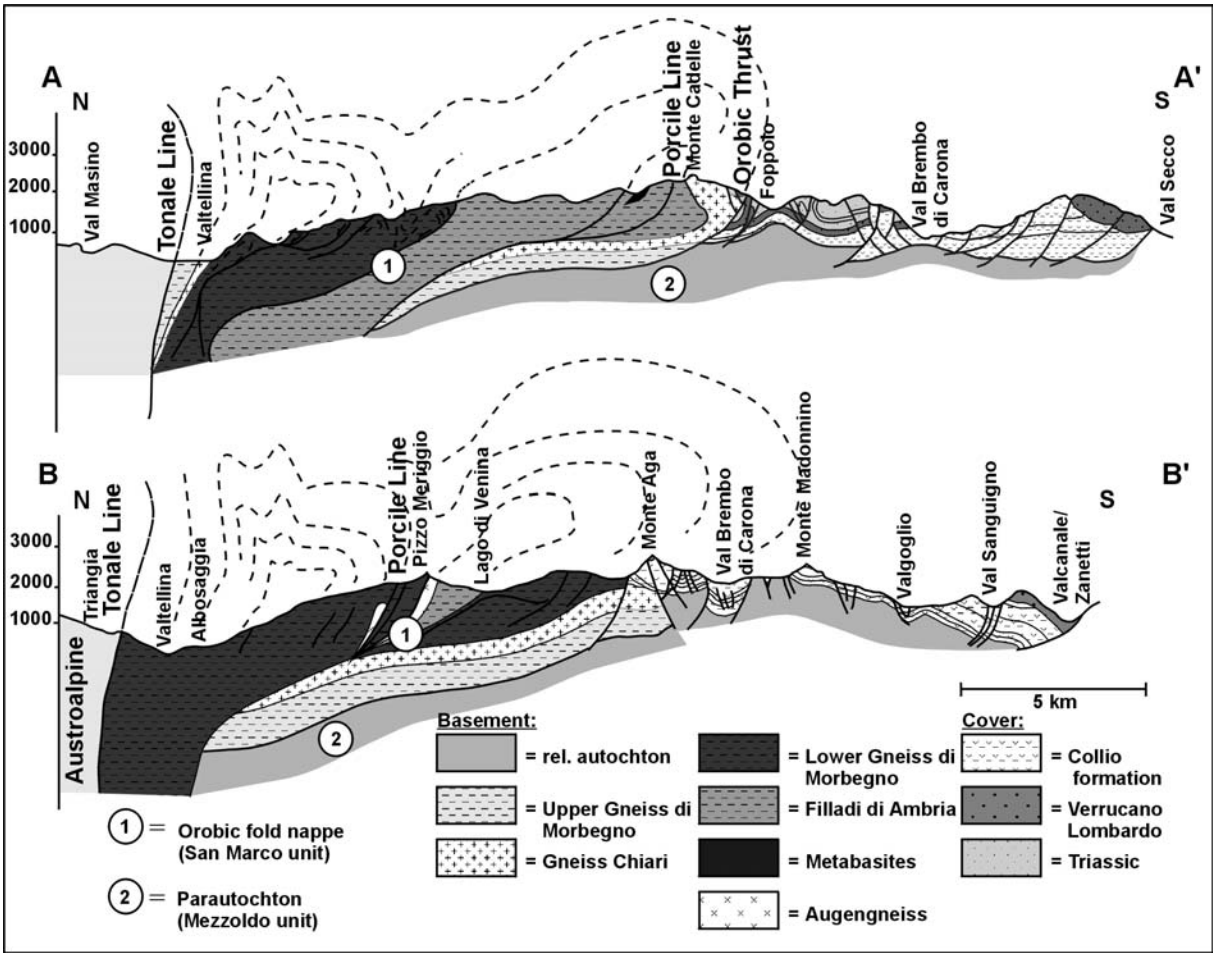
Fig. 2. N-S cross sections across the Orobic chain. Traces A-A' and B-B' are shown in Fig.1.

age of particular older sedimentary and volcanic protoliths of the Southern Alps is at minimum slightly older than an Ordovician event by which these units were affected. This orogenic phase was called the 'Sardic' event (Zurbriggen, et al., 1997; Handy et al., 1999) of which the D_2 'Ceneri phase' of Handy et al. (1999), was up to now only clearly identified in the 'Strona-Ceneri zone'. Special attention has been paid to possible equivalent pre-Variscan orogenic events in the Orobic basement and structural and geodynamic relationships between the Variscan and older phases. So far Ordovician igneous activity was only inferred for the Orobic basement (Colombo et al., 1994). A key-question is whether and how the Variscan tectono-metamorphic and magmatic development can be identified and reconstructed in this region and how the Variscan phases and anticipated earlier orogenic events can be distinguished. With the sparse published geochronological data, reviewed in Feijth et al. (in prep.) geochronological arrangement of the individual phases of the complex Palaeozoic development of the Central Orobic basement, is rather difficult or impossible. Therefore, apart from field-data mainly presented here, one of the fundaments of the model is a phase-petrographic study, which in combination with microtectonic analysis, thermo-barometry and isotopic dating ($^{40}Ar/^{39}Ar$ on muscovite and biotite, U-Th-Pb on monazite by EMP) enabled reconstruction of P-T-d-t-paths and tectonic development. Results on isotopic age-data are discussed in Feijth et al. (in prep.) and Feijth & Neubauer, (in prep.a, b). Variscan kinematic development is discussed in detail in Feijth (in prep. a, b). Phase petrographic analysis,

metamorphic development and thermobarometry are treated in Feijth & Franz (in prep.). To obtain a complete overview some of the conclusions of these investigations are included here.

2 Geological setting

The 'Orobic-Bergamasc Alps' are an east-west trending Alpine thrust belt extending from the 'Lago di Como' in the west to the 'Val Camonica' in the east (Fig. 1a). The majority of the Orobic basement is exposed north of the Orobic drainage-divide, in the northern part of the area in the province of Sondrio, in the Valtellina, a major Alpine valley of the Lombardian Southern Alps, and is separated from the Permian basins and their underlying basement by the Alpine south-verging 'Orobic thrust' (Fig. 1b, c).

The hanging- and footwall wall of the Alpine 'Orobic thrust' correspond respectively to the 'San Marco unit' and the 'Mezzoldo unit' (Fig. 2). Latter are names applied by Schönborn, (1990; 1992) and Schumacher et al. (1997). 'Upper'- and 'Lower Orobic nappe' are other names, applied for both Alpine units respectively by Schönborn (1994) and also by Schumacher (1997).

The 'Porcile line' (Fig. 1b) is another major Alpine structure north of the Orobic drainage-divide. It is an ENE-WSW fault-zone marked by black cataclasites with abundant pseudotachylytes and 'horses' of the Upper Permian 'Verrucano Lombardo'-, the Scythian 'Servino'- and Scythian to Anisian 'Carniola di Bovegno formations'. (For lithological descriptions see Appendix A.)

The Permian 'Collio-Orobico basin', with possibly Permo-Carboniferous 'Conglomerato Basale' and the 'Collio-Orobica'- and 'Ponteranica formations', is exposed in the weakly developed deca-kilometric scale 'Orobic'- and 'Trabuchello(-Cabianca) anticlines' (de Sitter, 1963) (Fig. 1b). The 'Cedegolo anticline', in which mainly the 'Verrucano Lombardo formation' is exposed as Permian formation, is situated east of the selected working area shown in Fig. 1.

The 'Orobic'- and 'Trabuchello(-Cabianca) anticlines' are for the most part located south of the Orobic drainage-divide, in the Bergamasc valleys 'Valle Brembana di Mezzoldo', -'di Valleve', -'di Carona', at the northern slopes of 'Val Stabina' and in the 'Valle Seriana'.

South of these structures, formed by Alpine basin inversion, there is a south-verging thrust belt, of mainly Mesozoic carbonates. At a complex boundary-zone with the 'Collio Orobico basin', in which opposite thrusting-vergence is recognisable, the Mesozoic formations are backthrusted over the inverted basin in a configuration of an intercutaneous wedge (terminology after McClay (1992) and references therein).

In this setting of a tectonically reworked orogen the disturbing influence of younger phases should be assessed before the interpretation of the oldest Palaeozoic tectonic phases can be carried out confidently. Rifting occurred between the Permian and Jurassic and affected the westernmost extension of the Orobic basement, the footwall of the 'Lugano-Val Grande rift-fault' (Mottana et al., 1985; Bernoulli et al., 1990; Diella et al., 1992; Bertotti et al., 1993; 1997; 1999; Siletto et al., 1990; 1993; Sanders et al., 1996; Gosso et al., 1997). The 'Monte Muggio zone', the hanging wall of this rift-fault, where there is no HT-overprint, is in direct continuity with the outcrops of the 'Orobic fold nappe' in the area under discussion.

Alpine overprint is developed as shortening (Werner et al., 1977; Trümpy, 1980; Schmid et al., 1987; Roeder, 1985, 1989, 1992; Schönborn, 1990, 1992; Carminati et al. ,1997;

Carminati & Siletto, 1997). Aerial balanced cross sections (Schönborn, 1990, 1992a,b, 1994; Schönborn & Schumacher, 1994; Schumacher, 1997; Schumacher et al., 1997) brought useful insights to the distribution of Alpine shortening and the recognition of Alpine structural units. The Alpine deformation depends on the Variscan basement structure, and in the cover mainly on the competence contrasts that define certain decollement levels, like the lower Triassic 'Servino'- and 'Carneola di Bovegno formations'. Shortening is mainly accommodated by thrusts, in the basement marked by black cataclasites with pseudotachylytes. These and also undeformed basement are locally intruded by hornblende-diorite dykes, of Oligocene age according to Zanchi et al. (1990), which occasionally have been deformed by repeated movement along faults. Internal Alpine deformation of all units is relatively modest. In the basement it depends strongly on lithology. The predominantly pelitic units, mainly present in the eastern Orobic basement, show Alpine kink-folds of various scales. Carminati et al. (1997) and Carminati & Siletto (1997) investigated thrust-kinematics and internal deformation of Alpine age in this eastern Orobic basement. The basement of the western-central area of the Orobic Alps, the area of investigation, is dominated by the 'Gneiss di Morbegno' which are much more competent and generally almost devoid of Alpine structures.

Alpine metamorphism of the Southern Alps is seen as metamorphic overprint, but of lowermost grade. Bocchio et al. (1981), Diella et al. (1992) and Spalla et al., (1999) recognised retrograde mineral reactions like chloritisation of biotite and sercitisation of chlorite while Crespi et al. (1981, 1982) observed stilpnomelane replacing chlorite, which has replaced primary biotite, and which occurred along Alpine faults at both sides of the Valtellina. In the Orobic basement chlorite, white mica and stilpnomelane grew on alpine cleavage planes and in alpine veins (Carminati, 1992, Carminati et al., 1997; Albini et al., 1994).

The 'Collio Orobico formation' locally shows a well-defined Alpine secondary foliation, formed by pressure solution. Specifically arenites, siltstones and shales of the 'Upper sedimentary member' (Cadel et al., 1996), the 'Scisti di Carona', show many evident pressure-solution structures, like tension gashes with antitaxial fibrous quartz veins, which are folded due to shortening across a well developed sub vertical foliation. These processes of pressure-solution are related to activity of the 'Orobic thrust system', events that were dated by the $^{40}Ar/^{39}Ar$-method, which indicate at least three periods of Alpine intracrystalline rejuvention of the $^{40}Ar/^{39}Ar$ isotopic system, Maastrichtian, Paleocene to late Eocene and early Eocene (Feijth & Neubauer, in prep.a, b). Illite crystallinity was measured on phyllosilicates of pelites of the Collio (Keller, 1986; Riklin, 1983), 'Servino' (Schönborn, 1986) and 'Prezzo' (Keller, 1986) formations, and indicates anchimetamorphic conditions with temperatures between 200 °C and 300 °C. From field-observations it can be concluded that in the selected area Alpine tectonic and metamorphic structures can easily be distinguished from higher-grade imprints resulting from Pre-Mesozoic events.

This analysis forms the basis for investigations of geochronological, structural, kinematic and metamorphic development to be published in the nearby future (Feijth, in prep. a, b, c; Feijth & Franz, in prep.; Feijth & Neubauer, in prep. a, b).

3 Results

3.1 Identification of the main Palaeozoic structural units

A subdivision of the Orobic basement in structural units, each with a different depositional origin, intruded by different igneous units and with a distinguishing tectonic imprint, is introduced here to reveal the Palaeozoic structural development. The hanging wall of the 'Orobic thrust' comprises of an almost monoclinic recumbent fold, a pre-Alpine structure, in Palaeozoic context called the 'Orobic fold nappe'. Its ENE-WSW striking hinge-zone is clearly exposed inbetween 'Val Budria' and 'Val Cervia' (Fig. 1). East- and westwards it can be deduced from lithology, contained tectonic structures and layering-orientation. NNE-NE-dipping transtensional detachments formed in this fold nappe during Variscan phases and were active also during Permian phases. These separate the relatively autochtonous basement below the 'Collio Orobico basin', called the parautochton, from basement belonging to the 'Orobic fold nappe' (Fig. 2). These shear-zones, that crosscut the Orobic nappe, are rooted in this detachment. The parautochton coincides with the basement of the 'Mezzoldo unit' of Schönborn (1990, 1992) and Schumacher et al. (1997).

The core of the 'Orobic fold nappe' is reactivated as a thrust, the 'Porcile line' (Fig 1b), which approximately coincides with the hinge zone. Therefore the 'Porcile line' can also be considered as a structure inherited from the Palaeozoic structural configuration.

Facies distribution of the Permian Collio-sediments N and S of the 'Orobic thrust' E of the 'Porcile line' shows that Alpine reactivation between both units is relatively small in comparison to the other major Alpine thrusts of the 'Orobic-Bergamasc Alps', like the thrusts in the Mesozoic cover which displacements are up to 20 km. West of the point where both faults join, the displacement of the 'Orobic thrust' is equally large as the displacement of the major thrusts in the Mesozoic cover sequence and the Permian volcano-sedimentary units are dissected by this thrust. This implies closely related Variscan development of the 'San Marco'- and 'Mezzoldo units' east of the merging point of both faults up to the Middle Permian.

The 'Orobic fold nappe' and the parautochton together are called 'infrastructure' of the Orobic basement, because in the eastern Orobic Alps a unit of greenschist facies rocks overlies the 'Orobic fold nappe' trough a thrust-contact. This Upper unit, consisting of the 'Scisti di Edolo' is called 'suprastructure' (Fig. 3).

3.2 The basement lithologies

Lithologic units of the three tectonic units of the Orobic basement, including the metaigneous and igneous suites, which concentrate in specific stratigraphic units, are described here. A schematic overview is given in Fig. 3. Apart from the Late Ordovician to Silurian depositional age of the 'Scisti di Edolo' (Gansser & Pantić, 1988) the age of other protoliths is still unknown and protolith ages from Archean to Lower Palaeozoic have been considered (Bocchio et al., 1981; Mottana et al., 1985).

The succession starts with the 'Filladi di Ambria'. These generally consist of well-developed centimetre- to decimetre-scale layered schists, quartzitic-schists and chlorite-schists with subordinate thinner meta-greywackes and quartzites. Garnet and amphibole are locally common. Massive lenses of quartzite without internal structure occur as well, but mainly,
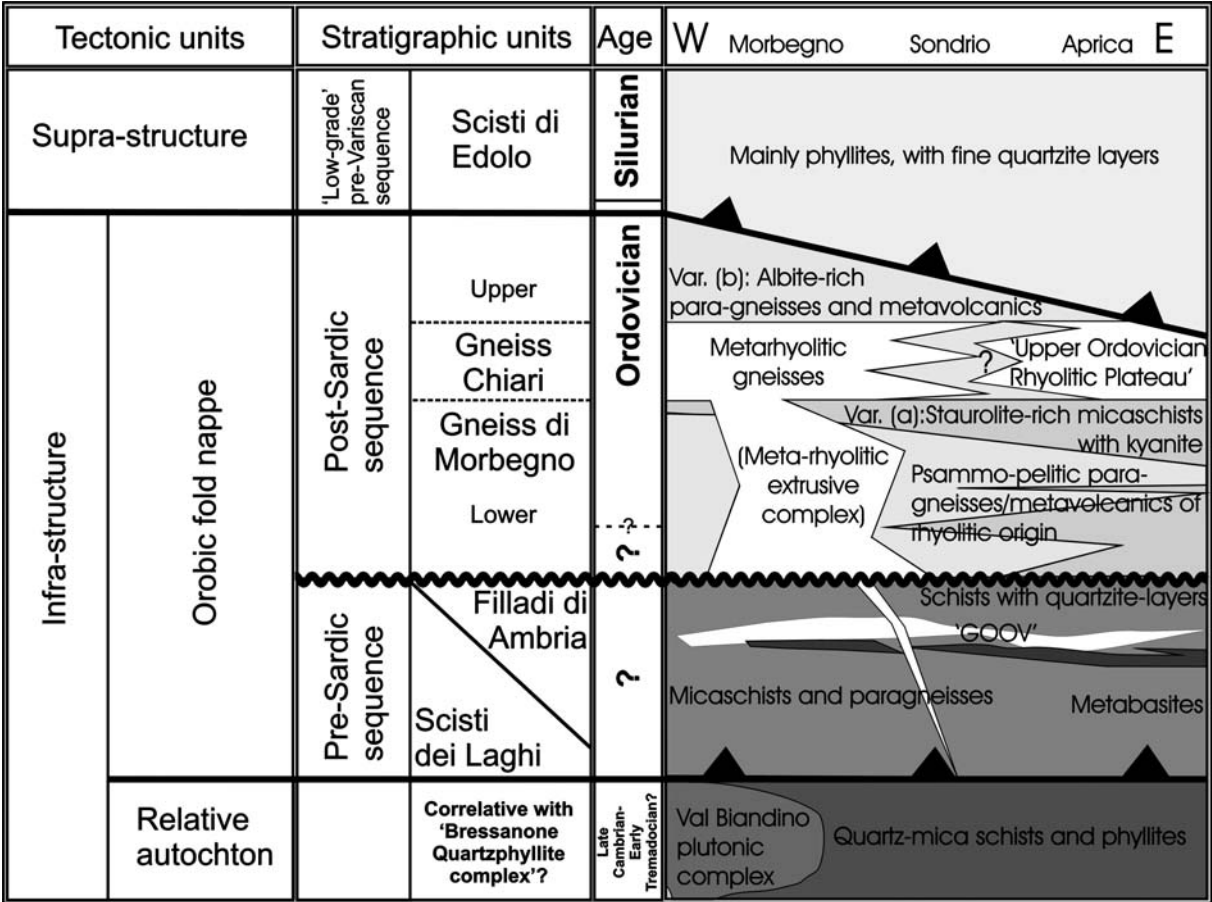
Fig.3. Schematic overview of the stratigraphy of the Orobic basement.

outside the working area, in the eastern Orobic Alps between the 'Val Caronella' and the 'Valle Camonica'. The 'Filladi di Ambria', are interpreted as a sequence of clastic meta-sediments derived from a continental source area, with a general eastward increase of meta-pelite.

The 'Filladi di Ambria' include bodies of metabasitic rocks which appear at km-scale length and up to 100 metres, but generally some tens of metres thickness. The metabasites are exposed in the core of the 'Orobic fold nappe' and can roughly be grouped in two major classes:

(1) Amphibolite schists and epidote-amphibolite-schists (Fig. 4a) with garbenschiefer-varieties, with zoned amphibole and locally with some garnet. Some of the amphibolite-layers have moderately defined, occasionally chaotic bedding. Cross bedding and laminations have been observed in the layered amphibolites, which have been interpreted as meta-sediments or are of meta-volcano-sedimentary origin. Folds with amplitudes of cm- to dm-scale with axial planes parallel to general layering orientation are present and indicate that this relatively incompetent rock was favourably folded during shear sub-parallel to layering. These schists might represent meta-ashes and -tuffs likely deposited in an aquous depositional environment.

(2) A complex of fine-grained meta-amphibolitic sills of up to 3m thickness consisting of fine-grained euhedral magmatic amphibole in a matrix of symplectitic plagioclase and epidote. Weakly developed pillow-structures in the dykes, separated by plagioclase-rich zones, indicate intrusion in wet sediments. Locally, at the base of the sills, there are subangular to rounded, occasionally angular, xenoliths of meta-gabbro, meta-amphibolite and
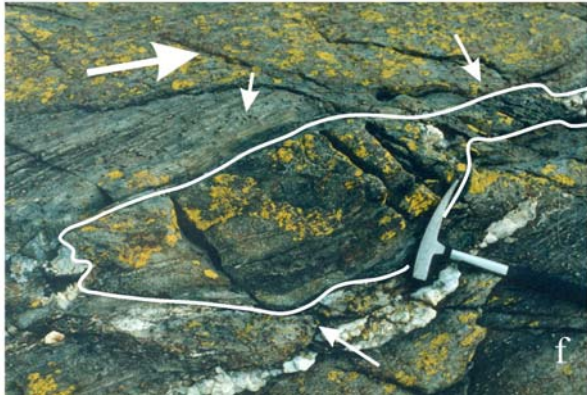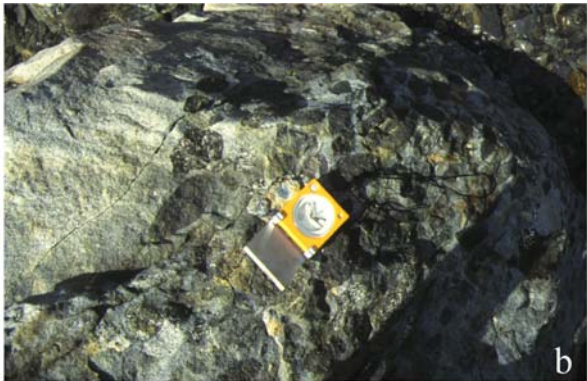
Fig. 4.

a. *Metavolcanics, exposed as folded amphibolite-schists and epidote-amphibolite-schists. (Photograph taken nearby Cima di Lemma.).*

b. *Lithology of an amphibolite-sill with a matrix of fine-grained amphibole with symplectitic plagioclase and epidote, containing rounded xenoliths of up to 10 cm diameter of amphibole, gabbro and of ultramafic composition. (Photograph taken at the Val Lunga.)*

c. *The amphibolite-sills have slightly discordant relationships at their contacts with layering of the host rock (pointed at with pencil and arrow). (Photograph taken at the Val Lunga.)*

d. *Sharp contacts of the 'GOOV' with the metabasites. The metabasites have thin contact-metamorphic zones and the 'GOOV' thin chilled margins. Within the metabasites a primary layering is still identifiable (at arrow). (Photograph taken at Val Lunga.)*

e. *Discordant contact of 'GOOV' with 'Filladi di Ambria'. A younger foliation, activated during intense shearing, crosscuts the contact and obliquely overprinted primary layering of the 'Filladi di Ambria. (Photograph taken at Val Lunga.)*

f. *Slightly sheared apophyse of an -intrusive body (outlined) of 'Gneiss Occhiadini Orobico-Valtellinese' in the upper 'Val Lunga', surrounded by 'Filladi di Ambria' with garnet-porphyroblasts (some indicated by small arrows). (A small shear zone indicated by the large arrow.)*

ultramafic rock of up to ~l dm size (Fig. 4b). These xenoliths are mostly matrix-supported, but at the base of the magmatic layers the xenoliths are denser packed and more frequently xenolith-supported, which might suggest gravitative settling. At their base and top the sills have slightly discordant relationships with layering of the host rock (Fig. 4c).

Numerous intrusions of slightly peraluminious and subalkaline (Colombo et al., 1994) granodioritic augengneisses are spatially associated with the metabasites and occur in the 'Filladi di Ambria'. Contacts with the bodies of metabasite, which occur dispersed along the 'Porcile line' (Fig. 4d), are frequent. These contacts and also those with the overlying metasedimentary unit, as well as the occurrence of metabasite-xenoliths in the granodioritic augengneisses clearly indicate that these augengneisses intruded the metabasites and associated metasediments. The contacts are sharp, with thin margins in the metabasites affected by contactmetamorphism and chilled margins within the 'GOOV' (Fig. 4d), indicating a shallow intrusion level. Also the shape of the bodies, sills and stocks, are typical for relatively shallow intrusions. Additionally the structural and metamorphic relationships of garnets in the halos around and within the 'GOOV' indicate a similar sequence of events.

Different names have been given to the individual bodies, the most important and voluminous of which are the 'Monte Fioraro'-'Monte Pedena' (Colombo et al., 1994) and 'Pizzo Meriggio' (Liborio & Mottana, 1971) gneisses. The 'Gneiss del Monte Pallone de Sopressà' (Liborio & Mottana, 1969) of the eastern Orobic Alps might be equivalent as suggested by its structural position. All these augengneisses are called here 'Gneiss Occhiadini Orobico-Valtellinese' (GOOV), to emphasise the common origin of all occurrences and regional distribution. They are all light grey to dark meta-granodioritic augengneisses, locally mylonitic, with centimetre-large porphyroblasts of K-feldspar (often replaced by chessboard albite) and albite in a matrix of quartz, white mica, biotite and chlorite. Often at the contacts to the host rock they are darker, show a diffuse transition zone, and a cataclastic overprint.

The contacts are either parallel to layering and foliation or oblique and the main foliation of the host rock, which continues into the 'GOOV' overprints the contact (Fig. 4e). Locally up to 2½ centimetres large garnets occur as swarms in different concentrations and sizes in banded paragneisses and phyllites of the country rock (Fig. 4f). Because size and concentration of the garnets are inversely proportional to the distance from the contact their growth is possibly related to the shallow intrusion of the 'GOOV'. Garnet also occurs inside the intrusive bodies, mainly along the boundaries, but not as abundant as in the zones around the intrusives. The almandine-grossular rich garnet is of metamorphic origin and found in previously metasomatic Fe-, and Ca- enriched zones, caused by the shallow intrusions of 'GOOV'. These garnets are particularly well developed nearby occurrences of the metabasites around the core of the 'Orobic fold nappe'. Metabasites and paragneisses, similar to the intruded hostrock occur as xenoliths, particularly in the 'Val Budria', some of them even with folds, indicating that a folding phase preceded intrusion.

Psammo-pelitic paragneisses and rhyolitic meta-volcanics, the 'Gneiss di Morbegno' and the 'Gneiss Chiari del Corno Stella', in the following abbreviated as 'Gneiss Chiari', follow in the succession (Fig. 3). The transition from the 'Filladi di Ambria' is in many cases a zone of intense Variscan and Alpine shear-deformation, but there are indications of an angular unconformity at this level. The different tectonic developments of the lower and upper sequences indicate an unconformity or a tectonic contact inbetween. In contrast to the sequence below, which contains mainly basic volcanic components, the upper sequence contains mainly meta-rhyolites. Characteristic is the higher, dominantly albitic, feldspar- and quartz content in the overlying 'Gneiss di Morbegno'. This unit is exposed mainly in the western sector of the Orobic Alps and in the 'Val Colla zone', that forms part of the 'Strona Ceneri zone'. Two typical lithotypes (a) and (b) occur in this stratigraphic unit immediately below and above the 'Gneiss Chiari', amongst the other less distinctive usually garnet-bearing psammo-pelitic rocks:

(a) Garnet-staurolite-white mica schist containing occasionally some kyanite and tourmaline. This Al-rich meta-pelite occurs mainly around the Orobic drainage-divide along the contacts to 'Gneiss Chiari', particularly below. It is also exposed in the upper 'Valle Vicima' in combination with some thin layers of 'Gneiss Chiari'. These lithologies are predominantly present below the 'Gneiss Chiari' and in absence of latter usually below the level where the 'Gneiss Chiari'-horizon usually occurs, but similar lithologies also occur at other levels.

(b) Biotite and albite-rich paragneisses with typical albite-blasts, the 'Albitknotengneise' of Cornelius & Cornelius-Furlani (1930). These rocks display slightly- to well preserved layering, possibly bedding of volcano-sedimentary origin, mainly because of its variable composition and thickness, but within the beds the rock locally resembles metadiorite. The origin of this character, dehydration melting of biotite (±muscovite) is discussed in Feijth & Franz (in prep.). This lithology grades laterally into rocks without foliation or layering. Albite porphyroblasts with fine garnet-, biotite-, quartz- and occasional muscovite inclusions are typical. These porphyroblasts are surrounded by circular concentrations of irregularly shaped biotite. White varieties of this lithology without biotite are also present. Most of these rocks of lithologic variety (b) occur especially in the 'Valle del Bitto' near 'Bema' and 'Sacco', around the 'Monte Piscino', in the Orobic foothills of the 'Valtellina' near 'Selvetta', 'Fusine' and 'Cedrasco' and in the 'Val Tartano' around the 'Crap del Mezzodi'. Other occurrences, with

well-defined layering, seem to be bounded to stratigraphically similar positions above the 'Gneiss Chiari', and are exposed north of the Orobic drainage-divide.

Rocks of transitional type between (a) and (b) occur as well. Quartzite has been found as diffuse intercalations in (a) and (b), in general with layer-thickness of a few cm to dm, but locally in considerable abundance.

The distinctive 'Gneiss Chiari', generally occurs at a specific stratigraphic level of the 'Gneiss di Morbegno', between Al-rich meta-pelites below and biotite- and albite rich paragneisses and meta-volcanics above, but at places the exposed upper sequence is entirely made up of 'Gneiss Chiari'. Exposures of this calc-alkaline unit (Boriani & Colombo, 1979; samples from between 'Valsesia' and the 'Lago di Como') are mainly exposed along the Orobic drainage-divide between Bellano and 'Val Venina', roughly along the hinge-zone of this folded horizon. Massive bodies of around 1000m minimum preserved thickness occur around the 'Monte Cadelle' and the 'Pizzo Zerna'. Exposures West of the 'Valle del Bitto di Gerola' belong to the overturned limb. Northeastward the intrusive bodies diminish in thickness and disappear below the 'Orobic fold nappe'. These massive homogeneous leucocratic coarse-grained rocks have a granoblastic and rarely flaser texture with typical large K-Feldspar porphyroblasts. The main macroscopically recognisable constituents are: quartz, K-feldspar, muscovite and minor albite. Thin muscovite layers, with or without chlorite, that curve around layers and lenses of quartz and granoblastic feldspars, form the main foliation. This foliation is roughly concordant with layering and main foliation of the 'Gneiss di Morbegno' below and on top. Prismatic tourmaline was occasionally observed on the foliation planes. Stronger foliated and finer grained varieties, with more chlorite, biotite and some garnet, can be observed. Subordinately lithotypes enriched in quartz occur, as well as zones with more or less mylonitic structures. Variability is mainly due to a more or less porphyritic structure or to different content of phyllosilicates. Original deposition-related layering of cm to metres scale is locally well visible and the transition is to the 'Gneiss di Morbegno' is gradual at many locations. Locally enclaves of 'Gneiss di Morbegno', usually parallel to the main foliation, have been found in the 'Gneiss Chiari'.

The 'Gneiss di Morbegno' and 'Gneiss Chiari' should be considered together, making up a meta-volcano-sedimentary system with massive rhyolitic complexes. Laterally away from those rhyolitic complexes the proportion of beds of meta-rhyolite in the upper sequence decreases and meta-volcanoclastic beds become more prominent.

These field-based observations are in accordance with the interpretation of an alkali-rhyolitic nature of the 'Gneiss Chiari' (Boriani & Colombo, 1979), which is based on petrographical and geochemical data.

There are also some occurrences of meta-rhyolitic masses which are less porphyritic than the 'Gneiss Chiari' and have more mafic minerals, in particular biotite, potassian-ferroan pargasite/tschermakite, ferro-hornblende, calcian gedrite and zoisite/clinozoisite possibly indicating a change toward a higher mafic content of the volcanic protoliths.

The parautochton (Fig. 3) is exposed in windows in the Permo-Mesozoic cover, the 'Orobic'- and 'Trabuchello anticlines' (Fig. 1c) and generally consist of quartz-mica schists, phyllites and meta-conglomerates, which have a strong overprint of phases of pre-Alpine and Alpine shearing. Variscan layering-parallel shearing whereby low-angle extensional shear-bands developed, gave the rock either a strong planar character or, due to the shear-bands, a wavy

appearance. There are rootless folds in quartzite-layers and the meta-conglomerates contain strongly flattened and sheared clasts. Alpine overprint is mainly cataclastic. Occasionally the quartz mica schists and phyllites contain some garnet and at the 'Upper Val Brembo di Carona' there are amphibolite-schists as intercalations. This parautochton hosts the distinctive 'Val Biandino plutonic complex', which is exposed along the western border of the study area, in the 'Val Sassina', 'Val Biandino' and 'Val Stabina'. This complex consists of stocks and laccoliths of Variscan syn-late tectonic tonalites, granites, quartz-diorites and gabbro-diorites with a large contactmetamorphic aureole are exposed. The intrusions are generally conformable to folded layering of the host rock, but at places discordant, especially at the apophyses (De Capitani et al., 1988). The contactmetamorphic aureole consists of sillimanite-, cordierite- and andalusite- bearing hornfelses, indicating a depth of intrusion of at maximum 10-12 km (De Capitani et al., 1988).

The 'Scisti di Edolo' form the highest unit of the Orobic metasedimentary succession and belong to the 'suprastructure' (Fig. 3). They are characterised by finely laminated phyllites with thin quartzitic layers and are the only basement-rocks of the Orobic Alps with a known depositional age (Silurian and subordinate Ordovician; Gansser & Pantić, 1988). The dominant phyllitic appearance in the field suggests relatively weak metamorphism compared to the underlying units.

3.3 Structure, metamorphic and igneous relationships
3.3.1 Field-relationships

A first-order structure recognised in the field is the monoclinic 'Orobic fold nappe', exposed south of the approximately E-W-striking 'Tonale line', from the 'Adamello massif' up to 'Lago di Como' (Fig. 1a). Across 'Lago di Como' it might be traceable into the 'Strona-Ceneri zone', where it has been mapped as a synform (Giobbi Origoni et al., 1997). Early-Middle Jurassic to Alpine southward rotation (Handy, 1986; 1987; Handy et al., 1999) might be the cause of this orientation. Appearance of this 'Orobic fold nappe' in the field is not as prominent as its size suggests. Once the hinge was recognised in the upper 'Val Lunga' and 'Val Madre' (Fig. 5) the structure could be inferred from the distribution of the metabasites, Filladi di Ambria and other characteristic stratigraphic levels, including the almost conformable sills and some stocks of 'GOOV' and generally stratiform 'Gneiss Chiari' intercalated in characteristic lithologies of 'Gneiss di Morbegno'.

At several locations around the hinge-zone it is possible to observe the 100m- to km-scale curvature of bedding and foliation of all lithologies, related to the hinge-zone of the 'Orobic fold nappe'. This indicates that nappe folding and related deformation in the substructure occurred after development of the main foliation in the upper sequence. Because in the following structural and metamorphic relationships are discussed in more detail symbols will be introduced to indicate the metamorphic and structural events. Metamorphic cycles are indicated as $M_{n/m}$, whereby n is the cycle and m is an identifiable stage of this cycle, either by metamorphic or tectonic analysis. Here m is either represented by the prograde path, including the metamorphic peak, (m=1) or the retrograde path (m=2). The corresponding deformation phase is indicated as $D_{n/m}$. Bedding is indicated as S_0, whereas main foliation, lineations and fold axes are indicated as $S_{n/m}$, $L_{n/m}$ and $F_{n/m}$, where the suffixes correspond to those of the phases of formation.
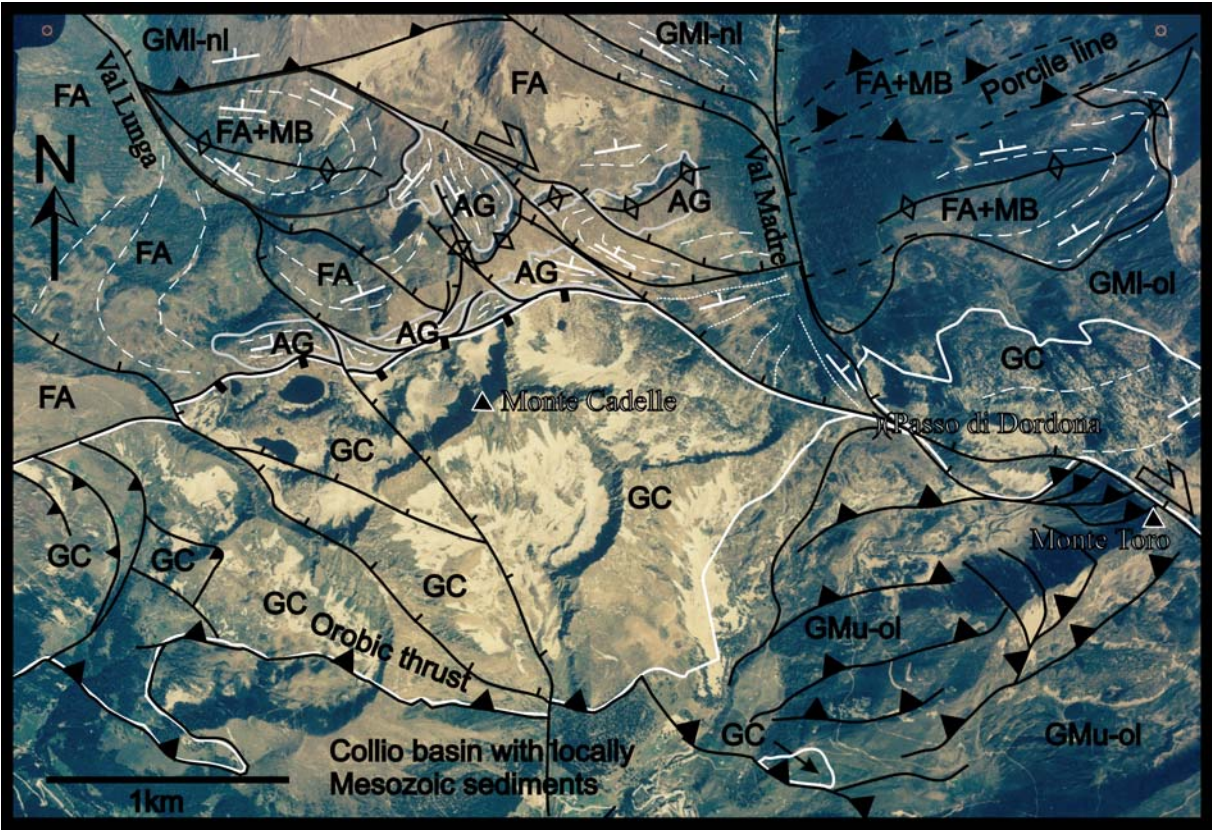
Fig. 5. Areal photograph of the 'Laghi di Porcile'-'Monte Cadelle'-'Passo di Dordona' area, showing the core of the 'Orobic fold nappe', with metabasites surrounded by 'Gneiss Occhiadini Orobico-Valtellinese' and 'Filladi di Ambria. The massive bodies of 'Gneiss Chiari' are also visible, as well as NNE- to NE-dipping transtensional shear-zones, which sense of shear is indicated by offset of characteristic lithologies. Dip- and strike symbols indicate orientation of bedding and main foliation, which are also traced by thin dashed lines. Other symbols as in Fig. 1. Lithologic units: FA: Filladi di Ambria; MB: Metabasites; AG: Augengneiss; GM: Gneiss di Morbegno; GC: Gneiss Chiari; extensions '-nl' and '-ol' indicate normal- and overturned limb respectively. Photograph from REGIONE LOMBARDIA: Concession No. 118 (22.03.1996) of the MINISTERO DELLA DIFESA-AERONAUTICA to COMPAGNIA GENERALE RIPRESEAREE (Parma)

The 'GOOV', which igneous emplacement postdates M_1 and D_1 (Fig. 4e) and represents the youngest identifiable event in the lower sequence, have been found in the metabasites and particularly in the 'Filladi di Ambria'. The larger bodies, like the stocks of 'Monte Fioraro', 'Monte Lago', 'Pizzo Scala' and the folded sill of 'Alpe Cuminello', have a core with rather undeformed magmatic fabrics and in the 'Monte Fioraro'-area these have been called 'Monte Fioraro granite' (Colombo et al., 1994). Towards the margins and especially in apophyses, as well as in the thinner sills and laccoliths, penetrative $D_{2/2}$-fabrics are stronger, manifested as SL-, LS- and, particularly at the boundaries, even L-tectonites. The $D_{2/2}$ foliated 'GOOV' in the upper 'Valle del Bitto di Albaredo' have locally been called 'Monte Pedena orthogneisses' (Colombo et al., 1994), even when these were in continuation with the undeformed cores of 'Monte Fioraro granites or granodiorites'. They are well developed along characteristic NE-dipping dextral shear-zones that affected all units (see discussion). In the lower sequence of the fold nappe, in the core of the fold nappe (Fig. 1) structures of an old phase (D_1) are deformed by $D_{2/2}$-folds and overprinted by $D_{2/2}$-crenulations. Typical macroscopic structures

and minerals of the older phase are: (a) D_1-folds of up to 50 m scale, most frequently dm to 2 m, that have been folded by $D_{2/2}$-folds that also affected the upper sequence of the fold nappe (Fig. 6).

Fig. 6. Type 3 overprint-relationship (Ramsay, 1967) of folds of the lower sequence of the 'Orobic fold nappe' ('Filladi di Ambria'). (Photograph taken near the 'Laghi di Porcile'.)

The folds of the first generation have also been overprinted by the other typical $D_{2/2}$-structures like extensional shear-zones, extensional shearbands, stretching lineations, foliations and a metamorphic phase. (b) A foliation, folded by D_2-folds, which is less developed as the main foliation in the upper sequence that transposes layering (c) M_2-garnets with internal S_1-quartz fabrics. In the lower sequence the $S_{2/1}$-main foliation is less developed as in the upper sequence and D_2-structures appear to be developed more locally and variably below the unconformity.

Bedding and main foliation of the complete sequence of the fold nappe generally dip in NW-direction (Fig. 5 in Feijth, in prep. b). The orientation of strike of bedding planes, that differ from the expected original orientation parallel to the regional E-W strike of the fold nappe, is interpreted to be caused by rotation of individual fault blocks, separated by NE-dipping transtensional shear-zones related to $D_{2/2}$ (Fig. 1, 5 and 7). Most important are those in the 'Valle del Bitto', 'Val Tartano', 'Campo-Pizzo Gerlo' and 'Val Caronno'. This deformation and related rotation of the fault blocks occurred during and after the formation of the fold nappe and is related to internal deformation of the fold nappe in connection to wrenching along the root-zone. The individual fault blocks, separated by the transtensional shear-zones, rotated in an anticlockwise to the horizontal plane, simultaneous with rotation of the hanging-
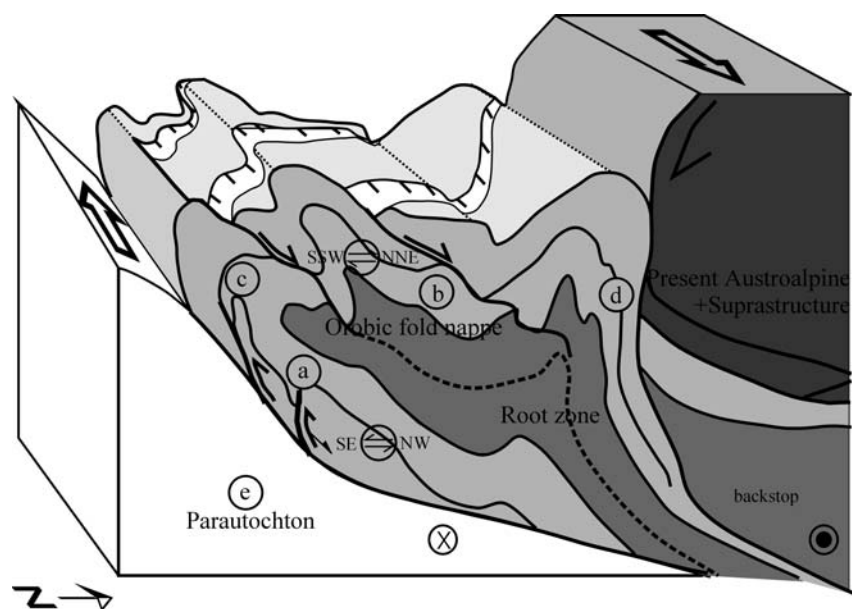
Fig. 7. Schematic overview of the 'Orobic fold nappe' with internal structures. The zones of different kinematic developed, mentioned in the text, are indicated (a) to (e). Within the 'Orobic fold nappe' the lower sequence is indicated in darker grey than the upper sequence.

walls around a horizontal axis according to the orientation of the NE-dipping transtensional shear-zones. Most prominent shear zones of this type and size are those of 'Valle del Bitto', 'Val Tartano', 'Campo-Pizzo Gerlo' and 'Val Caronno' (Fig. 1). Particularly along these $D_{2/2}$-shear-zones, but also at other locations, the main foliation ($S_{2/1}$), also of the 'Gneiss Chiari' and 'GOOV', is overprinted by linear fabrics ($L_{2/2}$), like stretching lineations, crenulations and up to decametric scale $D_{2/2}$-folds. Plunge of these structures range from NNE- to NW-plunging (Fig. 5 in Feijth, in prep. b).

$D_{2/2}$-deformation structures related to the main folding- and nappe-formation of the 'Orobic fold nappe' have developed differently depending on position within the structure according to the local deformation regime. Zones with different structural development are: (a) the overturned limb, (b) the normal limb, (c) the hinge-zone, (d) the root zone and (e) the parautochton. Areal allocation of these zones is shown in Fig. 1. Structures of each of these zones, structural evolution and the involved mechanisms are discussed in detail in Feijth (in prep. a, b) and can be summarised as follows:

Structures of the root zone are extensional shear-bands and -flexures, locally occuring in association with outcrop- to km scale diapirs that have evolved, to various degrees, into extrusional folds (Feijth, in prep. b). All these strucures are related to extrusion of a diapiric ridge that evolved into the South-verging recumbent 'Orobic fold nappe'. Feijth (in prep. b) interpreted that extensional shear-bands and -flexures formed at least partly as a result of adjustment, minimising the potential energy in the gravity field under superposed tectonic shortening perpendicular to the rootzone, as the structural orientations suggest.

Also the normal limb contains extensional shearbands that together with the superposed extensional lineations indicate a top to the NNE sense of shear related to extrusion of the diapiric ridge, gravitational adjustment and collapse of the nappe by southward spreading.

The vergence of occasional compressional structures in the overturned limb is SW to WSW, in accordance with the direction resulting from the combination of extrusion and nappe-

spreading with a dextral wrench-component along the root zone. The NE-dipping dextral transtensional shear zones, also related to wrenching along the root zone, and in the north rooted in this zone, crosscut the entire nappe structure and together form the decollement between the fold nappe and the parautochton. The orientation patterns of stretching lineations, fold axes and crenulations in the overturned limb (Fig. 5 in Feijth, in prep. b) are a result of interference of orthogonal compression/underplating and extension obliquely oriented with respect to strike of the 'Orobic fold nappe'. The compressional and underplating structures respectively are related to combined extrusion and wrenching and the extensional structures to gravitational collapse and spreading of the fold nappe. It is important to note that these indications of interference imply concurrent extrusion, collapse and wrenching. The abundant low-angle shearbands and layering-parallel shearzones in outcrops around the contact between the 'Orobic fold nappe' and the parautochton, indicate a relative high degree of decoupling between both units. Brittle overprint along the contact could either be related to a Permian detachment, Alpine faulting activity or both.

The base of the tectonic unit consisting of the sequence of 'Scisti di Edolo' is intensely sheared parallel to layering. Also some quartzitic layers are folded related by a pre-Alpine phase. A xenolith of folded mylonite was found in a hornblende-porphyritic dyke (Lardelli, 1981), which hornblende was dated at 96-80 Ma (Mc Dowell, 1970). These dykes have only been weakly affected by post-intrusive events. The difference in metamorphic grade between the 'Scisti di Edolo' that make up the 'suprastructure' and the 'infrastructure' suggests that the contact between higher grade 'infrastructure' and the 'suprastructure' is an extensional or transtensional shearzone extending downwards in the hanging wall of the root zone.

3.3.2 Microfabrics, petrography, temperature-sensitive micofabrics

In order to extract the structural and metamorphic evolution of the Orobic basement, including the evolution of the 'Orobic fold nappe', an analysis of the development of the petrography, microfabric and microtectonic relationships is required. The analysis presented here is mainly focused on interpretation of overprinting relationships to derive relative age relationships of tectonic events and kinematic parameters and the structural configuration. A mineral crystallisation-deformation-diagram (Fig. 8) shows a schematic overview of the development. Shear sense indicators are discussed separately in Feijth (in prep. b), because they are important for the interpretation of fold nappe development. Additional description of microfabric and petrography and phase-relationships, essential for thermo-barometric analysis is presented in Feijth & Franz (in prep.).

Lower sequence of the 'Orobic fold nappe'
The bulk of the investigated lithologies of the central Orobic basement contain assemblages with garnet and biotite as index minerals, together with quartz, albite and white mica. This is also the case for the 'Filladi di Ambria', which belongs to the lower sequence of the 'Orobic fold nappe'. Locally, especially close to the metabasites, some alumino-tschermakite, schermakite zoisite and clinozoisite also occurs.

Presence of high concentrations of large garnet in the halos around the 'GOOV' underlines the important conclusion that there was a metamorphic phase that post-dates the igneous emplacement of 'GOOV' and related metasomatic Fe- and Ca- enrichment in these zones.
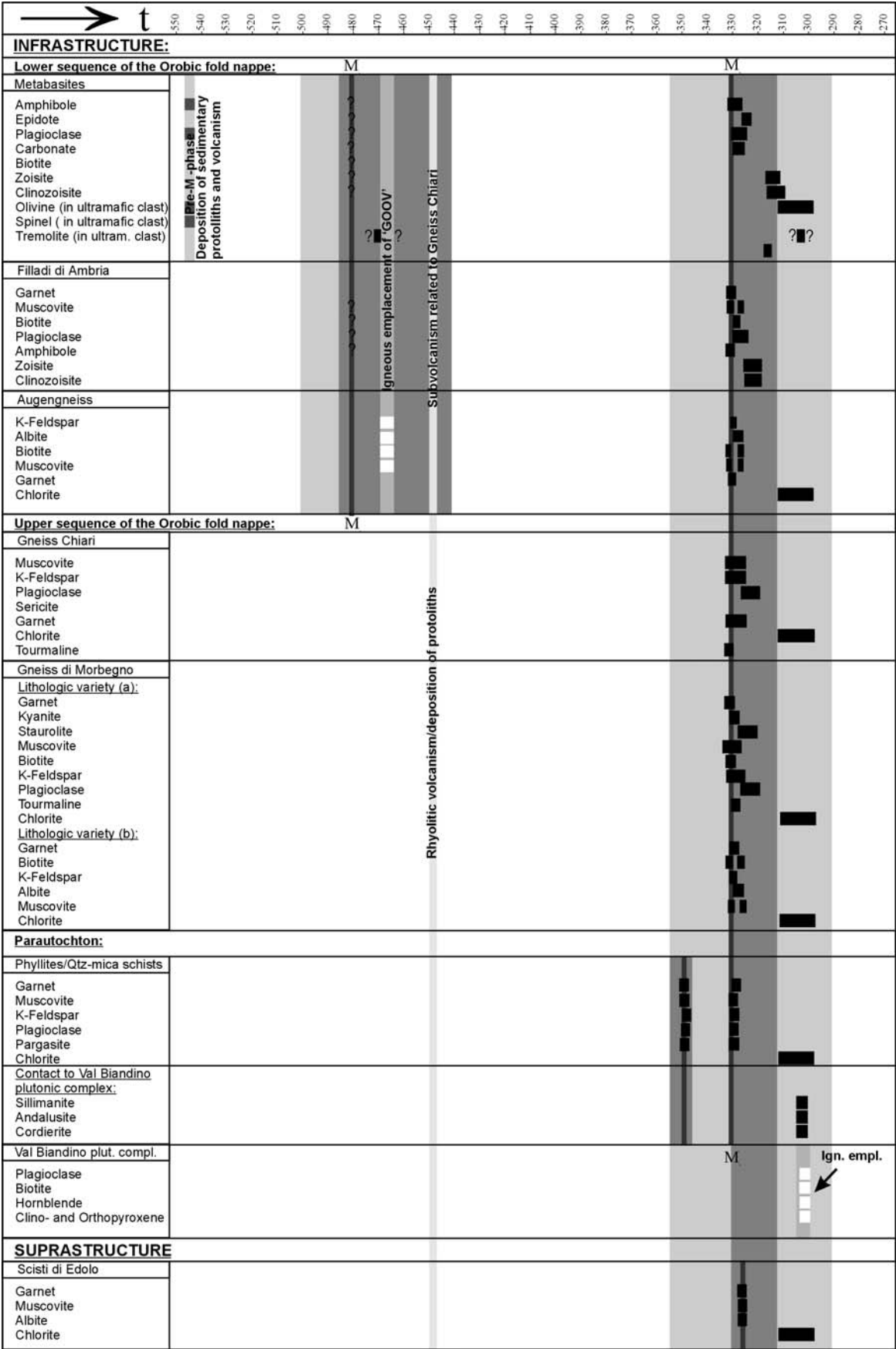
Fig. 8. Mineral-crystallisation-deformation diagram.

The garnets in these halos contain undulous quartz inclusions with subgrains and deformation lamellae, which indicate that the growth of these garnets should postdate an earlier tectono-metamorphic phase. This fabric, overgrown by the garnets, cannot related to M_2, because $D_{2/2}$-microshears, that form an extensional crenulation cleavage affecting the M_1-foliation, are concentrated around these porphyroblasts, and some garnets are also broken and disrupted by $D_{2/2}$-shear along the main foliation and mentioned microshears. The garnets are therefore pre-tectonic with respect to $D_{2/2}$ and post-tectonic in relation to an earlier tectono-metamorphic phase (D_1/M_1 or early-$D_{2/1}/M_{2/1}$) and should have started growing on the prograde path of M_2.

Also zoisite of the 'Filladi di Ambria', in a pegmatite vein close to the metabasites is sheared in a brittle-ductile manner during the same event that affected the garnets, with the cracks in the undulous zoisite filled by younger clinozoisite. Amphibole in the 'Filladi di Ambria', that especially occurs close to the metabasites, is usually alumino-tschermakite, tschermakite or occasionally magnesio-hornblende. These rocks also contain undulous clinozoisite, locally very abundant, with conspicuous younger micro-fissure-filling Fe-richer clinozoisite. These fissures are a product of ductile-brittle $D_{2/2}$-shearing. This ductile-brittle event also affected quartz and $M_{2/1}$-garnet that contains inclusions of an overgrown quartz-fabric that was deformed during an earlier metamorphic phase, as their undulous extinction and deformation lamellae indicate.

The intercalations of metabasites in the 'Filladi di Ambria' have above been subdivided in two main types, (a) meta-amphibolitic tephra-layers and (b) meta-amphibolite sills containing mafic and ultramafic xenoliths:

(a) The meta-ashes and –tuffs, occur as amphibolite- and epidote-amphibolite-schists and coarser 'Garbenschiefer'-varieties consisting of amphibole, biotite and calcite parallel to the main foliation and occasionally garnet, in a matrix of finer grained groundmass of plagioclase, some quartz and epidote, zoisite and clinozoisite. Some portions consist almost entirely of (clino?-)zoisite. The locally abundantly dispersed (clino?-)zoisite is sheared in a similar brittle-ductile manner as the clinozoisite in the pegmatite vein in the 'Filladi di Ambria'. Fe-richer fissure-filling clinozoisite was also here formed along these fissures, probably during the brittle-ductile tectonic event.

Compositional layering and parallel metamorphic fabric of the amphibolite-schists is locally D_1-folded with axial planes parallel to general layering orientation. (b) The meta-amphibolite sills consist of fine-grained euhedral magmatic amphibole in a matrix of symplectitic finer plagioclase and epidote. The amphibole of the groundmass is clearly of magmatic origin. They are euhedral with a magmatic outer zonation, in a finer grained symplectitic groundmass of albite and epidote. This magmatic rock locally contains mafic and ultramafic xenoliths. These xenoliths consist of foliated meta-gabbro and garnet-amphibolite, pyroxenite and ultramafic rock, latter with relics of olivine and some spinel in a crystalline groundmass of serpentine and talc overgrown by some tremolite. Amphibole and plagioclase of the xenoliths of meta-gabbro grew in two generations the second before being included into the magma. These minerals have magmatic cores that were overgrown by a rim that grew in a preferred orientation parallel to the foliation or lineation of these xenoliths during a pre-D_1 tectonic phase. This could be the Canobbio phase (Handy et al., 1999) identified in the 'Strona-Ceneri Zone', but should be further investigated.

The augengneiss (GOOV) contains quartz, often perthitic K-feldspar, biotite, plagioclase (0-

17 % An), epidote/zoisite and occasionally garnet ($Al_{58-69}Py_{3-7}Gr_{21-31}Sp_{2-12}$), latter especially at the boundaries of the sills and stocks. Apatite, zircon, tourmaline, rutile and opaques occur as accessory minerals. Epidote is occasionally abundant. Biotite and white mica form the main foliation and the $D_{2/2}$-related shearplanes and C'-shearbands, which form an anastomosing conjugate cleavage around the K-feldspar σ-blasts, garnet, albite and quartz of the microlithons. Garnet and K-feldspar porphyroblasts predate ductile-brittle $D_{2/2}$-shearing. Locally it can be recognised that a local $S_{2/1}$-foliation crenulates an older foliation. Quartz displays a granoblastic interlobate structure; with subgrains along the bounding foliation shear planes. $D_{2/2}$-related dynamic recrystallisation was followed by static recovery, which caused euhedral subgrain-shapes. Locally quartz-lenses show crystal-preferred orientations. Biotite and garnet are occasionally replaced by chlorite. Perthitic unmixing of K-feldspar might indicate a high T overprint and following slow cooling.

Upper sequence of the 'Orobic fold nappe'
Albite- and garnet-porphyroblasts from a zone of intense layering parallel shear-deformation at the base of the sequence of 'Gneiss di Morbegno' along the main unconformity of the 'Orobic fold nappe', contain older relics of sedimentary layering expressed as inclusion trails of fine opaques in the garnet (Fig. 9a). In the albite-porphyroblasts these layers of opaques indicate an original primary layering which is parallel to the main foliation, consisting of muscovite and biotite. This secondary foliation is deflected by the rigid garnet-porphyroblasts. Interpretation of these garnets with inclusion trails require awareness of the ongoing discussion of rotation or non-rotation of spiral-S_i porphyroblasts between Bell (1985), Bell & Johnson (1989), Passchier et al. (1992) and Johnson (1993 a,b) whether spiral- S_i porphyroblasts rotated with respect to kinematic axes of bulk flow, or with respect to geographical co-ordinates. In this case it is obvious that the garnets rotated with respect to bedding and main foliation during their syn $M_{2/1}$ growth, because the inclusion trails overgrown by the garnets and those outside the garnets, e.g. in the plagioclase, are of similar origin. Shearing parallel to the main foliation and a stretching lineation on the combined foliation- and bedding-plane caused the rotation. Because the stretching lineation was sub-parallel to the shear direction indicated by the garnets the kinematic axes would have rotated only slightly with respect to the reference frame. The inclusion trails indicate an up to 90° rotation of the garnets.

Composition of these syn-tectonic garnets gradually changes from core to boundary from $\sim Al_{60}Py_3Gr_{25}Sp_{12}$ to $\sim Al_{67}Py_{10}Gr_{21}Sp_2$, a prograde zonation as indicated by microprobe analyses.

The 'Gneiss di Morbegno' of lithotype (a) contains much muscovite, garnet-, kyanite-, staurolite- and plagioclase-porphyroblasts. Usually, particularly in the staurolite-richer rocks of lithotype (a) there is no or very little biotite. Kyanite overgrew bedding-parallel muscovite in a parallel preferred orientation aligned with the transposed main foliation. The relatively abundant staurolite commonly has inclusions of almandine-garnet$_{(2/1)}$ ($Al_{70}Py_8Gr_{17}Sp_1$) (Fig. 9b). The main foliation represents an early-$M_{2/1}$ foliation, parallel to the main foliation of the 'Gneiss Chiari'. Signs of older phases of penetrative foliation are absent in this sequence. Garnet grew during prograde $M_{2/1}$ metamorphism, followed by kyanite in a later stage of $M_{2/1}$.
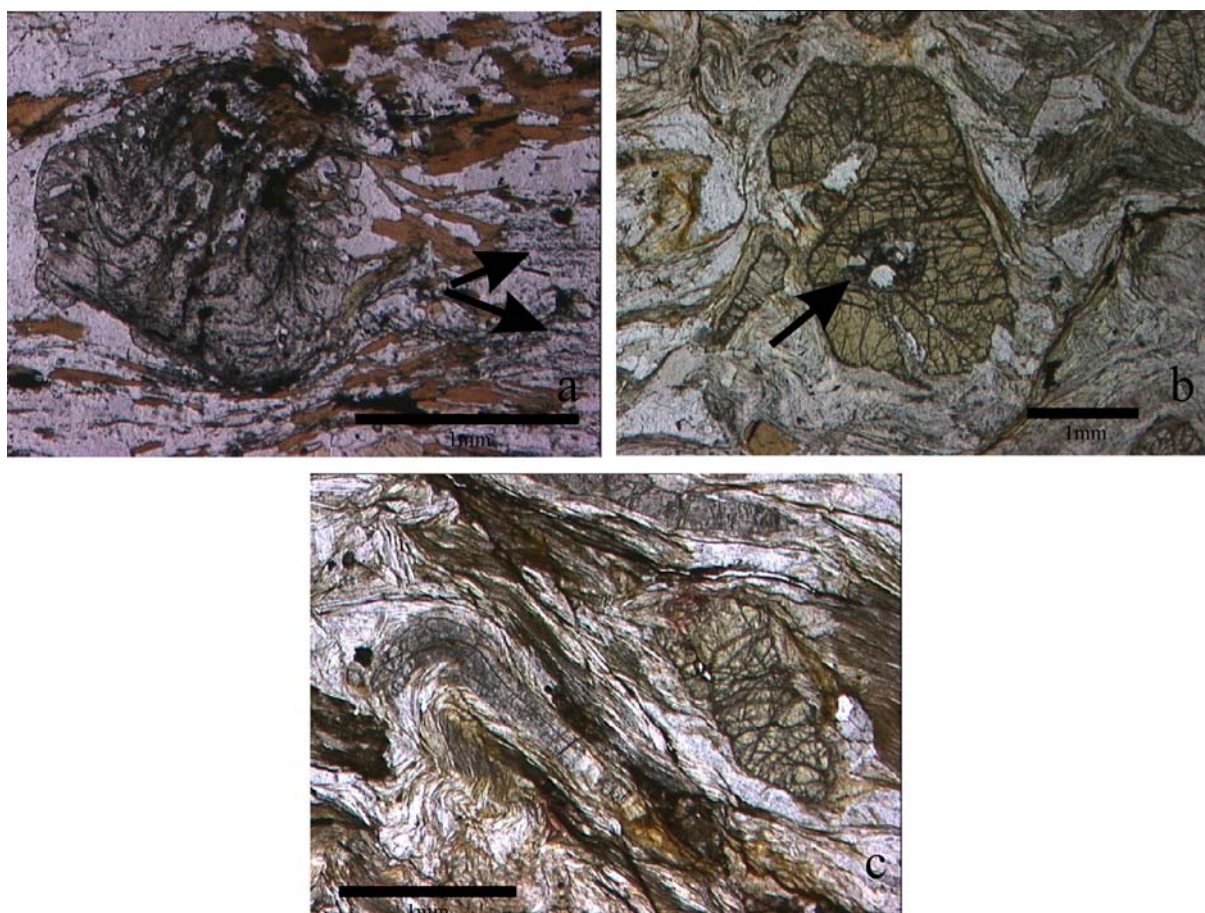
Fig. 9.

a. Syn-tectonic garnet with inclusion trails of fine opaques representing sedimentary bedding as 'primary foliation' and a deflected foliation of secondary origin of muscovite and biotite. Plagioclase with similar inclusions is indicated with arrows. Thin section from a Variscan shear-zone at the base of 'Gneiss di Morbegno'. Thin section 98.2-1 from Val Lunga, plane polarised light.

b. Staurolite with an inclusion of garnet that also contains quartz (arrow). Thin section 31.7a5 from a sample from the 'Monte Valetto'-'Passo Salmurano' area, plane polarised light.

c. $D_{2/2}$-folded kyanite and staurolite in a groundmass of muscovite and plagioclase. The sample is from the 'Gneiss di Morbegno', lithologic variety a, from a NE-dipping shear-zone in the Monte Valetto-Passo Salmurano area. Thin section 31.7a2, plane polarised light.

Kyanite is a product of muscovite dehydration melting at peak-conditions of at least 750 °C (Feijth & Franz, in prep.). Additional kyanite has possibly either been formed by the continuous reaction

$$grt + mu \longrightarrow bt + Al_2SiO_5 + qz \quad \text{(Thomson, 1982)} \tag{1}$$

at the low-T side of the dry dehydration melting reaction of muscovite (Feijth & Franz, in prep., Fig. 11b.) and/or by the back-reaction of the biotite dehydration melting reaction (Feijth

& Franz, in prep., Fig. 11b).

Garnet- and kyanite porphyroblasts predate the culmination of $D_{2/2}$, because the main foliation including the kyanite-porphyroblasts is $D_{2/2}$-folded (Fig. 9c), boudinaged and sheared in $D_{2/2}$-transtensional shear-zones.

Staurolite-porphyroblasts grew on a temperature retrograde path immediately after peak-conditions, by the reaction

$$grt + bt + as \longrightarrow st \qquad\qquad (Spear\ \&\ Cheney,\ 1989) \quad (2)$$

at around 700 °C (Feijth & Franz, in prep.). This led to the formation of staurolite around garnet (Fig. 9b).

$D_{2/2}$-folded white mica has overgrown porphyroblastic albite (~20 % An) before folding. Kyanite and plagioclase are often sericitised, staurolite is occasionally replaced by sericite and chlorite whilst garnet not included in staurolite is often pseudomorphic replaced to various degrees by chlorite during retrogression. Chlorite veins crosscut albite. Quartz occurs as grain aggregates with seriate-interlobate and younger polygonal subgrains, which formed after dynamic recrystallisation. Undulous extinction and deformation lamellae are common.

A lithology with typical abundant relatively large albite-porphyroblasts$_{(2/1)}$, biotite$_{(2/1)}$ and small garnet$_{(2/1)}$, chlorite, almost devoid of muscovite was above introduced as variety type (b). In thin sections and samples from few locations in the Orobic foothills of the Valtellina and in the field also staurolite- and kyanite-relics have been recognised both in thin section (Crespi et al., 1980), and in the field but these are generally rare in this type of rock. The porphyroblasts of kyanite are aligned with muscovite and are surrounded by albite and biotite (Tavola II, Fig. 2 of Crespi et al., 1980).

These typical phases have been overgrown and are surrounded by albite and biotite. Irregularly shaped biotite forms circular concentrations around the plagioclase porphyroblasts (Feijth & Franz, in prep., Fig. 4c, d), occasionally bedding-parallel cleavage domains as well as fine synthetic and antithetic C'-type extensional shearbands. The conspicuous albite-porphyroblasts have small garnet, laths of biotite, quartz and very fine mica as inclusions (Fig. 4c, d and e in Feijth & Franz, in prep.). These albite porphyroblasts seem to have pseudomorphically replaced a mineral with an orthorhombic symmetry, as indicated by the alignment of the phyllosilicate inclusions. The replaced mineral that has given this rock its remarkable character might have been an anorthite- and orthoclase-richer feldspar, possibly K-feldspar, a product of biotite dehydration melting. The fabric as a whole represents a product of incomplete biotite dehydration melting during a metamorphic event ($M_{2/1}$), which culmination preceded $D_{2/2}$-deformation (Feijth & Franz, in prep.). In the majority of lithologic variety (b) back-reaction would have been possible because segregation of the melt beyond mesoscopic scale did not really start (Feijth & Franz, in prep.). $D_{2/2}$-extensional shearbands, $D_{2/2}$-flexures, stretching lineations, $D_{2/2}$-folds and boudins of meso- to outcrop scale developed synchronously with or postdate this melting in these meta-greywackes. The relative abundance of these types of structures in these lithologies suggests a relationship between lithology and deformation. The presence of microscopically thin veneers of melt, related to dry melting of biotite before and during related growth of the relatively large amount of albite porphyroblasts, might have induced deformation and rheological changes accomodating early

$D_{2/2}$-strain.

Quartz, orthoclase, large granoblastic microcline, albite-oligoclase and muscovite are the primary constituents of the 'Gneiss Chiari', of which microcline is certainly magmatic. The cleavage domains, a spaced foliation that is found anastomosing around the K-feldspars, and quartz, contains large muscovite, sericite and chlorite. Albitic plagioclase is evenly distributed between cleavage domains and microlithons. The microstructure of the 'Gneiss Chiari' shows a development similar to that of the 'GOOV': The grain size generally becomes finer towards these cleavage domains, where undulous extinction is more common, suggesting that these acted as micro-shear-zones. Granoblastic microcline with perthitic structure was formed by slow post magmatic cooling from high temperatures. The subgrains in this microcline are a product of $D_{2/2}$-shearing. Pertithic veins are oriented perpendicular to foliation shearplanes. The outer zones of large quartz crystals consist of dominantly anhedral subgrains and deformation lamellae, indicating dynamic recrystallisation. Minor recovery by grain boundary area reduction is suggested in view of their slight modification towards polygonal crystal shapes. Relics of S_0, expressed as compositional changes between centimetres to metres scaled layers, are most clearly preserved close to the contacts with 'Gneiss di Morbegno' and are often visible in the field.

Muscovite, often sheared parallel to foliation, gives the rock a slight schistose- or flaser character, and is concentrated in a spaced foliation of thin wavy cleavage domains, which take approximately 5 % of the rock volume. Late brittle deformation is represented by brittle fractures in microlithons of quartz and K-feldspar filled with sericite and microcracks filled with ore. Occasionally tourmaline and chloritised garnets are present in the cleavage domains.

The parautochton

Mineralogy and microstructure of the quartz-mica schists and phyllites exposed in windows in the Permo-Mesozoic cover differs from both sequences of the 'Orobic fold nappe' and from the 'Scisti di Edolo'. Undulous quartz with preferred orientations, minor plagioclase and white mica are the main constituents, with garnet occasionally present. Some pargasite-rich intercalations were identified in samples from the upper 'Val Brembana di Carona'.

The 'Val Biandino plutonic complex' consists of a variety of lithologies, granites, aplitic granites, quartzdiorites/tonalites granodiorites and gabbrodiorite. The investigated samples of quartzdiorites contain plagioclase, quartz, biotite, K-feldspar, usually ferri- and ferrian-magnesio-hornblende, orthopyroxene and occasionally clinopyroxene.

The 'suprastructure'

These sericitic phyllites have a mm-scale disjunctive cleavage parallel to the shear plane. Undulous quartz is very fine grained with moderately to well-developed preferred orientation. Albite is also present in the quartzitic microlithons. The cleavage domains are made up of sericitic white mica and biotite and the garnets have strain shadows with fine-grained quartz. Garnet is generally fully replaced by post-tectonic chlorite.

The presence of biotite and garnet indicate a metamorphism that exceeds Alpine conditions, next to the folded mylonite in hornblende-porphyritic dykes mentioned above is a second argument for pre-Alpine mylonite formation.

4 Discussion of the basement evolution

4.1 Pre-Variscan development, particularly the Sardic event (M_1/D_1)

For the revelation of the tectono-metamorphic evolution of the Southern Alps it is essential to realise that the 'Orobic fold nappe' consists of two sequences, which are separated by an unconformity, as recognised in the Orobic Alps for the first time. The lower sequence is affected by two tectono-metamorphic events (M_1/D_1 and M_2/D_2), whilst the upper sequence only by the youngest of both events.

The relative ages of the events of the metamorphic-, folding- and igneous events that affected the lower sequence are well-constrained: Metamorphism and folding should have preceded the igneous phase of 'GOOV'-intrusion, because the 'GOOV' is not affected by the oldest folding phase (D_1). Locally the 'GOOV' cut the foliation of the host rock and xenoliths with folds have been identified. The minimum age of the 'GOOV' is best constrained by the discordant contacts of the shallow intruded 'GOOV' with D_1 folded and M_1 metamorphosed 'Filladi di Ambria' (Fig. 4e) and metabasites. Garnets, that grew in the around the 'GOOV', during $M_{2/1}$ acted as rigid objects during $D_{2/2}$-shearing. This $D_{2/2}$-shearing also affected the 'GOOV'.

So far, due to high grade of the $M_{2/1}$-$M_{2/2}$ metamorphic overprint, no isotopic ages are available for the M_1 phase in the Orobic basement and finding suitable minerals for isotopic dating of this phase might pose a problem.

The identification that the lower and upper sequences correlate tectonically and stratigraphically with the 'Scisti dei Laghi'- and 'Strona Ceneri sequences' respectively of the 'Strona Ceneri Zone', which is exposed West of the working area is a fortunate circumstance, because isotopic age data are available for the 'Scisti dei Laghi sequence'. The 'Scisti dei Laghi'-sequence contains granodiorites similar to the 'GOOV' and a unit with metabasites called 'Strona Ceneri Border Zone' (SCBZ), described and latest mentioned by Handy et al. (1999) and named by Boriani & Giobbi Origoni (1992).

The interpretation of the ages of the M_1 metamorphism, D_1 deformation and intrusion of the 'GOOV' are discussed in detail in Feijth et al. (in prep.). According to latter mentioned publication and references therein all these events are related to the 'Sardic' event, whereby the metamorphic- and folding-events occurred in the early Ordovician, most likely at 473 or 480 Ma, immediately followed by the igneous phase, most likely during the early to middle Ordovician. Eclogite xenoliths in the 'Ceneri granitoid' of the 'Strona Ceneri Zone' (Zurbriggen et al., 1997) provide the important information that the early- to middle-Ordovician granitoids and thus also igneous emplacement of the 'GOOV' postdate accretion and subduction.

Buletti (1983) investigated the trace element characteristics of garnet amphibolites of the 'SCBZ'. The results indicate that at least this lithology originally comprised tholeitic ocean floor basalt. The clasts with a foliation and lineation included in the metabasite sills indicate a 'pre-M_1' deformation phase, which would also be older than depositional age of the lower sequence.

The metamorphosed 'pre-Sardic' sequence forms the basement of the upper sequence with 'Gneiss di Morbegno' and 'Gneiss Chiari' that were deposited post M_1 and D_1 during a phase of rhyolitic volcanism. The albite- quartz-, muscovite- and occasionally microcline-bearing

(Liborio & Mottana, 1969) porphyroid-gneisses called 'Gneiss di Cima Fraitina', exposed between the 'Val Caronella' and 'Val Brandet' and the 'Formazione di Forno d'Allione' of the 'Val Camonica' occur at a similar stratigraphic position as the 'Gneiss Chiari del Corno Stella'. The 'Gneiss di Cima Fraitina' has discordant, concordant and lateral interfingering relationships with the metasedimentary host rock, which have been described by Liborio & Mottana (1969) and are not uncommon for rhyolitic volcanic units. The 'Gneiss Chiari' and these related formations might have affinities with the 'pre-Hercynian rhyolitic plateau' of Sassi & Zirpoli (1968). This unit coincides with the 'Porphyroid-Platte of Mostler (1970), which is similar to the 'Upper Ordovician Rhyolitic Plateau' of Belieni & Sassi (1981) and Sassi et al. (1984). Related rhyolitic volcanics are exposed in the 'Northern'- and 'Eastern Greywacke Zones', the 'Nock series', the 'Gurktaler Alpen' and the 'Carnic Alps'. Samples from sequences belonging to the 'Upper Ordovician Rhyolitic Plateau', all contain lithologies that are geochemically comparable. Representative analyses of the major elements of the 'Blasseneck' porphyroid of the 'Eastern Greywacke Zone' (Loeschke & Heinisch, 1990) and of the 'Gneiss Chiari' from inbetween 'Valsesia' and the 'Lago di Como' (Boriani & Colombo, 1979) suggest a similar rhyolitic origin for both occurrences. The 'Mantello gneisses', exposed near Dubino in the Southalpine basement of the Valtellina, have a very similar composition, microstructure and appearance, partly even identical, which suggests that also these orthogneisses could be equivalent to the 'Gneiss Chiari', as already suggested by Bonsignore et al. (1971). Other sequences of the Southalpine with 'Gneiss Chiari' west of the Orobic Alps (Lehner, 1952; Boriani & Colombo, 1979; Handy et al., 1999) and units with similar rocks in the Austroalpine (Hess, 1953; Doessegger, 1974; Martina, 1958) the 'Cassana phyllites' of the Valtellina (Neubauer & Sassi, 1993 and references therein) contain similar 'porphyroid' gneisses, many of which called 'Gneiss Chiari' and might be equivalent as well.

Assuming similar stratigraphic relationships across the 'Insubric lineament', isotopic and palynological data available can be used to reveal whether these rhyolitic ignimbrites might be used as a time marker throughout the Austroalpine and Southern Alps. The metapelitic series of the 'Northern Greywacke Zone' below the rhyolitic porphyroids would then correspond to the lower 'Gneiss di Morbegno'. Biostratigraphic dating with conodonts by Flajs & Schönlaub (1976) indicate that the metapelitic series of the 'Northern Greywacke Zone' was deposited around the 'Caradoc-Ashgill'-boundary (~450 Ma).

However, the Southalpine rhyolitic volcanism can be up to 30-35 Ma older, as suggested by recently dated zircons from Eastern Southalpine metavolcanics, the Comelico porphyroids, which yielded ages of 479 ± 8 Ma and 485 ± 8 Ma (Meli and Klötzli, 2001). Also the age of deposition of associated metasediments is older than metasediments in the 'Northern Greywacke Zone'; palynologic assemblages from the Col di Foglia Formation suggest a late Early Cambrian to Early Ordovician (Tremadocian) age (520-475 Ma) for the sedimentation, the late Cambrian being more probable (Sassi et al., 1984). Metamorphic U-Pb ages of 480 Ma of staurolite of the 'Strona Ceneri Zone' (Romer & Franz, 1998) indicate an upper limit for the age of rhyolitic volcanism in the West-Italian Southalpine basement and diachronous relationships.

These data indicate that since the M_1-metamorphic peak, that affected the pre-'Sardic' sequence, and before deposition of the upper sequence of the Orobic basement a significant crustal section has been eroded in the Orobic Southalpine zone.

For Early- to Middle Ordovician magmatic suites of similar character in southern Sardinia Carmignani et al. (1994) has proposed a magmatic arc setting, based on the felsic, subalkaline character of these rocks. This agrees with the speculative palaeo-geographic reconstructions of Stampfli (1996) and von Raumer (1998), who have located the southern Variscides, including Sardinia and the Southern Alps along the northern margin of Gondwana in mid-Ordovician time. Agreeing with this setting Handy et al. (1999) has adopted the name 'Sardic event' for Ordovician tectono-metamorphic phases in the Southern Alps between 440 and 480 Ma.

According to above reconstruction of the 'Sardic' Orobic evolution the main unconformity between the pre- to syn 'Sardic' and post-'Sardic' sequences would represent rearrangement of the plate-tectonic setting and possibly the start of a change to an early stage of a backarc extensional setting suggested first by Neubauer & Frisch (1988).

The origin of the 'Gneiss Chiari' that has long been debated (de Sitter & de Sitter Koomans, 1949; Graeter, 1951; Reinhard, 1953, 1964; Mottana, 1963; El Tahlawi, 1965; Liborio & Mottana, 1971; Köppel & Grünenfelder, 1971; Boriani & Colombo, 1979; Zurbriggen et al., 1997; Handy et al., 1999) seems to be solved now. It should however be confirmed that all lithologies that have been mentioned as 'Gneiss Chiari' or 'Gneiss Chiaro' (Graeter, 1951; Lehner, 1952; Reinhard, 1953, 1964; Mottana, 1963; El Tahlawi, 1965; Liborio & Mottana, 1971; Köppel & Grünenfelder, 1971; Zurbriggen et al., 1997; Handy et al., 1999), also in the Austroalpine realm (Hess, 1953; Martina, 1958; Doessegger, 1974; Neubauer & Sassi, 1993), are identical and have a similar origin. As demonstrated above, the 'Gneiss Chiari'-horizon could well serve as an important marker to correlate Variscan units and crustal levels across the 'Insubric lineament'.

4.2 Variscan structural and metamorphic evolution (M_2/D_2)

A plausible evolutionary sequence of the interpreted Variscan development is shown in the sequential sketches of Fig. 10. Main conclusion from the presented field- and microstructural data is that the formation 'Orobic fold-nappe' started when Variscan peak metamorphic conditions of uppermost amphibolite facies grade and dehydration melting of muscovite and biotite were reached when this unit was situated at the orogenic root. Prograde Variscan fabrics are rare, and occur as garnet with weak relic prograde zonation in a shearzone at the contact between the pre-'Sardic' and post-'Sardic' sequences. Retrogression started with the start of formation of the 'Orobic fold-nappe'. The recently available isotopic ages obtained by EMP on monazite (Feijth et al., in prep.) constrain peak conditions, whereas $^{40}Ar/^{39}Ar$-ages of white mica and biotite from the Orobic basement and of detrital white mica from the Permian 'Collio Orobico basin' and U-Th-Pb constrain the following cooling. The $M_{2/1}$ event under P ≤ 1.3 GPa and T around 750°C (Feijth & Franz, in prep.), is tied geochronologically very well at 330-320 Ma (Feijth et al., in prep.), because monazite was used for U-Th-Pb-dating and peak-tempertures were obtained by monazite-xenotime thermometry. Collapse-related cooling ($M_{2/2}$) through the closure temperatures of the $^{40}Ar/^{39}Ar$ isotopic system of white mica occurred at approximately 325-305 Ma (Feijth et al., in prep.).

Oblique orientations of these $D_{2/2}$ extrusion- and $D_{2/2}$ collapse-related transtensional within the fold nappe suggest that combined diapirism, extrusion and gravitational collapse were at least partly coincident with a shearing of the fold nappe with a transcurrent component parallel to
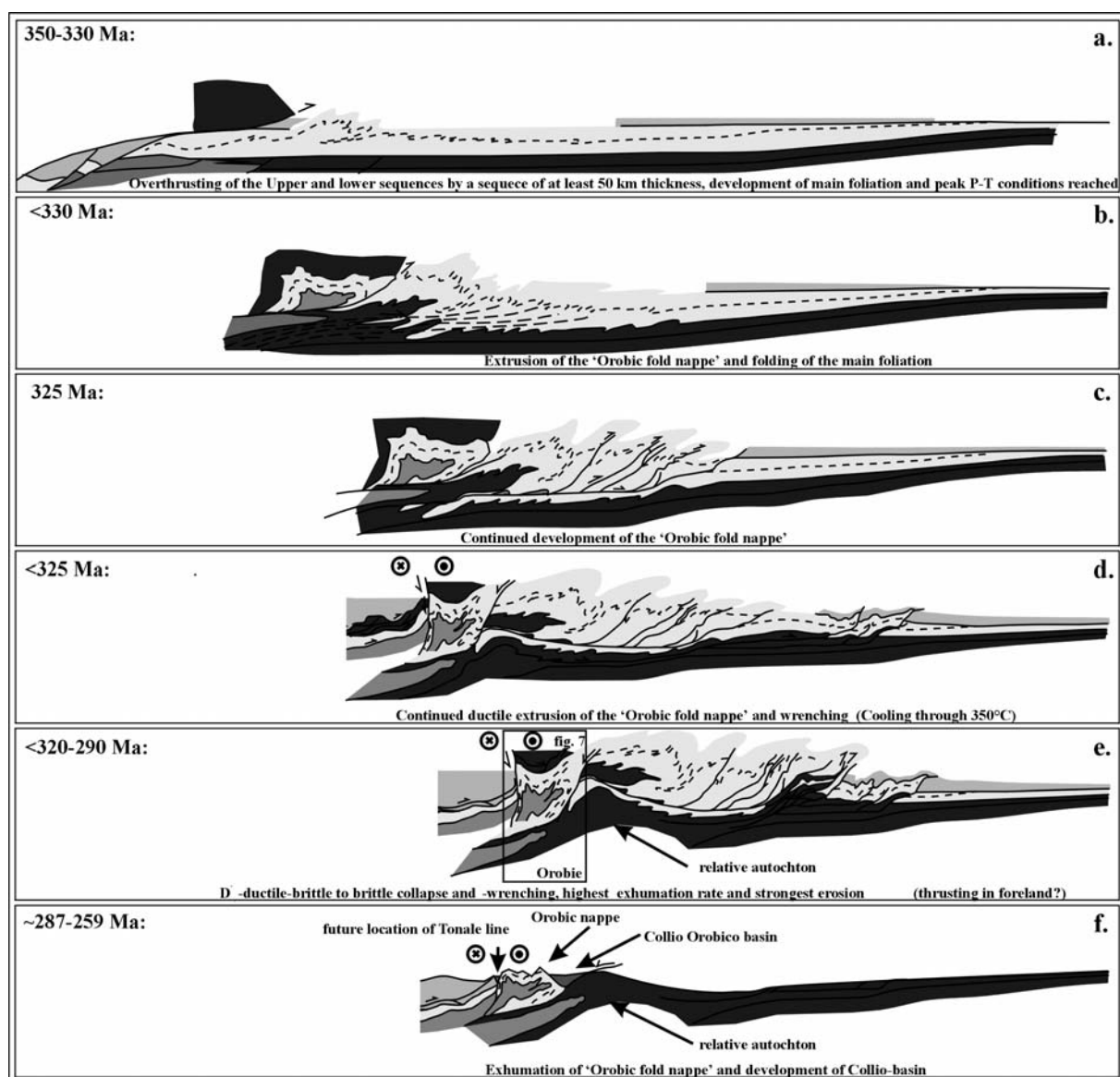
Fig. 10. *Evolutionary model of the Variscan and Permian tectonic development of the Orobic belt. Six stages (a-f) are illustrated:*

a. *350-330 Ma: Burial by at least 50 km of crust of the 'pre-Sardic' and 'post-Sardic' sequences during a ($D_{2/1}$)-phase of crustal shortening; development of main foliation and peak P- and T-conditions reached.*

b. *<330 Ma: Extrusion of the 'Orobic fold nappe' and folding of the main foliation (start of $D_{2/2}$).*

c. *325 Ma: Continued development of the 'Orobic fold nappe'.*

d. *<325 Ma: Continued $D_{2/2}$ ductile extrusion of the 'Orobic fold nappe' and wrenching parallel to strike of the structure (Cooling by uplift through the window of 350 °C).*

e. *320-290 Ma: $D_{2/2}$ ductile brittle to brittle collapse and -wrenching, highest exhumation rate and strongest erosion.*

f. *~287-259 Ma: Exhumation of 'Orobic fold nappe' and development of the 'Orobic Collio basin'.*

the root-zone (Feijth, in prep.a, b) (Fig. 10d). The structure would have developed from a gravitationally instable structure, formed by dehydration melting-related bouyancy (Feijth & Franz, in prep.) and extrusion by superposed tectonic shortening (Fig. 10a), and soon in this stage gravitational collapse and spreading could start playing a role in deformation. This dehydration melting (with positive $\triangle V_{melting}$) has been identified in lithologic varieties (a) and (b), as shown above and in Feijth & Franz (in prep.). In fact this sequence of development implies structuration directly related to horizontal convergence and crustal thickening with collapse starting syn-convergent.

According to the model of Aerden (1998) and Aerden & Malavieille (1999) gravitational nappes spread outwards from the orogenic belt over a cooler relatively undeformed footwall, a configuration also envisaged for the Orobic complex. The parautochton below the 'Orobic fold nappe' may extend to external zones of the Orogenic belt. Near the 'Orobic fold nappe' it was intruded by the relatively undeformed Val Biandino intrusive granodiorite-complex. This occurred at Eo-Variscan times (307-271 ± 9Ma) (De Capitani et al., 1988) and according to geobarometric results (Feijth & Franz, in prep.) at depths of <5 km. The biotite cooling ages of 291 (± 6) and 292 (± 9) Ma for samples from Campo (Bocchio et al., 1981) and Bema/Fumasi (Mottana et al., 1985) respectively provide an indication for the effectivity of the exhumation processes during the late stages of $D_{2/2}$, immediately preceding the formation of a molasse basin containing the 'Conglomerato Basale' and the superposed 'Collio Orobico basin'. Particularly the NE-dipping transtensional shear-zones that crosscut the 'Orobic fold nappe' must have contributed much in this process of exhumation.

This $D_{2/2}$-phase is correlative in age with the 'Schlingen-phase' in the 'Strona Ceneri Zone' of Zurbriggen (1997, 1998). Zurbriggen (1997) however interpreted that Schlingen folding was accompanied by prograde metamorphism. Boriana & Villa (1997) dated the 'Schlingen phase' at 290 Ma. Boriani & Giobbi Origoni (1992) have interpreted the origin of the Schlingen-folds as related to drag-folding along the 'Cossato-Mergozzo-Brisago line', which implies a considerable lateral component and could also have been transmitted along the precursor of the 'Tonale line', the rootzone of the 'Orobic fold nappe'.

  The 'Scisti di Edolo', which make up the 'suprastructure', lack an imprint of the main Variscan high pressure event and also the ductile $D_{2/2}$ dehydration melting-, extrusion- and collapse-related deformation identified in the 'infrastructure'. The pre-Alpine greenschist metamorphic grade (chlorite, biotite ± garnet) (Gansser & Pantić, 1988; Feijth & Franz, in prep.) of the 'Scisti di Edolo' and greenschist-facies bedding-plane parallel shearing structures at the base of the 'Scisti di Edolo' differ clearly from the structural and metamorphic development of all sequences of the 'infrastructure' and might be related to one single tectono-metamorphic event.

The fabric of the 'Scisti di Edolo' indicates intense bedding-parallel shear, together with the lower metamorphic grade suggesting that the 'Scisti di Edolo' represent metamorphic rocks of a hanging-wall sequence of a thin-skinned thrust-system, that during activity of a drop-fault along the northern margin of the rootzone of the 'Orobic fold nappe' became juxtaposed to the higher grade substructure (Fig. 10d, e). In contrast Gansser & Pantić (1988) reported grading from 'Gneiss di Morbegno' to 'Scisti di Edolo', but based on the differing metamorphic evolution and other structural development a tectonic contact inbetween, as suggested above, is more probable. More data from the Southern- and Austroalpine Alps need

to be acquired to solve these relationships regionally. At the base of the 'Thurntal quartzphyllites', which are equivalent to the 'Scisti di Edolo' and are exposed in the Austroalpine, a situation similar to the configuration in the Val Cortena at the basal contact of the 'Scisti di Edolo', has been observed. The 'Thurntal quartzphyllites', that reached only low pressures (Sassi, 1972; Sassi & Spiess, 1992; Giudotti & Sassi, 1986), overly higher grade, kyanite, staurolite and sillimanite-bearing paragneisses and micaschists. The contact is tectonic, as pointed out by Sassi & Zanferrari (1972) and emphasised by Heinisch & Schmidt (1976).

It seems most probable that the rocks of the 'Orobic fold nappe' have tectono-metamorphic, depositional and volcanic affinities to the Austroalpine basement, as suggested by the distribution of the 'Gneiss Chiari'whereas the 'Austroalpine quartzphyllites' correlate with the 'Scisti di Edolo'. Apart from lithological similarity the Variscan P-T-conditions and timing of the events indicate this equivalence. This suggests that both, the upper sequence of the 'Orobic fold nappe' and 'Scisti di Edolo' might have a common origin with Austroalpine units and might have been deposited in the same backarc basin as the one suggested by Neubauer & Frisch (1988), Neubauer & Sassi (1993) and Loeschke & Heinisch (1993) and are related to the 'Sardic' event of Handy et al. (1999).

The origin of the parautochton remains unclear, but a hypothesis, based on few data is proposed. No lithologies that can be correlated with certainty with the Orobic nappe and the suprastructure were found in this unit but the ages of few detrital micas from the basal conglomerates as well as from the basal series of the 'upper sedimentary unit' of the 'Collio Orobico formation', which single grain total fusion ages are 338,1 ± 5,7, 341,7 ± 8,4 and 350,6 ± 5,4 Ma (Feijth & Neubauer, in prep. a) indicate a possible solution for this problem. These ages indicate an uplift or cooling phase around the Devonian-Carboniferous boundary and the grains that supplied these ages are certainly not derived from the 'Orobic fold nappe'.

That the Devonian-Early Carboniferous detrital white micas were sourced by the 'Scisti di Edolo' is unlikely as well because cooling ages of equivalent rocks, the Austroalpine 'quartzphyllites' are much younger. Previously unpublished K/Ar cooling ages of muscovite from the 'quartzphyllites' of the Austroalpine Kreuzeck mountains of ca. 300 (+320?) Ma obtained by Brewer were published by Hoke (1990). A unit of the same depositional and tectonic origin as the 'Brixen- and Agordo quartzphyllite complexes' could be a possible source, because isotopic ages from the 'Brixen quartzphyllite complex', a Rb-Sr muscovite-garnet-WR isochron of 354 ± 10 Ma (Del Moro et al., 1980), and from the 'Agordo quartzphyllite complex', a Rb-Sr WR isochron of 347 ± 17 Ma (Cavazzini et al., 1991) falls in the same range as the oldest white micas of the 'Collio Orobico formation' and the 'Conglomerato Basale'. A more convincing argument for the parautochton as source unit, might be that muscovite from the basement below the 'Collio Trumplino basin', with an equivalent structural position, has cooling ages of 364-340 Ma (Mottana, shown in Martin et al. (1996). The 'Brixen quartzphyllite complex' was also overprinted by the younger Variscan Phase dated at 321 ± 1 Ma (Rb-Sr biotite-Kfs-WR isochron) (Del Moro et al., 1984), 319 ± 5,5 (Ar-Ar muscovite), 316 ± 8 Ma (K-Ar muscovite) and 314 ± 5 Ma (Rb-Sr muscovite and Rb-Sr biotite) (Hammerschmidt & Stöckhert, 1987). Biostratigraphic data, only available for the 'Agordo phyllites', where acritarch assemblages refer to deposition between Late Cambrian to Early Tremadocian (Sassi et al., 1995), indicate a unit which protoliths are older

than the age of deposition of lithologies of the Orobic fold, the Austroalpine 'quartzphyllites' and 'Scisti di Edolo'. The 'Agordo phyllites', and very likely also the parautochton, could be jointly Gondwana-derived. In fact all pre-Silurian/Devonian units of the Southalpine basement and Austroalpine that belong to the 'Noric-Bosnian terrane' can be considered as Gondwana-derived, but in contrast to units that docked at the north Gondwana margin before opening of the Orodovician-Silurian backarc, the parautochton, the 'Agordo phyllites' and 'Brixen quartzphyllites' might have been part of Gondwana before the 'Sardic phase'.

Chapter 2

P-T Conditions of Variscan and Mesozoic phases in the Orobic chain (Southern Alps, Italy)

Abstract

Metamorphic conditions of the Variscan phase that affected the Orobic basement were determined by petrographic study and thermobarometry. Peak temperatures of 750 °C occurred at 330-320 Ma, indicated by monazite-xenotime-thermometry in combination with U-Th-Pb-isotopic dating with monazite. At this time fluid-absent/deficient dehydration melting of the hydrous phases white mica and biotite occurred. Related metamorphic assemblages, -fabrics and -structures related to this phase are particularly abundant in metagrauwackes exposed in the rootzone of the 'Orobic fold nappe'. The phengite barometer (Massone & Schreyer, 1987) indicates a peak pressure of $\leq$ 1.3 Gpa. Related bulk volume increase, and thus density decrease, would have triggered the buoyant rise of a diapiric ridge, a precursor of the 'Orobic fold nappe', which further structuration occurred by superposed, chronologically partly overlapping tectonic strain. Freezing-in occurred after incomplete dehydration melting of the phyllosilicates, before significant segregation and separation of melt beyond micro- to mesoscale could take place in the bulk of the exposed lithologies. The garnet-staurolite-thermometer was applied on staurolite with garnet-inclusions of garnet-staurolite-white mica schists. Combined with the garnet-plagioclase-muscovite-quartz and garnet-plagioclase-Al_2SiO_5-quartz barometers this resulted in early-retrogressive conditions of 675 °C ± 20 at 1.0 GPa ± 0.05, conditions in a clockwise P-T path close to the position of the retrograde reaction garnet + biotite + kyanite $\longrightarrow$ staurolite, which has formed conspicious staurolite with garnet-inclusions. Later retrogressive development, with a concentration of results at 600 °C at around 1.0 Gpa, was constrained by various geothermobarometric methods, like combinations of garnet-biotite, garnet-phengite and muscovite-biotite thermometers combined with various calibrations of the garnet-plagioclase-biotite-quartz, garnet-plagioclase-muscovite-quartz and garnet-plagioclase-muscovite-biotite-quartz barometers. P- and T dependent clinozoisite phase-relationships in a pegmatite vein that formed immediately after peak conditions indicate very similar conditions. The garnet-hornblende and amphibole-plagioclase thermometers in combination with the Al-in hornblende and garnet-plagioclase-hornblende-quartz barometers were applied on metabasites, particularly of the pre-Variscan sequence of the 'Orobic fold nappe', that has a metamorphic overprint of the Ordovician 'Sardic phase'. This resulted in various other points on the Variscan retrograde P-T-path. Due to the metamorphic overprint of the 'Sardic phase' at least the rocks of the lower sequence must have been H_2O-poor or H_2O-absent at peak-Variscan metamorphism. This would explain the relative rarity of melt and migmatites. Conditions were thus close to the granulite and eclogite facies, but according to lacking typical eclogite facies assemblages and the limited degree of dehydration melting, conditions could not have been much higher. Monazite-xenotime and two feldspar thermometry revealed a hydrothermal overprint between 320 and 350 °C, related to Mesozoic magmatism and rifting of the Lombardian basin.

1 Introduction

The Southern Alps are very well suited for studies of Palaeozoic tectono-metamorphic development, because the Alpine metamorphic overprint of the well-exposed early Palaeozoic to Permian rocks is relatively weak. Also intense Mesozoic overprint doesn't play an important role in the part of the Southern Alps selected for this purpose, the 'Orobic chain' (Fig. 1a, c). Diella et al. (1992) stresses the difference of metamorphic development between the 'Lario basement', near the eastern shores of the 'Lago di Como', and the 'Val Vedello basement' of the central Orobic Alps. The 'Lario basement' has been affected by LP/HT metamorphism related to Tethyan rifting, in the 'Val Vedello basement' Pre-Permian phases prevail.

The recent discovery of two tectonic units, consisting of sequences with different tectonic and metamorphic development, within the 'Orobic fold nappe' (Feijth, in prep. a.) enabled the distinction of two Palaeozoic tectono-metamorphic phases, the Ordovician 'Sardic' (D_1/M_1) and the Variscan (D_2/M_2). The identification of the structural and metamorphic imprint of each of the two Palaeozoic structural and tectonic phases forms an important part of this analysis and is essential for a proper geothermobarometric analysis. How both phases can be distinguished in the field and in thin section is presented in more detail in Feijth (in prep.a). When Diella et al. (1992) and Spalla et al. (1999) presented their thermobarometric data of the Orobic basement, the 'Orobic fold nappe' and its newly identified sequences were not known yet. Because Spalla et al. (1999) studied an area where only the lower sequence of the 'Orobic fold nappe' is exposed their thermobarometric evaluation is based on analyses from lithologies that were affected by both Palaeozoic phases. Spalla et al. (1999) attributed structures and metamorphic imprint of both Palaeozoic phases to the Variscan orogeny, in contrast to the evolution proposed by Feijth (in prep. a). Diella et al. (1992) and Spalla et al. (1999) calculated significantly lower P and T than the conditions presented in this paper, possibly having used M_1-relics.

Because of these favourable conditions the Variscan P- and T-development of the Orobic basement could be revealed, supporting a recent model of Variscan structural development of Feijth (in prep. a, b, c). As this study shows, fluid-absent and -deficient (dehydration) melting reactions of phyllosilicates at high grade metamorphic conditions are capable of changing rheological conditions, rock density and structure dramatically, triggering a chain of events that initiated retrogression. A connection between peak metamorphic conditions and development of the recently identified 'Orobic fold nappe' (Feijth, in prep. a, b, c) is suggested. Initial stages of dehydration melting were attained in some lithologies of this recumbent fold nappe during the initial stages of nappe-folding and possibly only for a short time interval, during which segregation of the melts did not yet occur beyond micro- to mesoscopic scale.

Timing of the formation of the 'Orobic fold nappe' is constrained by $^{40}Ar/^{39}Ar$ isotopic dating on muscovite and biotite and U-Th-Pb on monazite by EMP (Feijth et al., in prep.). It was formed at ~330-320 Ma during the Variscan phase (M_2), preceding the formation of the Permian 'Orobic Collio basin'.

Due to the strong Variscan imprint only few aspects of the pre-Variscan metamorphism could be revealed by the study presented here. The presented interpretation of P-T development is based on field-data, phase-petrographic study, combined with microtectonic analysis and

Fig. 1. a. Location of the investigation area in the Orobic Alps. b. Simplified geological map of the Orobic Alps showing only the main Alpine structures c. Overview of the investigated area of the Orobic Alps. The main Variscan-Permian structures are shown. The sample locations of the samples used for geothermobarometry are indicated with their sample numbers.

thermobarometry. The structural and kinematic development of the 'Orobic fold nappe' is discussed in detail in Feijth (in prep. b, c).

A Mesozoic phase, although weaker than in the 'Lario basement', was clearly identified in some thermobarometric and isotopic age-data from the selected area. Thermobarometric aspects of this hydrothermal event are also discussed.

2 Geological setting, structural configuration, and post-Variscan overprint

The Orobic basement is located in the Alpine thrust belt of the Italian Southern Alps, and has a complex multiphase development. The location and extent of the study area are shown in Fig. 1a and 1c and a schematic north-south cross section with the main Variscan units is displayed in Fig. 2. The Orobic Palaeozoic basement is mainly exposed in the northern part of the area, in the Valtellina, a major Alpine Valley of the Lombardian Southern Alps. The Orobic drainage-divide is the border with the Bergamasc valleys 'Valle Brembana' and 'Valle Seriana' to the south, where the Permian 'Orobic Collio basin' is situated. The 'Tonale fault', a segment of the 'Periadriatic lineament', separates the Austroalpine and Penninic realms of the Central Alps of Alpine greenschist to amphibolite facies grade from the E-W striking Orobic basement with a completely different Alpine metamorphic development. Although the Palaeozoic structures and metamorphic assemblages are overprinted by younger Mesozoic and Alpine phases in the Orobic Alps, the Palaeozoic metamorphic relationships and structures are still quite well-preserved.

Alpine metamorphic overprint of lowermost grade accompanied shortening (Roeder, 1985, 1989, 1992; Schönborn, 1990, 1992; Schönborn & Schumacher, 1994; Carminati et al. ,1997; Carminati & Siletto, 1997) (Fig. 1b). Bocchio et al. (1981), Diella et al. (1992) and Spalla et al., (1999) recognised retrograde Alpone mineral reactions like chloritisation of biotite and sercitisation of chlorite whilst Crespi et al. (1981, 1982) observed stilpnomelane replacing chlorite, a replacement of primary biotite. Both latter types of recrystallisation occurred along Alpine faults at both sides of the Valtellina. In the Orobic basement chlorite, white mica and stilpnomelane grew on alpine cleavage and in Alpine veins (Carminati, 1992, Carminati et al., 1997; Albini et al., 1994).

Illite "crystallinity" was measured on phyllosilicates of pelites of the 'Collio'- (Keller, 1986), (Riklin, 1983), 'Servino'- (Schönborn, 1986) and 'Prezzo' (Keller, 1986) formations. All these data indicate anchimetamorphic conditions with temperatures between 200°C and 300°C and it can be concluded that in the selected area there is no problem to distinguish Alpine tectonic and metamorphic structures from dominantly higher-grade pre-Mesozoic events. Solution transfer- and crystallisation processes, related to the activity of the Orobic thrust, were dated by the $^{40}Ar/^{39}Ar$-method on detrital white mica from the Collio Orobico basin at ~40 Ma (Feijth & Neubauer, in prep.).

Between the Permian and Jurassic rifting has left a strong HT overprint with growth of sillimanite only in the footwall of the 'Lugano-Val Grande rift-fault', the 'Dervio-Olgiasca zone' (Bernoulli et al., 1990; Diella et al., 1992; Bertotti et al., 1993, 1999; Siletto et al., 1993; 1999; Gosso et al., 1997). In the 'Dervio-Olgiasca zone' pre-Westphalian metamorphic relics and structures were, at least partially, obliterated by this phase of formation of the Lombardian basin. The tectono-metamorphic evolution of the 'Monte Muggio zone', the hanging wall of the 'Lugano-Val Grande fault', shows the typical Orobic evolution with two
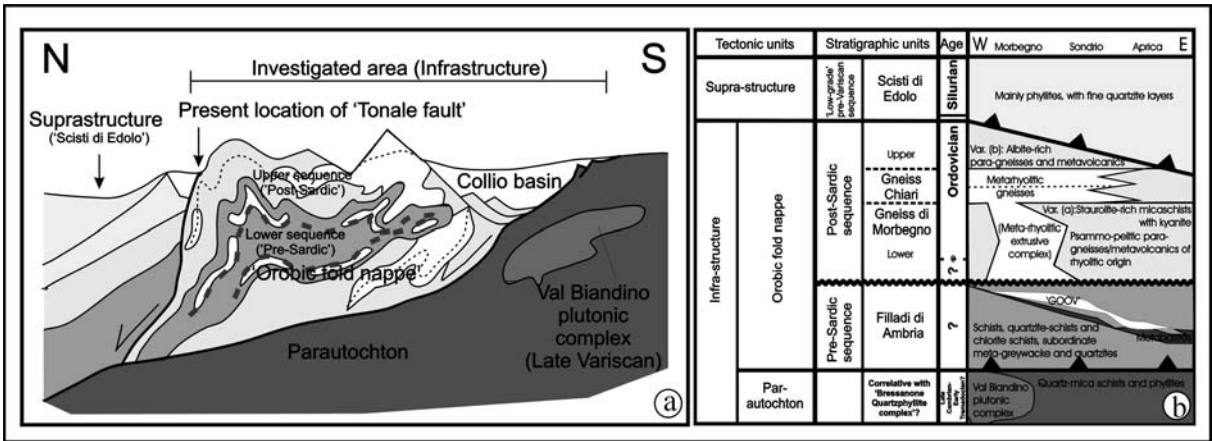
Fig. 2.
a. *Schematic N-S cross-section showing the Variscan-Permian structural configuration of the investigated area.*
b. *Schematic overview of the stratigraphy of the Orobic basement.*

Palaeozoic orogenic phases (Mottana et al., 1985; Siletto et al., 1993). The 'Dervio-Olgiasca zone' and the 'Monte Muggio zone' together form the westernmost extension of the Orobic basement that was not investigated in this study.

In spite of reactivation of the main Variscan faults as thrusts, the Variscan-Permian structure (Fig. 2) is largely preserved. Its infrastructure consists of the 'Orobic fold nappe', exposed mainly N of the Orobic waterdivide, and an underlying parautochton. The 'Orobic fold nappe' developed initially by buoyancy and tectonic extrusion into a diapiric ridge that spread gravitationally over the parautochton (Feijth, in prep. a, b, c). The lower-grade sequence of 'Scisti di Edolo', overlying and juxtaposed trough a fault contact, makes up the 'suprastructure'.

The Permian 'Collio-Orobico formation' and the 'Ponteranica formation', overlying mainly the parautochton, are exposed in the weakly developed deca-kilometric scale 'Orobic'-, 'Trabuchello(-Cabianca)'- and 'Cedegolo anticlines' (de Sitter, 1963) (Fig. 1b). The former two of these anticlines are exposed in the area of investigation. These structures, formed by Alpine basin inversion, are located between the Orobic basement in the north and a thrust belt, consisting of mainly Mesozoic carbonates in the south. The parautochton is visible in inliers in the 'Orobic'- and 'Trabuchello(-Cabianca)'anticlines. The Orobic basement that is exposed north of the Orobic waterdivide, the 'Orobic fold nappe', is separated from the Permian basins and their underlying basement by the Alpine south-verging Orobic thrust (Fig. 1b). The Alpine 'Porcile fault' can be found along the core of this fold nappe (more details in Feijth, in prep. a).

3 The basement sequences and lithologies

The Orobic basement consists of several meta-clastic sequences, which protoliths were deposited at different times in various tectonic settings (Feijth, in prep. a; Feijth, et al., in prep.). A schematic sketch of the stratigraphy is shown with the structural profile in Fig. 2. The individual successions can shortly be characterised as follows:

(1) Lower sequence of the 'Orobic fold nappe':
The 'Filladi di Ambria' consist of cm- to dm-scale layered schists, quartzitic-schists and chlorite-schists with subordinate meta-greywacke and quartzites. The equivalent 'Scisti dei Laghi sequence' in the 'Strona Ceneri Zone' is a possible western continuation of this stratigraphic unit (Feijth, in prep. a). It also includes a horizon of metabasites, the 'Strona Ceneri Border Zone' (SCBZ) (Boriani & Giobbi Origoni, 1992).
Metabasites are exposed in the 'Filladi di Ambria' as a thin discontinuous horizon with lenses of several metres to 200m thickness. These rocks have been grouped in two major classes (Feijth, in prep. a):
(1) Up to 200 m thick sequences with foliated (epidote-)amphibole-schists, locally with some garnet, and 'garbenschiefer'-varieties which might represent volcanic rocks.
(2) Up to 3 m thick sills of fine-grained euhedral magmatic amphibole in a bimodal size-distribution, in a matrix of symplectitic plagioclase and epidote. The lower parts of these sills locally contain subangular to rounded, occasionally angular, meta-gabbroic, meta-amphibolite and ultramafic xenoliths of up to ~l dm size, which are only clast-supported at the base, suggesting gravitative settling. These xenoliths are derived from a previously deformed and metamorphosed basement.
At the stratigraphic level of the metabasites there are mainly sills and some stocks of granodioritic augengneisses, called 'Gneiss Occhiadini Orobico-Valtellinese' ('GOOV') (Feijth, in prep. a). These slightly peraluminious and subalkaline igneous rocks correlate in age with the Ordovician granodiorites of the Strona Ceneri zone (Feijth, in prep. a), occurring in equivalent host rocks and with similar structural, igneous and petrographic relationships.
The relative ages of metamorphic-, folding- and igneous events that affected the lower sequence are well-constrained: (1) Metamorphism and ductile folding at mesoscopic to 10 m scale should have preceded the igneous phase of 'GOOV'-intrusion, because the 'GOOV' are not affected by the oldest metamorphic- and folding phase and the igneous bodies locally cut the foliation and the folded layering of the host rock. (2) According to relationships discussed in Feijth (in prep. a) garnets in and around the 'GOOV' grew during the second metamorphic phase during which a foliation overprinted the 'GOOV'. This second phase jointly affected the lower sequence and the upper sequence of the 'Orobic fold nappe' obviously following igneous emplacement of the granitoid protoliths of the 'GOOV'. In amphibole-bearing 'Filladi di Ambria' a few metres from the metabasites, there are thin amphibole-, clinozoisite-, plagioclase-, biotite-, quartz- and garnet-bearing pegmatite veins (Fig. 3a, b). Melting-related fabrics, like leucosome, either as discontinuous lenses or concentrated in boudins (Fig. 3c) have been identified in several parts of the 'Filladi di Ambria'.
(2) Upper sequence of the 'Orobic fold nappe':
Psammo-pelitic paragneisses and rhyolitic meta-volcanics, the 'Gneiss di Morbegno' and the 'Gneiss Chiari del Corno Stella', in the following just called 'Gneiss Chiari', overly the lower sequence. The boundary between both sequences is generally developed as a ductile shearzone and locally as Alpine thrusts, most likely along an older unconformity. Particularly the garnet-mica schists at the base of the 'Gneiss di Morbegno' are strongly sheared parallel to the layering. This basal contact with syntectonic prograde garnets is discussed in the next section.
The upper sequence of the 'Orobic fold nappe' was deposited on a metamorphosed lower
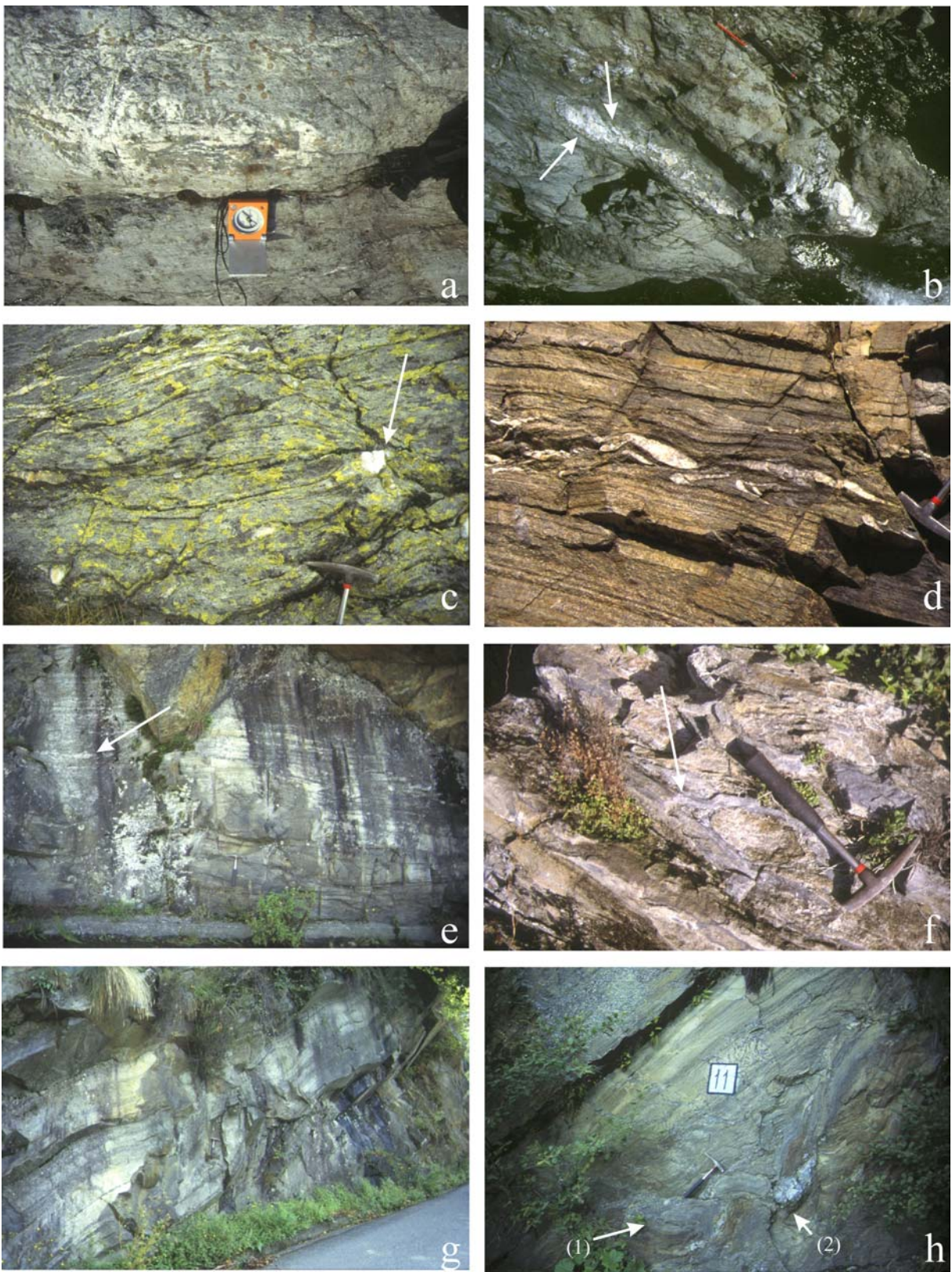
Fig. 3. Melting-related field-relationships and structures:

a. Metabasite-derived pegmatite vein, in amphibole-bearing 'Filladi di Ambria', in a transition zone toward the metabasites. The surface of the outcrop coincides with the orientation of the vein. Location: 'Fienili Arale' in 'Val Tartano'.

b. Metabasite-derived pegmatite-vein along metabasite-sills of the lower sequence. Arrows point to garnets along the boundary of the vein. Pencil and hammer are on a sill-boundary. Location: 'Fienili Arale' in 'Val Tartano'.

c. Leucosome in boudin in the Filladi di Ambria of the upper 'Valle di Bomino'. Some discontinuous (lensoid) leucosome is visible at the top left of the photograph. Leucosomes are generally quite rare in the study area.

d. 'Gneiss di Morbegno' of 'lithological variety (b) with abundant albite-porphyroblasts, which concentration and abundance varies according to layering. Leucosome is also present. Photograph from behind Rifugio Fratelli Longo.

e. Layering-parallel leucosomes in lithological variety (b) (best visible at arrow). Photograph from along the road to Campo (Val Tartano).

f. Melt veins cutting primary layering (arrow) and partly parallel to this layering in an outcrop above Sirta within lithological variety (b).

g. Melt-related pinch- and swell structures, caused by compositional and deformational anisotropy during the dehydration melting-phase. Lithologies above and below the extended layer, with a more favourable composition for the muscovite- and biotite-melting to occur and/or with a higher a_{H2O}, have undergone a positive dilatation, causing extension, pinch and swell structures and boudinage in the enclosed layers. Outcrop along the road to Campo (Val Tartano).

h. Composite structures related to melting and certainly not purely of tectonic origin. A tectonic origin can be excluded because extension and contraction of individual layers in similar directions occurred almost simultaneously and intermittently. Formation of these structures during the phase of dehydration melting (at peak P and T) is obvious. These extension and compression are due to varying dilation from one layer to the other, each having extended to other degrees and at different moments during the (M_2) melting event and having affected the surrounding layers. The variation in degree and time of melting of the individual layers is related to varying composition and a_{H2O} of the individual layers. Note the layer indicated with arrow (1), which was at first boudinaged and compressed in a later stage of the melting-event. This resulted in overlapping boudins. Arrow (2) points to a pod of leucosome.

sequence. The 'Gneiss di Morbegno' and 'Gneiss Chiari' belong to a meta-volcano-sedimentary system of which the 'Gneiss Chiari' forms massive rhyolitic complexes locally originally at least 1000 m thick. Thickness of the metarhyolites decreases distally within these complexes. The sheets of 'Gneiss Chiari' meta-rhyolite are situated within meta-volcano-sedimentary rocks of the 'Gneiss di Morbegno' with commonly rust-brown colours, related to Fe-oxidation by weathering. A good example is the 'Monte Cadelle meta-rhyolitic complex'. 'Gneiss Chiari' of this complex directly overlies the lower sequence and is in close proximity to the 'GOOV'.

These massive homogeneous leucocratic coarse-grained 'Gneiss Chiari' have a granoblastic

and rarely flaser texture with typical large K-feldspar porphyroblasts. The main macroscopically recognisable constituents are: quartz, K-feldspar, muscovite and minor albite. Variability is mainly due to a more or less porphyritic structure and to different content of phyllosilicates. Original deposition-related layering of centimetres to metres scale is locally well visible and the transition to the 'Gneiss di Morbegno' is gradual at many locations. Locally enclaves of 'Gneiss di Morbegno', usually parallel to the main foliation, have been found in the 'Gneiss Chiari'. Stronger foliated and finer grained varieties, with more chlorite, biotite and some garnet, can be observed. The main foliation is formed by thin muscovite layers, with or without chlorite that curve around layers and lenses of quartz and granoblastic feldspars. This main foliation transposes primary layering, alike in the 'Gneiss di Morbegno' below and on top. The main foliation in the 'Gneiss di Morbegno' is continuous across the boundary to the 'Gneiss Chiari'. Subordinately quartz-enriched lithotypes occur, as well as zones with more or less mylonitic structures and there are some possible relic cylindrical vents with varieties of 'Gneiss Chiari' with more mafic minerals, like amphibole. Deposition of the protoliths of the 'Gneiss Chiari' might be related to a phase of rhyolitic volcanism during which also the 'Upper Ordovician Rhyolitic Plateau' of Bellieni & Sassi (1981) and Sassi et al. (1984) was formed, which is coincident to porphyroids in the 'Eastern Greywacke Zone' in the eastern Austroalpine, (Feijth, in prep. a; Feijth et al, in prep.).

Among the other less distinctive psammo-pellitic rocks of the 'Gneiss di Morbegno' characteristic lithologic varieties (a) and (b) require particular attention because they play an important role in the thermobarometric evaluation, rheological behaviour and structural development.

Lithologic variety (a) are garnet-staurolite-white mica schists containing kyanite and occasionally tourmaline, occurring mainly immediately below 'Gneiss Chiari' or, where latter is absent, in the lower part of the 'Gneiss di Morbegno' succession.

The Al-poorer lithologic variety (b) was called 'Albitknotengneise' by Cornelius & Cornelius-Furlani (1930) and has a bulk chemistry of meta-greywackes. Albite-blasts are very characteristic and abundant in these psammo-pelitic gneisses (Fig. 3d) and are often surrounded by relatively large biotite crystals. Garnet is common and occurs as inclusions in both albite and biotite. Metamorphic conditions were high enough to cause melting, but segregation of melt beyond microscopic- to mesoscopic scale occurred only very locally. Only at a few isolated locations in the 'Gneiss di Morbegno' clear leucosome was identified, mostly in discontinuous lensoid bedding-parallel leucosomes in lithologic variety (b) (Fig. 3d, e and h).

Melting-related deformation is very common in lithologic variety (b), particularly in the foothills of the Valtellina. This deformation has been identified as such, because approximately layering-parallel extension of some layers and compression of others in the same direction must have occurred simultaneously during a phase of melting. In outcrop there are various structures, particularly pinch and swell structures (Fig. 3g) and boudins and locally folds, which are related to compositional anisotropy, leading to different degrees of dilation of individual layers during the dehydration melting-phase. The enclosed layers might have had a higher a_{H2O}, hampering dehydration melting or possibly even causing fluid-present melting, which goes along with a volume decrease. This caused extension, pinch and swell structures and boudinage in the enclosed layers. Such field-structures, that are related to

different degrees of melting of individual layers, are shown in Fig. 3g and h. In case of rocks that underwent higher degrees of dehydration melting than their enclosing lithologies, the enclosed rocks were folded or deformed by other constrictional deformation (Fig. 3h). Well-developed migmatites are generally absent.

(3) The parautochton:

The parautochton consists of intensely sheared phyllitic schists and quartzites, with occasional garnet. This unit of lower grade is exposed in the inliers in the 'Orobic'- and 'Trabuchello'(- 'Cabianca') anticlines. Along the south-western border of the study area, in the 'Val Sassina', 'Val Biandino' and 'Val Stabina', stocks and laccoliths of Variscan syn-late tectonic tonalites, granites, quartz-diorites and gabbro-diorites of the 'Val Biandino plutonic complex' are present in this parautochton. They have large contact metamorphic aureoles, with sillimanite-, cordierite- and andalusite- bearing hornfelses and have conformable contacts to the folded bedding of the host rock, but also, especially at the apophyses discordant contacts (De Capitani et al., 1988).

(4) The 'suprastructure':

The 'supra structure' is characterised by finely laminated phyllites, micaschists and fine quartzitic layers of the 'Edolo micaschists'. Particularly at the base these lithologies are intensely sheared parallel to bedding, but the typical black cataclasites and pseudotachylytes, indicative of Alpine thrusting, are very scarce. Therefore an Alpine age of shearing seems unlikely (Feijth, in prep. a; Feijth et al., in prep.). Ductile folding is associated with this shear zone. The Silurian and subordinate Ordovician age of deposition has been determined with spores and acritarchs (Gansser & Pantić, 1988). The Alpine 'Tonale fault', part of the 'Periadriatic lineament', forms the upper boundary of this unit. Only phengite-barometry (Massone & Schreyer, 1987) was applied on this unit, and the dominant phyllitic appearance in the field and preservation of spores and acritarchs suggests relatively weak metamorphism compared to the underlying units, greenschist metamorphic grade according to Gansser & Pantić (1988) and Feijth (in prep.a).

4 Structure and Palaeozoic development

Metamorphic- and deformation phases related to the two identified Palaeozoic tectono-metamorphic events introduced above are indicated below as M_1 and D_1 and M_2 and D_2 respectively, with the prograde stage indicated as $M_{2/1}$ and $D_{2/1}$ respectively and the retrograde stages are $M_{2/2}$ and $D_{2/2}$.

Field-structures enabled identification of the Variscan 'Orobic fold nappe' with a root-zone (Fig. 2). This structure was originally formed by an elongate zone of diapirism and extrusion with vertical and horizontal components and gravitational spreading of the diapiric ridge over the parautochton (Feijth, in prep. a, b, c). This was accompanied by wrenching parallel to the root-zone, leading to a dextrally sheared nappe-structure, as it is exposed at present (Feijth, in prep. a, b, c).

5 Petrography and microstructural relations of the geothermobarometry-samples

Each of the sequences of the Orobic basement has a different structural and metamorphic development. The metamorphic- and age-relationships of the individual lithologies are discussed in Feijth (in prep. a.) where also a mineral-crystallisation-deformation diagram is

presented. Following petrographic overview concentrates on the structural and metamorphic relationships of the individual samples used for geothermobarometry. All locations from where the samples for thermobarometry were taken are illustrated in Fig. 1c. Table I gives an overview of these samples, with the sampling locations and their mineral-assemblages.

(1) Lower sequence of the 'Orobic fold nappe':
Metabasites:
Sample 34.2 is a garnet-amphibolite xenolith from the lavas or ash flow units of the metabasites. The sample consists of (Al-)tschermakite and some included grossular-rich almandine-garnet with pyrope. A photomicrograph of the matrix of a sill with another type of xenolith of ultramafic composition, consisting of relics of olivine and some spinel in a crystalline groundmass of serpentine and talc overgrown by some tremolite, is shown in Fig. 4a.

Sample 58.6b was taken from the meta-ashes and –tuffs. It is an amphibole- and epidote-amphibole-schist, consisting of amphibole, biotite and calcite in preferred orientation parallel to the main foliation in a matrix of plagioclase, some quartz, zoisite and epidote (no garnet). Compositional layering and parallel metamorphic fabric of the amphibole-schists is D_1-folded with axial planes parallel to general bedding orientation.

Filladi di Ambria:
Sample 40.9A is from the boundary of the pegmatite-vein shown in Fig. 3b. Garnets grew in the host rock along the contact with this and other similar veins. These contain aligned quartz inclusions. These inclusions are mutually related, because across the enclosing garnet their fabric with subgrains, undulous extinction and deformation lamellae, is continuous. Garnet is thus post-tectonic with respect to the included quartz-fabric and the related early overgrewn foliation. A younger deformation phase affected the coarse-crystalline quartz, plagioclase, usually alumino-tschermakite, tschermakite or magnesio-hornblende and zoisite of the vein surrounding the garnet. Garnet was deformed brittle. The coarse quartz outside the garnets was deformed by intense brittle-ductile shearing, leaving undulous crystals with deformation lamellae and quartz-filled fissures. The clinozoisite is crosscut by simple-shear-related microshearzones and cracks with are related to the sheared microstructure in the surrounding quartz and plagioclase. Along these fissures younger Fe-richer clinozoisite replaced the original clinozoisite (Fig. 4b). These tectonic microfabrics, as well as the chemical changes of zoisite, are related to phase of brittle-ductile deformation in the host rock of the vein, the D_2 simple shearing under retrograde P-T conditions.

'GOOV':
Samples 33.6, 33.6rand, 69.2aI, 32.4 and VdL are all from 'GOOV'. Generally the 'GOOV' contains quartz, often perthitic K-feldspar, biotite, plagioclase (0-17 % An), epidote, zoisite and most samples contain garnet $(Al_{58-69}Py_{3-7}Gr_{21-31}Sp_{2-12})$ (samples 33.6, 33.6rand, 69.2aI and 32.4). Apatite, zircon, tourmaline, rutile and opaques occur as accessory minerals. Zoisite and clinozoisite are occasionally abundant and monazite was not found. Biotite and white mica form the main foliation and the $D_{2/2}$-related shearplanes and C'-shearbands, which form an anastomosing conjugate cleavage around the K-feldspar σ-blasts, garnet, albite and quartz of the microlithons. Sample 69.2aI has a strong linear fabric related to $D_{2/2}$. Garnet and K-feldspar porphyroblasts thus obviously predate $D_{2/2}$-shearing. Quartz displays a granoblastic

Table I: Overview of all samples applied for geothermobarometry.

	Sample No.	Sample location	Coordinates (UTM)	Altitude (m)	Formation & position (if determinable)/Lithologal variety and lithological characteristics/Main mineral constituents
Filladi di Ambria	34.2	'Val Lunga', below 'Fienili Arale'	1554300-5103438	1451	Garnet-amphibolite clast or xenolith from amphibolite-sill in 'metabasites'/(Al-)tschermakite, garnet, plagioclase
	58.6b	'Upper Val Lunga' near 'Cima di Lemma' ('Val Tartano')	1554745-5101555	2200	'metabasites'/quartz, plagioclase, amphibole (tschermakite and hornblende), epidote, zoisite, rutile, titanite
	40.9A	'Upper Val Lunga' upstream from 'Fienili Arale' (='Cesure')	1555618-51029500	290	'Filladi di Ambria'/contact of pegmatite-vein with host rock/ quartz, plagioclase, Al-tschermakite, garnet, biotite, zoisite, clinozoisite, chlorite
GOOV	33.6	'Alpe Cul' ('Val Bitto di Albaredo')	1547801-5099717	1935	'GOOV', boundary zone/ quartz, plagioclase, K-feldspar, white mica, biotite, garnet, zoisite, epidote, carbonate, chlorite
	33.6 rand	'Alpe Cul' ('Val Bitto di Albaredo')	1547801-5099717	1935	'GOOV', boundary zone/ quartz, plagioclase, K-feldspar, white mica, biotite, garnet, zoisite, epidote, carbonate, chlorite
	69.2aI	'Upper Val Budria'	1550775-5102382	1592	'GOOV', boundary zone/ quartz, plagioclase, K-feldspar, white mica, biotite, epidote
	32.4	'Valle della Pietra' below 'Il Piazzo' ('Valle del Bitto di Gerola')	1540970-5099580	1985	'GOOV'/ quartz, plagioclase, K-feldspar, white mica, biotite, garnet, epidote, chlorite
	VdL	'Val dei Lupi' ('Val Tartano')	1556880-5101640	2058	'GOOV', close to boundary/ quartz, plagioclase, K-feldspar, white mica, biotite, chlorite
Gneiss di Morbegno	98.2-1/ 98.2-2	'Val Lunga', near 'San Antonio' ('Val Tartano')	1553552-5105233	1272	Basal 'Gneiss di Morbegno'/intensely sheared/ quartz, plagioclase, muscovite, garnet, biotite, zoisite, Mg-chlorite, staurolite, rutile, tourmaline
	65.5aI/ 65.5aII/ 65.5bI/ 65.5bIII	'Valle di Bomino'	1543600-5101819	1237	'Gneiss di Morbegno'/With well developed $D_{2/2}$ crenulation and lineation/ quartz, plagioclase, white mica, garnet, biotite, chlorite, tourmaline
	38.1/ 38.1-1°/ 38.1-3a	Between ‚Albaredo' and 'Passo di San Marco' ('Valle del Bitto di Albaredo')	1547855-5105510	1435	'Gneiss di Morbegno'/ quartz, plagioclase, white mica, garnet, (Al-)tschermakite, biotite, chlorite, rutile
	91.2aI	near 'Passo di Publino' ('Val del Livrio')	1563450-5100722	2132	'Gneiss di Morbegno'/Lithologic variety (a)/ quartz, plagioclase, white mica, garnet, staurolite (partly sericitised), biotite, chlorite
	31.7a2/ 31.7a5/ 31.7a2	Between 'Passo Salmurano' and 'Monte Valetto'	1545100-5096697	2148	'Gneiss di Morbegno'/Lithologic variety (a)/ quartz, plagioclase, white mica, kyanite, garnet, staurolite, biotite, chlorite
	48.10	'Foppa delle Uccelli' ('Val Madre')	1558277-5108765	1140	'Gneiss di Morbegno'/Lithologic variety (b)/ quartz, plagioclase , white mica, biotite, garnet, chlorite
	92.2	In 'Bema' ('Valle del Bitto')	1543650-5106325	805	'Gneiss di Morbegno'/Lithologic variety (b)/ quartz, plagioclase, white mica, garnet, biotite, chlorite
	94.2	Road to 'Campo', 'Crap del Mezzodi' ('Val Tartano')	1550111-5111503	620	'Gneiss di Morbegno'/Lithologic variety (b)/ quartz, plagioclase, white mica, garnet, biotite, chlorite
Gneiss Chiari	142.2	'Sirta' ('Valtellina')	1542350-5111850	290	'Gneiss Chiari'/rare amphibole- and biotite containing variety/ quartz, K-feldspar, plagioclase, amphibole, allanite, clinozoisite, biotite, white mica
	39.2	Near 'Passo dei Lupi' ('Val Madre')	1557801-5101815	2250	'Gneiss Chiari'/relatively coarse grained/ quartz, K-feldspar, plagioclase, white mica (incl. sericite), chlorite
	80.1	'Lago Pescegallo'	1545302-5098435	1866	'Gneiss Chiari'/ quartz, K-feldspar, plagioclase, muscovite (incl. sericite)
	82.13I	NE-flank of 'Pizzo Zerna' ('Val del Livrio')	1564302-5100110	2292	'Gneiss Chiari'/ quartz, K-feldspar, plagioclase, muscovite (incl. sericite)
	89.2II	Below 'Pizzo Rotondo' ('Val Brembo di Valleve')	1553755-5099940	1908	'Gneiss Chiari'/ quartz, K-feldspar, plagioclase, muscovite (incl. sericite)
	82.17	'Passo di Publino' ('Valle Sambuzza')	1563822-5099600	2260	'Gneiss Chiari'/ quartz, K-feldspar, plagioclase, muscovite (incl. sericite)
VB	71.5b	Between 'Torrente Troggia' and 'Mondoro' ('Val Sassina')	1536015-5094062	1120	'Val Biandino Plutonic Complex'/ quartz, plagioclase, biotite, orthopyroxene, clinopyroxene
SdE	SdE	Road to 'Galleno' ('Val Cortena')	1594750-5113425	980	'Scisti di Edolo'/ quartz, albite, sericitic white mica, biotite, garnet, chlorite
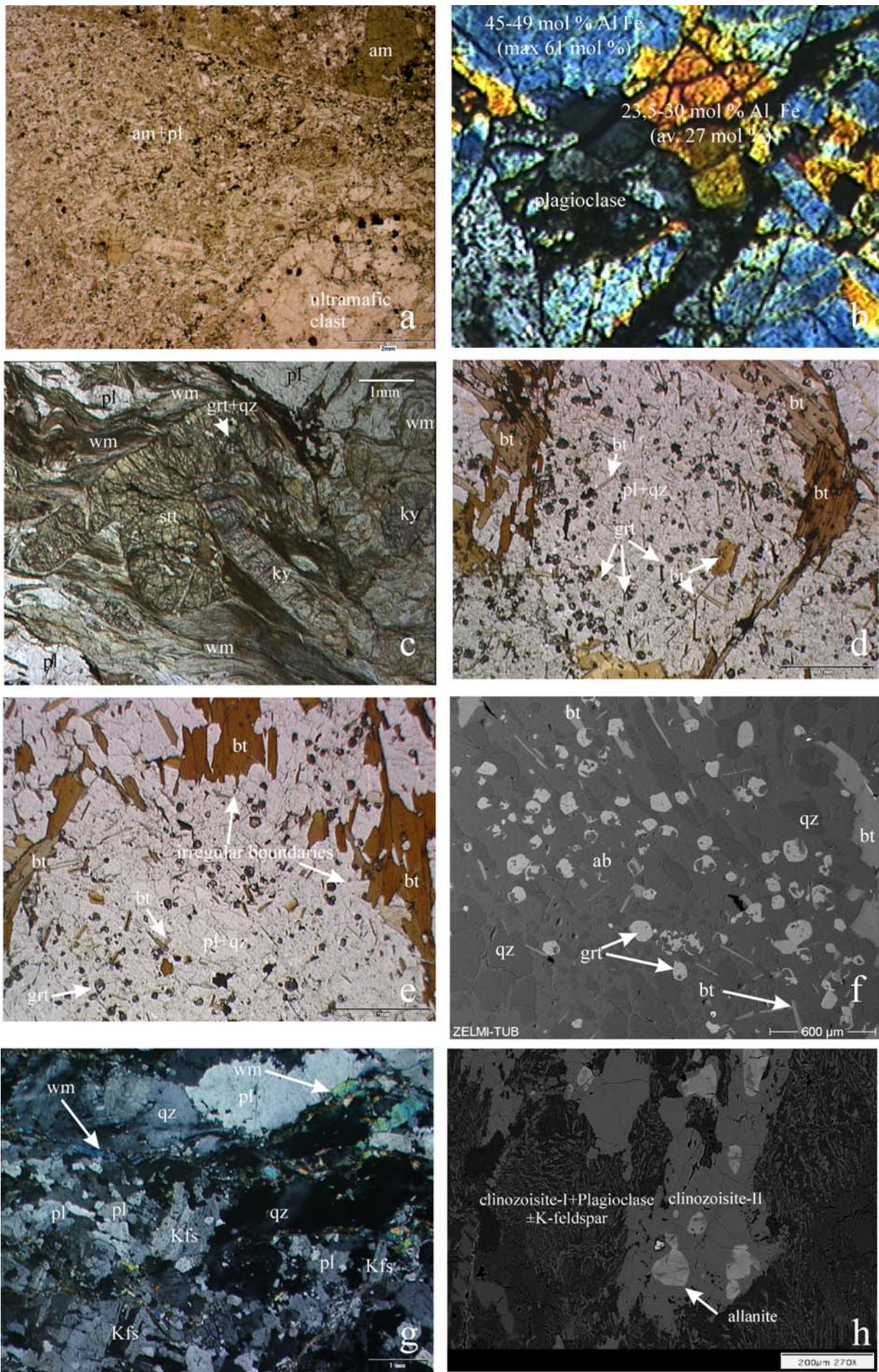
Fig. 4.

a. *Microphotograph of an amphibolite-sill with ultramafic clast or xenolith (sample 34.2). This xenolith consists of relics of olivine and some spinel in a crystalline groundmass of serpentine and talc overgrown by some tremolite. The large amphibole crystal in the top right corner, situated within the finer grained matrix, indicates a crystalline matrix. Plane polarised light.*

b. *Microphotograph of primary clinozoisite and young Fe-richer clinozoisite (yellow) and plagioclase in a pegmatite vein (sample 40.9A).*

c. *Sample 31.7a-3 of lithologic variety (a) with a staurolite-porphyroblast with small inclusions of garnet(+quartz). Kyanite is also present at the staurolite porphyroblast. This composite of porphyroblasts is a product of the reaction grt + bt + as ⟶ st, wherby biotite has reacted completely and garnet and kyanite are excess phases with respect to this reaction. Plane polarised light.*

d. *An albite-porphyroblast surrounded by biotite, typical of lithological variety (b). Porphyroblast includes fine garnet, quartz and biotite-laths. The regular, orthorhombic, orientation patterns of biotite and some white mica are notable. Plane polarised light. (Sample 92.2)*

e. *Lithological variety (b), sample 92.2, with typical albite-porphyroblast surrounded by biotite. In this photograph the irregular boundaries of the remnant biotite are pronounced. Otherwise the photograph shows a similar fabric as Fig. 4d and e. Plane polarised light.*

f. *REM-photograph of lithological variety (b), sample 92.2. Inclusions in garnet of quartz, plagioclase and biotite are well visible.*

g. *Microstructure of Gneiss Chiari (sample 39.2) with microshearzone along foliation plane with fine white mica. Undulous extinction is well developed in quartz along this microshearzone and some dynamic recrystallisation has occurred in some of the quartz grains, where subgrains started to form. Crossed polars.*

h. *Clinozoisite-plagioclase symplectites and older phases of allanite and clinzoisite in a variety of Gneiss Chiari of sample 142.2.*

interlobate structure, with subgrains along the bounding foliation shear planes. $D_{2/2}$-related dynamic recrystallisation was followed by static recovery, which caused euhedral subgrain-shapes. Locally quartz-lenses show crystal-preferred orientations. Biotite and garnet are occasionally replaced by chlorite, particularly in sample 32.4. Perthitic unmixing of K-feldspar indicates high temperatures followed by slow cooling after growth.

(2) Upper sequence of the 'Orobic fold nappe':

Gneiss di Morbegno lithologic variety (a):

The samples 31.7 and 91.2aI were taken from 'Gneiss di Morbegno' of litho-type (a). Sample 31.7 contains much muscovite, garnet, kyanite, staurolite, plagioclase-porphyroblasts and chlorite. Muscovite forms the transposed main foliation around kyanite and is separated by relatively weakly developed microlithons of plagioclase and K-feldspar. Staurolite, occasionally very abundant, has inclusions of almandine-garnet ($Al_{70}Py_{11}Gr_{15}Sp_4$) and is surrounded by muscovite and kyanite (Fig. 4c). Sample 91.2aI is rich in biotite, contains staurolite, but no kyanite. Garnet should represent a prograde Variscan relic. Kyanite is a later

phase and staurolite formed during early retrogression. Garnet- and kyanite-growth certainly predate the culmination of deformation, because the kyanite-porphyroblasts are $D_{2/2}$-folded (Fig. 9c in Feijth, in prep.a.). Quartz occurs as grain aggregates with seriate-interlobate and younger polygonal subgrains, indicating static recovery after dynamic recrystallisation. Undulous extinction and deformation lamellae are common. Kyanite and plagioclase are often sericitised, staurolite is occasionally replaced by sericite and chlorite whilst the garnet not included in staurolite is often replaced by chlorite during retrogression. Porphyroblastic albite (~20 mol % An) is an early-$M_{2/2}$ phase replacing microcline.

Gneiss di Morbegno lithologic variety (b) and other lithologies:

Samples 92.2 and 94.2 are from the rootzone of the 'Orobic fold nappe' and have the typical mineralogical composition and microfabric of lithologic variety (b). It is a lithology with a rather isotropic fabric with abundant albite-porphyroblasts, surrounded by relatively large biotite with irregular boundaries (Fig. 4d, e), as principal constituents. Numerous small garnets and biotite, latter oriented in oblique orthorhombic patterns within the albite, are very conspicuous (Fig. 4d, e). Muscovite crystals, oriented according to the same patterns as biotite, are small and relatively rare. The large albite-porphyroblasts also include blobs of quartz (Fig. 4d, e). All included garnet-crystals have inclusions of biotite, quartz and plagioclase (Fig. 4f). The inclusion patterns of phyllosilicate indicate that albite is a pseudomorphic replacement of possibly an anorthite and orthoclase-richer feldspar.

Samples 38.1, 48.10, 65.5 and 98.2 are also from the 'Gneiss di Morbegno'. Basically the mineralogical content of these samples is similar to lithologic variety (b), but a much more pronounced anisotropic and tectonic fabric is developed, particularly in sample 98.2, which is from the base of the upper sequence. Samples 48.10 and 65.5 have a strong linear and penetrative fabric. Sample 38.1 additionally includes some alumino-tschermakite that encloses garnet. Garnets crystals in these samples are generally larger than in samples 92.2 and 94.2 and not included in plagioclase, but plagioclase is common in their strain shadows.

Albite- and relatively large garnet-porphyroblasts of sample 98.2 contain older relics of sedimentary layering (S_i). The inclusion trails of fine opaques (Fig. 9a in Feijth, in prep. a) in the prograde garnet (zonation from core to boundary: $Al_{60}Py_3Gr_{25}Sp_{12}$ to ~$Al_{67}Py_{10}Gr_{21}Sp_2$) represent relics of sedimentary bedding. Growth of these garnets can only have occurred during the Variscan event. In the albite-porphyroblasts these layers of opaques indicate an original bedding which is parallel to the main foliation, formed by muscovite and biotite. This secondary foliation is deflected by the rigid garnet-porphyroblasts. The spiral shaped inclusion trails in the garnets indicate an up to 90° rotation with respect to the bedding plane and main foliation during their growth in when this zone accommodated bedding-parallel shear (Feijth, in prep. a).

In the investigated thin sections there are several modes of occurrence of monazite, with and without xenotime, providing information on the degree and mode of overprint. Fig. 5 shows some examples. In sample 31.7a-2 monazite occurs as relatively small and abundant homogeneous crystals with Variscan ages. The ratio monazite:xenotime is approximately 25:1 in this sample, where the homogeneous monazites (Fig. 5a) indicate that these are unaffected by younger overprint. Coexistence of these grains with xenotime of similar grainsize (Fig. 5b) suggest that thermobarometric results give peak-Variscan ages and temperatures. In samples 65.5 bI and 65.5 bIII monazite was found mainly as primary peak Variscan monazite with

allanite-epidote coronas (Fig. 5c, d), a replacement similarly described by Finger et al. (1998) indicating amphibolite-facies overprint of monazite. In this sample also primary monazite without coronas occurs. Overprint in sample 91.2a is indicated by relatively low values of X_Y. Generally the monazites in this sample are homogeneous, but some primary monazites have thin allanite and epidote seams along their boundaries (Fig. 5e).

Gneiss Chiari:

Quartz, orthoclase, large granoblastic microcline, albite-oligoclase and muscovite are the main constituents of the 'Gneiss Chiari' of samples 39.2, 80.1, 82.13I, 82.17, 89.2II and 142.2. The cleavage domains, a spaced foliation that is found anastomosing around K-feldspar and quartz, contains large muscovite, sericite, albitic plagioclase and chlorite (Fig. 4g). In a rare variety, from a possible vent, (142.2) also biotite and amphibole are present as well as plagioclase-clinozoisite symplectites (Fig. 4h). The microstructure of the 'Gneiss Chiari' shows a development similar to that of the 'GOOV': The grain size generally becomes finer towards these cleavage domains, where undulous extinction is more common, suggesting that these acted as micro-shear-zones. The outer zones of large quartz crystals consist of dominantly anhedral subgrains and deformation lamellae, indicating dynamic recrystallisation. Minor recovery by grain boundary area reduction is suggested in view of their slight modification towards polygonal crystal shapes. A primary compositional layering related to deposition (S_0) is locally well preserved, also close to the contacts with 'Gneiss di Morbegno' and is often visible in the field.

A slight schistose- or flaser character, concentrated in a spaced foliation of thin wavy cleavage domains, is formed by approximately 5 vol % muscovite and is often sheared parallel to foliation. Late brittle deformation is represented by brittle fractures in microlithons of quartz and K-feldspar. These are filled with sericite as well as galena and Fe-oxide. Occasionally tourmaline and chloritised garnet (sample 39.2) are present in the cleavage domains.

In Fig. 5f a monazite-grain of sample 82.13I is shown, which EMP-analyses of U, Th and Pb gave Mesozoic ages (Feijth et al., in prep.). This monazite has xenotime and apatite at its edges, which significance is discussed below. Monazite of samples 80.1 and 82.17 is homogeneous and lacks corona-structures.

Parautochton, Val Biandino plutonic complex:

Sample 71.5b, from the 'Val Biandino plutonic complex' is a quartzdiorite with granoblastic fabric, containing plagioclase, quartz, biotite, K-feldspar, usually ferri- and ferrian-magnesio-hornblende, orthopyroxene and occasionally clinopyroxene.

Scisti di Edolo:

At microscopic scale the sericitic phyllites of sample SdE have a mm-scale disjunctive cleavage parallel to the shear plane. Undulous quartz is very fine grained with moderately to well-developed preferred orientation. Fine albite is also present in the quartzitic microlithons. The cleavage domains are made up of sericitic white mica and the garnets have strain shadows with fine quartz. The presence of biotite and garnet indicates a metamorphism that exceeds Alpine conditions, next to the folded mylonite in hornblende-porphyritic dykes mentioned above, a second argument for pre-Alpine mylonite formation. Garnet is generally replaced by post-tectonic chlorite.
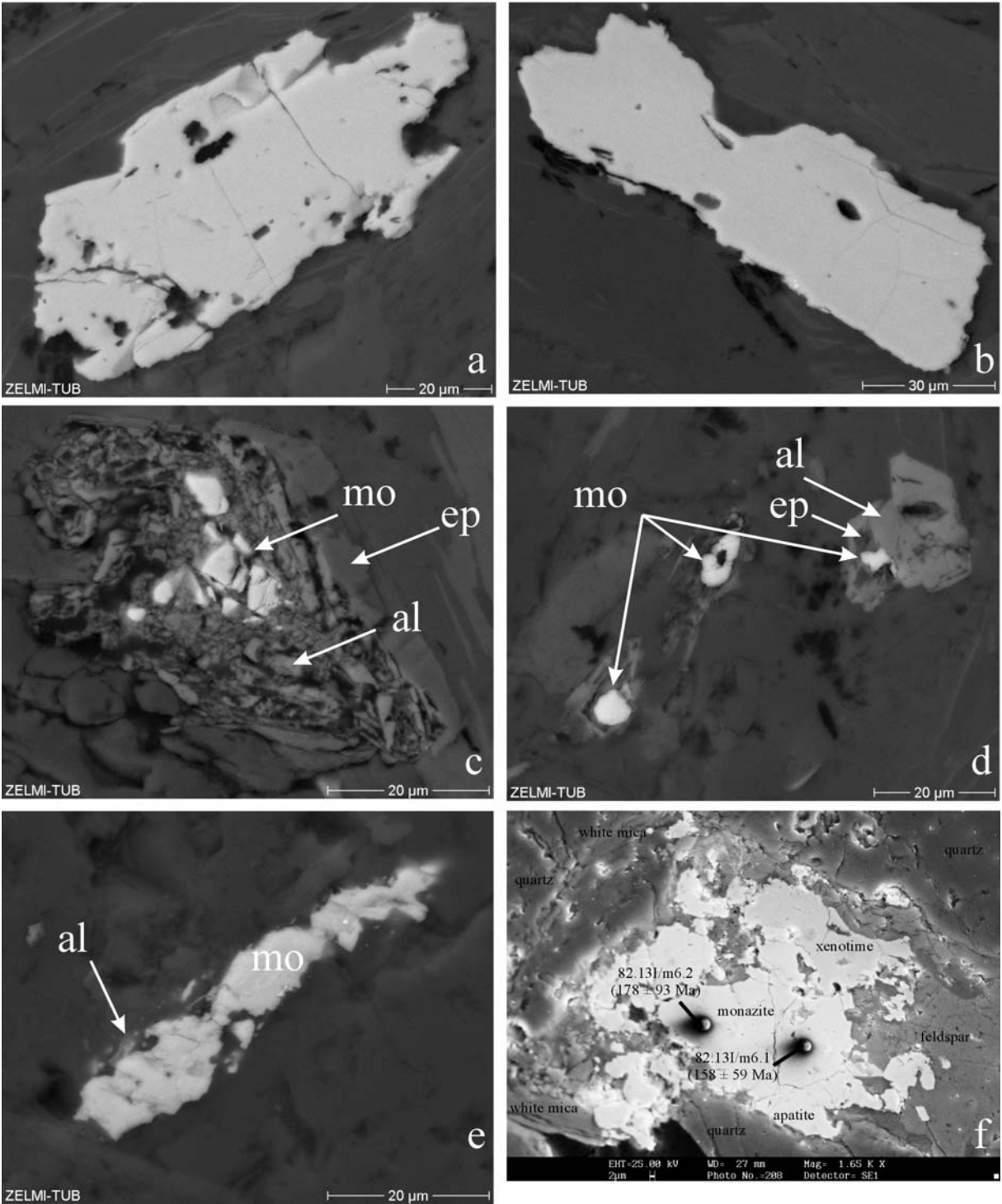
Fig. 5. REM-photographs of various habits of monazite and xenotime of the Orobic basement.
a. Homogeneous monazite from sample 31.7a-2.
b. Homogeneous xenotime from sample 31.7a-2.
c. Monazite of sample 65.5bIII with coronas of allanite and epidote, indicating amphibolite-facies overprint, accordig to the interpretation related to Variscan retrogression.
d. Three monazite-grains of sample 65.5bIII with coronas of allanite and epidote, indicating amphibolite-facies overprint, according to the interpretation related to retrogression.
e. A monazite-grain affected slightly by amphibolite-facies overprint (M_2-retrogression). Sample 91.2a.
f. Composite grain of monazite, xenotime and apatite (Sample 32.13I). The monazite was re-equilibrated during a Mesozoic hydrothermal phase, expelling Y, and producing xenotime at its boundary. The holes produced by microprobe analyses are visible. U-Th-Pb-ages of both analyses are indicated.

6 Mineral chemistry

Measurements on the selected minerals were carried out on a Jeol JXA-8800L microprobe equipped with four wavelength-dispersive spectrometers at the 'Institut für Mineralogie' of the 'Museum für Naturkunde', Humboldt Universität Berlin. The operating parameters were: 15 kV accelerating voltage, 15 nA beam current and a 3 μm wide beam. Calibration was against a set of standard natural minerals, and the ZAF correction procedure was applied.

Representative chemical compositions of the analysed minerals from the different lithologies are shown in Appendix 1. For the thermobarometric calculations we used only mineral compositions within the range of compositions of the calibration datasets of each of the individual geo-thermobarometric methods.

Garnet

Garnet-analyses from different lithologies of the Orobic basement are shown in Fig. 6a and 6b. Garnets from all lithologies are rich in almandine (49-65 mole %), with grossular (13-33 mole %) and pyrope (11-31 mole %) relatively abundant. Some differences in the ranges of garnet composition from and within the different units are obvious: garnets from the xenoliths of garnet-amphibolite in the meta-amphibolite sills of the metabasites (sample 34.2) are generally relatively rich in grossular, up to 36 mole %. The possibility that they might be related to a metamorphic phase in the source area predating the deposition of the lower sequence, is discussed below.

The garnets of the 'GOOV' show the largest range in composition, with almandine, varying from 95 to just below 40 mole %, and grossular (+Ad+Sp+Uv), ranging from 5 to just above 60 %. Pyrope content is generally between 2½ and 6 mole %. This variability can possibly be attributed to the various degrees of igneous and metasomatic assimilation with the host rock and type of host rock which is locally carbonate-richer. All samples from the 'GOOV' used for geothermobarometry are from the marginal zones of the 'GOOV', which is variably rich in mafic minerals, dependent on distance from the host-rock and type of host rock.

The range in composition of garnet-analyses from the 'Gneiss di Morbegno', also principally consisting of almandine (52-76 mole %) and grossular (0-47 mole %) can partly be attributed to the zonation, which has been identified in garnets from the basal 'Gneiss di Morbegno'.
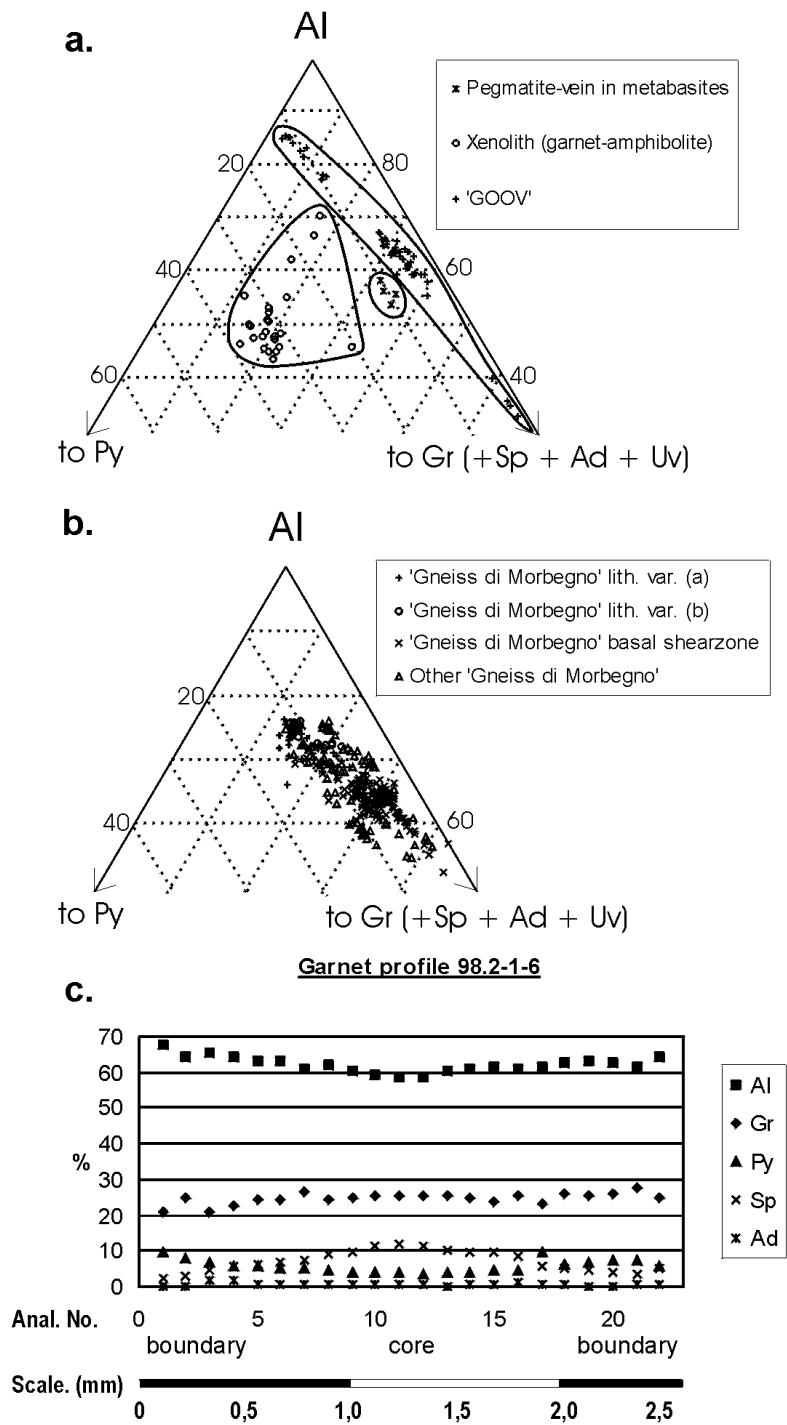
Fig. 6.

a. Ternary diagram with compositions of garnets from the lower sequence of the 'Orobic fold nappe', different symbols indicate individual lithologies (see legend).

b. Ternary diagram with compositions of garnets from the upper sequence of the 'Orobic fold nappe', different symbols indicate individual lithologies (see legend).

c. Profile through a garnet from sample 98.2-1, from the base of the 'Gneiss di Morbegno', showing weakly preserved relic zonation.

Fig. 6c shows the relic prograde zonation of garnets from the basal 'Gneiss di Morbegno'. There is also distict difference in garnet-composition of the garnets from the different lithologic varieties of the 'Gneiss di Morbegno'. The garnets included in the staurolite of lithologic variety (a) and those of the small garnets of lithologic variety (b) are richer in almandine.

The few analysed garnets of the pegmatite-vein in the 'Filladi di Ambria' that occur in close association with alumino-tschermakite and tschermakite (samples 40.9A) are similar in composition to those of the 'Gneiss di Morbegno'.

Kyanite

Kyanite contains some Ti (Av. 0,0127 wt. % TiO_2) and Fe (Av. 0,124 wt. % FeO).

Staurolite

Cations p.f.u. of microprobe analyses of staurolite were calculated on the basis of 48 oxygens. X_{Fe} is in the range 0,68 to 0,92, generally 0,82-0,92 allowing the application of the garnet-staurolite thermometer (Koch-Müller, 1997) for which this value should exceed 0,6. Zn-contents (p.f.u.) varies from 0,004 to 0,179, generally being in the range 0,075 to 0,123.

Amphibole

Amphibole analyses from the 'Gneiss di Morbegno' and the metabasites (Fig. 7) give an overview of the range of compositions analysed for this study according to the classification of Leake (1978). Pargasitic hornblende occurs in a particular variety of 'Gneiss Chiari' (sample 142.2).
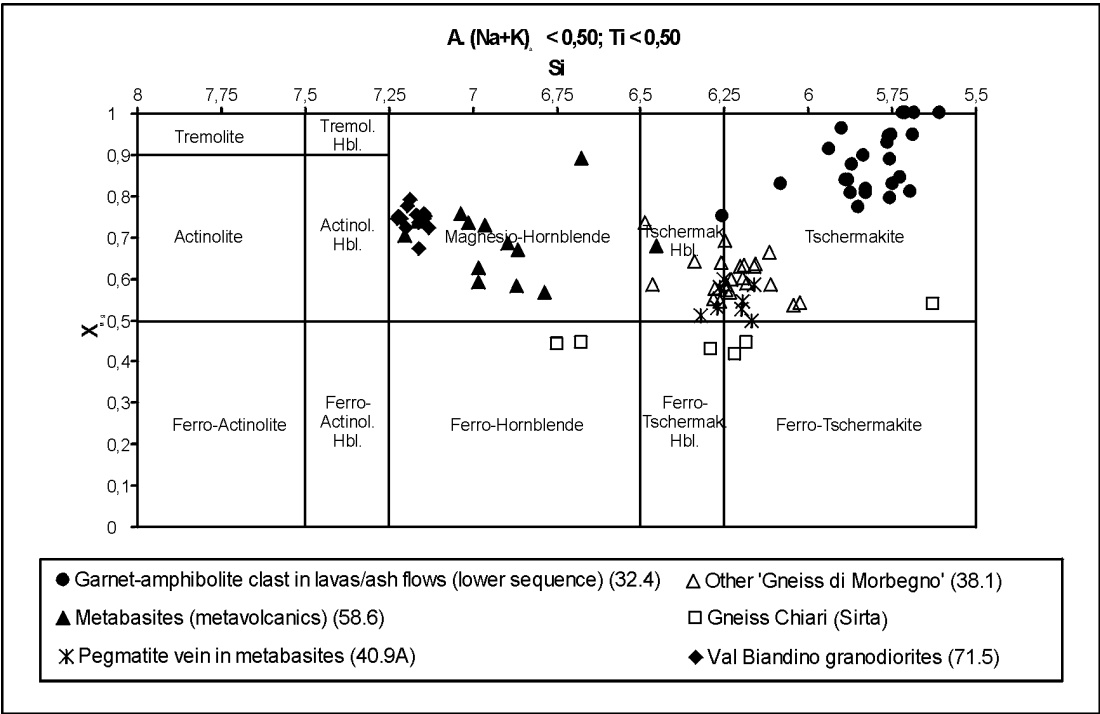
Fig. 7. *Compositions of the amphiboles from various lithologies of the Orobic basement. Classification according to Leake (1978). Four analyses of sample 142.2, for which no diagram is shown, are pargasitic hornblendes and pargasites. These fall in the range (Na + K)$_A$ > 0,50 with Ti < 0,50 / Fe^{3+} < Al^{VI}.*

White mica

In all lithologies, but to a lesser extent in the 'Scisti di Edolo', (Fe + Mg) correlate negatively with $Al^{[VI]}$. For white mica of particularly the 'Gneiss di Morbegno', 'Gneiss Chiari' and 'GOOV' Mg-tschermakite-substitution is thus proven. Accordingly there is a positive correlation of $(Fe^{2+} + Mg)^{[VI]}$ (p.f.u.) against Si (p.f.u.) of white mica of all lithologic units, idicated by different symbols in Fig. 8a. Ideally all points in Fig. 8a should plot on the line that indicates theoretical phengite substitution, but due to the Fe^{3+}-contents most points plot somewhat below.

Another influence on the Si^{4+} content of white mica is controlled by the paragonite-content. This effect plays a role where Pg > 0,1 (Bailey, 1984), which is the case for part of the analyses of white mica of the 'Gneiss di Morbegno' and 'GOOV' (Fig. 8b). However, because the phengite content correlates negatively with the paragonite content it is suggested that high values of on Si^{4+} represent a high T stage that was followed by a lower T overprint.
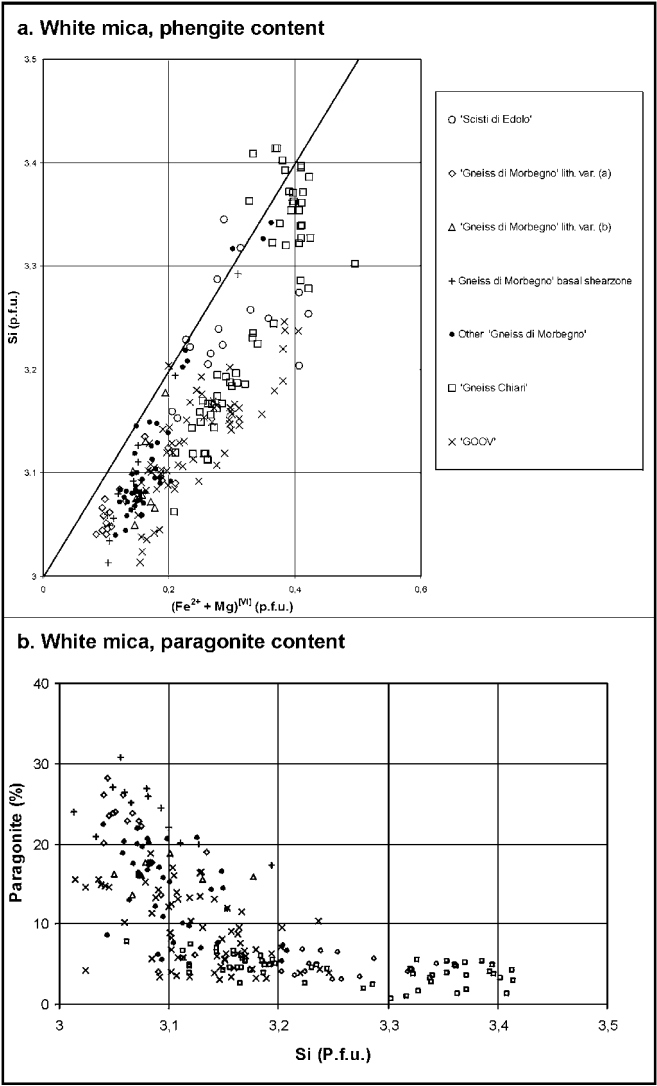
Fig. 8.

a. $(Fe^{2+}$ and $Mg)^{[VI]}$ content (p.f.u.) versus Si (p.f.u) content of white mica of various lithologies of the Orobic basement. The line indicates theoretical phengite substitution.

b. Plot showing the relationship between paragonite-content (%) and Si (p.f.u.) (the same symbols as in Fig. 8 a).

Biotite
Dark micas are Mg-biotite and Fe-biotite (Fig. 9) defined by Guidotti et al. (1975). Biotite from the 'GOOV' is exclusively Fe-biotite, whereas the 'Gneiss di Morbegno' contains Mg- and Fe-biotite. In the basal 'Gneiss di Morbegno' exclusively Mg-biotite was found, whereas higher up in the sequence, particularly in lithologic variety (b) and associated rocks Fe-biotite is more prominent or the main biotite-phase. This biotite from lithological variety (b) is Ti-enriched in comparison to biotite of the other lithologies. Ti reaches values up to 0.25 with an average of 0.23. In most lithologies the composition of biotite falls outside the narrow range of compositions allowed to apply the muscovite-biotite thermometer of Hoisch (1989).
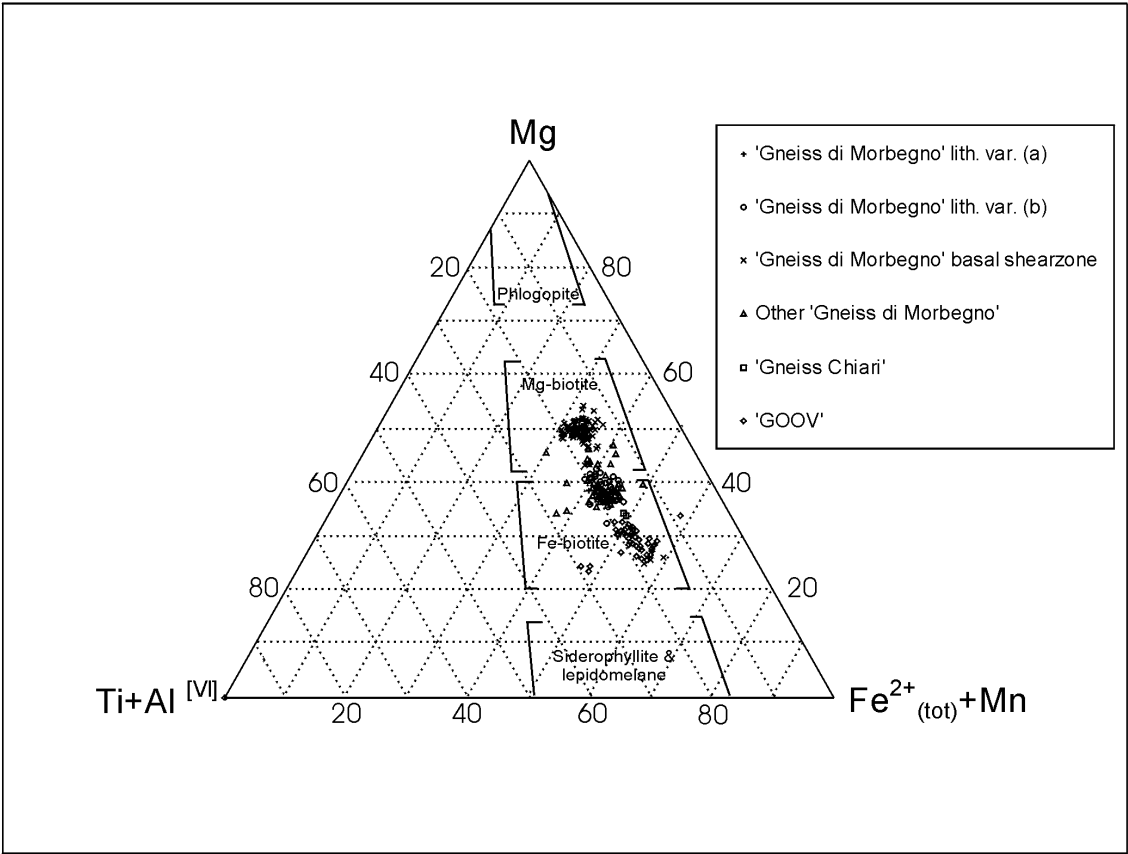
Fig. 9. Ternary diagram for biotite-compositions (Guidotti et al., 1975), showing that the composition of the analysed biotite is either Mg-biotite or Fe-biotite and rather strongly dependent on lithology, as the different symbols (see legend) indicate.

Clinozoisite
Zoisite of a pegmatite vein in the amphibole-bearing 'Filladi di Ambria' nearby metabasites (sample 40.9A) was analysed. The primary zoisite, a clinozoisite, that formed during formation of the vein, has 23.5 to 30 mole % $Ca_2Al_2FeSi_3O_{12}(OH)$, abbreviated in the following as 'mole % Al_2Fe' and, neglecting minor components such as Cr and Mn, calculated as Fe/(Al-2)). Along $D_{2/2}$-related cracks zoisite has been transformed to clinozoisite with up to 61.4 mole % Al_2Fe, whereby most analyses fall in the range of 45-50 %. These analyses might partly represent transition zones.
Clinozoisite of an original magmatic rock-variety of 'Gneiss Chiari' of sample 142.2 occurs in three habits (1) REE-rich cores of large older crystals which Al_2Fe-content ranges from 0 to

46 mole % with an average at 32 %, (2) thick rims of these large older crystals with an Al_2Fe-content ranging from 6 to 53 mole % and an average at 37 % and (3) fine symplectite needles with an Al_2Fe-content ranging from 1 to 28 mole % and an average at 11 %.

Feldspars

The feldspars of the epidote-amphibolite-schists of the metabasites of the lower sequence are dominantly albite. Feldspars of the analysed pegmatite-vein of the lower sequence (sample 40.9A) have an anorthite content of 24-25 %. In the 'GOOV' the feldspars are mainly of albite-composition whereas some plagioclase with 11-17 % anorthite and orthoclase was also analysed.

In the 'Gneiss di Morbegno' feldspars are dominantly plagioclase with anorthite contents in the range 16-27 % (lithological variety (a) 16-27 %, lithological variety (b) 20-26 %, other lithologies of the 'Gneiss di Morbegno' 18-26 %). Exceptions are the amphibole-bearing sample 38.1, which contains anorthite richer plagioclase (18-37 % An), and sample 48.10, which is albite-rich.

The 'Gneiss Chiari' contains albite and orthoclase. Plagioclase of a special variety of 'Gneiss Chiari' of sample 142.2 occurs as original magmatic crystals, which range in anorthite content of 32 to 63 % and an average of 41 %. Plagioclase in symplectite has an average anorthite content of 13 % and a range from 0.3 to 22 %.

In the 'Scisti di Edolo' albite is the dominant feldspar.

Feldspar of the 'Val Biandino Granodiorites' occurs either as plagioclase with 36-70 % anorthite or sodium rich (9-16 %) orthoclase.

Monazite

Monazite-analyses are available due to U-Th-Pb-dating. Because Y and Ce were also measured application of the monazite-xenotime thermometer, calibrated empirically by Heinrich et al. (1997) and experimentally by Gratz & Heinrich (1997) was also possible. Composition of all analysed grains of the samples of Table IV (88.0-97.9 % monazite (Ce PO_4), 1.2-9.9 % brabantite (Ca Th $(PO_4)_2$) and also 0.5-5.7 % huttonite ($ThSiO_4$)) are indicated in Fig. 10. From this diagram it is obvious that the monazites of 'Gneiss Chiari', where the U-Th-Pb isotopic system of a relatively large proportion of monazite crystals are affected by a young hydrothermal overprint, contain a higher huttonite-component. This might represent a generally higher content of Th of this lithology.
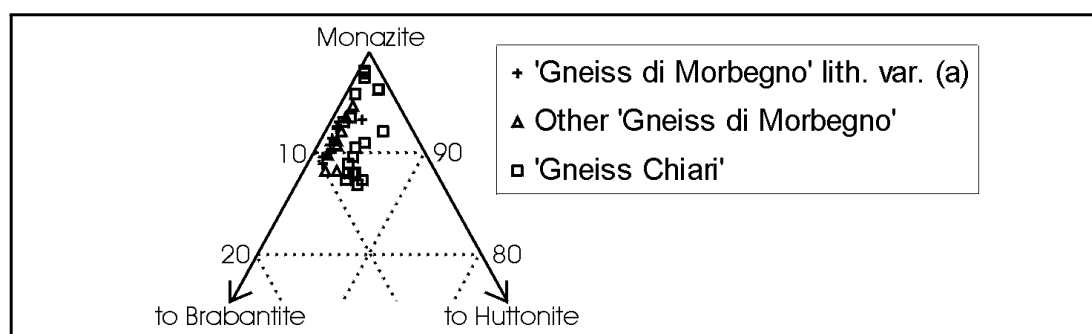
Fig. 10. Triaxial plot of compositions of monazite, in terms of monazite (CeREEPO4), brabantite (CaTh(PO4)2) and huttonite (ThSiO4) component.

7 Thermobarometry and P-T evolution

Attempts were made to determine P- and T-conditions of the 'Sardic' phase, prograde Variscan metamorphism, peak Variscan conditions ($M_{2/1}$), various retrograde Variscan stages ($M_{2/2}$) and Mesozoic imprint related to rifting. The 'Sardic phase only affected the lower sequence of the 'Orobic fold nappe', but, as mentioned above, the search for suitable assemblages to obtain 'Sardic' metamorphic (M_1) conditions by geothermobarometry in the lower sequence of the Orobic fold nappe was unsuccessful, mainly due to the high grade of Variscan overprint. The upper sequence of the 'Orobic fold nappe' has only been affected by Variscan metamorphism and subsequent very low-grade phases.

Prograde metamorphism leading to $M_{2/1}$:
Despite of high grade overprint prograde Variscan conditions are still identifiable in relatively large zoned garnets from the 'Gneiss di Morbegno' at the base of the upper sequence of the Orobic fold nappe (sample 98.2; Fig. 9a in Feijth, in prep. a), but at the attained peak conditions, it is unlikely that the phengite-, biotite- and plagioclase-compositions calculated from the EMP-analysis are still the same as during growth of garnet on the prograde path. Also the boundaries of the garnets that grew during this phase will not have retained their original composition. Therefore conducting P- and T-calculations will not lead to meaningfull results.

Peak $M_{2/1}$:
Phengite geobarometry (Massone & Schreyer, 1987) has been used in combination with Monazite-Xenotime thermometry (Franz et al., 1996; Gratz & Heinrich, 1997; 1998; Andrehs & Heinrich, 1998) and the petrogenetic grid to obtain the peak-conditions. Results of the phengite geobarometry, which relies on Mg-tschermakite-substitution, are shown in Table II and the relevant isopleths in Fig. 11 a and b. A first impression of the attained pressures is given by the maximum Si^{4+} contents of white mica reaches up to 3.4 p.f.u., whereas most analyses indicate values of around 3.3 p.f.u.. These highest values are typical for samples from 'Gneiss Chiari' (Table II, Fig. 8a), being generally higher than those in the 'Gneiss di Morbegno', which underwent the same tectonic evolution. The ideal limiting assemblage should include K-feldspar, biotite and quartz (Massone & Schreyer, 1987), of which biotite is generally missing in the 'Gneiss Chiari'. The missing biotite or another Mg, Fe silicate in the 'Gneiss Chiari' has as consequence that the obtained pressures are minimum values. As discussed below, this might not be a great disadvantage, and the determined P-conditions are very likely close to those really attained. Because re-equilibration and homogenisation of phengitic mica under lower P-conditions is extremely sluggish (Massone & Schreyer, 1987), the relic Si^{4+} contents are likely to indicate pressures close to peak conditions. The isopleths of 3.3 and 3.4 (Si^{4+} p.f.u.) are indicated in Fig. 11a, b and c.
The monazite-xenotime thermometer (Franz et al., 1996; Gratz & Heinrich, 1997; 1998; Andrehs & Heinrich, 1998) relies on X_Y (= Y/Ce + Y) of the solid solution (Ce,Y)PO_4, which, when xenotime (YPO_4) has been coexisting during monazite growth or re-equilibration, indicates formation- or recrystallisation temperature. High contents of Y indicate high temperatures of formation. If no xenotime is present X_Y is a measure of minimum temperature of monazite growth or recrystallisation. The relevant data for monazite-xenotime

Table II: Geothermobarometric results sorted by lithological unit. The internally consistent dataset of Holland & Powell (1990) was applied in their program Thermocalc for determination of a_{H2O} during $M_{2/2}$. A list of the reactions applied in this internally consistent dataset is given in Table III. Thermocalc version 3.1 (June 2001) was used with the datafile of 14.05.2001.

Lith. Unit	Sample No.	Thermometer [reference number for Fig.11a.]	Barometer [reference number for Fig. 11a.]	T (°C)	P (GPa) / Si⁴⁺
		Considered equilibria in Thermo-calc (for reactions see Table III) and applied a_{H2O}			
Filladi di Ambria (metabasites)	34.2	grt-hbl (Graham & Powell, 1984) [1]	Al in hbl (Hollister, 1987) [1]	751±23	1.26±0.04
		grt-hbl (Graham & Powell, 1984) [1]	Avg.: Al in hbl (Hollister, 1987; Hammarstrom & Zen, 1986; Johnson & Rutherford, 1989; Schmidt, 1992) [2]	751±23	1.13±0.03
		grt-hbl (Graham & Powell, 1984) [1]	Al in hbl (Anderson & Smith, 1995) [3]	751±23	0,98±0.07
	58.6b	am-pl(+qtz) (Holland & Blundy, 1994) [2]	Al in hbl (Anderson & Smith, 1995) [3]	771±2	1,44±0.01
	40.9A	grt-hbl (Graham & Powell, 1984) [1]	grt-pl-hbl-qz (Kohn & Spear, 1990) (P_Fe) [4] grt-pl-hbl-qz (Kohn & Spear, 1990) (P_Mg) [5]	602±6	0.99±0.01 0.92±0.02
Gneiss Occhiadini Orobico-Valtellinese	33.6	grt-bt (Kleemann & Reinhardt, 1994) [3]	grt-pl-bt-mu-qz (Ghent & Stout, 1981) (P_Fe) [6] grt-pl-bt-mu-qz (Ghent & Stout, 1981) (P_Mg) [7]	581±7 574±7	0.87±0.01 0.76±0.01
			grt-pl-bt-mu-qz (Hodges & Crowley, 1985) [8]	590±7	1.00±0
		grt-phe (Green & Hellmann, 1982) [4]	grt-pl-bt-mu-qz (Ghent & Stout, 1981) (P_Fe) [6] grt-pl-bt-mu-qz (Ghent & Stout, 1981) (P_Mg) [7]	599±4 593±4	0.89±0.01 0.77±0.01
			grt-pl-bt-mu-qz (Hodges & Crowley, 1985) [8]	607±4	1.04±0.01
		-	Si⁴⁺_max of phengite (Massone & Schreyer, 1987)	-	3.20 p.f.u.
		Internally consistent thermodynamic dataset (Holland & Powell, 1990); reactions: 1, 2, 3, 4, 5, 6, 7; $a_{H2O} = 0.005$		495±110	1.24±0.38
	33.6rand	grt-bt (Kleemann & Reinhardt, 1994) [3]	grt-pl-bt-mu-qz (Ghent & Stout, 1981) (P_Fe) [6] grt-pl-bt-mu-qz (Ghent & Stout, 1981) (P_Mg) [7]	619±14 615±21	0.99±0.01 0.89±0.01
			grt-pl-bt-mu-qz (Hodges & Crowley, 1985) [8]	632±15	1.18±0.01
			grt-pl-mu-qz (Hodges & Crowley, 1985) (P_Fe) [9] grt-pl-mu-qz (Hodges & Crowley, 1985) (P_Mg) [10]	626±21 658±24	1.10±0 1.58±0.01
		grt-phe (Green & Hellmann, 1982) [4]	grt-pl-bt-mu-qz (Ghent & Stout, 1981) (P_Fe) [6] grt-pl-bt-mu-qz (Ghent & Stout, 1981) (P_Mg) [7]	580±6 577±6	0.92±0.01 0.87±0.01
			grt-pl-bt-mu-qz (Hodges & Crowley, 1985) [8]	586±7	1.03±0.01
			grt-pl-mu-qz (Hodges & Crowley, 1985) (P_Fe) [9] grt-pl-mu-qz (Hodges & Crowley, 1985) (P_Mg) [10]	581±9 607±9	0.95±0 1.45±0.01
		-	Si⁴⁺_max of phengite (Massone & Schreyer, 1987)	-	3.19 p.f.u.
		Internally consistent thermodynamic dataset (Holland & Powell, 1990); reactions: 1, 2, 3, 5, 6, 8, 9; $a_{H2O} = 0.002$		486±114	1.28±0.42
	69.2aI	grt-bt (Kleemann & Reinhardt, 1994) [3]	grt-pl-bt-mu-qz (Ghent & Stout, 1981) (P_Fe) [6] grt-pl-bt-mu-qz (Ghent & Stout, 1981) (P_Mg) [7]	477±6 473±6	0.80±0.02 0.68±0.02
			grt-pl-bt-mu-qz (Hodges & Crowley, 1985) [8]	476±6	0.76±0.02
			grt-pl-bt-qz (Hoisch, 1990) (P_Fe) [11] grt-pl-bt-qz (Hoisch, 1990) (P_Mg) [12]	495±7 493±7	1.24±0.01 1.19±0.01
			grt-pl-mu-qz (Hodges & Crowley, 1985) (P_Fe) [9] grt-pl-mu-qz (Hodges & Crowley, 1985) (P_Mg) [10]	472±6 504±7	0.68±0.01 1.46±0.02
		grt-phe (Green & Hellmann, 1982) [4]	grt-pl-bt-mu-qz (Ghent & Stout, 1981) (P_Fe) [6] grt-pl-bt-mu-qz (Ghent & Stout, 1981) (P_Mg) [7]	502±2 494±2	0.83±0.02 0.69±0.02
			grt-pl-bt-mu-qz (Hodges & Crowley, 1985) [8]	501±2	0.82±0.02
			grt-pl-bt-qz (Hoisch, 1990) (P_Fe) [11] grt-pl-bt-qz (Hoisch, 1990) (P_Mg) [12]	524±2 523±2	1.31±0.01 1.13±0.01
			grt-pl-mu-qz (Hodges & Crowley, 1985) (P_Fe) [9] grt-pl-mu-qz (Hodges & Crowley, 1985) (P_Mg) [10]	497±2 534±2	0.74±0.01 1.52±0.02
		Internally consistent thermodynamic dataset (Holland & Powell, 1990); reactions: 1, 2, 3, 10, 11, 12, 13; $a_{H2O} = 0.01$		502±118	1.17±0.39
	32.4	grt-chl (Perchuk, 1989) (P-independent)	-	634±13	-
		-	Si⁴⁺_max of phengite (Massone & Schreyer, 1987)	-	3.20 p.f.u.
	VdL	-	Si⁴⁺_max of phengite (Massone & Schreyer, 1987)	-	3.24 p.f.u.
Gneiss di Morbegno	98.2	grt-bt (Kleemann & Reinhardt, 1994) [3]	grt-pl-bt-mu-qz (Ghent & Stout, 1981) (P_Fe) [6] grt-pl-bt-mu-qz (Ghent & Stout, 1981) (P_Mg) [7]	542±4 528±4	0.95±0.02 0.70±0.02
			grt-pl-bt-mu-qz (Hodges & Crowley, 1985) [8]	554±4	1,14±0.01
			grt-pl-bt-qz (Hoisch, 1990) (P_Fe) [11] grt-pl-bt-qz (Hoisch, 1990) (P_Mg) [12]	510±11 513±11	0.98±0.03 1.03±0.02
			grt-pl-mu-qz (Hodges & Crowley, 1985) (P_Fe) [9] grt-pl-mu-qz (Hodges & Crowley, 1985) (P_Mg) [10]	543±11 559±12	0.97±0.02 1.25±0.03
		grt-phe (Green & Hellmann, 1982) [4]	grt-pl-bt-mu-qz (Ghent & Stout, 1981) (P_Fe) [6] grt-pl-bt-mu-qz (Ghent & Stout, 1981) (P_Mg) [7]	574±56 564±55	0.93±0.02 0.73±0.05
			grt-pl-bt-mu-qz (Hodges & Crowley, 1985) [8]	581±57	1.06±0.01
			grt-pl-bt-qz (Hoisch, 1990) (P_Fe) [11] grt-pl-bt-qz (Hoisch, 1990) (P_Mg) [12]	601±23 605±23	1.18±0.03 1.26±0.03
			grt-pl-mu-qz (Hodges & Crowley, 1985) (P_Fe) [9] grt-pl-mu-qz (Hodges & Crowley, 1985) (P_Mg) [10]	592±23 604±23	1.02±0.02 1.25±0.04
		-	Si⁴⁺_max of phengite (Massone & Schreyer, 1987)	-	3.29 p.f.u.

Lith. Unit	Sample No.	Thermometer [reference number for Fig.11a.]	Barometer [reference number for Fig.11a.]	T (°C)	P (GPa) / Si^{4+}
		Considered equilibria in Thermo-calc (for reactions see Table III) and applied a_{H_2O}			
Gneiss di Morbegno	65.5	grt-bt (Kleemann & Reinhardt, 1994)[3]	grt-pl-bt-mu-qz (Ghent & Stout, 1981) (P$_{Fe}$)[6]	527±20	0.84±0.02
			grt-pl-bt-mu-qz (Ghent & Stout, 1981) (P$_{Mg}$)[7]	515±20	0.69±0.03
			grt-pl-bt-mu-qz (Hodges & Crowley, 1985)[8]	526±20	0.89±0.01
			grt-pl-bt-qz (Hoisch, 1990) (P$_{Fe}$)[11]	530±26	1.10±0.01
			grt-pl-bt-qz (Hoisch, 1990) (P$_{Mg}$)[12]	532±27	1.12±0.02
			grt-pl-mu-qz (Hodges & Crowley, 1985) (P$_{Fe}$)[9]	523±19	0.83±0.02
			grt-pl-mu-qz (Hodges & Crowley, 1985) (P$_{Mg}$)[10]	540±19	1.13±0.05
		grt-phe (Green & Hellmann, 1982)[4]	grt-pl-bt-mu-qz (Ghent & Stout, 1981) (P$_{Fe}$)[6]	526±8	0.85±0.01
			grt-pl-bt-mu-qz (Ghent & Stout, 1981) (P$_{Mg}$)[7]	519±8	0.69±0.01
			grt-pl-bt-mu-qz (Hodges & Crowley, 1985)[8]	529±8	0.92±0.01
			grt-pl-bt-qz (Hoisch, 1990) (P$_{Fe}$)[11]	527±12	1.09±0.01
			grt-pl-bt-qz (Hoisch, 1990) (P$_{Mg}$)[12]	528±12	1.13±0.01
			grt-pl-mu-qz (Hodges & Crowley, 1985) (P$_{Fe}$)[9]	513±9	0.85±0.07
			grt-pl-mu-qz (Hodges & Crowley, 1985) (P$_{Mg}$)[10]	524±9	1.05±0.02
		mu-bt (Hoisch, 1989)[5]	grt-pl-bt-mu-qz (Ghent & Stout, 1981) (P$_{Fe}$)[6]	527±27	0.85±0.03
			grt-pl-bt-mu-qz (Ghent & Stout, 1981) (P$_{Mg}$)[7]	482±29	0.63±0.06
			grt-pl-bt-mu-qz (Hodges & Crowley, 1985)[8]	550±26	0.96±0.01
			grt-pl-bt-qz (Hoisch, 1990) (P$_{Fe}$)[11]	613±24	1.26±0.04
			grt-pl-bt-qz (Hoisch, 1990) (P$_{Mg}$)[12]	684±21	1.60±0.02
			grt-pl-mu-qz (Hodges & Crowley, 1985) (P$_{Fe}$)[9]	520±27	0.81±0.02
			grt-pl-mu-qz (Hodges & Crowley, 1985) (P$_{Mg}$)[10]	642±22	1.40±0.06
		-	Si$^{4+}_{max}$ of phengite (Massone & Schreyer, 1987)	-	3.21 p.f.u.
		Internally consistent thermodynamic dataset (Holland & Powell, 1990); reactions: 1, 2, 3, 5, 10, 16, 17; a_{H_2O} = 0.01		511±84	1.24±0.32
	38.1	grt-bt (Kleemann & Reinhardt, 1994)[3]	grt-pl-bt-mu-qz (Ghent & Stout, 1981) (P$_{Fe}$)[6]	625±8	0.71±0.02
			grt-pl-bt-mu-qz (Ghent & Stout, 1981) (P$_{Mg}$)[7]	618±8	0.62±0.01
			grt-pl-bt-mu-qz (Hodges & Crowley, 1985)[8]	644±9	0.94±0.02
			grt-pl-bt-mu-qz (Hoisch, 1990) (P$_{R5}$)[13]	648±9	0.98±0
			grt-pl-bt-mu-qz (Hoisch, 1990) (P$_{R6}$)[14]	656±9	1.08±0
			grt-pl-bt-qz (Hoisch, 1990) (P$_{Fe}$)[11]	582±181	1.09±0.04
			grt-pl-bt-qz (Hoisch, 1990) (P$_{Mg}$)[12]	581±181	1.08±0.03
			grt-pl-mu-qz (Hodges & Crowley, 1985) (P$_{Fe}$)[9]	647±9	0.98±0.01
			grt-pl-mu-qz (Hodges & Crowley, 1985) (P$_{Mg}$)[10]	661±9	1.14±0.06
		grt-phe (Green & Hellmann, 1982)[4]	grt-pl-bt-mu-qz (Ghent & Stout, 1981) (P$_{Fe}$)[6]	557±29	0.64±0.01
			grt-pl-bt-mu-qz (Ghent & Stout, 1981) (P$_{Mg}$)[7]	555±29	0.61±0.01
			grt-pl-bt-mu-qz (Hodges & Crowley, 1985)[8]	563±29	0.76±0.02
			grt-pl-bt-mu-qz (Hoisch, 1990) (P$_{R5}$)[13]	568±29	0.86±0.02
			grt-pl-bt-mu-qz (Hoisch, 1990) (P$_{R6}$)[14]	568±29	0.85±0.02
			grt-pl-bt-qz (Hoisch, 1990) (P$_{Fe}$)[11]	573±29	0.96±0.03
			grt-pl-bt-qz (Hoisch, 1990) (P$_{Mg}$)[12]	572±29	0.98±0.02
			grt-pl-mu-qz (Hodges & Crowley, 1985) (P$_{Fe}$)[9]	563±29	0.76±0.01
			grt-pl-mu-qz (Hodges & Crowley, 1985) (P$_{Mg}$)[10]	575±29	1.00±0.06
		grt-hbl (Graham & Powell, 1984)[1]	grt-pl-hbl-qz (Kohn & Spear, 1990) (P$_{Fe}$)[4]	599±25	1.08±0.09
			grt-pl-hbl-qz (Kohn & Spear, 1990) (P$_{Mg}$)[5]	599±25	0.97±0.09
		-	Si$^{4+}_{max}$ of phengite (Massone & Schreyer, 1987)	-	3.13 p.f.u.
		Internally consistent thermodynamic dataset (Holland & Powell, 1990); reactions: 1, 2, 3, 6, 10, 14, 18; a_{H_2O} = 0.005		507±109	1.22±0.35
	91.2a-I	grt-bt (Kleemann & Reinhardt, 1994)[3]	grt-pl-bt-mu-qz (Ghent & Stout, 1981) (P$_{Fe}$)[6]	647±11	0.84±0.04
			grt-pl-bt-mu-qz (Ghent & Stout, 1981) (P$_{Mg}$)[7]	641±10	0.78±0.04
			grt-pl-bt-mu-qz (Hodges & Crowley, 1985)[8]	667±1	1.11±0.05
			grt-pl-bt-mu-qz (Hoisch, 1990) (P$_{R5}$)[13]	684±11	1.32±0.08
			grt-pl-bt-mu-qz (Hoisch, 1990) (P$_{R6}$)[14]	689±11	1.39±0.08
			grt-pl-bt-qz (Hoisch, 1990) (P$_{Fe}$)[11]	689±11	1.39±0.07
			grt-pl-bt-qz (Hoisch, 1990) (P$_{Mg}$)[12]	690±11	1.40±0.07
			grt-pl-mu-qz (Hodges & Crowley, 1985) (P$_{Fe}$)[9]	671±11	1.16±0.04
			grt-pl-mu-qz (Hodges & Crowley, 1985) (P$_{Mg}$)[10]	678±11	1.25±0.05
		grt-phe (Green & Hellmann, 1982)[4]	grt-pl-bt-mu-qz (Ghent & Stout, 1981) (P$_{Fe}$)[6]	600±4	0.79±0.03
			grt-pl-bt-mu-qz (Ghent & Stout, 1981) (P$_{Mg}$)[7]	599±4	0.76±0.04
			grt-pl-bt-mu-qz (Hodges & Crowley, 1985)[8]	610±4	0.97±0.05
			grt-pl-bt-mu-qz (Hoisch, 1990) (P$_{R5}$)[13]	623±5	1.21±0.08
			grt-pl-bt-mu-qz (Hoisch, 1990) (P$_{R6}$)	622±5	1.12±0.07
			grt-pl-bt-qz (Hoisch, 1990) (P$_{Fe}$)[11]	624±5	1.24±0.07
			grt-pl-bt-qz (Hoisch, 1990) (P$_{Mg}$)[12]	623±5	1.21±0.06
			grt-pl-mu-qz (Hodges & Crowley, 1985) (P$_{Fe}$)[9]	611±5	0.99±0.04
			grt-pl-mu-qz (Hodges & Crowley, 1985) (P$_{Mg}$)[10]	619±5	1.13±0.05
		-	Si$^{4+}_{max}$ of phengite (Massone & Schreyer, 1987)	-	3.09 p.f.u.
		Internally consistent thermodynamic dataset (Holland & Powell, 1990); reactions: 1, 2, 3, 5, 6, 18, 19; a_{H_2O} = 0.001		471±114	1.18±0.44

Table II (Continued)

Lith. Unit	Sample No.	Thermometer [reference number for Fig.11a.]	Barometer [reference number for Fig. 11a.]	T (°C)	P (GPa) / Si⁴⁺
		Considered equilibria in Thermo-calc (for reactions see Table III) and applied a_{H_2O}			
Gneiss di Morbegno	31.7	grt-stt (Perchuk, 1969/1991) [6]	grt-pl-mu-qz (Hodges & Crowley, 1985) Fe* [15]	677±20	1.03±0.04
			grt-pl-mu-qz (Hodges & Crowley, 1985) Mg* [16]	678±20	1.05±0.06
			grt-pl-as-qz (Newton & Haselton, 1981) Ky* [17]	678±20	1.05±0.04
			Grt-pl-as-qz (Hodges & Spear, 1982) Ky* [18]	677±11	0.94±0.04
			grt-pl-as-qz (Ganguly & Saxena, 1984) Ky* [19]	675±20	0.94±0.05
			grt-pl-as-qz (Hodges & Crowley, 1985) Ky* [20]	677±20	1.00±0.05
			grt-pl-as-qz (Hodges & Crowley, 1985) Kyev* [21]	677±20	1.00±0.04
			grt-pl-as-qz (Koziol, 1989) Ky* [22]	679±20	1.09±0.04
			grt-pl-as-qz (Koziol & Newton, 1988) Ky_T* [23]	679±20	1.10±0.05
			grt-mu-as-qz (Hodges & Crowley, 1985) Ky* [24]	678±20	1.04±0.01
		grt-phe (Green & Hellmann, 1982) [4]	grt-pl-mu-qz (Hodges & Crowley, 1985) Fe* [15]	683±11	1.04±0.04
			grt-pl-mu-qz (Hodges & Crowley, 1985) Mg* [16]	684±11	1.06±0.06
			grt-pl-as-qz (Newton & Haselton, 1981) Ky* [17]	685±11	1.07±0.04
			grt-pl-as-qz (Hodges & Spear, 1982) Ky* [18]	677±11	0.94±0.04
			grt-pl-as-qz (Ganguly & Saxena, 1984) Ky* [19]	678±11	0.95±0.05
			grt-pl-as-qz (Hodges & Crowley, 1985) Ky* [20]	681±11	1.01±0.05
			grt-pl-as-qz (Hodges & Crowley, 1985) Kyev* [21]	681±11	1.01±0.04
			grt-pl-as-qz (Koziol, 1989) Ky* [22]	687±11	1.11±0.04
			grt-pl-as-qz (Koziol & Newton, 1988) Ky_T* [23]	687±11	1.11±0.05
			grt-mu-as-qz (Hodges & Crowley, 1985) Ky* [24]	686±11	1.09±0.01
		-	Si⁴⁺max of phengite (Massone & Schreyer, 1987)	-	3.13 p.f.u.
		Internally consistent thermodynamic dataset (Holland & Powell, 1990); reactions: 20, 21, 22, 23, 24, 25, 26, 27, 28; a_{H_2O} = 0.25		513±61	1.16±0.28
	48.10	grt-bt (Kleemann & Reinhardt, 1994) [3]	grt-pl-bt-mu-qz (Ghent & Stout, 1981) (P_Fe) [6]	608±219	0.91±0.02
			grt-pl-bt-mu-qz (Ghent & Stout, 1981) (P_Mg) [7]	599±216	0.78±0.04
			grt-pl-bt-mu-qz (Hodges & Crowley, 1985) [8]	623±225	1.11±0.02
			grt-pl-mu-qz (Hodges & Crowley, 1985) (P_Fe) [9]	626±186	1.09±0.02
			grt-pl-mu-qz (Hodges & Crowley, 1985) (P_Mg) [10]	645±190	1.40±0.13
		grt-phe (Green & Hellmann, 1982) [4]	grt-pl-bt-mu-qz (Ghent & Stout, 1981) (P_Fe) [6]	575±15	0.89±0.02
			grt-pl-bt-mu-qz (Ghent & Stout, 1981) (P_Mg) [7]	571±15	0.81±0.05
			grt-pl-bt-mu-qz (Hodges & Crowley, 1985) [8]	582±15	1.04±0.02
			grt-pl-mu-qz (Hodges & Crowley, 1985) (P_Fe) [9]	583±15	1.05±0.04
			grt-pl-mu-qz (Hodges & Crowley, 1985) (P_Mg) [10]	596±15	1.35±0.13
		mu-bt (Hoisch, 1989) [5]	grt-pl-bt-mu-qz (Ghent & Stout, 1981) (P_Fe) [6]	613±18	0.79±0.02
			grt-pl-bt-mu-qz (Ghent & Stout, 1981) (P_Mg) [7]	601±18	0.73±0.04
			grt-pl-bt-mu-qz (Hodges & Crowley, 1985) [8]	663±16	1.08±0.06
			grt-pl-mu-qz (Hodges & Crowley, 1985) (P_Fe) [9]	657±17	1.04±0.05
			grt-pl-mu-qz (Hodges & Crowley, 1985) (P_Mg) [10]	691±15	1.23±0.07
		-	Si⁴⁺max of phengite (Massone & Schreyer, 1987)	-	3.34 p.f.u.
		Internally consistent thermodynamic dataset (Holland & Powell, 1990); reactions: 1, 2, 3, 19, 14, 6, 18; a_{H_2O} = 0.003		461±96	1.24±0.40
	92.2	grt-bt (Kleemann & Reinhardt, 1994) [3]	grt-pl-bt-qz (Hoisch, 1990) (P_Fe) [11]	618±3	0.87±0.05
			grt-pl-bt-qz (Hoisch, 1990) (P_Mg) [12]	619±3	0.89±0.05
		-	Si⁴⁺max of phengite (Massone & Schreyer, 1987)	-	3.18 p.f.u.
		Internally consistent thermodynamic dataset (Holland & Powell, 1990); reactions: 1, 2, 3, 6, 14, 18, 19; a_{H_2O} = 0.007		518±105	1.09±0.38
	94.2	grt-bt (Kleemann & Reinhardt, 1994) [3]	grt-pl-bt-qz (Hoisch, 1990) (P_Fe) [11]	598±14	0.74±0.07
			grt-pl-bt-qz (Hoisch, 1990) (P_Mg) [12]	602±14	0.80±0.05
		-	Si⁴⁺max of phengite (Massone & Schreyer, 1987)	-	3.13 p.f.u.
		Internally consistent thermodynamic dataset (Holland & Powell, 1990); reactions: 1, 2, 3, 5, 6, 14, 29; a_{H_2O} = 0.005		514±111	1.10±0.42
Gneiss Chiari	142.2	am-pl (+qtz) (Holland & Blundy, 1994) [2]	al in hbl (Anderson & Smith, 1995) [3]	593±29	0.99±0.17
			al in hbl (Hollister, 1987) [1]	593±29	1.01±0.03
			Avg.: Al in hbl (Hollister, 1987; Hammarstrom & Zen, 1986; Johnson & Rutherford, 1989; Schmidt, 1992) [2]	593±29	0.92±0.03
	39.2	-	Si⁴⁺max of phengite (Massone & Schreyer, 1987)	-	3.41 p.f.u.
		2-feldspar (Stormer & Whitney, 1985)	-	335±19	-
	82.13I	-	Si⁴⁺max of phengite (Massone & Schreyer, 1987)	-	3.41 p.f.u.
		2-feldspar (Stormer & Whitney, 1985)	-	351±17	-
	89.2II	-	Si⁴⁺max of phengite (Massone & Schreyer, 1987)	-	3.41 p.f.u.
Val Biandino Plutonic Complex	71.5b	am-pl (Blundy & Holland, 1990)	Avg.: Al in hbl (Hollister, 1987; Hammarstrom & Zen, 1986; Johnson & Rutherford, 1989; Schmidt, 1992)	729±20	0.93±0.19
SdE	SdE	-	Si⁴⁺max of phengite (Massone & Schreyer, 1987)	-	3.34 p.f.u.

Table III: Considered reactions in Thermocalc (Holland & Powell, 1990).

(1)	mu + 2phl + 6qz = 3cel + py
(2)	mu + 2ann + 6qz = 3fcel + alm
(3)	phl + 3an = mu + py + gr
(4)	ma + py + gr + mic = phl + 4an
(5)	mu + 3fcel + 2phl + 6qz = 6cel + alm
(6)	pa + 2ann + mic + 6qz = 3fcel + alm + ab
(7)	30fcel + 6ma + 15phl + 39qz = 45cel + 10alm + 2gr + 6H_2O
(8)	ma + py + gr + mic = phl + 4an
(9)	30fcel + 6ma + 15phl + 39qz = 45cel + 10alm + 2gr + 6H_2O
(10)	3cel + 2ma = 2mu + phl + 2an + 3qz + 2H_2O
(11)	mu + phl + ann + 6qz = 3fcel + py
(12)	3cel + 2pa = 2mu + phl + 2ab + 3qz + 2H_2O
(13)	pa + 2phl + mic + 6qz = 3cel + py + ab
(14)	3fcel + py = 3cel + alm
(15)	2ma + gr + 3qz = 5an + 2H_2O
(16)	3ma + 9ann + 4py + 3mic + 24qz = 12cel + 9alm + gr
(17)	3cel + 4pa + alm + gr + mic = 3fcel + 3ma + phl + 4ab
(18)	3cel + ma + alm + gr + mic = 3fcel + phl + 4an
(19)	15cel + 6ma = 10mu + 5phl + 2gr + 21qz + 6H_2O
(20)	gr + 2ky + qz = 3an
(21)	12ma + 8py + 13gr + 60ky = 6mst + 51an
(22)	6mst + 75an = 8py + 25gr + 96ky + 12H_2O
(23)	3mu + py + 4qz = 3cel + 4ky
(24)	4mu + 2mst + 4mic + 15qz = 8cel + 22ky
(25)	3mu + alm + 4qz = 3fcel + 4ky
(26)	4mu + 2fst + 4mic + 15qz = 8fcel + 22ky
(27)	8mu + 2mst + 4ab + 15qz = 8cel + 4pa + 22ky
(28)	4py + 6mnst + 12mic + 29qz = 12cel + 8spss + 50ky
(29)	9cel + 4ma + 2alm + 3gr = 6fcel + 3phl + 13an + 4H_2O

thermobarometry are listed in Table IV.

Monazite can grow at low-grade conditions up to granulite facies conditions, can crystallise from melt and can re-equilibrate by hydrothermal overprint. This implies that identification of different generations of monazite is essential in order to understand the results of the monazite-xenotime geothermometry. This can be done by plotting X_Y, which is proportionate to the temperature of equilibration, against the corresponding U-Th-Pb monazite-age of each analysis (Fig. 12). Monazite coexisting with xenotime (analyses of samples 31.7a-2, 65.5bI, 65.5bIII, 82.13I, 82.17 and 91.2a-1 in this diagram shows roughly two point groups, a Variscan group and a Mesozoic group. The group with lower X_Y is younger, according to the lower values of X_Y of probable hydrothermal origin or re-equilibrated by hydrothermal overprint. Some intermediate points, and points with lower X_Y, represent Variscan monazites affected by Variscan amphibolite facies overprint and/or by Mesozoic hydrothermal overprint. Monazite without coexisting xenotime (open symbols in Fig. 12) shows consistently lower X_Y.

Legend for a and b:
Lower unit:
- ◆ 'Gneiss Occiadini Orobico-Valtellinese' (GOOV)
- ▫ Metabasites: xenolith in sill
- ○ Metabasites: epidote-amphibolite schist
- △ Filladi di Ambria: pegmatite vein
Upper unit:
- ● Gneiss di Morbegno
- ▲ Gneiss Chiari (sample 142.2)
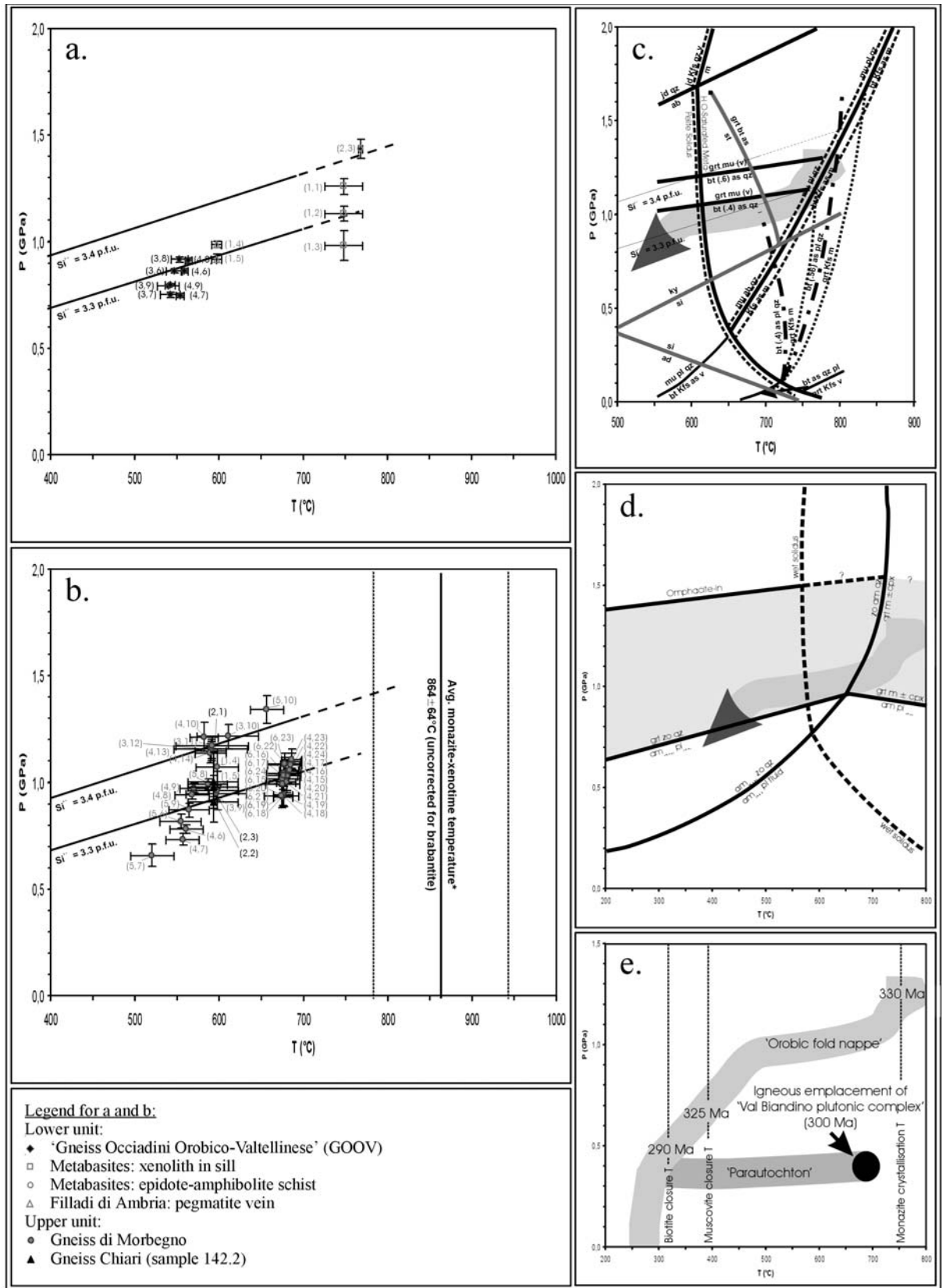
Fig. 11.

a. Geothermobarometric results of some important lithologies of the lower sequence of the 'Orobic fold nappe'.

b. Geothermobarometric results of some important lithologies of the upper sequence of the 'Orobic fold nappe'.

c. Pressure-temperature diagram showing the conditions of dehydration melting of biotite in metapellites (from Le Breton & Thompson, 1988) and dehydration melting of muscovite (Petö, 1976). Further shown are, the H_2O-saturated metapelite solidus (Thompson, 1982), the Al_2SiO_5 phase-relations and the reaction grt + bt + as $\longrightarrow$ st (both from Spear & Cheney, 1989), the Si^{4+}-isopleth of 3.4 p.f.u. (Massone & Schreyer, 1987) and the biotite sides (X_{Mg} = 0.4, 0.6) of the continuous reaction with muscovite, garnet, Al_2SiO_5, quartz (Thompson, 1982, Fig. 6). The interpreted Variscan P-T-loop is also indicated.

d. Phase diagram for the fluid-absent melting of mid ocean ridge basalt (MORB) saturated with quartz/coesite at subsolidus conditions. (From Vielzeuf & Schmidt, 2001). The interpreted Variscan P-T-loop is also indicated.

e. P-T-t relationships of the 'Orobic Fold nappe' and the 'Val Biandino plutonic complex'. Geochronological data are from Feijth et al. (in prep.).

Analyses with a low Y_2O_3-content (< 1) indicate hydrothermal overprint, during which Y was obviously released from metamorphic monazite. Hydrothermal and/or retrograde Variscan overprint has obviously affected the monazite from samples 65.5bI, 65.5bIII and 91.2a from the 'Gneiss di Morbegno' samples 80.1 and 82.17 from 'Gneiss Chiari'.

Temperatures were calculated with the xenotime-monazite thermometer (Gratz & Heinrich, 1997) for the samples where xenotime and monazite are coexisting. Temperatures were only calculated for samples where monazite has a reasonably high X_Y and SiO_2 < 1 (because of the huttonite component, as discussed below), which is the case for all analyses indicated with filled points in Fig. 12 and marked in Table IV. In all other samples with Variscan ages and where xenotime is missing monazite-xenotime-temperatures should be regarded as minimum Variscan temperatures, which are also given in Table IV. Discussion of the conditions calculated for Mesozoic overprint follows in an especially dedicated section below. For calculation of an average temperature considering all relevant samples with the monazite-xenotime thermometer a pressure input is required. The selection of the most realistic value for input is based on phase relationships, particularly of dehydration melting reactions of white mica and biotite.

These phase relationships indicate conditions far beyond the H_2O-saturated metapelite solidus and the existence of the mineral paragenesis of lithologic variety (a) and the other meta-pelite paragenesis of the Orobic basement at these P and T imply very low values of a_{H2O}, as shown in Table II. Values of P and T around muscovite dehydration melting determined by Petö (1976) (Fig. 11c) must have been reached because muscovite dehydration melting has occurred in lithologic variety (a) and produced kyanite by the reaction

$$\text{mu} + \text{pl} + \text{qz} \longrightarrow \text{bt} + \text{Kfs} + \text{ky} + \text{m,} \tag{1}$$
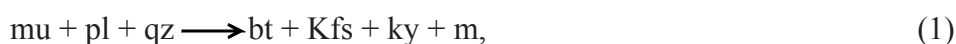
Table IV: Isotopic ages and results of monazite-xenotime thermometry. Complete analytical results are shown in Feijth et al. (in prep.). Analyses with $Y_2O_3 > 1$ are shown in grey lines.
Analyses with Mesozoic ages are typed in italic. Bold typed temperatures are values corrected for the Huttonite-component. Underlined temperatures can clearly be related to specific events, either peak Variscan or Mesozoic.
(* P = from barometers mentioned in text; 1.3 GPa; ** P = 0.34 GPa (Aalenian overburden))

Sample	Age	Error	Weighted average	Ce_2O_3	Y_2O_3	Ce	Y	Mo	Br	Hu	X_t(monazite)	$P_{applied}$ (GPa)	T (Peak Variscan)*	T_av (Peak Variscan w.a.)*	T (Hydrothermal)**	T (mo. and xe. not coexisting)*
Gneiss di Morbegno:																
31.7a-2/m1.1	327	± 60		28,34	1,61	0,412	0,034	89,97	8,64	1,39	0,0765		949 / **936**			
31.7a-2/m2.1	288	± 53		28,68	1,56	0,426	0,034	89,68	9,31	1,02	0,0732		929 / **919**			
31.7a-2/m3.1	316	± 66		29,60	1,27	0,438	0,027	92,98	6,22	0,80	0,0588		826 / **820**			
31.7a-2/m4.1	362	± 67		28,70	1,27	0,431	0,028	92,69	6,59	0,72	0,0602		838 / **832**			
31.7a-2/m5.1	323	± 55	319 ± 25	28,30	1,28	0,425	0,027	91,51	7,58	0,90	0,0608		842 / **834**	877 ± 50 / 868 ± 48		
65.6bIII/m1.1	291	± 87		29,98	0,99	0,448	0,021	94,69	4,26	1,05	0,0456					
65.6bIII/m2.1	351	± 48		28,12	1,50	0,422	0,033	88,21	9,88	1,91	0,0718		920 / **902**			
65.6bIII/m3.1	295	± 52		27,73	0,32	0,432	0,007	88,22	8,95	2,83	0,0165					
65.6bIII/m4.1	334	± 58	324 ± 28	29,38	1,40	0,442	0,031	92,18	6,50	1,32	0,0648		872 / **861**	890 ± 24 / 881 ± 21		
65.6bI/m1.1	311	± 60		28,93	1,00	0,446	0,022	91,19	7,51	1,30	0,0478					730 / **720**
65.6bI/m2.1	316	± 53		29,86	0,80	0,453	0,018	90,82	7,69	1,49	0,0376					
65.6bI/m3.1	393	± 72		31,16	0,52	0,469	0,011	93,42	5,48	1,10	0,0239					
65.6bI/m4.1	300	± 63	322 ± 29	29,07	1,19	0,438	0,026	89,77	8,99	1,24	0,0563			-		806 / **796**
91.2a/m1.1	376	± 63		30,99	0,87	0,443	0,018	92,35	6,83	0,82	0,0393					
91.2a/m2.1	324	± 49		29,69	0,92	0,438	0,020	89,93	8,81	1,27	0,0433					
91.2a/m3.1	300	± 71		30,48	0,79	0,454	0,017	93,25	4,11	2,64	0,0365					
91.2a/m4.1	311	± 46		27,70	1,18	0,417	0,026	88,84	9,83	1,33	0,0582		822 / **811**			
91.2a/m5.1	326	± 56	326 ± 25	28,14	1,22	0,424	0,027	90,67	8,34	0,99	0,0593		830 / **822**	826 ± 4 / 816 ± 6		
Gneiss Chiari:																
80.1/m1.1	-			34,05	0,36	0,509	0,008	96,32	1,20	2,48	0,0152					
80.1/m2.1	181	± 62		31,51	0,26	0,484	0,006	91,03	4,90	4,08	0,0119					
80.1/m3.1	365	± 54		31,66	0,90	0,486	0,020	90,53	6,01	3,46	0,0398					
80.1/m4.1	247	± 45		30,11	1,01	0,462	0,022	88,09	7,85	4,06	0,0464					716 / **687**
80.1/m4.2	237	± 44		30,21	0,67	0,466	0,015	88,01	7,62	4,37	0,0312					
80.1/m4.3	238	± 44		30,22	1,05	0,464	0,024	88,00	7,41	4,58	0,0462					734 / **700**
80.1/m5.1	283	± 38	-	29,89	1,02	0,469	0,023	86,73	7,85	5,42	0,0473			-		725 / **685**
82.13/m3.1	252	± 216		34,486	0,108	0,508	0,002	97,50	1,67	0,83	0,0045					
82.13/m6.1	158	± 59		31,256	0,572	0,473	0,013	92,21	2,83	4,95	0,0259		964 / **916**	964 / 916		
82.13/m7.1	-			34,888	0,276	0,515	0,005	98,19	1,34	0,46	0,0114					
82.13/m6.2	178	± 93		33,709	0,357	0,507	0,008	93,64	4,93	1,43	0,0151				327 / 322	
82.13/m5	318	± 333	-	34,843	0,201	0,534	0,004	97,90	1,55	0,55	0,0083					
82.17/m1.1	318	± 46		29,99	1,81	0,453	0,040	89,54	6,71	3,75	0,0605		973 / **936**			797 / **761**
82.17/m2.1	262	± 38		29,38	1,18	0,448	0,028	87,24	7,01	5,74	0,0552					
82.17/m3.1	325	± 47		27,97	0,76	0,434	0,017	87,24	8,51	4,25	0,0382					
82.17/m4.1	295	± 149		36,34	0,12	0,544	0,003	95,77	3,36	0,87	0,0048					
82.17/m3.2	300	± 121		33,93	0,00	0,529	0,000	92,97	5,98	1,05	0,0000					
82.17/m1.2	316	± 47	300 ± 30	30,60	1,27	0,466	0,028	88,81	7,45	3,74	0,0563		806 / **776**	890 ± 83 / 856 ± 80		

Av.: 864 ± 80
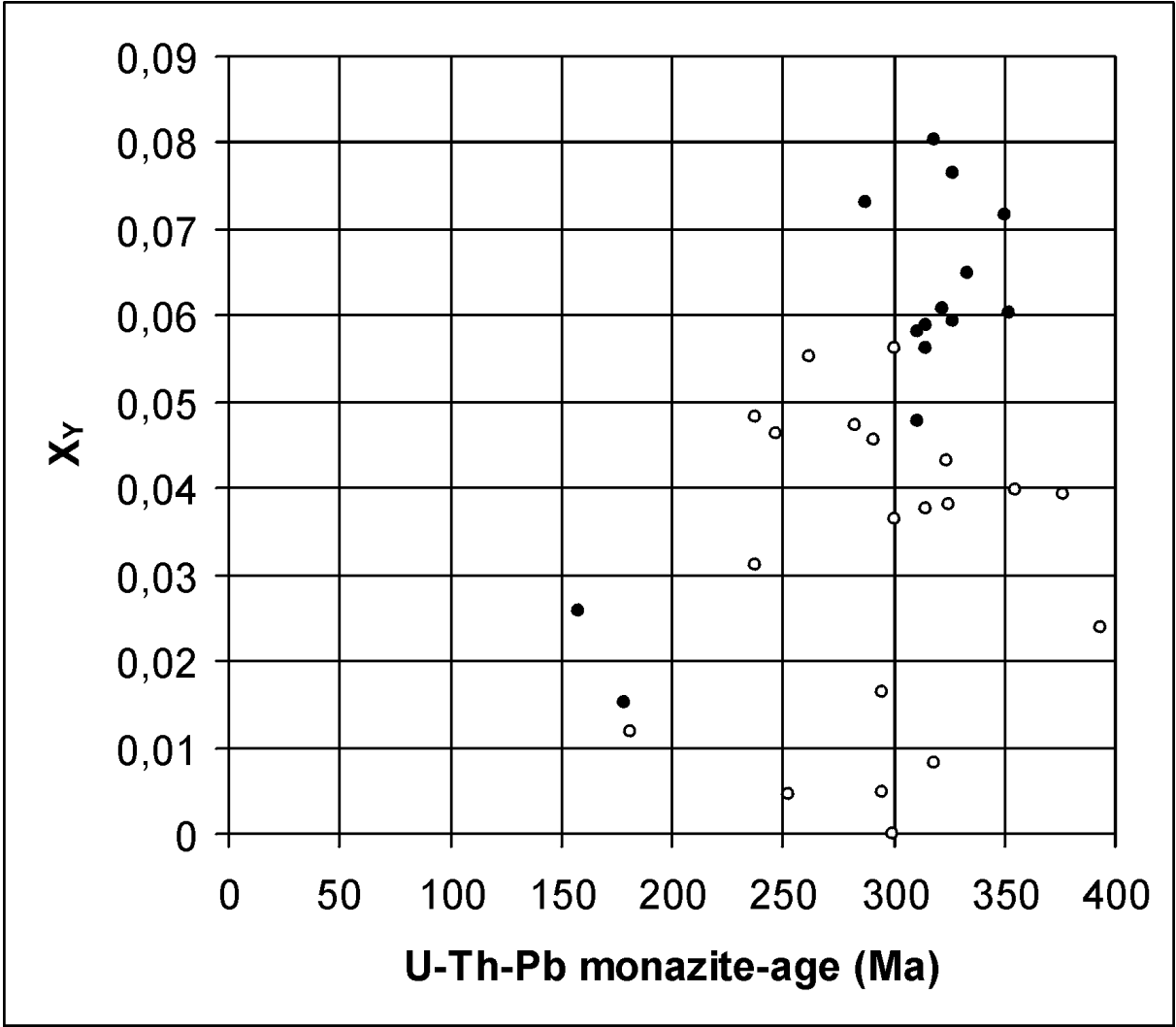
Fig. 12. Plot of monazite-age of the individual analyses versus the corresponding X_Y. The filled points represent analyses with coexistent xenotime. Two point-groups of monazite equilibrated with xenotime are identifiable, a Variscan group and a Mesozoic point group. Latter point group equilibrated at lower T.

which is the relic kyanite preserved in these rocks. More kyanite has possibly either been formed at the low-T side of the dry dehydration melting reaction of muscovite by the continuous reaction

$$grt + mu \longrightarrow bt + ky + qz \qquad (Thomson, 1982) \qquad (2)$$
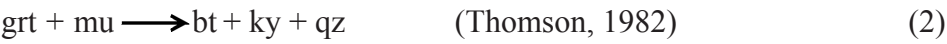
(Fig. 11c) and/or by the back-reaction of the biotite dehydration melting reaction (Fig. 11c). This second generation of kyanite has subsequently completely been removed by the retrograde reaction

$$grt + bt + as \longrightarrow st \qquad (Spear \& Cheney, 1989) \qquad (3)$$

and resulted in the characteristic staurolite crystals with garnet inclusions. The remaining included garnet fortunately remained in coexistence with staurolite, allowing application of

the garnet-staurolite thermometer of Perchuk (1969/1991). The calculated equilibration temperature is 675 ± 20 °C, indicating that these mineral compositions were frozen in immediately after completion of reaction (3) which P-T-condition in the system KFMASH (Fig.11b) was taken from Spear & Cheney (1989). This interpretation and these results indicate that lithologic variety (a) has reached conditions beyond dry muscovite dehydration melting and that a significant part of the retrograde path was at the low T-side of the dry muscovite melting reaction where the P-sensitive continuous reaction (2) (Fig. 11c) could produce significant amounts of biotite and kyanite that were used up in reaction (3).

In metagreywacke with only biotite and no white mica dehydration melting of biotite would proceed according to the reaction

$$bt\ [+ab + qz] \longrightarrow grt + m\ [+Kfs], \tag{4}$$

until the reaction

$$bt\ [+ab + qz] \longrightarrow opx + grt + m\ [+Kfs] \tag{5}$$
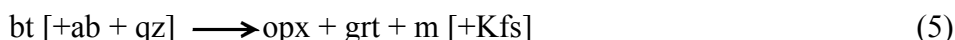
is reached.

If some white mica was originally present and pressures were below the intersection region of muscovite and biotite dehydration-melting reactions in Fig. 11c the dehydration melting reaction of this phase would have occurred before dehydration melting of biotite.

At pressures higher than the intersection region of muscovite and biotite dehydration-melting reactions in Fig. 11c, which location depends on X_{Mg} (biotite), both micas will undergo simultaneous dehydration-melting through the reaction

$$bt + mu + pl + qz \longrightarrow grt + Kfs + m\ \text{ (Le Breton & Thompson, 1988)} \tag{6}$$
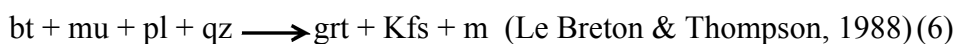
According to Le Breton & Thompson (1988) this reaction is similar to the plagioclase-free reaction sketched by Thompson (1982, Fig. 6b, reaction 49).

Due to its very low Al-content, and/or pressures higher than the intersection region of muscovite and biotite dehydration-melting reactions, the purest form of the lithologic variety (b) doesn't contain any kyanite. Kyanite is very occasionally present in few Al-richer biotite-bearing rocks of 'Gneiss di Morbegno' of lithologic variety (b), as shown in Crespi et al. (1980, their plate II). The sillimanite occurrence, observed only near 'Traona' in the 'Gneiss di Morbegno' and described by Crespi et al. (1980), is probably related to a younger intrusion (possibly similar to the one in the 'Culmine di Dazio') and according to the analyses presented here only a local feature.

Characteristics of the microfabric of lithologic variety (b) indicate that dehydration melting reactions (4) and (6) has occurred. Lithologic variety (b) of the 'Gneiss di Morbegno' has exceeded temperatures of fluid-absent dehydration melting of biotite (Fig. 4d e and f), which at <1.5 GPa (and for X_{Mg} (biotite) > 0.56) occurs at higher T than muscovite dehydration melting. The melting-related fabric was frozen, resulting in the characteristic albite-porphyroblasts that include garnet, biotite, white mica and quartz (Fig. 4d and e) surrounded by large biotite-crystals with irregularly shaped edges.

The albite porphyroblasts with included orthorhombic inclusion patterns of the fine aligned muscovite and biotite indicate that this phase is a replacement of anorthoclase and anorthite richer feldspar. Most likely K-feldspar formed by biotite-dehydration melting and was replaced by plagioclase by retrograde back-reaction. The absence of orthopyroxene and presence of biotite in all samples of lithologic variety (b) indicates that temperatures for reaction (5) were not reached.

The fabric in the albite porphyroblasts of lithologic variety (b) is very similar to the experimental products of Vielzeuf & Montel (1994; Figs. 1A-F), with the exception that the glass-phase is not existent and the space it may have occupied taken by albite and quartz. The fine garnet have inclusions of quartz, plagioclase and biotite (Fig. 4f), phases that must have been present before reaction (4) took place. Interestingly the fabric of lithologic variety (b) has close similarity with the experimental products of Vielzeuf & Montel (1994; Figs. 1E-F). This fabric has been frozen under approximate isobaric cooling at the muscovite and biotite melting reactions. According to Clemens & Droop (1998) isobaric cooling after fluid-absent melting without melt segregation at mesoscopic scale allow the melt-reactions to react back on a T-retrograde path, because melt and restite remain in intimate contact. This would lead to transitory migmatites, and would have occurred in lithologic variety (b). The coarse biotite in lithologic variety (a) is relic partly melted biotite, as the irregular rims and included garnet and K-feldspar(?) indicate. The biotite within the plagioclase could be a retrograde product related to back-reaction, following a short phase of incomplete dehydration melting. Conclusively, according to melting relations discussed by Le Breton & Thomson (1988) and Vielzeuf & Schmidt (2001) (Fig. 11c) and appearance of the run products of experiments by Vielzeuf & Montel (1994), P and T are very well constrained by the rather unobtrusive mineral paragenesis of lithologic variety (b) with the characteristic fabric.

Temperatures calculated with the calibration of Kleemann & Reinhardt (1994) for these garnet- and biotite-bearing assemblages and all other investigated equilibria are in the range 400 to 600 °C (Table II). These are retrograde temperatures because before the system was frozen in cooling was obviously too slow in relation to the rate of re-equilibration of the garnet- and biotite-phases by net exchange reactions and diffusion. In this light the small size of the individual garnets of the metagreywackes of lithological variety (b) plays an important role. It is also important whether analyses were made at the cores or close to the boundaries. Results of the garnet-phengite thermometer (Green & Helmann (1982) suggest similar limitations for this thermometer.

Biotite has probably been present in the Gneiss Chiari before dehydration melting of muscovite. Some isolated chloritised garnet crystals have been identified, representing another Mg-and Fe-bearing phase at peak Variscan conditions. Mg and Fe of this garnet and prograde metamorphic biotite are likely to have been added to white mica on the prograde path. Subsequently, during retrograde cooling trough the dry-melting curve of white mica, all biotite, the product of white mica dry melting that includes the Mg- and Fe of previously present biotite and garnet, reacted into white mica. Therefore the Si^{4+}-values (p.f.u.) of white mica would indicate quite well the pressures of retrograde back-reaction at the dry muscovite melting-curve very close to the attained peak-conditions and therefore this from phengite content inferred minimum pressure is close to the real value during peak metamorphism.

This pressure of 1,3 GPa, a value around, but nececarilly below the intersection of the biotite

and muscovite dehydration reaction curves, would be the right value to apply in the monazite-xenotime thermometer, which leads to an average temperature for the relevant analyses of 864 °C ± 64 (Table II), most likely unrealistically high.

Correction for the huttonite-content of monazite (Seydoux-Guillome et al., (in press), as was done, slightly reduces the temperatures and pressures, as listed in table II. The $ThSiO_4$-content of huttonite in monazite reduces the temperatures obtained by the monazite-xenotime thermometer of Gratz & Heinrich (1997) by approximately 1 % per mole % huttonite, as experimental data (at 0.2 Gpa) of Seydoux-Guillome et al., (in press) indicated. Monazite-xenotime thermochronometry applied on an orthogneiss sample from the Nepalese Himalya (Viskupic & Hodges, 2001) potentially indicates an even larger influence of the Th-content of monazite, which indicates the required finetuning of the monazite-xenotime thermometer.

The M_2-metamorphic conditions derived from the metapelites and metagreywackes are thus in the uppermost amphibolite facies, close to the granulite and eclogite facies. Metamorphism of mafic rocks under eclogite facies metamorphism involves some marked mineralogical changes such as the appearance of the assemblage garnet + omphacite and the disappearance of plagioclase (Fig. 11d), but these changes are not observable in the metabasites of the lower sequence of the Orobic basement and the very rare occurrences of lithologies with mafic minerals in the upper sequence. The typical minerals occurring in these metabasites of the Orobic basement are amphibole, zoisite/clinosoisite, epidote, plagioclase garnet and quartz, which according to Vielzeuf & Schmidt (2001) indicate a possible pressure-range of 1.0-1.5 GPa. In following overview of the geothermobarometric results of these metabasites are discussed. There also some emphasis is layed on the, in terms of P- and T-indicative minerals, relatively indistinctive mineralogical development.

The P and T determined for metabasites of sample 58.6b (Metabasites) do not differ much from the peak conditions obtained from the metapelites and metagreywackes. The highest P and T for metabasites were determined for this sample from the lower sequence of an amphibolite schist consisting of quartz, plagioclase, alumino-subsilicic ferro-tschermakite/ ferrian-(subcalcic-) magnesio-hornblende, epidote, zoisite, rutile and titanite, but no garnet. The P- and T-results, 1.44 Gpa ± 0.01 at 771 °C ± 2 , were calculated with the amphibole-plagioclase (+quartz) thermometer (Holland & Blundy, 1994) combined with the Al-in hornblende barometer (Anderson & Smith, 1995).

Slightly lower conditions, fitting with the retrograde path suggested for lithologic variety (a), were calculated from analyses of garnet and ferri (-subsilicic-) tschermakite from sample 34.2. The EMP-analyses were performed on garnet and amphibole of a mafic garnet-amphibolite- xenolith without plagioclase from a meta-amphibolite sill. Temperatures were calculated with the garnet-hornblende barometer of Graham & Powell (1984). The pressure from the Al in hornblende barometer of Hollister (1987) and the average pressure calculated from the calibrations of Hollister (1987), Hammarstrom & Zen (1986), Johnson & Rutherford (1989) and Schmidt (1992) lays very close to the peak-conditions determined for the metapelites and metagreywackes. Because equilibration on a retrograde path should be accounted for it is suggested that the calculated P/T conditions are related to a pre-M_2 phase, possibly a metamorphic phase predating the 'Sardic' phase.

In a sample 142.2, a variety of Gneiss Chiari containing quartz, K-feldspar, white mica, amphibole, biotite, clinozoisite with allanite cores and wherein plagioclase-clinozoisite

symplectites have developed abundantly (Fig. 4h). Similar symplectites, with plagioclase, zoisite and kyanite have been described by Ruby (1998) who relates their growth to the sudden availability of H_2O. Microprobe analyses of clinozoisite and plagioclase of indicate two populations of each mineral, the original magmatic crystals with higher anorthite content and those of the symplectites. The Fe-content of the symplectite-needles (calculated as mole % $Ca_2Al_2FeSi_3O_{12}(OH)$, abbreviated in the following as mole % Al_2Fe, calculated as Fe/(Al-2), neglecting minor components such as Cr and Mn) indicate, according to Fig. 3 of Rubie (1998) pressures at peak conditions close to 1.3 GPa, indicating the growth of these symplectites with clinozoisite-I at peak conditions, which seems very likely when the required H_2O was supplied by the dehydration of biotite of lithological variety (b), which is very abundant close to the outcrop of the rock with symplectites. Temperatures of around 750 °C seem realistic for this formation of clinozoisite I with Al_2Fe-content of ~10 mole %, according to the zoisite-clinozoisite phase realtionships of Brunsmann (2000). In this specific case, even when applying element mapping, kyanite has not been found, which according to Wayte et al. (1989) may be due to the large activation energy of this mineral at intracrystalline sites (dislocations and twin boundaries) in plagioclase in the absence of fluid.

As already stated above, clinopyroxene is not present in any of the samples, which unsurprisingly confirms that temperatures were significantly lower than the amphibolite-out. Still the rarity of garnet in the metabasites at the conditions calculated is remarkable, but not unexceptional. Vielzeuf & Schmidt (2001) reviewed numerous experimental results (for references it is referred to their publication) and concluded that the position of the garnet-in curve of the reaction

$$am + pl \longrightarrow grt + zo + qz. \tag{7}$$

varies as a function of the bulk composition and is located between 0.9 and 1.4 GPa in the temperature interval 800-1000 °C. The generally plagioclase-rich composition of the metabasites of the lower sequence of the Orobic fold-nappe might be one of the reasons, because the M_2-peak was at the high end of this pressure-range. Another important control on the first appearance of garnet is the water content, at dryer conditions garnet appears by the reaction

$$zo + am + qz \longrightarrow grt + m \, (\pm cpx), \tag{8}$$
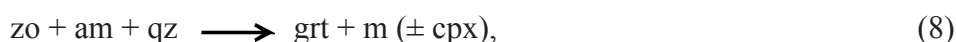
at higher T in the pressure-range between 1.0 and 2.5 GPa (Fig. 11d). The petrography and thermobarometric data of the metapelites and metagreywackes have already shown that a_{H_2O} in the melt did not exceed values of around 0.5, because dry dehydration melting of biotite and muscovite occurred.

Various stages of $M_{2/2}$ retrogression:
The further P-T path is shown in Fig. 11f and is based on the application of numerous geothermetric and geobarometric calibrations on different samples, mainly from the 'Gneiss di Morbegno'. The thermometers applied are garnet-biotite (Kleemann & Reinhardt, 1994),

garnet-phengite (Green & Hellmann, 1982) and muscovite-biotite (Hoisch, 1989). A compilation of the results, diplayed as averaged P and T values for averaged successfull combinations of geothermometer and barometer per lithologic unit, is shown in Fig. 11 a and b.

This development complies also with well constrained by the zoisite-clinozoisite phase-relationships in a pegmatite-vein in amphibole-bearing 'Filladi di Ambria', close to the metabasites.

The contact zone of this pegmatite-vein to the metabasites contains quartz, plagioclase, Al-tschermakite, M_2-garnet, biotite, clinozoisite and chlorite. The garnet-hornblende thermometer of Graham & Powell (1984) was applied in combination with the grt-pl-hbl-qz-barometer of Kohn & Spear (1990), giving a P and T well on the retrograde path at 600 °C and just below 1.0 GPa. The garnet in this sample is a higher-grade relic originally formed by reaction (8) and/or (7) and seemingly overgrew an older quartz-fabric, as indicated in the sample description. Latter and all other phase-relationships of importance for fluid-absent melting in metabasites are shown in Fig. 11d. Clinozoisite and amphibole in this pegmatite-vein are most likely a product of the retrograde back-reaction of reaction (8). Amphibole can also have been formed retrograde by the reaction (7), whereby also plagioclase would have been formed.

The vein, with clinozoisite, plagioclase, quartz, garnet, amphibole and some biotite must have formed during the earliest retrogressive phases, when the Fe-poorer clinozoisite (Al_2Fe 23.5 to 30 mole %, avg. ± 27 mole %) was formed by the back-reaction of reaction (8), after some melt had formed by this reaction on the prograde path. Relationships along $D_{2/2}$-microshearzones indicate very clearly the transformation of the primary clinozoisite to a Fe-richer clinozoisite during the deformation retrogressive $D_{2/2}$-phase of wrenching and collapse. Semi-quantitative thermobarometry could be applied to assess the conditions of the P-T development between peak conditions and the retrogressive phase of $D_{2/2}$ and during $D_{2/2}$.

First of all the range in Al_2Fe-content observed by Schmidt (1993), from 24 to 63 mole % corresponding to respective pressures of 15 and 6 ≤kbar gives some indication of the conditions to be expected in the Orobic basement. The upper pressure limit inferred corresponds thus very well with the peak-pressures (1.3 GPa) presented above for the Orobic basement. Application of the zoisite-clinozoisite phase-relationships of Brunsmann (2000) points to temperatures for the primary zoisite of around 700 °C at these peak-pressures. These phase relationships of Brunsmann (2000) indicate that the primary zoisite should be clinozoisite I. Petrographic microscopy confirms that these are orthorhombic crystals. The younger Fe-richer phase, formed by chemical transformation along fissures in the primary crystals, with Al_2Fe-contents of up to 61.4 mole % and most in the range 45 to 49 mole %, indicate pressures of approximately 10 GPa and temperatures of ~600 °C. This assessment is based on Brunsmann (2000), from which can be inferred that the new phase is clinozoisite II, as well as the ranges indicated by Schmidt (1993) and the $D_{2/2}$-phase would thus have occurred just before or when these conditions were reached. These are very similar conditions as obtained by applying grt-hbl thermometry (Graham & Powell, 1984) and grt-pl-hbl-qz geobarometry on this sample.

Application of grt-hbl thermometry (Graham & Powell, 1984) and grt-pl-hbl-qz geobarometry (Kohn & Spear, 1990) on sample 38.1, with concentrations of tschermakitic hornblende and

tschermakite surrounding garnet and as other phases present plagioclase, biotite, white mica and quartz, resulted in the same P and T as calculated for the pegmatite vein.

Another of the very few other samples of the upper sequence of the 'Orobic fold nappe' that contain amphibole is sample 142.2, a rare variety of 'Gneiss Chiari' already discussed above in connection with the peak condztions. In this sample also biotite is present. Amphibole-plagioclase thermometry and several calibrations of Al in hornblende barometry were applied, which results are listed in Table II. Application of the am-pl (+qz)-thermometer of Holland & Blundy (1994) with the Al in hbl-barometer calibration of Anderson & Smith (1995) fits best with the other data on the retrogressive part of the P-T-path listed in Table II.

Local P-T-conditions of later stages of the exhumation were calculated for late- to post-tectonic (late- to post-$M_{2/2}$) emplacement of the 'Val Biandino plutonic complex' in the parautochton. P-conditions on the retrogressive path around the Westphalian-Stephanian boundary are constrained by the occurrence of andalusite and sillimanite in the contactmetamorphic aureole of the Val Biandino intrusive complex (Pasquarè, 1967), indicating a depth of intrusion of at maximum 10-12 km (De Capitani et al., 1988). The in this study applied amphibole-barometer of Anderson & Smith (1995) and the amphibole barometer of Hollister et al. (1987) indicate pressures of 0,102 and 0,065 GPa respectively indicate a shallower intrusion level. Related temperatures in the 'Val Biandino Granodiorites' were then 729 °C, as calculated using the am-pl thermometer of Blundy & Holland (1990). The emplacement of this plutonic complex post-dates folding (Pasquarè, 1967).

Younger retrogression, either Late-Variscan or Alpine, is recorded in most exposed lithologies. At least below anchimetamorphic conditions no distinction is possible between the retrograde imprint of both orogenic phases, for which suitable geobarometers are lacking.

Mesozoic hydrothermal overprint

Different habits of monazite, resulting from different types of overprint, were identified and described above. In combination with the U-Th-Pb dating results this allows identification of suitable monazite grains to apply monazite-xenotime thermometry for calculation of temperature-conditions during Mesozoic hydrothermal overprint. The monazite-xenotime thermometer (Gratz & Heinrich, 1997) was applied on the two analyses of monazite from a composite monazite-xenotime grain of sample 82.13I for which Feijth et al. (in prep.) defined Mesozoic U-Th-Pb ages of 178 ± 93 Ma and 158 ± 59 Ma (Fig. 12). Formation of xenotime within and along the boundary of this originally Y-richer Variscan monazite grain, shown in Fig. 5f, would have been caused by concentration of Y from the original monazite in the newly grown xenotime-phase that thus most likely occurred during the Late Triassic to Jurassic.

From both respective analyses that revealed the hydrothermal age the calculated equilibration-temperatures (corrected for huttonite content) are 322 °C and 712 °C, assuming an Aalenian overburden of 9 km (P = 0.34 GPa), inferred from stratigraphic diagrams of Schönborn (1992). Latter calculated temperature is presumably less meaningful and too high. It is possible that X_Y within the grain has locally remained above equilibrium values, due to insufficient re-equilibration of internal parts of the grain during the hydrothermal phase.

As an independent check two-feldspar (K-feldspar and plagioclase) equilibration-temperatures (Stormer & Whitney, 1985) were calculated for the Gneiss Chiari and were 339

± 18 °C (see Table II) when applying an Aalenian overburden of 9 km (= 0.35 GPa) on all mineral pairs of samples 39.2 and 82.13I. The ages calculated for the individual samples are given in Table IV. These results corresponds very well with the monazite-temperature of 322 °C and explains also why the $^{40}Ar/^{39}Ar$ isotopic system of biotite was in many cases reset and white mica has Variscan ages (Feijth et al., in prep.).

8 Discussion and conclusions
8.1 Variscan development
Peak mineral assemblages and structures that formed in the prograde path, like the main foliation in the upper sequence and S_2 in the lower sequence, predate structures related to nappe-folding (Feijth, in prep. a, b). This indicates that dehydration melting at uppermost amphibolite facies conditions predates the formation of 'Orobic fold nappe'. Fortunately the age of this event could be very clearly defined, due to the fact that monazite was used for U-Th-Pb-isotopic dating by EMP (Feijth et al., in prep.) as well as for monazite-xenotime thermometry (Gratz & Heinrich, 1997), defining the peak temperatures.

Realising that start of dehydration melting occurred around the temperatures obtained by the monazite-xenotime thermometer, the age of the peak metamorphism and incipient melting can be pinpointed at 330-320 Ma (Fig. 11e). This would be the turning point to retrograde metamorphism, because the melting-phase was very short durated, too short for the melt to be segregated in the majority of the lithologies enabling (incomplete?) back reaction through the dehydration melting reactions. Dehydration melting-related structures (Fig. 2) and petrographic relationships thus suggest a sudden change; (1) in rheological behaviour and (2) from prograde metamorphism to retrogression, as soon as the conditions of fluid-absent melting in hydrous systems, with biotite, muscovite and, to a lesser extent amphibole and zoisite, were reached.

These changes are suggested not to be by pure coincidence, but there seems to be a causal relationship between the start of the short phase of dehydration melting and a sequence of events triggered as a consequence. Dehydration melting reactions of hydrous phases, in contrast to fluid-present melting have positive dP/dT slopes and are accompanied by bulk volume increase (positive $\triangle V_{melting}$) that would have been in the order of 0-20 % (Mawer et al., 1988; Clemens & Mawer, 1992). Consequently the density of the rock lowers, which creates gravitational instability and initiates buoyancy. A change in rheological properties has occurred simultaneously, whereby the rock became more ductile. Additionally the melting of phyllosilicates reduces the fabric anisotropy (Weber, 1986). The combined effect would have been the growth of a diapiric ridge, initially brachyanticlinal-shaped in profile. Fig. 2 of Perchuk & Geyra (1998) shows a development similar to the probable first stages of the formation of the 'Orobic fold nappe'. Amplification of such large-scale fold structures will cause piercing of the overlying crust in the form of a large 'injective' fold (Weber, 1986; Perchuk et al., 1992; Perchuk & Geyra, 1998), like the granulite facies concentric domes in N. China described by Dirks et al. (1997). Simultaneously active tectonic shortening would produce granulite facies asymmetrical fold-structures or nappes (Weber, 1986) or, like in this case of uppermost amphibolite facies metamorphism the formation of the 'Orobic fold nappe'. Because dry melting is a slow endothermic reaction freezing in is sensitive to P or T changes. The formation of the 'Orobic fold nappe', marks the initiation of retrogression and freezing

in, thus before significant segregation and separation of melt beyond micro- to mesoscale could occur in the bulk of the exposed lithologies. Feijth (in prep. b) gives structural details on the development of this structure in the Orobic basement and its further development. As Variscan peak-conditions were reached before development of the 'Orobic fold nappe' one could argue why no folded isograds and inverted metamorphic gradient have been recognised. This can be explained with the scale of the 'Orobic fold nappe' and the thickness of the folded sequence. The initial thickness of the sequence of the 'Orobic fold nappe' of up to around 5000 m was too small to identify any isograds in the field. Additionally, dealing with uppermost amphibolite facies metamorphism close to granulite- and eclogite facies conditions, one would be surprised to expect any important identifiable isograds. Variability of bulk chemistry of the rocks or variation of a_{H_2O} would have an as much as large effect on petrographic relationships.

The upper limits of a_{H_2O} and metamorphic conditions have been attempted to be constrained. Values of a_{H_2O} close to unity would have caused much more migmatites and melts by fluid present melting reactions than observed. Values of a_{H_2O} at peak P and T were assessed with the internally consistant thermodynamic dataset of Holland & Powell (1990). The determined conditions near the intersection of the dehydration reaction curves of biotite and white mica require values of a_{H_2O} allmost as low as those applied and shown in Table II. Slightly higher values would be allowed for the metamorphic peak, because the values of a_{H_2O} indicated in Table II refer to the conditions forming the present assemblage on the retrograde path, where H_2O might have been consumed by the formation of the hydrous phases white mica and biotite. In the lower sequence of the 'Orobic fold nappe', these dry conditions can be related to the older 'Sardic' metamorphic phase, which would have caused dehydration of the rock. Higher-grade metamorphic conditions would have caused: (1) the dehydration reactions of white mica and biotite to have proceded much further, and (2) typical eclogite facies assemblages in the metabasites, particularly in the lower sequence of the 'Orobic fold nappe'. Both of these metamorphic fabrics or assemblages have not been observed. A temperature-limit is given by the clinozoisite bearing pegmatite veins, occuring near the metabasites (e.g. sample 40.9A). Formation of such veins is typical of conditions of at least upper amphibolite facies around 650 - 700 °C (Fig. 11d).

This development of a diapiric ridge by gravitational instability, and followed by nappe-folding and collapse is very well compatible with the identified Variscan structural configuration in the Orobic Chain, with a high-grade fold nappe overlying a relatively low grade 'parautochton' and an extensional 'drop-fault' as contact between 'infrastructure' and lower grade 'suprastructure'. The diapiric rise and particularly the tectonic extrusion of the initial nappe-structure would have brought the relatively high grade 'Orobic fold nappe' in contact with the 'parautochton'.

Spalla et al. (1999), who reconstructed the tectonometamorphic development of another area in the then not yet identified 'Orobic fold nappe', have concluded that the development of the Orobic basement is a single, temperature-prograde polyphase event. Having worked in an area in the lower sequence of the 'Orobic fold nappe', they identified two metamorphic assemblages. Their prograde Variscan assemblage cld+bt$_I$+grt+ ms$_I$+pl+qtz was interpreted to be formed at 480-540 °C / 0.75-0.95 GPa, whereas the assemblage st+bt$_{II}$+grt+ms$_{II}$+pl+qtz

marks the Variscan peak at 570-660 °C / 0.85-1.15 Gpa, followed by greenschist retrogression. Their prograde Variscan assemblage would correspond to the 'Sardic' phase in this paper, whereas their peak-Variscan assemblage geochronologically corresponds. Chlorotoid was preserved by deformation partitioning would have been preserved by the deformation partitioning as suggested by Spalla et al. (1999) and other chloritoid crystals are also preserved within garnet crystals. It could also be suggested that conditions would have been dryer within the microlithons, as opposed to along the foliation planes that formed at peak conditions.

The 'Val Biandino plutonic complex' intruded at 307-271 ± 9 Ma (De Capitani et al., 1988) after the event of nappe folding, because intrusions are at places, especially at the apophyses, discordant to folded layering of the host rock and generally conformable (De Capitani et al., 1988). This occurred after tectonic emplacement of the 'Orobic fold nappe' on the parautochton. Parts of the 'Val Biandino plutonic complex' have been found subcropping below the volcano-sedimentary succession of the 'Collio-Orobico basin' and clasts of these plutonic rocks are present in the alluvial fan conglomerates of the Lower Permian 'Ponteranica' formation, that is part of this volcano-sedimentary succession.

8.2 Mesozoic hydrothermal phase

Hydrothermal overprint at ~335 °C confirms that the investigated part of the Orobic chain forms part of the hanging wall of the 'Lugano-Val Grande fault'. Sillimanite formed during LPHT metamorphism of the footwall (Diella et al., 1992) of up to 500 to 700 °C Bertotti et al. (1999) and greenschist mylonites to cataclasites occur in the fault zone (Bertotti et al., 1999). However temperatures are significantly higher than the 200-250 °C calculated by Bertotti et al. (1999) for the immediate hanging wall of the 'Lugano-Val Grande fault'. Also timing of the activity of this fault-system (Bertotti et al., 1999) is compatible with the age of the hydrothermal overprint, dated by the U-Pb-Th-method on monazite (Feijth et al., in prep.). The thermal gradient calculated from the geothermometric results and the thickness of the Aalenian overburden was 39 °C km^{-1}, falling exactly in the middle of the range between 20 and 60 °C km^{-1} calculated by Bertotti et al. (1999) for this event. This would have been a typical metamorphic development of the hanging walls of the rift-faults of the 'Lombardian basin', because the investigated area is situated in the hanging wall of opposite-dipping sets of rift faults, in the west the 'Lugano-Val Grande'- and 'Lago Maggiore faults' and in the east the 'Sebino'- and 'Garda faults'.

APPENDIX 2.1

Representative electron microprobe analyses

Garnet (O=12)

	Metabasites, (xenolith)		Filladi di Ambria		GOOV		Gneiss di Morbegno						Paragneisses, phyllites & schists	
							Lith. var. (a)			Lith. var.(b)				
Anal. No.	34.2-5 grt1	34.2-6 grt2	40.9-A-grt4	40.9-A-grt5	33.6/2-3-grt1	69.2a-1-grt2	31.7a5-3-grt2	31.7a5-4-grt4	31.7-a6-grt1	92.2-1-grt1	92.2-2-grt2	92.2-2-grt3	38.1-1a-3-grt1	65.5aII-4-grt1
SiO_2	37,65	38,66	38,16	38,21	37,64	38,24	37,46	37,68	38,28	37,17	37,54	37,42	38,39	37,46
TiO_2	0	0,19	0,10	0,07	0,13	0,01	0	0,01	0,07	0,11	0,01	0,02	0,02	0,06
Al_2O_3	21,97	22,36	21,86	21,66	21,69	21,38	21,41	21,85	21,68	21,44	21,97	21,88	22,05	21,58
Fe_2O_3	0,23	0,22	0	0	0	0,83	0	0	0	0	0	0	0,46	0
FeO	29,51	23,91	25,22	26,46	29,93	18,29	36,67	31,69	30,84	33,07	33,55	33,84	27,90	31,53
MnO	1,62	1,00	4,20	3,63	1,13	4,22	3,06	2,36	0,25	2,74	2,88	2,93	1,22	0,34
MgO	5,34	8,37	2,53	2,53	0,82	0,39	3,38	0,76	2,42	2,92	2,83	2,65	2,88	1,21
CaO	3,85	5,42	8,11	7,79	9,67	18,29	2,62	0,70	7,11	3,03	2,67	2,68	9,44	7,94
Total	100,17	100,13	100,18	100,35	100,99	101,14	100,60	100,97	100,64	100,49	101,46	101,41	102,33	100,12
Si	2,96	2,96	3,01	3,01	2,98	2,98	2,99	2,98	3,02	2,97	2,97	2,97	2,97	2,99
Al^{IV}	0,04	0,04	0	0	0,02	0,02	0,01	0,02	0	0,03	0,03	0,03	0,03	0,01
Al^{VI}	2,00	1,99	2,03	2,01	2,01	1,95	2,00	2,02	2,01	2,00	2,02	2,02	1,98	2,03
Cr	0	0	0	0	0	0	0	0	0	0	0	0	0	0
Fe^{3+}	0,01	0,01	0	0	0	0,05	0	2,35	0	0	0	0	0,03	0
Ti	0	0,01	0,01	0	0,01	0	0	0	0	0	0	0	0,01	0
Mg	0,63	0,96	0,30	0,30	0,10	0,05	0,40	0,38	0,28	0,35	0,33	0,31	0,33	0,14
Fe^{2+}	1,94	1,53	1,66	1,75	1,98	1,19	2,18	2,10	2,03	2,21	2,22	2,25	1,81	2,11
Mn	0,11	0,07	0,28	0,24	0,08	0,28	0,21	0,16	0,02	0,19	0,19	0,20	0,08	0,02
Ca	0,33	0,45	0,69	0,66	0,82	1,48	0,22	0,35	0,60	0,26	0,23	0,23	0,78	0,68
Total	8,01	8,01	7,97	7,98	8,00	8,00	8,01	8,00	7,97	8,01	8,00	8,00	7,98	7,99
Uv.	0	0	0	0	0	0	0	0	0	0	0	0	0	0
Ad.	1	1	0	0	0	3	0	0	0	0	0,03	0	1	
Gr.	10	14	23	22	27	47	7	12	20	8	7,59	8	25	23
Al.	65	51	57	59	67	40	72	70	69	74	74,67	75	60	71
Sp.	4	2	10	8	3	9	7	5	1	6	6,50	7	3	1
Py.	21	32	10	10	3	2	13	13	10	12	11,22	10	11	5

Biotite (O=22)
Gneiss di Morbegno

Anal. No.	GOOV			Lith. var. (a)			Lith. var. (b)			Paragneisses, phyllites & schists			Val Biandino granodiorites	
	32.4-3-bt1	33.6-2-bt2	33.6 rand-9-bt2	91.2a-5-bt2	91.2a-6-bt1	91.2a-6-bt5	92.2-1-bt2	92.2-3-bt3	94.2-8-bt1	38.1-1a-1-bt4	65.5aI-2-bt3	98.2-1-12-bt10	71.5b-2-bt2	71.5b-6-bt2
SiO_2	34,67	35,78	36,46	35,00	35,57	35,39	36,82	34,65	35,80	37,65	36,41	36,26	37,69	37,44
TiO_2	2,08	1,80	2,00	1,63	1,96	1,79	1,80	1,94	2,17	1,54	1,63	1,59	3,55	3,48
Al_2O_3	19,18	18,47	18,20	18,72	19,60	19,13	18,99	19,40	19,21	17,62	18,33	18,96	14,66	14,73
FeO	25,09	23,52	21,94	20,62	19,08	19,81	18,39	21,12	20,41	16,09	20,78	15,46	20,17	20,23
MnO	0,07	0,14	0,22	0,11	0,11	0,11	0,04	0,05	0,15	0,09	0,05	0,04	0,21	0,32
MgO	6,70	7,89	7,78	9,57	9,33	9,11	10,77	10,81	9,67	12,67	10,07	13,09	11,75	11,49
CaO	0,08	0,07	0,03	0	0,01	0	0	0,01	0	0,04	0,11	0	0	0,08
Na_2O	0,08	0,06	0,14	0,17	0,17	0,15	0,08	0,07	0,22	0,07	0,10	0,14	0,12	0,12
K_2O	9,73	8,95	9,41	8,80	0,65	9,54	8,85	8,28	8,67	9,48	7,93	8,96	9,10	8,79
F-	0	0	0	0	0	0	0	0	0	0	0	0,012	0,005	0,008
Total	97,74	96,67	96,20	94,65	95,48	95,05	95,73	96,33	96,30	95,25	95,42	97,35	97,65	96,92
Si	5,30	5,46	5,55	5,39	5,40	5,42	5,51	5,23	5,39	5,62	5,51	5,39	5,63	5,62
Al^{IV}	2,70	2,54	2,45	2,61	2,60	2,59	2,49	2,77	2,61	2,38	2,49	2,61	2,37	2,38
Sum^{IV}	8,00	8,00	8,00	8,00	8,00	8,00	8,00	8,00	8,00	8,00	8,00	8,00	8,00	8,00
Al^{VI}	0,76	0,77	0,82	0,78	0,90	0,87	0,85	0,69	0,80	0,72	0,78	0,72	0,21	0,23
Ti	0,24	0,21	0,23	0,19	0,22	0,21	0,20	0,22	0,25	0,17	0,19	0,18	0,40	0,39
Fe^{2+}	3,21	3,00	2,80	2,66	2,42	2,54	2,30	2,67	2,57	2,01	2,63	1,92	2,52	2,54
Mn	0,01	0,02	0,03	0,01	0,01	0,02	0,01	0,01	0,02	0,01	0,01	0,01	0,03	0,04
Mg	1,53	1,79	1,77	2,20	2,11	2,08	2,40	2,43	2,17	2,82	2,27	2,90	2,62	2,57
Sum^{VI}	5,75	5,79	5,64	5,84	5,67	5,70	5,76	6,01	5,80	5,74	5,87	5,73	5,78	5,79
Ca	0,01	0,01	0,01	0	0	0	0	0	0	0,01	0,02	0	0	0,01
Na	0,02	0,02	0,04	0,05	0,05	0,04	0,02	0,02	0,06	0,02	0,03	0,04	0,04	0,04
K	1,90	1,74	1,83	1,73	1,87	1,86	1,69	1,60	1,67	1,81	1,53	1,70	1,73	1,68
Total	15,69	15,56	15,52	15,62	15,59	15,61	15,47	15,63	15,53	15,57	15,45	15,64	15,56	15,53
XFe	0,68	0,63	0,61	0,55	0,53	0,55	0,49	0,52	0,54	0,42	0,54	0,40	0,49	0,50

White mica (O=22)
Gneiss di Morbegno

Anal. No.	GOOV		Lith. var. (a)		Lith. var.(b)		Paragneisses, phyllites & schists			Gneiss Chiari		Scisti di Edolo	
	33.6/2-1-mu2	33.6rand-8-mu4	92.2-5-mu1	92.2-5-mu3	94.2-5-mu3	31.7a5-3-mu1	31.7a5-7-mu4	38.1-4-mu1	48.10-3-mu2	98.2-1-8-mu3	39.2-4-mu8	82.13I-2-mu5	SdE-1-mu1	SdE-5-mu3
SiO_2	47,06	48,51	49,11	47,87	46,53	46,18	46,23	45,98	49,98	46,72	50,43	52,63	49,24	49,12
TiO_2	0,48	0,61	0,62	0,71	0,72	0,48	0,21	0,47	0,35	0,46	0,10	0,23	0,39	0,21
Al_2O_3	34,09	33,33	34,37	36,03	36,61	36,49	36,93	35,81	29,45	35,43	27,75	30,63	31,41	32,36
FeO	1,82	2,42	1,23	1,08	1,24	0,89	0,87	0,94	1,96	0,79	5,52	4,94	3,07	2,60
MnO	0	0,04	0	0,02	0	0,05	0	0,03	0,01	0,01	0,11	0,08	0	0,03
MgO	1,17	1,48	1,33	0,87	0,80	0,54	0,48	0,87	2,54	1,01	0,98	1,04	1,62	1,38
CaO	0,01	0,03	0,03	0,01	0,02	0,04	0	0,02	0	0,03	0,04	0,09	0	0,05
Na_2O	1,20	0,59	1,16	1,37	1,12	1,83	1,82	0,93	0,86	1,83	0,27	0,12	0,20	0,46
K_2O	9,25	10,79	9,31	9,01	8,81	8,87	7,83	9,46	8,95	8,57	10,57	6,05	9,89	9,73
F-	0	0	0	0	0	0	0	0	0	0	0	0	0	0
Total	95,07	97,79	97,16	96,96	95,86	95,36	94,38	94,50	94,09	94,85	95,77	95,80	96,19	96,14
Si	6,26	6,33	6,36	6,20	6,10	6,10	6,12	6,13	6,68	6,18	6,79	6,83	6,52	6,48
Al^{IV}	1,74	1,67	1,65	1,80	1,90	1,90	1,88	1,87	1,32	1,82	1,21	1,17	1,48	1,52
Sum^{IV}	8,00	8,00	8,00	8,00	8,00	8,00	8,00	8,00	8,00	8,00	8,00	8,00	8,00	8,00
Al^{VI}	3,60	3,46	3,77	3,70	3,76	3,77	3,88	3,76	3,33	3,71	3,20	3,51	3,41	3,51
Ti	0,05	0,06	0,05	0,07	0,07	0,05	0,02	0,05	0,04	0,05	0,01	0,02	0,04	0,02
Fe^{2+}	0,20	0,26	0,10	0,12	0,14	0,10	0,10	0,10	0,22	0,09	0,62	0,54	0,34	0,29
Mn	0	0	0,01	0	0	0,01	0	0	0	0	0,01	0,01	0	0
Mg	0,23	0,29	0,11	0,17	0,16	0,11	0,10	0,17	0,51	0,20	0,20	0,20	0,32	0,27
Sum^{VI}	4,08	4,07	4,05	4,06	4,12	4,03	4,09	4,08	4,07	4,04	4,04	4,28	4,12	4,09
Ca	0	0	0,01	0	0	0,01	0	0	0	0	0,01	0	0	0,01
Na	0,31	0,15	0,47	0,34	0,29	0,47	0,47	0,24	0,22	0,47	0,07	0,03	0,05	0,12
K	1,57	1,80	1,49	1,49	1,47	1,49	1,32	1,81	1,53	1,45	1,82	1,00	1,67	1,64
Total	13,96	14,02	13,88	13,89	13,88	14,00	13,95	13,93	13,93	13,97	13,94	13,32	13,85	13,09
Si^{4+} p.f.u.	3,13	3,17	3,05	3,10	3,05	3,05	3,06	3,07	3,34	3,09	3,40	3,41	3,26	3,24

Staurolite (O=48)

Gneiss di Morbegno Lith. var. (b)

Anal. No.	31.7a5-3-st1	31.7a6-st1
SiO_2	28,39	28,45
TiO_2	0,587	0,600
Al_2O_3	56,05	55,43
FeO	12,33	11,93
ZnO	0,59	0,57
MnO	0,22	0,23
MgO	1,14	1,25
Na_2O	0,05	0,02
K_2O	0	0
Total	99,35	98,49
Si	8,04	8,12
Al^{IV}	0,31	0,23
Al^{VI}	18,41	18,40
Ti	0,13	0,13
Mg	0,48	0,53
Fe^{2+}	2,92	2,85
Mn	0,053	0,06
Zn	0,12	0,12
Total	30,49	30,44
XMg	0,14	0,16

Amphibole (O=23)

	Metabasites (xenolith)		Metabasites		Filladi di Amb.	Gn. di Morb. Paragn	Val Biandino granodiorites	
Anal. No.	34.2-1 am5	34.2-6 am3	58.6b-1-am4	58.6b-1-am6	40.9-A-am2	38.1-1a-3-am2	71.5a-6-am5	71.5a-1-am3
SiO_2	39,60	39,76	46,90	44,36	43,14	42,76	49,73	48,30
TiO_2	1,26	1,46	0,26	0,29	0,39	0,54	0,58	0,66
Al_2O_3	18,05	17,33	10,14	12,64	17,61	17,97	6,02	5,87
Cr_2O_3	0	0	0	0	0	0	0,02	0,06
Fe_2O_3	12,72	15,41	17,30	8,11	4,19	5,37	10,10	6,33
FeO	1,18	0	2,50	9,06	10,69	9,51	7,56	10,56
MnO	0,06	0,12	0,41	0,19	0,17	0,10	0,40	0,38
MgO	12,11	12,03	11,25	10,73	8,89	9,25	12,70	12,07
ZnO	0	0	0,02	0,02	0,01	0,06	0	0
CaO	10,65	9,63	8,50	11,04	10,79	10,94	10,12	10,74
Na_2O	1,80	1,53	1,43	1,64	1,85	1,72	0,87	0,86
K_2O	0,75	0,73	0,25	0,33	0,37	0,41	0,51	0,55
F-	0,002	0,012	0	0	0	0	0,023	0
Total	100,28	100,16	101,07	100,46	100,71	100,17	100,88	98,63
Si	5,69	5,71	6,68	6,46	6,16	6,25	7,15	7,16
Al^{IV}	2,31	2,29	1,32	2,17	1,84	1,75	0,85	0,84
Al^{VI}	0,75	0,65	0,38	1,54	1,21	1,26	0,17	0,19
Ti	0,14	0,16	0,03	0,03	0,06	0,04	0,06	0,07
Fe^{3+}	1,38	1,67	1,85	0,89	0,58	0,46	1,90	0,71
Fe^{2+}	0,14	0	0,30	1,10	1,15	1,30	0,91	1,31
Mn	0,01	0,01	0,05	0,02	0,02	0,01	0,05	0,05
Mg	2,59	2,58	2,39	2,33	1,99	1,92	2,72	2,67
Zn	0	0	0	0	0,01	0	0	0
Ca	1,64	1,48	1,30	1,72	1,69	1,68	1,56	1,71
Na	0,50	0,43	0,39	0,46	0,48	0,52	0,24	0,25
K	0,14	0,13	0,05	0,06	0,07	0,07	0,09	0,10
F	0	0,01	0	0	0	0	0,01	0
Total	17,28	17,11	16,74	17,25	17,24	17,26	16,90	17,07

Pyroxene (O=6)

Val Biandino granodiorites

Anal. No.	71.5b-3-cpx1	71.5b-4-opx3
SiO_2	53,32	55,02
TiO_2	0,02	0,29
Al_2O_3	0,46	0,68
Cr_2O_3	0	0,07
MgO	12,19	16,09
CaO	21,66	2,14
MnO	0,62	1,22
FeO	11,45	24,53
Na_2O	0,22	0,07
K_2O	0,06	0,03
Total	100,00	100,13
Si	2,01	2,07
Ti	0	0,01
Al	0,02	0,03
Cr	0	0
Mg	0,69	0,90
Ca	0,87	0,09
Mn	0,02	0,04
Fe^{2+}	0,36	0,77
Na	0,02	0,01
K	0	0
Total	3,99	3,91
XMg	0,66	0,54

			Plagioclase (O=8) Gneiss di Morbegno						Albit (O=8)		K-feldspar (O=8)			
	Meta-basites	GOOV	Lith. var. (a)		Lith. var.(b)	Paragneisses, phyllites & schists	Gneiss Chiari	Val B. gran. (magm HT plag.)	GOOV		Gneiss Chiari		Val Biandino granodiorites	
Anal. No.	58.6b-1-pl5	33.6/2-2-pl2	92.2-4-pl1	94.2-6-pl2	31.7a5-5-pl3	98.2-2-7-pl4	39.2-8-pl4	71.5a-6-pl2	33.6/2-3-kf2	33.6/2-3-kf3	39.2-2-kf1	39.2-4-kf2	71.5a-3-kf2	71.5a-3-kf3
SiO$_2$	68,15	64,76	61,46	63,75	62,38	61,77	68,06	55,70	67,82	68,346	65,27	64,46	66,24	66,08
Al$_2$O$_3$	19,95	22,32	24,29	23,60	23,36	23,44	20,42	28,29	20,02	20,32	18,68	18,54	18,88	19,16
MgO	0	0	0	0,02	0	0,01	0,02	0,01	0	0,01	0	0	0	0
CaO	0,37	2,66	4,78	3,88	4,26	4,71	0,61	10,42	0,45	0,52	0,03	0	0,15	0,06
MnO	0	0	0	0,01	0	0	0	0,07	0	0,03	0	0	0,03	0
FeO	0	0,07	0,08	0,06	0,08	0,07	0,03	0,13	0,08	0,10	0	0	0,04	0,02
BaO	0	0	0	0	0	0	0	0	0	0	0	0	0,26	0,88
Na$_2$O	11,11	10,30	9,05	9,55	9,31	9,00	10,43	4,93	11,83	11,85	0,24	0,54	1,54	1,23
K$_2$O	0,05	0,06	0,08	0,06	0,12	0,05	0,11	0,28	0,05	0,04	15,82	16,23	13,53	14,13
Total	99,63	100,17	99,74	100,94	99,52	99,03	99,67	99,82	100,25	101,22	100,04	99,78	100,67	101,56
Si	2,98	2,85	2,73	2,79	2,78	2,76	2,97	2,51	2,96	2,96	3,00	2,99	3,01	2,99
Al	1,03	1,16	1,27	1,22	1,23	1,24	1,05	1,50	1,03	1,04	1,01	1,01	1,01	1,02
Ca	0,02	0,13	0,23	0,18	0,20	0,23	0,03	0,50	0,02	0,02	0	0	0,01	0
Ba	0	0	0	0	0	0	0	0	0	0	0	0	0,01	0,02
Na	0,94	0,88	0,78	0,81	0,80	0,78	0,88	0,43	1,00	1,00	0,02	0,05	0,14	0,11
K	0	0	0,01	0	0,01	0	0,01	0,02	0	0	0,93	0,96	0,79	0,82
Total	4,98	5,01	5,02	5,01	5,02	5,01	4,95	4,97	5,02	5,02	4,97	5,01	4,95	4,96
Ab	98	87	77	81	79	77	96	45	98	97	2	5	15	11
An	2	12	22	18	20	22	3	53	2	2	0	0	1	0
Or	0	0	0	0	1	0	1	2	0	0	98	95	84	87

	Clinozoisite (O=25) Pegmatite vein in Filladi di Ambria	
Anal. No.	40.9a-3-Ep3	40.9a-3-Ep9
SiO$_2$	39,46	38,54
TiO$_2$	0,10	0,17
Al$_2$O$_3$	31,30	27,04
Fe$_2$O$_3$	4,72	10,51
MgO	0,08	0,01
CaO	24,39	24,59
MnO	0,32	0,27
Na$_2$O	0,01	0,03
K$_2$O	0	0,01
Total	99,91	100,10
Si	5,93	5,89
Ti	0,01	0,02
Al	5,55	4,87
Fe^{3+}	0,53	1,21
Mg	0,02	0
Ca	3,93	4,03
Mn	0,04	0,04
Total	16,02	16,06
X$_{Ps}$	0,09	0,20
Al$_2$Fe (mole %)	27	61

Chapter 3

Geochronology of the Orobic Alps (Lombardy, Italy): (I) Evolution of the basement, constrained by U-Th-Pb-ages of monazite and ^{40}Ar/^{39}Ar-ages of biotite and muscovite

Abstract

Radiometric dating of Palaeozoic metamorphic and tectonic events of the basement of the Orobic Alps (Central Southern Alps, Lombardy, Italy) was carried out. This basement consists of the 'Orobic fold nappe', overlying a parautochton. These units together form an infrastructure that is separated from the suprastructure, consisting of 'Scisti di Edolo', by a Variscan normal fault. The two sequences of the 'Orobic fold nappe' can be seen as different tectonic units separated by a tectonically reactivated unconformity. The lower sequence, which includes metabasites that were deposited as extrusive volcanics and intruded by amphibolite sills, was affected by a tectono-metamorphic phase (M_1/D_1), followed by intrusion of granodiorites ('Gneiss Occhiadini Orobico-Valtellinese') and a second tectono-metamorphic phase (M_2/D_2). The upper sequence consists of volcano-sedimentary complexes related to a phase of rhyolitic volcanism. It is made up of 'Gneiss Chiari' meta-rhyolites and the related meta-volcano-sedimentary 'Gneiss di Morbegno'. The first tectono-metamorphic phase to affect the upper sequence was M_2/D_2, of uppermost amphibolite facies grade (750 °C/ ≤ 1.3GPa).

Structural and metamorphic relationships indicate that the formation of the 'Orobic fold-nappe' and related cooling occurred immediately after the peak P and T were reached. The age of peak-conditions of this phase is constrained by the U-Th-Pb-dating on monazite. Monazite was found in the upper sequence, in meta-psammites and -pelites of the 'Gneiss di Morbegno' and the meta-rhyolitic 'Gneiss Chiari'. This monazite provided an age of 330-320 Ma. At 325-305 Ma the 'Orobic fold-nappe' cooled below the closure temperature of white mica, as the results of the ^{40}Ar/^{39}Ar-multigrain step heating method applied on samples of 'Gneiss Occhiadini Orobico-Valtellinese' ('GOOV'), the 'Gneiss di Morbegno' and 'Gneiss Chiari' show. No isotopic ages of the earlier Palaeozoic event were obtained, but the identified equivalence of the lower sequence to the 'Scisti dei Laghi sequence' of the 'Strona-Ceneri Zone', from where isotopic data are available, proved to be useful. Based on this correlation, the pre-Variscan metamorphic and following late- to post-orogenic igneous phase of the 'Gneiss Occhiadini Orobico-Valtellinese' in the lower sequence would be related to respective metamorphic and igneous phases of the Ordovician 'Sardic' event in the Middle to Late Ordovician. Also the protoliths of 'Gneiss Chiari' and 'Gneiss di Morbegno' can be related to the widespread post-Caradocian rhyolitic volcanism in the southern and eastern Alps, which would be related to the formation of an active marginal basin related to the 'Sardic' event. ^{40}Ar/^{39}Ar-multigrain step heating-results of all biotite- and only some white mica samples indicate Middle Permian and Mesozoic hydrothermal phases. The Permian hydrothermal phase is related to late volcanic activity of the Collio basin. The Mesozoic hydrothermal phase, related to a combination of Ladinian magmatic activity and Ladinain to Liassic rifting, has re-equilibrated the U-Th-Pb system of monazite at ~322 °C, as revealed by monazite-xenotime thermometry on samples of 'Gneiss Chiari'.

1 Introduction

In the Orobic chain, the Central part of the Italian Southern Alps (Fig. 1), the Palaeozoic depositional, structural and metamorphic sequence of the basement was analysed to identify the tectono-metamorphic development (Feijth, in prep. a, b; Feijth & Franz, in prep.). Relative ages of the identified Palaeozoic tectonic and metamorphic phases have been assigned in the Orobic Chain, based on structural, metamorphic and igneous relationships in meta-volcanic and meta-sedimentary sequences of different age and structural units.

Radiometric ages of the Palaeozoic orogenic phases are presented here. The U-Th-Pb method on monazite by electron microprobe, was applied to date metamorphic- and young metasomatic phases. Furthermore $^{40}Ar/^{39}Ar$-cooling-ages of white mica and biotite from the Orobic basement units were determined.

Correlation with other Southalpine and Austroalpine units was required to complete the geochronological interpretation, particularly for the pre-Variscan metamorphic- and igneous development.
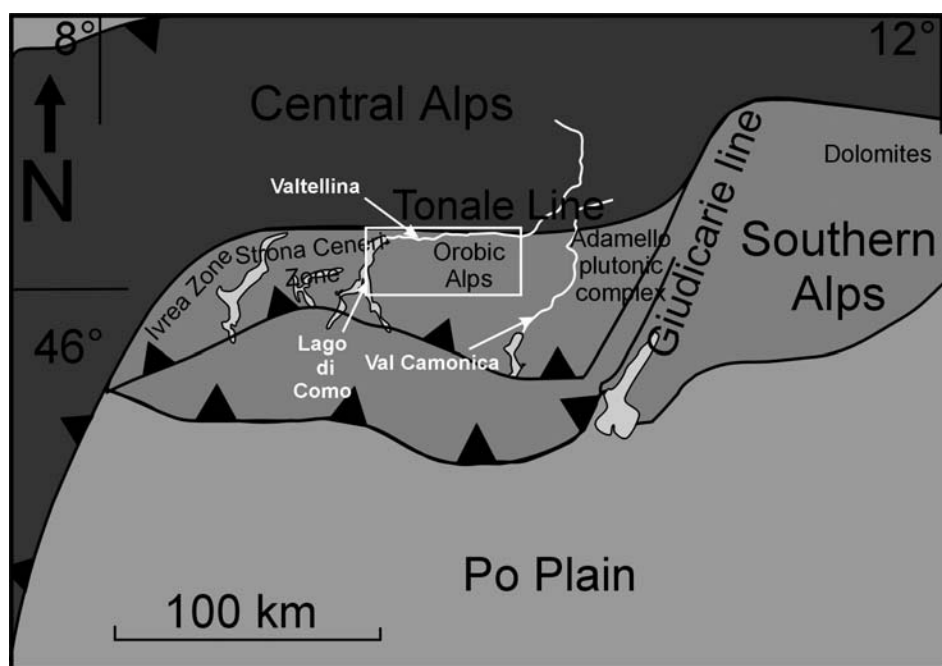
Fig. 1. Location of the investigated area in the Orobic Alps.

Areas of Permo-Triassic to Liassic rifting, as identified in the 'Lario basement', the western sector of the Orobic Alps (Diella et al., 1992; Bertotti et al., 1993, 1999), were avoided in this study as far as field-identification allowed. The tectonic units selected for this study, the 'Orobic fold nappe' and the parautochton, correspond by approximation to the Alpine 'San Marco'- and 'Mezzoldo Units' of Schönborn (1990, 1992, 1994) and Schumacher et al. (1997) (Fig. 2).

Compared to the Central Alps, the Alpine and Mesozoic metamorphic overprint of the Orobic Southern Alps is relatively weak (Bocchio et al., 1981; Crespi et al., 1981; 1982; Diella et al., 1992; Schönborn, 1992; Carminati, 1992, 1997; Albini et al., 1994; Spalla et at., 1999), which makes this zone well suited to identify the Palaeozoic tectono-metamorphic development. Although this conclusion still holds, some Alpine and Mesozoic ages were obtained and the Alpine overprint is discussed in Feijth & Neubauer (in prep. b).

Fig. 2. Simplified geological map of the Orobic Alps showing only the main Alpine faults. The area selected for this study is located East of the line Pizzo Slavello-Monte Rotondo-P. Melasc. For the Variscan and Permian structures see Feijth (in prep. a.). Location of sampling locations are indicated according to the legend.
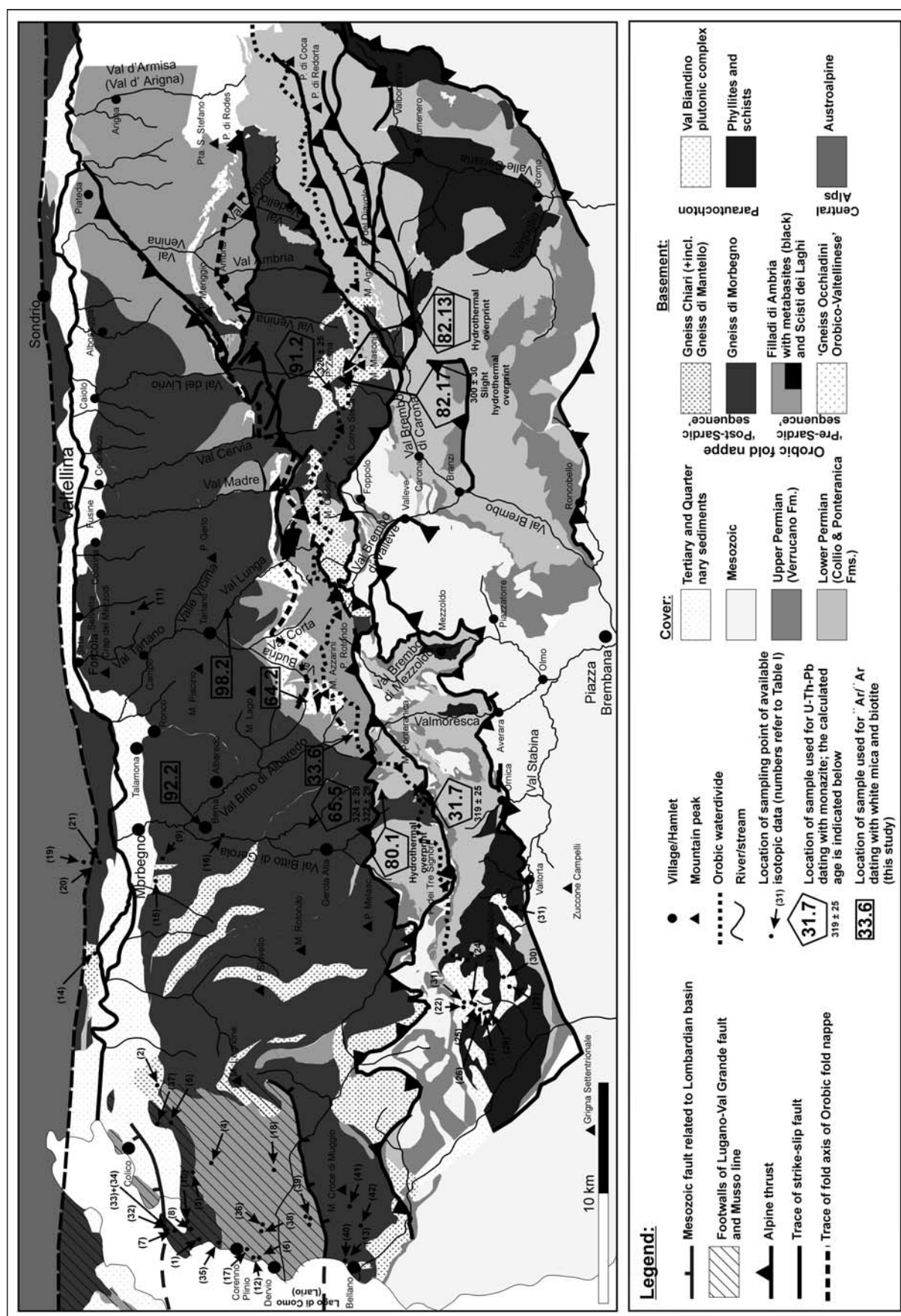
2 Geological setting

Exposures of the southern margin of the Variscan belt can be followed through Liguria, Tuscany, the 'Peloritani Mountains' and Calabria into Sardinia (Vai & Cocozza, 1986). In eastern direction the trend of this zone follows approximately the southern margin of the Alpine belt. The tectonic separation between the Variscan Southalpine basement and the Austroalpine is the Alpine 'Insubric'- or 'Tonale fault'. In the investigated central part of the Italian Southern Alps, the 'Orobic-Bergamasc Alps' (Figs. 1 and 2) the 'Tonale fault' is located along the northern slopes of the Valtellina. The Variscan units have been tectonically reworked and overprinted in an Alpine thrust belt, comprising of east-west trending zones of different character (Figs. 1 and 3). Because the Variscan 'Orobic fold nappe' and its root zone strike parallel to the 'Tonale fault' there seems to be a close genetic relationship between the Variscan and younger structural trends.

The Early Permian 'Orobic Collio basin', with the 'Collio-Orobico'- and 'Ponteranica'- formations, is exposed between the Orobic basement in the north and a thrust belt, consisting of mainly Mesozoic formations in the south (Figs. 2, 3). These are Alpine inversion-related large-scale gentle anticlines, the 'Orobic'-, 'Trabuchello'- and 'Cedegolo'- anticlines (de Sitter, 1963). Some inliers in the Permian sediments and -volcanics allow the observation of the parautochton below. The 'Orobic fold nappe' is separated from the parautochton by the south-verging Alpine 'Orobic thrust', which extends into the Permo-Mesozoic sedimentary cover. The 'Porcile fault', which is found along the core of a Variscan fold nappe crosses obliquely (ENE-WSW) the Orobic basement north of the 'Orobic thrust' and is steeper in ENE-direction. The 'Orobic thrust' and 'Porcile fault' have been active simultaneously. West of the junction of the 'Porcile fault' and 'Orobic thrust the approximately 20 km offset of the 'Porcile fault' adds to the displacement along the 'Orobic thrust'.
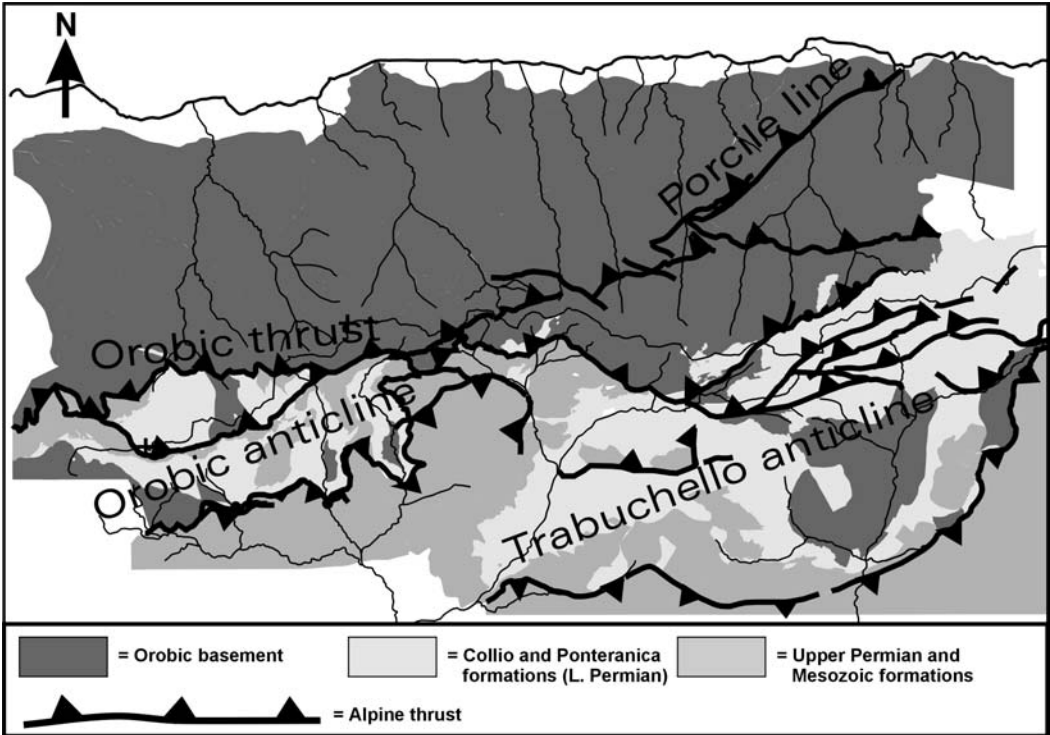

Fig.3. Overview of the principal Alpine structures in the investigated area Orobic Alps. For topography compare with Fig. 2.

So far Pre-Alpine, and particularly the Pre-Mesozoic, ages of metamorphism in the Orobic Alps are poorly constrained. All available isotopic data, except the $^{40}Ar/^{39}Ar$-age spectra of Bertotti et al. (1999) from the 'Lario basement', are shown in Fig. 2 and Table I.

K-Ar-ages of hornblende from an amphibolite-sample of Orobic basement 850 m from the vicinity of the 'Tonale fault' (near Mello) gave approximately 360 Ma (Wiedenbeck, 1986), the oldest age in the area, which is similar to Rb-Sr muscovite-ages of Schists of Val Trompia near the 'Collio-Trumplino basin' of 364 ± 15 Ma (Del Moro et al., 1983). Based on data from McDowell (1968a, 1968b), Wiedenbeck (1986) interpreted the result of the sample from Mello as a mixing of a Caledonian event between 440 and 390 Ma with an Hercynian overprinting at 315 Ma. Samples from locations north of the 'Tonale fault' supplied Alpine K-Ar ages of hornblende, biotite and muscovite and Rb-Sr ages of whole rock, hornblende, biotite and muscovite (Wiedenbeck, 1986).

Only two samples from the metapsammites and -pelites of the area of interest revealed Variscan K-Ar-cooling ages of muscovite, 306 ± 7 and 330 ± 10 Ma (Bocchio et al., 1981) (Fig. 2, Table I). Variscan regional metamorphic biotite K-Ar-cooling ages of 291 ± 6 (Bocchio et al., 1981) and 292 ± 9 Ma (Mottana et al., 1985) for samples from a lithologic variety of the 'Gneiss di Morbegno' called type (b) below, in Feijth (in prep. a) and in Feijth & Franz (in prep.).

Radiometric age determinations of the 'Val Biandino plutonic complex' in the southwest of the area, are also available (De Capitani et al., 1988). These are whole rock K-Ar ages of 214 ± 6 to 275 ± 8 Ma, K-Ar amphibole ages of 331 ± 10 to 348 ± 13 Ma and K-Ar biotite ages that vary from 271 ± 8 to 307 ± 9 Ma. The biotite ages probably represent the age of igneous emplacement (De Capitani et al., 1988).

Permo-Triassic resetting of the isotopic systems had only local influence in the central Orobic Alps but is certainly present, as indicated by the muscovite-age of 242 ± 7 Ma in a sample from 'Fumasi' (Fig. 2) (Mottana et al., 1985). In the Lario basement Permo-Triassic biotite-ages between 269 ± 9 and 218 ± 6 Ma (Mottana et al., 1985) show a relatively wide distribution, indicating a long Permo-Triassic period of extension that also affected the K-Ar and Rb-Sr isotopic systems of muscovite with Permo-Mesozoic ages varying from 286 (no error indicated) to 180 ±3 Ma (Bertotti et al., 1999; Hanson et al., 1966; Bocchio, 1981; Mottana et al., 1985).

Köppel & Grünenfelder (1971) attempted to date 'Gneiss Chiari' from the Val Colla zone, but protolith age and metamorphic ages remained unknown. Certainly the 'Gneiss Chiari' is older than Westphalian-B to -C age, because of the occurrence of pebbles of 'Gneiss Chiari' in the 'Manno conglomerates' (Graeter, 1951; Lehner, 1952; Reinhard, 1964).

Although Ordovician isotopic ages were not obtained so far for rocks of the Orobic basement, an Ordovician igneous phase has been considered, based on geochemistry of granodioritic 'Monte Fioraro metagranitoids' (Colombo et al., 1994). The different types of pre-Alpine structures, igneous and metamorphic events in the Orobic basement could not yet be related to specific orogenic phases, although a two-phase Variscan structuration was generally assumed in the most recent publications (Spalla et al., 1999; Cadel et al., 1996). Bocchio et al. (1981) concluded with a Caledonian intermediate pressure event followed by a Hercynian low pressure event, whereas Mottana et al. (1985) interpreted two Hercynian events, an intermediate pressure event followed by a retrograde low-pressure event.

Table I: Overview of published isotopic age data of the Orobic Alps.

Author	Location (numbers refer to Fig. 2)	Formation/Lithology	Method	Age (Ma)
Hanson et al. (1966)	(1)	Pegmatite	K-Ar Mu	207 ± 10
			Rb-Sr Mu	244
	(2)	Pegmatite	K-Ar Mu	219 ± 11
	(3)	Pegmatite	K-Ar Mu	215 ± 11
	(4)	Pegmatite	K-Ar Mu	218 ± 11
			Rb-Sr Mu	223
	(5)	Pegmatite	K-Ar Mu	198 ± 10
	(6)	Pegmatite	K-Ar Bt	239 ± 12
Bocchio et al. (1981)	(7)	Pegmatite	K-Ar Mu	228 ± 6
	(8)	Bt-Sil schist	K-Ar Bt	218 ± 6
			K-Ar Mu	190 ± 6
			K-Ar WR	264 ± 8
	(9)	Paragneiss	K-Ar Bt	276 ± 8
			K-Ar Mu	330 ± 8
			K-Ar WR	210 ± 5
	(10)	Bt-Sil schist	K-Ar Bt	223 ± 5
			K-Ar Mu	221 ± 5
			K-Ar WR	224 ± 5
	(11)	Fine-grained gneiss	K-Ar Bt	291 ± 6
			K-Ar Mu	306 ± 7
			K-Ar WR	315 ± 8
	(12)	Micaschist	K-Ar Bt	218 ± 6
			K-Ar Mu	180 ± 3
			K-Ar WR	247 ± 5
	(13)	Paragneiss	K-Ar Bt	331 ± 10
			K-Ar Mu	330 ± 10
			K-Ar WR	313 ± 9
Mottana et al. (1985)	(14)	Fine-grained gneiss	K-Ar Mu	170 ± 6
			K-Ar WR	134 ± 4
	(15)	Fine-grained gneiss	K-Ar Bt	229 ± 7
			K-Ar Mu	186 ± 6
			K-Ar WR	43 ± 2
	(16)	Paragneiss	K-Ar Bt	292 ± 9
			K-Ar Mu	242 ± 7
			K-Ar WR	228 ± 7
	(17)	Fine-grained gneiss	K-Ar Bt	252 ± 6
			K-Ar Mu	231 ± 5
			K-Ar WR	402 ± 9
	(18)	Fine-grained gneiss	K-Ar Bt	269 ± 9
			K-Ar Mu	238 ± 7
			K-Ar WR	259 ± 7
Wiedenbeck (1986)	(19)	Bergell Tonalite	K-Ar Hbl	28.8 ± 2.2
			K-Ar Bt	23.5 ± 0.5
				23.6 ± 0.5
		Tonale Series	K-Ar Hbl	40.8 ± 0.9
				39.5 ± 0.8
			K-Ar Mu	25.4 ± 0.5
				25.3 ± 0.5
			K-Ar Bt	23.9 ± 0.5
				24.1 ± 0.5
	(20)	Insubric Mylonite	K-Ar Mu	105.4 ± 2.1
				61.8 ± 1.3
	(21)	'Gneiss di Morbegno'	K-Ar Hbl	373 ± 7
				358 ± 14

Table I (continued)

Author	Location (numbers refer to Fig. 2)	Formation/Lithology	Method	Age (Ma)
De Capitani et al. (1988)	(22)	Granite	K-Ar Bt	246 ± 7
	(23)	Quartzdiorite	K-Ar Bt	275 ± 8
	(24)	Quartzdiorite	K-Ar Hbl	348 ± 13
			K-Ar Bt	282 ± 8
	(25)	Granite	K-Ar Bt	301 ± 9
	(26)	Quartzdiorite	K-Ar Bt	291 ± 9
			K-Ar WR	238 ± 7
	(27)	Quartzdiorite	K-Ar Bt	274 ± 8
			K-Ar WR	229 ± 7
	(28)	Quartzdiorite	K-Ar Hbl	331 ± 10
			K-Ar Bt	271 ± 8
			K-Ar WR	214 ± 6
	(29)	Granite	K-Ar Bt	290 ± 8
	(30)	Gabbrodiorite	K-Ar Bt	307 ± 9
			K-Ar WR	242 ± 7
	(31)	Tonalite	K-Ar Bt	294 ± 9
			K-Ar WR	275 ± 8
Bertotti et al. (1999)	(32)	Pegmatite	Rb-Sr Kfs-Mu	208 ± 2 / 215 ± 2
	(33)	Schist	Rb-Sr Mu-Bt	195 ± 2 / 213 ± 2
	(34)	Marble	Rb-Sr Ca-Mu	198 ± 2
	(35)	Schist	Rb-Sr Mu-Bt	197 ± 2
	(36)	Schist	Rb-Sr Mu-Bt	197 ± 2
	(37)	unspecified	Zircon f.t.	49 ± 7
	(38)	unspecified	Zircon f.t.	139 ± 28
	(39)	unspecified	Zircon f.t.	161 ± 28 / 144 ± 15 / 135 ± 14
	(40)	unspecified	Zircon f.t.	151 ± 31
	(41)	unspecified	Zircon f.t.	177 ± 34
	(42)	unspecified	Zircon f.t.	223 ± 40

The Orobic basement escaped the greenschist to amphibolite grade Alpine metamorphism, which overprinted the Austroalpine and Penninic Variscan basement to the north of the 'Tonale fault'. Alpine metamorphism reached high anchimetamorphic conditions (Schönborn, 1992) and the Collio sediments were locally deformed by pressure solution- and recrystallisation processes during the activity of the 'Orobic thrust' (Feijth & Neubauer, in prep. b). Alpine deformation is, except in few lithologies, not penetrative and predominantly located along specific thrust zones, some of which being reactivated Variscan structures, separating blocks which remained relatively undisturbed. In the basement these zones are characterised by black cataclasites with abundant pseudotachylytes, particularly along the 'Orobic thrust' and the 'Porcile fault'. In the cover sequence pressure solution and cataclasis are typical. Alpine deformation was more penetrative in rocks where phyllites and schists are more abundant, particularly as chevron folds of cm to 100 m scale. Such lithologies are more abundant in the eastern sector of the Orobic basement, in the 'Val Venina' and further east. Related tectonic phases were investigated in the 'Valle Belviso' and 'Val di Campovecchio' by Carminati et al. (1997). The age of these Alpine phases could so far be

determined by fault-relationships with the 'Adamello pluton', by relationships of Miocene sediments in the foreland (Schönborn, 1992) and by relationships with Alpine andesite dykes (Zanchi et al, 1990), a single Alpine K-Ar age of 43 ± 2 Ma (Mottana et al., 1985) and a zircon fission track age of 49, $4 \pm 7,4$ Ma (Bertotti et al., 1999). Additional Alpine ages are presented in Feijth & Neubauer, in prep. b).

The stratigraphy of Orobic basement, that consists of meta-sedimentary and -volcanic sequences and igneous rocks of different nature and age, is illustrated in Fig. 4. It is mainly exposed between the 'Tonale fault' and the 'Orobic thrust' (Fig. 2), in the 'Orobic fold nappe'. A schematic N-S cross-section of the Variscan-Permian configuration is shown in Fig. 5.
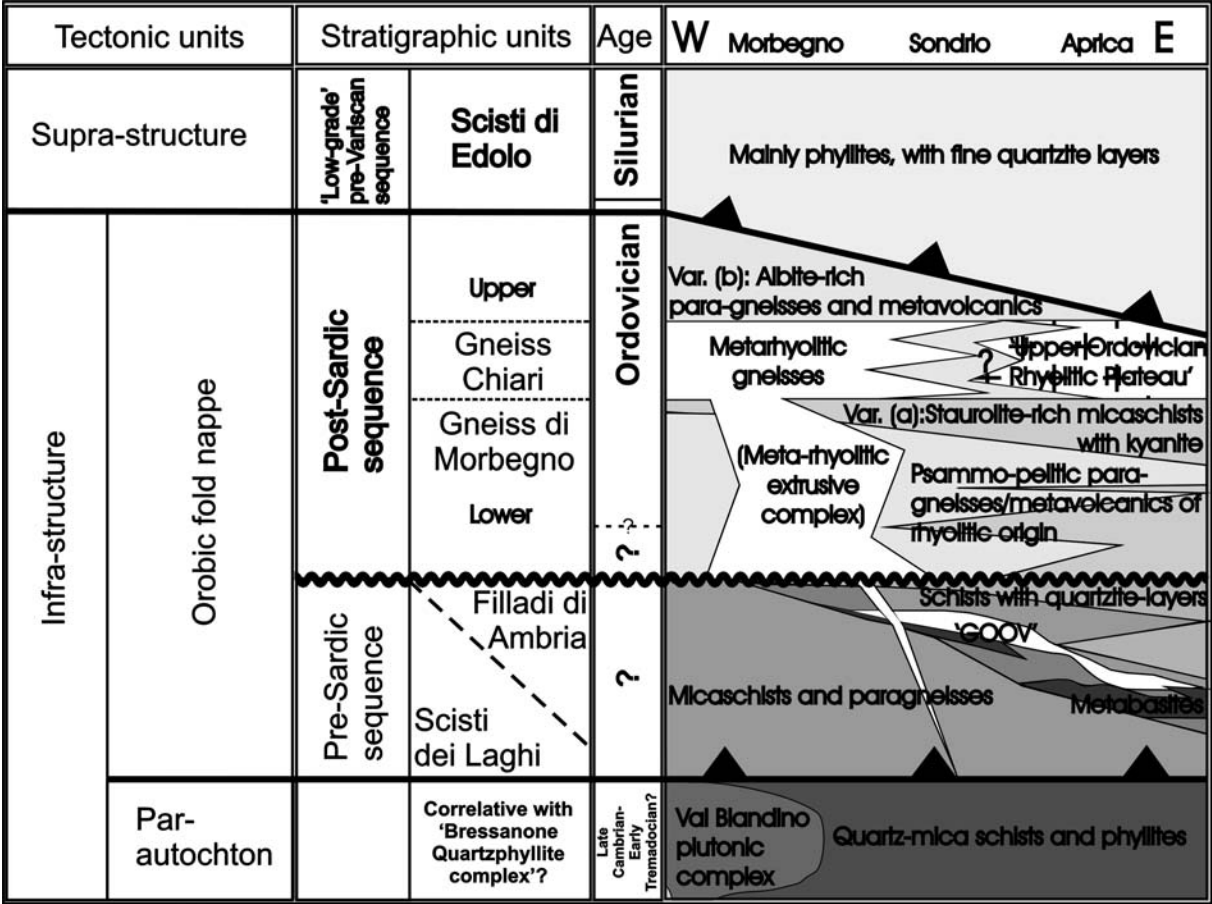

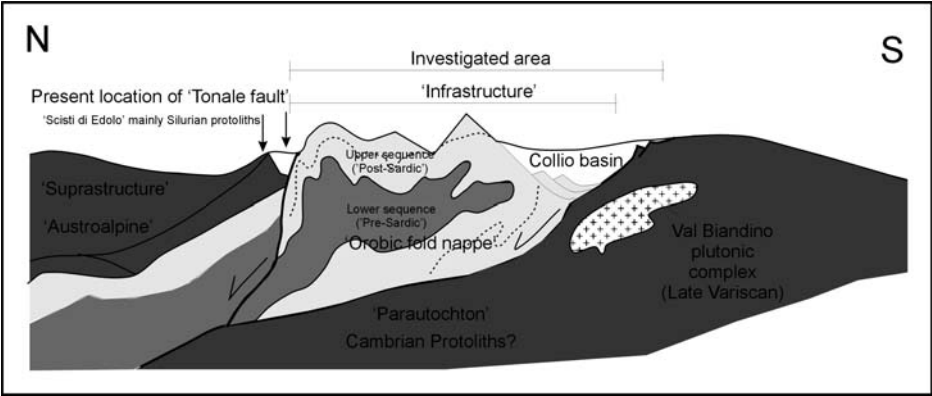*Fig. 4. Schematic overview of the stratigraphy of the Orobic basement.*

Fig. 5. Schematic N-S cross section showing the Permian structural configuration of the investigated area.

The 'Orobic fold nappe' and the parautochton make up the infrastructure and are overlain, through an extensional fault- contact, by the suprastructure that is of substantially lower metamorphic grade. Stratigraphic, petrographic and structural relationships of each of these units are described for each tectonic unit, starting with the two sequences of the 'Orobic fold nappe' and followed by the parautochton and the suprastructure. The two sequences of the 'Orobic fold nappe', separated by a tectonic contact and/or an angular unconformity, are discernable by their different structural and metamorphic development and might therefore be referred to as different tectonic units.

The lower sequence of the 'Orobic fold nappe' consists of the 'Filladi di Ambria', with lenses of metabasitic rocks at the contact. For reasons discussed in Feijth (in prep. a) we prefer to apply the name 'Filladi di Ambria' for the centimetre to decimetre scale layered schists, quartzitic-schists, chlorite-schists with subordinate thinner meta-grauwackes and quartzites, with typical garnet in the core of the 'Orobic fold nappe'. This is in contrast to Gansser & Pantić (1988) and Cadel et al. (1996) who apply the name 'Scisti di Edolo' for both, the formation of the suprastructure, that we wish to call 'Scisti di Edolo', and the unit that we call 'Filladi di Ambria'. Lenses and stocks of granodioritic 'augen gneisses', the 'Gneiss Occhiadini Orobico-Valtellinese' ('GOOV') (Feijth, in prep. a) are situated in the 'Filladi di Ambria', in particular along the contact with an horizon of metabasites of extrusive origin containing amphibolite-sills.

The lower sequence of the 'Orobic fold nappe' was affected by two pre-Mesozoic tectono-metamorphic phases, in contrast to the upper sequence, in which only one pre-Mesozoic phase was identified.

Sharp contacts with chilled margins within the 'GOOV' and juxtaposing up to 5cm thick contactmetamorphic zones in the metabasites clearly indicate that the igneous protoliths of the 'GOOV' intruded the metabasites and associated metasediments at a shallow intrusion level.

Primary layering of the 'Filladi di Ambria' and a metamorphic foliation, related to D_1-folding, is crosscut by the contacts of the 'GOOV', which contains folded xenoliths of metabasite.

In contrary to the lower sequence, that contains mainly basic meta-volcanics, the upper sequence contains felsic meta-volcanics, meta-rhyolites and derived metasediments. These are included in the psammo-pelitic 'Gneiss di Morbegno' with include rhyolitic meta-volcanics, the 'Gneiss Chiari', that is a separate stratigraphic unit. The contact to the 'Filladi di Ambria' is an angular unconformity, which in many cases has been activated as a Variscan shearzone and an Alpine fault-contact. The 'Gneiss di Morbegno' and 'Gneiss Chiari' can be regarded as a meta-volcano-sedimentary system with massive rhyolitic complexes of up to 1000 m thick there where extrusion took place, like the 'Monte Cadelle meta-rhyolitic complex'.

Laterally away from those rhyolitic complexes the proportion of meta-rhyolite in the upper sequence decreases and the meta-rhyolitic sheets of 'Gneiss Chiari' are situated between meta-volcano-sedimentary units with commonly rust-brown and greyish weathering colours. Amongst the other less distinctive, generally garnet-bearing, psammo-pellitic lithologies there are lithologic varieties (a) and (b) of the 'Gneiss di Morbegno', respectively characterised by metamorphic fabrics related to dehydration melting of white mica and biotite (Feijth & Franz, in prep.).

Lithologic variety (a) is represented by garnet-staurolite-white mica schist containing kyanite, related to dehydration melting of white mica (Feijth & Franz, in prep.), and tourmaline. It

occurs in the lower part of the 'Gneiss di Morbegno' succession, immediately below the level where the 'Gneiss Chiari'-horizon occurs. Their protoliths might be Al-rich meta-ashes and -tuffs or sedimentary reworked volcanics.

The Al-poorer lithologic variety (b) consists of biotite and albite-rich psammo-pelitic gneisses with usually garnet (seldom ± staurolite and ± kyanite), called 'Albitknotengneise' by Cornelius & Cornelius-Furlani (1930), because of the typical albite-blasts. This lithology with variably developed layering occurs mainly at the stratigraphic level of 'Gneiss Chiari' and above, either when latter is present or not.

The upper sequence has, together with the 'pre-Sardic sequence', been affected by the main metamorphic event of amphibolite facies grade at ≤ 1.3 Gpa and 750 °C (Feijth & Franz, in prep.), very close to the granulite and eclogite facies. Related dehydration melting of phyllosilicates marks the start of formation of the 'Orobic fold nappe'.

Bedding and main foliation of the upper sequence, and of coarse also the lower sequence, are folded in the 'Orobic fold nappe' and are overprinted by structures related to the event of nappe folding (Feijth, in prep. a, b).

The causes of formation of these structures and mechanisms of fold nappe development are discussed in detail in Feijth (in prep. a, b, c) and Feijth & Franz (in prep.). The resulting structure, shown in Fig. 6, can be described as a fold-nappe that, after diapirism related to dehydration melting, extruded by tectonically induced strain from a rootzone and was deformed internally, particularly along NE-dipping transtensional shearzones, by dextral wrenching along the rootzone. The rootzone is situated along the foothills of the 'Orobic
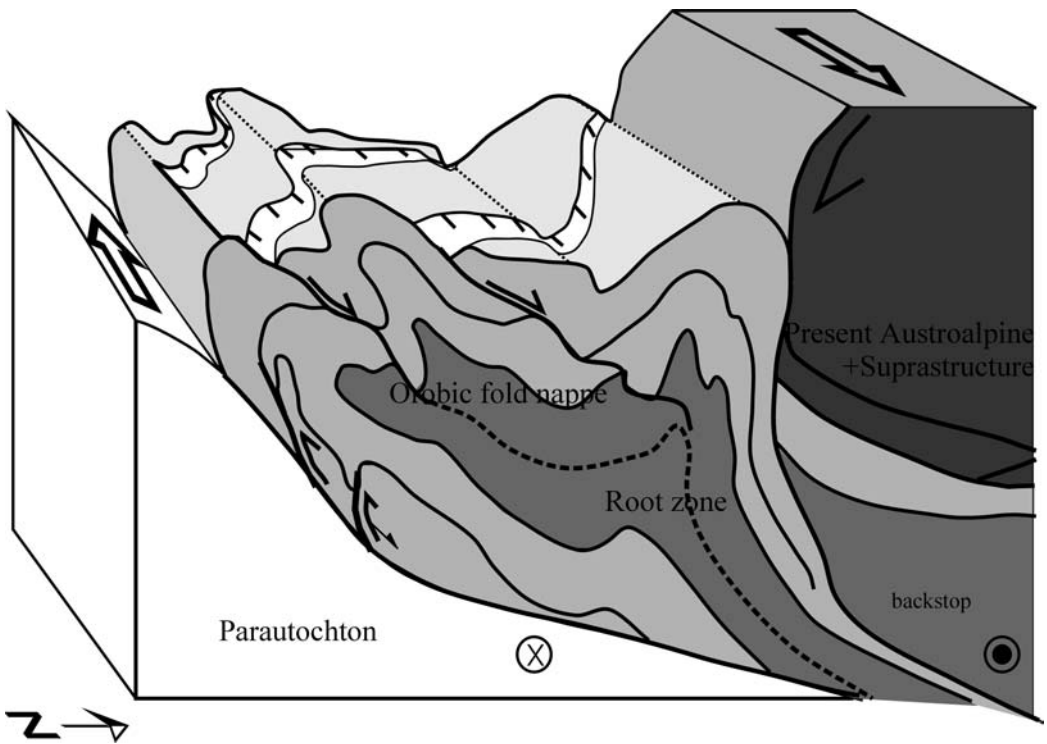

Fig. 6. Schematic overview of the 'Orobic fold nappe' with internal structures. Within the 'Orobic fold nappe' the lower sequence is indicated in the darker grey, whereas the upper sequence is indicated in the lighter grey.

chain' in the 'Valtellina' and the hinge zone is best exposed in the 'Upper Val Lunga' and 'Upper Val Madre'.

The parautochton, as exposed in the inliers in the 'Collio-Orobico basin' consists of phyllitic schists, schists, quartzitic phyllites, meta-conglomerates and quartzites, with occasionally garnet. These lithologies are intensely sheared parallel to bedding. The tectonic imprint, a strong planar fabric with extensional shear bands, is of combined pre-Alpine and Alpine origin. Along the south-western border of the study area, in the 'Val Sassina', 'Val Biandino' and 'Val Stabina', stocks and laccoliths of Variscan syn-late tectonic tonalites, granites, quartz-diorites and gabbro-diorites with a large contact metamorphic aureole are exposed in this parautochton. These Variscan intrusions of the 'Val Biandino plutonic complex' are exposed as syn-late tectonic stocks and laccoliths. Contacts of the intrusions are generally conformable to folded bedding of the host rock of the parautochton, but at places discordant, especially at the apophyses. The contactmetamorphic aureole consists of sillimanite-, cordierite- and andalusite- bearing hornfelses. Thermobarometry by Feijth & Franz (in prep.) indicates a depth of intrusion of at maximum 5 km.

The 'Edolo micaschists', that make up the suprastructure, are characterised by finely laminated phyllites, micaschists and fine quartzitic layers. These are the only basement-rocks of the Orobic Alps of which the age of deposition has been determined by biostratigraphic methods, which would certainly not have been possible for the higher grade sequences of the 'Orobic fold nappe'. The age of the identified spores and acritarchs is mainly Silurian and subordinate Ordovician (Gansser & Pantić, 1988). Particularly at the base these lithologies are intensely sheared parallel to bedding. This unit shows relatively weak pre-Alpine metamorphism of greenschist facies with biotite, chlorite and occasionally garnet that was obviously strongly chloritised after shearing. An Alpine age of the bedding-parallel shearing seems unlikely because the typical black cataclasites and pseudotachylytes, indicative of Alpine thrusting, are not very abundant. Ductile folding is associated with this shear zone. A xenolith of folded mylonite was found in a hornblende-porphyritic dyke (Lardelli, 1981), which hornblende was dated at 96-80 Ma (Mc Dowell, 1970). These dykes have only been weakly affected by post-intrusive events. At the upper boundary the Alpine 'Tonale fault' truncates the upper part of this succession.

3 Geochronological methods

3.1 U-Th-Pb-dating on monazite by EMP

The LREE-phosphate monazite ($CePO_4$) is widely reported as an accessory mineral in granite, pegmatite, felsic volcanic ash, felsic gneiss, pelitic schist and gneiss of medium to high metamorphic grade, and low-grade metasedimentary rocks, and as a detrital mineral in clastic and metaclastic sediments (Parrish, 1990). Despite its occurrence only as accessory mineral and generally small size, monazite is of outstanding geological importance. First, it is very useful for geochronology, applying the U-Th-Pb-method, because it incorporates large quantities of Th and U (Parrish, 1990; Montel et al., 1996). Second, monazite crystals typically carry between 40 and 80 % of the LREE content of their host rock (Bea, 1996; Schitter, 1997). Third, monazite can be applied as a geothermometer since monazite can contain xenotime (YPO_4). This is due to the restricted miscibility of xenotime and monazite,

which was calibrated empirically by Heinrich et al. (1997) and experimentally by Gratz & Heinrich (1997). Results of the application of the monazite-xenotime thermometer on the geochronologically dated samples are presented in Feijth & Franz (in prep.).

A great advantage of this the geochronological method applying monazite is that mother and daughter products remain within the monazite crystals. Since the U and Th contents of are generally high, a relatively short time-interval suffices to produce radiogenic Pb (^{208}Pb + ^{207}Pb + ^{206}Pb), which enables to use the EMP for geochronologic dating. A disadvantage of this U-Th-Pb-method is the rather poor precision (± 30-50 Ma). The concentrations of the daughter products determine the accuracy of the method, which therefore should not be applied on rocks younger than 200 Ma.

Monazite is stable under low- to high grade metamorphic conditions, the closure temperature being about 675-730 °C (Copeland et al., 1988), or 725 ± 25 °C Parrish (1990). Monazite often reacts to allanite or apatite at low-grade conditions (Overstreet, 1967; Bons, 1988; Ward et al., 1991; Smith & Barreiro, 1990; Lanzirotti & Hanson, 1996; Finger et al., 1998). Finger et al.,(1998) demonstrated that even monazite grains from granitoids affected by amphibolite facies metamorphic overprint exhibit a closed-system behaviour. It therefore appears to be very useful for constraining U-Th-Pb protolith ages, even in cases of metamorphic overprint up to amphibolite-facies conditions.

Measurements on the selected thin sections were carried out on a Jeol JX 8600 instrument equipped with three wavelength-dispersive spectrometers at the University of Salzburg. For the determination of total lead monazite model ages, which require a particularly precise measurement of Pb in the 0.1-0.2 wt % range, the probe current was increased to 250 nA at 15 kV. A relatively large beam size of 5-10 μm diameter was used to avoid damage to the sample. For the analysis of Pb, counting times were 100 s (peak) and 2 x 50 s (background). Counting times for Th and U were 30 s (2 x 15 s) and 50 s (2 x 25 s), respectively. Additionally, the elements La, Ce, Pr, Nd, Pr, Sm, P and Y were determined with 10 s (2 x 3s) counting times to enable a reasonable ZAF correction. A small Y interference on the Pb$M\alpha$ line was eliminated by measuring a Pb-free Yttrium standard and routinely correcting the monazite analysis by linear extrapolation (Montel et al., 1996).

For every measured point, the model age was calculated by solving the following equation (see Montel et al., 1996):

$$Pb = Th/232[\exp(\lambda^{232}\tau)-1]208 + (U/238.04)0.9928$$
$$x [\exp(\lambda^{238}\tau)-1]206 + (U/238.04)0.0072$$
$$x [\exp(\lambda^{235}\tau)-1]207$$

where U, Th and Pb concentrations are in parts per million, and λ^{232}, λ^{238} and λ^{235} are radioactive decay constants of ^{232}Th, ^{238}U and ^{235}U respectively (Steiger & Jäger, 1977). The 2σ errors for the single model ages were calculated by propagating the Th, U and Pb errors as resulting from the counting statistics of the microprobe (Montel et al., 1996). These were typically ± 0.04-0.05 wt % for the Th, ± 0.025-0.03 wt % for the U and ± 0.018-0.02 wt % for the Pb (all 2σ errors). To control the quality of the analysis, monazites with precisely known conventional concordant U-Pb ages were measured together with the unknown sample.

3.2 The ^{40}Ar/^{39}Ar-method on white mica and biotite

Concentrates of white mica and biotite of the fractions 125-250 and 250-500 μm were prepared. The sieve fractions were prepared to reduce the potential of contrasting populations. This was done by breaking the rock-samples, dry sieving, washing first in tap water, finally in distilled water, using an ultrasonic bath and drying. Phyllosilicates were separated from rounded grains according to their grain shapes. For the samples which contain both white mica and biotite this was done by magnetic separator. Finally the the separates of white mica and biotite were handpicked under a binocular microscope. For irradiation in the central position of the MTA-KFKI-reactor in Budapest the minerals were packed into Al-foil packets and sealed in quartz-vials. The samples were exposed to the radiation for 8 hours at a flux of c. 1,7 x 10^{18} n/cm^{2}s. Correction factors for production of interfering isotopes have been reported by Handler & Neubauer (in review) and are: ^{36}Ar/^{37}Ar$_{(Ca)}$ = 2.6025x10^{-4}, ^{39}Ar/^{37}Ar$_{(Ca)}$ = 6.5014x10^{-4}, and ^{40}Ar/^{39}Ar$_{(K)}$ = 1.5466x10^{-2}. Variation in the flux of neutrons were monitored with B4M white mica standard (Flisch, 1982) for which a ^{40}Ar/^{39}Ar plateau age of 18.555 ± 0.395 Ma has been reported (Burghele, 1987).

^{40}Ar/^{39}Ar analyses have been carried out in the ARGONAUT Laboratory at the Institute of Geology and Palaeontology at the University of Salzburg using a UHV Ar-extraction line equipped with a combined MERCHANTEK^{TM} UV/IR laser ablation facility, and a VG ISOTECH^{TM} NG3600 Mass Spectrometer following procedures described in Handler & Neubauer (in review). Samples were measured by stepwise heating of multigrain samples, using a 25 W CO$_2$-IR laser operating in Tem$_{00}$ mode at wavelengths between 10.57 and 10.63 μm. The laser was defocused to a spot size of ca. 1.0 mm. The laser was controlled from a PC, and the position of the laser beam on the sample was monitored through a double-vacuum window on the sample chamber via a video camera in the optical axis of the laser beam on the computer screen. Gas clean-up was performed using one hot and one cold Zr-Al SAES getter. Measurement was performed on an axial electron multiplier in static mode, peak jumping and stability of the magnetic field was controlled by a Hall-probe. For each increment the intensities of ^{36}Ar, ^{37}Ar, ^{38}Ar, ^{39}Ar and ^{40}Ar were measured, the baseline readings on mass 33.5 were automatically subtracted. Intensities are corrected for system blanks, background, post-irradiation decay of ^{37}Ar, and interfering isotopes. Ages and errors were calculated following suggestions of McDougall & Harrison (1988) and decay factors reported by Steiger & Jäger (1977) using our own MICROSOFT EXCEL^{TM} worksheet.

4 Sample locations and sample description

An overview of all samples applied for geochronology is given in Table II. Sampling locations of those samples that contained monazite and those that were dated by ^{40}Ar/^{39}Ar-step heating are indicated in Fig. 2.

Monazite-geochronology was originally intended to be applied to date the igneous phase of the 'GOOV' and the peak metamorphic conditions of the main phase of uppermost amphibolite facies grade (Feijth & Franz, in prep.) that affected the 'Orobic fold nappe'. Monazite was found only in samples of the upper sequence of the 'Orobic fold nappe', from

Table II: Overview of all samples applied for isotopic dating by the $^{40}Ar/^{39}Ar$-method on white mica and biotite and the U-Th-Pb-method on monazite.

Sample No.	Sample location	Co-ordinates (UTM)	Altitude (m)	Formation & position in formation (if determinable)/ Lithologal variety and lithological characteristics/ Main mineral constituents	U-Th-Pb on monazite applied:	Monazite (M), xenotime (X) and/or allanite (A) present	$^{40}Ar/^{39}Ar$-method applied white mica (=WM) biotite(=B)
33.6	'Alpe Cul' ('Valle del Bitto di Albaredo')	1547801-5099717	1935	'GOOV'/ Sample from boundary zone/quartz, plagioclase, K-feldspar, muscovite, biotite, garnet, zoisite, epidote, carbonate, chlorite	Sample unsuitable	M: No	WM B
64.2	'Val Pedena' ('Valle del Bitto di Albaredo')	1549415-5101755	1950	'GOOV'/ Sample from boundary zone/quartz, plagioclase, K-feldspar, muscovite, biotite, zoisite, epidote	Sample unsuitable	M: No	B
31.7a2	Between 'Passo Salmurano' and 'Monte Valetto'	1545100-5096697	2148	'Gneiss di Morbegno'/ Lithologic variety (a)/ quartz, plagioclase, muscovite, kyanite, garnet, staurolite, biotite, chlorite	Yes	M: Yes X: Yes	Not intended
65.5bI	'Valle di Bomino'	1543600-5101819	1237	'Gneiss di Morbegno'/ With well developed $D_{2/2}$ crenulation and lineation/ quartz, plagioclase, muscovite, garnet, biotite, chlorite, tourmaline	Yes	M: Yes X : No A : Yes	Not intended
65.5bIII	'Valle di Bomino'	1543600-5101819	1237	'Gneiss di Morbegno'/ With well developed $D_{2/2}$ crenulation and lineation/ quartz, plagioclase, muscovite, garnet, biotite, chlorite, tourmaline	Yes	M: Yes X : No A : Yes	Not intended
91.2aI	'Passo di Publino' ('Val del Livrio')	1563450-5100722	2132	'Gneiss di Morbegno'/ Lithologic variety (a)/ quartz, plagioclase, muscovite, garnet, staurolite (partly sericitised), biotite, chlorite	Yes	M: Yes	Not intended
92.2	'Bema' Marco' ('Valle del Bitto')	1543650-5106325	805	'Gneiss di Morbegno'/ Lithologic variety (b)/ quartz, plagioclase, muscovite, garnet, biotite, chlorite	Not intended		WM B
94.2	Road to 'Campo', 'Crap del Mezzodi' ('Val Tartano')	1550111-5111503	620	'Gneiss di Morbegno'/ Lithologic variety (b)/ quartz, plagioclase, muscovite, garnet, biotite, chlorite		M: Yes	Not intended
98.2	'Val Lunga', near 'San Antonio' ('Val Tartano')	1553552-5105233	1272	Basal 'Gneiss di Morbegno'/ intensely sheared/ quartz, plagioclase, muscovite, garnet, biotite, zoisite, chlorite, rutile, tourmaline	Not intended		WM B
39.2	Near 'Passo dei Lupi' (Val Madre')	1557801-5101815	2250	'Gneiss Chiari'/ relatively coarse grained/ quartz, K-feldspar, plagioclase, muscovite (incl. sericite), chlorite	Not intended		WM
80.1	'Lago Pescegallo' ('Val Bitto di Gerola')	1545302-5098435	1866	'Gneiss Chiari'/ quartz, K-feldspar, plagioclase, muscovite (incl. sericite)	Yes	M: Yes	Not intended
82.13I	NE-flank of 'Pizzo Zerna' ('Val del Livrio')	1564302-5100110	2292	'Gneiss Chiari'/ quartz, K-feldspar, plagioclase, muscovite (incl. sericite)	Yes	M: Yes	WM
82.17	'Passo di Publino' ('Valle Sambuzza')	1563822-5099600	2260	'Gneiss Chiari'/ quartz, K-feldspar, plagioclase, muscovite (incl. sericite)	Yes	M: Yes	Not intended

the meta-rhyolitic 'Gneiss Chiari' (80.1, 82.13I, 82.17) and of the meta-volcano-sedimentary lower 'Gneiss di Morbegno' (31.7a-2, 65.5-bI, 65.5-bIII, 91.2aI).

$^{40}Ar/^{39}Ar$-step heating was carried out on white mica and biotite multigrain samples on samples from different stratigraphic units of the metamorphic basement; 'GOOV' (33.6, 64.2), 'Gneiss Chiari' (39.2, 82.13I) and 'Gneiss di Morbegno' (92.2, 98.2).

Following petrographic overview concentrates on the structural and metamorphic

relationships of the individual samples applied.

'GOOV':

Two samples from the 'GOOV' were applied for $^{40}Ar/^{39}Ar$-step heating, 33.6 on white mica and biotite, 64.2 on biotite only. These samples of 'GOOV' contain quartz, often perthitic K-feldspar, biotite, plagioclase (0-17 % An), epidote, zoisite and both samples contain garnet ($Al_{58-69}Py_{3-7}Gr_{21-31}Sp_{2-12}Ad_{0-4}$). Microphotographs of samples 33.6 and 64.2 are shown in Figs. 7a and b. Apatite, zircon, tourmaline, rutile and opaques occur as accessory minerals. Zoisite and clinozoisite are occasionally abundant and monazite was not found in any of the investigated samples of 'GOOV'. Biotite and white mica form the main foliation and the $D_{2/2}$-related shearplanes and C'-shearbands, which form an anastomosing conjugate cleavage around the K-feldspar σ-blasts, garnet, albite and quartz of the microlithons. Sample 69.2aI has a strong linear fabric related to $D_{2/2}$. Garnet and K-feldspar porphyroblasts thus obviously predate $D_{2/2}$-shearing. Quartz displays a granoblastic interlobate structure, with subgrains along the bounding foliation shear planes. $D_{2/2}$-related dynamic recrystallisation was followed by static recovery, which caused euhedral subgrain-shapes. Locally quartz-lenses show crystal-preferred orientations. Chlorite, replacing biotite, is rather abundant in both samples (Fig. 7a). Perthitic unmixing of K-feldspar, indicates high temperatures followed by slow cooling after magmatic emplacement. In none of the samples of 'GOOV' monazite was found.

'Gneiss di Morbegno' lithologic variety (a):

The samples 31.7a-2 and 91.2aI, both applied for U-Th-Pb dating on monazite, were taken from 'Gneiss di Morbegno' of litho-type (a). Sample 31.7a-2 contains much muscovite, garnet, kyanite, staurolite, plagioclase-porphyroblasts and chlorite. Muscovite forms the transposed main foliation around kyanite and is separated by relatively weakly developed microlithons of plagioclase and K-feldspar. Staurolite, occasionally very abundant, has less of a preferred orientation and has inclusions of almandine-garnet ($Al_{70}Py_{11}Gr_{15}Sp_4$) and is surrounded by muscovite and remnant kyanite (Fig. 4c in Feijth & Franz, in prep.; Fig. 9b in Feijth, in prep. a). Sample 91.2aI is rich in biotite, contains staurolite, but no kyanite. Garnet should represent a prograde Variscan relic. Kyanite is a later phase and staurolite formed during early retrogression. Garnet- and kyanite-growth certainly predate the culmination of deformation, because the kyanite-porphyroblasts are $D_{2/2}$-folded (Fig. 9c in Feijth, in prep.a.). Kyanite is a product of dehydration melting of white mica (Feijth & Franz, in prep.) and staurolite formed by the retrograde reaction grt + bt + ky $\longrightarrow$ st (Feijth & Franz, in prep.). Quartz occurs as grain aggregates with seriate-interlobate and younger polygonal subgrains, indicating static recovery after dynamic recrystallisation. Undulous extinction and deformation lamellae are common. Kyanite and plagioclase are often sericitised, staurolite is occasionally replaced by sericite and chlorite whilst the garnet not included in staurolite is often pseudomorphic replaced to various degrees by chlorite during retrogression.

Porphyroblastic albite (~20 % An) is an early-$M_{2/2}$ phase replacing a microcline-richer feldspar. Sample 31.7a-2 contains relatively small homogeneous monazite and xenotime (Fig.5 a,b in Feijth & Franz, in prep.) in the approximate proportion 1:25. In sample 91.2a monazite is more abundant than xenotime. Monazite is generally homogeneous with slight
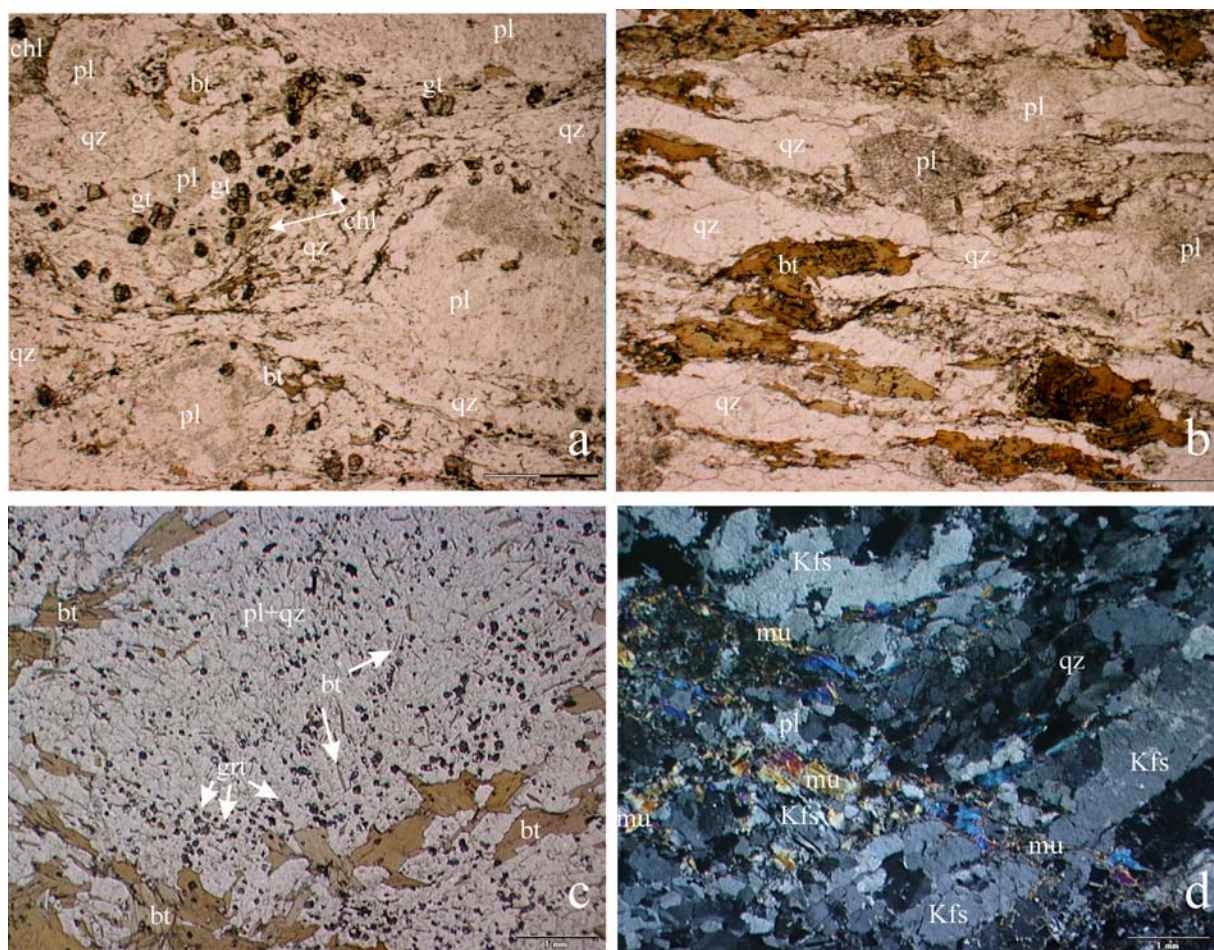
Fig. 7.

a. Microstructure of sample 33.6 of 'Gneiss Occhiadini Orobico-Valtellinese'. This sample was taken from nearby the boundary-zone of an intrusive body. Plane polarised light.

b. Microstructure of sample 64.2 of 'Gneiss Occhiadini Orobico-Valtellinese' with strong planar fabric realted to the formation of the 'Orobic fold nappe'. Plane polarised light.

c. Microstructure of sample 92.2 of 'Gneiss di Morbegno' lithological variety (b), showing an albite-porphyroblast with inclusions of quartz, garnet, very small biotite and white mica. The irregular shapes of the biotite-crystals surrounding the albite are related to dehydration melting. Plane polarised light.

d. Microstructure of sample 39.2 of 'Gneiss Chiari'. White mica has maximum Si^{4+} (p.f.u.) - values of 3.3 to 3.4, independent of grain size. Crossed polars.

signs of amphibolite-facies overprint, as indicated by some allanite and epidote along the edges (Fig. 5e in Feijth & Franz, in prep.).

'Gneiss di Morbegno' lithologic variety (b) and related lithologies:
Samples 92.2, applied for $^{40}Ar/^{39}Ar$-step heating on white mica and biotite, is from the rootzone of the 'Orobic fold nappe' and has the typical mineralogical composition and metamorphic fabric of lithologic variety (b). This fabric was frozen in after incomplete dehydration melting of biotite and some back-reaction (Feijth & Franz, in prep.). It is a metagreywacke with microscopically a rather isotropic fabric with typical abundant albite-

porphyroblasts, surrounded by relatively large remnant biotite with irregular boundaries (Fig. 7c), as principal constituents. Numerous small garnets and fine laths of biotite, latter a product of back-reaction and oriented in oblique orthorhombic patterns within the albite are very conspicuous (Fig. 7c). Muscovite crystals, oriented according to the same patterns as biotite, are small and relatively rare. The large albite-porphyroblasts also include blobs of quartz (Fig. 7c; Fig. 3e in Feijth & Franz, in prep.). All included garnet-crystals have inclusions of biotite, quartz and plagioclase (Fig. 3e in Feijth & Franz, in prep. b). The inclusion patterns of phyllosilicate indicate that albite is a pseudomorphic replacement of an orthorhombic mineral, possibly an anorthite and orthoclase-richer feldspar.

Thin section samples 65.5bI, 65.5bIII and 98.2 are also from the 'Gneiss di Morbegno', but from localities where the base of the formation is exposed. Former two were used for U-Th-Pb dating on monazite, whereas sample 98.2 was applied to date white mica and biotite by $^{40}Ar/^{39}Ar$-step heating. Basically the mineralogical content of these samples is similar to lithologic variety (b), but a much more pronounced anisotropic and tectonic fabric is developed. Samples 65.5bI and 65.5bIII show a strong linear and penetrative fabric, whereas sample 98.2 shows signs of relative intense layering-parallel shear and has a planar fabric. Garnets, particularly of sample 98.2, are generally larger than in sample 92.2 and not included in plagioclase, but plagioclase is common in their strain shadows.

Albite- and relatively large garnet-porphyroblasts of sample 98.2 contain older relics of sedimentary layering (S_i). The inclusion trails of fine opaques (Fig. 9a in Feijth, in prep. a.) in the prograde garnet (zonation from core to boundary: $Al_{60}Py_3Gr_{25}Sp_{12}$ to $\sim Al_{67}Py_{10}Gr_{21}Sp_2$) represent relics of sedimentary bedding. Growth of these garnets can only have occurred during the Variscan event. In the albite-porphyroblasts these layers of opaques indicate an original bedding which is parallel to the main foliation, formed by muscovite and biotite. This secondary foliation is deflected by the rigid garnet-porphyroblasts. The spiral shaped inclusion trails in the garnets indicate an up to 90° rotation with respect to the bedding plane and main foliation during their growth in when this zone accommodated bedding-parallel shear (Feijth, in prep. a). Samples 65.5bIII and 65.5bI have been used for U-Th-Pb dating with monazite. Particularly in sample 65.5bIII monazite has well-developed allanite-epidote coronas (Fig. 5c, d in Feijth & Franz, in prep.), similar to those described by Finger et al. (1998) who relate these coronas to amphibolite facies overprint. However, also homogeneous monazite-grains without coronas have been found in these samples.

Gneiss Chiari:
Quartz, orthoclase, large granoblastic microcline, albite-oligoclase and muscovite are the primary magmatic constituents of the 'Gneiss Chiari' of samples 39.2, 80.1, 82.13I and 82.17. The cleavage domains, a spaced foliation that is found anastomosing around the K-feldspars and quartz, contains muscovite, sericite, albitic plagioclase and chlorite (Fig. 7d).

The microstructure of the 'Gneiss Chiari' shows a development similar to that of the 'GOOV': The grainsize generally becomes finer towards these cleavage domains, where undulous extinction is more common, suggesting that these acted as micro-shear-zones. The outer zones of large quartz crystals consist of dominantly anhedral subgrains and deformation lamellae, indicating dynamic recrystallisation. Minor recovery by grain boundary area reduction is suggested in view of their slight modification towards polygonal crystal shapes.

A primary compositional layering related to deposition (S_0) is locally well-preserved close to the contacts with 'Gneiss di Morbegno' and is often visible in the field.

A slight schistose- or flaser character, and is concentrated in a spaced foliation of thin wavy cleavage domains is formed by muscovite which takes approximately 5 % of the rock volume and is often sheared parallel to foliation. Late brittle deformation is represented by brittle fractures in microlithons of quartz and K-feldspar. These are filled with sericite as well as galena- and Fe-oxide. Occasionally tourmaline and chloritised garnets (sample 39.2) are present in the cleavage domains. Except for sample 39.2 all were used for U-Th-Pb dating with monazite. Monazite and xenotime were both found in sample 82.13I, where the xenotime seems to have been growing on the edges of monazite by expelling Y during hydrothermal overprint from a Variscan monazite (Fig. 5f in Feijth & Franz, in prep.). Monazite of samples 80.1 and 82.17 is homogeneous and lacks corona-structures.

5 Geochronological results

5.1 U-Th-Pb-dating on monazite by EMP

Analytical results, including analyses of U, Th and Pb, are shown in Table III. Clear consistent ages, 319 ± 25 Ma, 322 ± 29 Ma, 324 ± 28 Ma and 326 ± 25 Ma, were obtained for the samples 31.7a-2 (from nearby 'Monte Valetto'), 65.5-bI, 65.5-bIII (both from Valle di Bomino) and 91.2aI (from Upper 'Valle del Livrio') respectively. The monazites of sample 31.7a-2 are homogeneous, indicating that overprint did not have any effect on them. Secondary apatite-allanite-coronas in the other samples of the 'Gneiss di Morbegno', particularly sample 65.5-bI and –bIII and to a lesser extent sample 91.2aI, (Fig. 5c, d and e in Feijth & Franz, in prep.) indicate a younger, probably lower grade metamorphic overprint.

U-Th-Pb data of the other samples, all from the 'Gneiss Chiari', indicate a probable Variscan origin of the monazites, and at least one prominent younger phase of either recrystallisation or crystallisation. This was not so clearly seen in sample 82.17. In this sample there is an age-distribution of the individual monazite-measurements of sample 82.17 of the 'Gneiss Chiari', ranging from 318 ± 46 to 262 ± 38 Ma, with an average age of 300 ± 30 Ma. The main metamorphic phase of this sample can thus be regarded Variscan, but a younger lower grade overprint is evident. Overprint of at least one possible young Permo-Mesozoic hydrothermal event was indentified in sample 80.1 and sample 82.13I. Analyses 82.13*I/m6.2*, for which an age of 178 ± 93 Ma was re-equilibrated at 322 °C as calculated applying the monazite-xenotime thermometer (Feijth & Franz, in prep.) on a composite monazite-xenotime grain (Fig. 5f in Feijth & Franz, in prep.). The Early- to Mid Carboniferous event of monazite growth (from 330 or earlier to 320 Ma indicates the peak of the main Variscan phase because conditions of dehydration melting of white mica and biotite were just reached at around 750 °C and $1,3 \leq$ GPa, as determined by Feijth & Franz (in prep.) applying also monazite-xenotime thermometry and phengite content of white mica (Massone & Schreyer, 1987).

Table III: Microprobe-results of monazite-analyses from the 'Gneiss di Morbegno' and 'Gneiss Chiari', and geochronological results.

	SiO2	PbO	ThO2	UO2	Nd2O3	Pr2O3	Ce2O3	La2O3	CaO	P2O5	Y2O3	Total	Si	Pb	Th	U	Nd	Pr	Ce	La	Ca	P	Y	tetr.	oct.	Mo	Br	Hu	Th	U	Pb	Th*	Age	Error	Weighted average
Gneiss di Morbegno:																																			
31.7a-2/m1.1	0,33	0,11	4,58	1,12	10,63	3,30	28,34	14,03	1,03	30,31	1,61	95,39	0,013	0,001	0,041	0,010	0,151	0,048	0,412	0,206	0,044	1,020	0,034	1,03	0,95	90,0	8,6	1,4	4,02	0,96	0,11	7,22	327	± 50	
31.7a-2/m2.1	0,24	0,09	5,36	0,73	10,51	3,19	28,68	13,34	0,99	29,57	1,56	94,24	0,010	0,001	0,049	0,007	0,152	0,047	0,426	0,200	0,043	1,015	0,034	1,02	0,96	89,7	9,3	1,0	4,71	0,64	0,09	6,78	288	± 53	
31.7e-2/m3.1	0,19	0,08	3,14	0,93	10,60	3,40	29,60	14,94	0,69	29,69	1,27	94,54	0,008	0,001	0,029	0,008	0,153	0,050	0,438	0,223	0,030	1,017	0,027	1,02	0,96	93,0	6,2	0,8	2,76	0,82	0,08	5,42	315	± 66	
31.7a-2/m4.1	0,17	0,09	3,40	0,82	10,82	3,33	28,70	14,19	0,69	29,40	1,27	92,89	0,007	0,001	0,032	0,008	0,159	0,050	0,431	0,215	0,030	1,021	0,028	1,03	0,95	92,7	6,6	0,7	2,99	0,72	0,08	5,35	352	± 67	
31.7a-2/m5.1	0,21	0,10	3,94	1,07	10,58	3,23	28,30	14,28	0,78	29,37	1,26	93,11	0,009	0,001	0,037	0,010	0,155	0,048	0,425	0,216	0,034	1,019	0,027	1,03	0,95	91,5	7,6	0,9	3,46	0,95	0,09	6,54	323	± 55	319 +- 25
65.5bII/m1.1	0,25	0,06	1,55	0,97	11,59	3,57	29,98	14,65	0,64	29,31	0,99	93,56	0,010	0,001	0,014	0,009	0,169	0,053	0,448	0,221	0,028	1,014	0,021	1,024	0,965	94,7	4,3	1,1	1,362	0,858	0,054	4,144	291	± 87	
65.5bII/m2.1	0,44	0,13	5,58	0,91	10,32	3,25	28,12	12,06	1,18	29,23	1,50	92,71	0,018	0,001	0,052	0,008	0,151	0,049	0,422	0,182	0,052	1,014	0,033	1,032	0,950	88,2	9,9	1,9	4,902	0,800	0,117	7,508	351	± 48	
65.5bII/m3.1	0,63	0,10	5,38	0,74	10,15	3,24	27,73	12,09	1,15	28,08	0,32	89,61	0,027	0,001	0,052	0,007	0,154	0,050	0,432	0,189	0,052	1,011	0,007	1,037	0,945	88,2	9,0	1,3	4,732	0,654	0,090	6,853	295	± 52	
65.5bII/m4.1	0,30	0,10	2,49	1,41	10,26	3,35	29,38	12,93	0,86	29,44	1,40	91,92	0,012	0,001	0,023	0,013	0,151	0,050	0,442	0,196	0,038	1,024	0,031	1,036	0,944	92,2	6,5	1,3	2,187	1,247	0,093	6,242	334	± 58	324 +- 28
65.5bl/m1.1	0,30	0,09	3,81	0,92	10,98	3,43	28,93	11,93	0,87	28,49	1,00	90,74	0,012	0,001	0,037	0,009	0,165	0,053	0,446	0,185	0,039	1,015	0,022	1,028	0,956	91,2	7,5	1,3	3,349	0,807	0,083	5,969	311	± 60	
65.5bl/m2.1	0,35	0,10	3,37	1,33	10,91	3,47	29,86	13,04	1,02	28,60	0,80	92,87	0,015	0,001	0,032	0,012	0,162	0,052	0,453	0,199	0,045	1,004	0,018	1,018	0,975	90,8	7,7	1,5	2,963	1,175	0,095	6,780	315	± 53	
65.5bl/m3.1	0,25	0,09	2,50	0,96	10,78	3,73	31,16	12,81	0,69	29,30	0,52	92,81	0,010	0,001	0,023	0,009	0,158	0,056	0,469	0,194	0,030	1,020	0,011	1,030	0,953	93,4	5,5	1,1	2,201	0,847	0,087	4,968	393	± 72	
65.5bl/m4.1	0,29	0,10	4,58	0,97	10,71	3,25	29,07	12,90	1,07	28,96	1,19	93,11	0,012	0,001	0,043	0,009	0,158	0,049	0,438	0,196	0,047	1,010	0,026	1,022	0,967	89,8	9,0	1,2	4,028	0,859	0,091	6,817	300	± 53	322 +- 29
91.2a/m1.1	0,20	0,10	3,67	0,85	11,37	3,60	30,99	14,19	0,78	30,91	0,87	97,53	0,008	0,001	0,033	0,007	0,159	0,051	0,443	0,205	0,033	1,023	0,018	1,03	0,95	92,4	6,8	0,8	3,23	0,75	0,10	5,68	376	± 63	
91.2a/m2.1	0,30	0,11	4,97	1,01	10,77	3,20	29,69	13,79	0,98	29,64	0,92	95,39	0,012	0,001	0,046	0,009	0,155	0,047	0,438	0,205	0,042	1,011	0,020	1,02	0,98	89,9	8,8	1,3	4,36	0,89	0,10	7,27	324	± 49	
91.2a/m3.1	0,62	0,07	3,15	0,96	11,19	3,56	30,48	14,04	0,64	29,06	0,79	94,42	0,025	0,001	0,029	0,007	0,163	0,053	0,454	0,211	0,029	1,001	0,017	1,03	0,96	93,3	4,1	2,6	2,77	0,70	0,07	5,05	300	± 71	
91.2a/m4.1	0,31	0,12	5,58	0,99	10,51	3,07	27,70	13,10	1,01	29,26	1,18	92,81	0,013	0,001	0,052	0,009	0,154	0,046	0,417	0,199	0,045	1,001	0,026	1,03	0,95	88,8	9,8	1,3	4,90	0,87	0,11	7,74	311	± 46	
91.2a/m5.1	0,23	0,10	4,53	0,83	10,64	3,16	28,14	13,31	0,87	29,38	1,22	92,40	0,009	0,001	0,042	0,008	0,156	0,047	0,424	0,202	0,038	1,023	0,027	1,03	0,95	90,7	8,3	1,0	3,99	0,74	0,09	6,38	326	± 56	326 +- 25
Gneiss Chiari:																																			
80.1/m1.1	0,59	0,00	2,50	0,10	11,46	3,99	34,05	13,03	0,27	28,73	0,36	95,08	0,024	0,000	0,023	0,001	0,167	0,059	0,509	0,196	0,012	0,993	0,008	1,017	0,975	96,3	1,2	2,5	2,195	0,088	0,000	2,475	*		
80.1/m2.1	0,93	0,05	6,11	0,16	12,72	4,32	31,51	8,25	0,59	27,71	0,26	92,62	0,039	0,001	0,058	0,001	0,191	0,066	0,484	0,128	0,026	0,985	0,005	1,024	0,962	91,0	4,9	4,1	5,368	0,141	0,047	5,822	181	± 62	
80.1/m3.1	0,81	0,11	6,25	0,40	9,63	3,43	31,66	11,82	0,66	27,59	0,90	93,25	0,034	0,001	0,060	0,004	0,144	0,052	0,486	0,183	0,030	0,979	0,020	1,013	0,979	90,5	6,0	3,5	5,490	0,349	0,105	6,625	355	± 54	
80.1/m4.1	0,99	0,10	7,91	0,38	10,84	3,80	30,11	9,23	0,80	27,71	1,01	92,81	0,039	0,001	0,075	0,004	0,162	0,058	0,462	0,143	0,036	0,963	0,022	1,022	0,963	88,1	7,9	4,1	6,951	0,332	0,088	8,024	247	± 45	
80.1/m4.2	1,01	0,09	7,90	0,42	11,40	3,74	30,21	9,33	0,82	27,27	0,67	92,87	0,043	0,001	0,076	0,004	0,172	0,057	0,466	0,145	0,037	0,974	0,015	1,016	0,973	88,0	7,6	4,4	6,946	0,374	0,086	8,155	237	± 44	
80.1/m4.3	1,06	0,09	7,96	0,42	11,26	3,69	30,22	9,15	0,81	27,39	1,05	93,13	0,045	0,001	0,076	0,004	0,169	0,056	0,464	0,142	0,037	0,973	0,024	1,017	0,972	88,0	7,4	4,6	7,014	0,368	0,087	8,202	238	± 44	
80.1/m5.1	1,24	0,13	9,23	0,45	8,66	3,17	29,89	11,10	0,78	26,38	1,02	92,05	0,053	0,001	0,090	0,004	0,132	0,050	0,469	0,175	0,036	0,957	0,023	1,010	0,981	86,7	7,8	5,4	8,112	0,396	0,119	9,395	283	± 38	.
82.13/lm3.1	0,204	0,020	1,554	0,104	7,931	3,507	34,486	19,352	0,221	29,345	0,108	96,83	0,008	0,000	0,014	0,001	0,114	0,051	0,508	0,287	0,010	1,000	0,002	1,008	0,988	97,5	1,7	0,8	1,366	0,092	0,019	1,664	252	± 216	
82.13/lm6.1	1,159	0,046	6,511	0,118	9,860	3,620	31,256	13,458	0,292	27,742	0,572	94,63	0,048	0,001	0,061	0,001	0,146	0,055	0,473	0,205	0,013	0,972	0,013	1,019	0,967	92,2	2,8	5,0	5,722	0,104	0,043	6,056	158	± 59	
82.13/lm7.1	0,112	0,000	1,055	0,088	10,147	4,134	34,888	15,066	0,163	29,705	0,276	95,63	0,004	0,000	0,010	0,001	0,146	0,061	0,515	0,224	0,007	1,014	0,006	1,019	0,969	98,2	1,3	0,5	0,928	0,077	0,000	1,173	*		
82.13/lm6.2	0,342	0,033	4,022	0,110	9,757	4,047	33,709	13,149	0,540	28,724	0,357	94,79	0,014	0,000	0,038	0,001	0,143	0,061	0,507	0,199	0,024	0,998	0,008	1,012	0,980	93,6	4,9	1,4	3,535	0,097	0,031	3,848	178	± 93	
82.13/lm5	0,132	0,016	0,962	0,081	8,081	3,662	34,843	17,391	0,250	28,024	0,201	93,64	0,006	0,000	0,009	0,001	0,121	0,056	0,534	0,288	0,011	0,993	0,004	0,999	1,005	97,9	1,6	0,5	0,845	0,071	0,015	1,077	318	± 333	
82.17/m1.1	0,88	0,12	7,07	0,56	10,46	3,44	29,99	11,20	0,68	28,07	1,81	94,26	0,036	0,001	0,066	0,005	0,154	0,052	0,453	0,170	0,030	0,960	0,040	1,016	0,971	89,5	6,7	3,7	6,211	0,493	0,111	7,812	318	± 46	
82.17/m2.1	1,35	0,12	9,41	0,93	10,41	3,39	29,38	11,16	0,71	27,11	1,18	94,61	0,056	0,001	0,089	0,004	0,155	0,051	0,448	0,171	0,032	0,956	0,026	1,012	0,978	87,2	7,0	5,7	8,272	0,348	0,110	9,397	262	± 38	
82.17/m3.1	0,96	0,12	7,78	0,27	13,82	3,86	27,97	7,51	0,99	27,38	0,76	91,42	0,041	0,001	0,075	0,003	0,209	0,060	0,434	0,117	0,045	0,984	0,017	1,024	0,963	87,2	8,5	4,2	6,840	0,239	0,111	7,618	325	± 47	
82.17/m4.1	0,21	0,03	2,36	0,12	12,00	4,57	36,34	10,09	0,43	28,93	0,12	95,18	0,009	0,000	0,022	0,001	0,175	0,068	0,544	0,152	0,019	1,002	0,003	1,010	0,984	95,8	3,4	0,9	2,070	0,101	0,032	2,399	295	± 149	
82.17/m3.2	0,25	0,04	2,94	0,13	12,66	4,55	33,93	8,97	0,90	27,50	0,00	91,86	0,011	0,000	0,029	0,001	0,193	0,071	0,529	0,141	0,041	0,991	0,000	1,002	1,004	93,0	6,0	1,1	2,585	0,115	0,040	2,958	300	± 121	
82.17/m1.2	0,87	0,12	7,46	0,40	9,57	3,48	30,60	10,93	0,76	27,95	1,26	93,38	0,036	0,001	0,071	0,004	0,142	0,053	0,466	0,168	0,034	0,984	0,028	1,020	0,965	88,8	7,5	3,7	6,558	0,353	0,108	7,704	315	± 47	300 +- 30

5.2 The $^{40}Ar/^{39}Ar$-method on white mica and biotite

Results of the step heating measurements are illustrated in Fig. 8 and listed in Appendix 1. A Variscan event, at 325-305 Ma is very obvious in the step-heating measurements of white mica (39.2, 82.13I, 92.2, 98.2) (Fig. 8) and can be considered the main event of closure of white mica of the of the 'Orobic fold nappe' and possibly of the entire substructure. These mid- to late-Carboniferous ages of white-mica represent cooling following the peak metamorphic event that was dated by monazite at 330-325 Ma.

Step heating of multigrain samples of biotite from the 'GOOV' (33.6, 64.2) and from the 'Gneiss di Morbegno' (98.2, 92.2) (Fig. 8, Appendix 3) indicate thermal activity related to Middle Permian and Mesozoic metasomatic- or hydrothermal events. For the nice plateaux of samples 64.2 and 98.2, average ages of 159.9 ± 1.6 Ma and 255.3 ± 2.5 Ma were calculated (Fig. 8). The older of these two events, a Middle Permian phase, might also have overprinted multigrain white mica sample 33.6 (Fig. 8). The Variscan biotite ages of Bocchio et al. (1981) and Mottana et al. (1985), mentioned in the introduction, remain the only Variscan biotite ages available for the Orobic basement that give cooling ages of the main Variscan regional event related to cooling after the peak conditions at 330-320 Ma.

6 Discussion of the geochronological results and implications

6.1 Pre-Variscan development and orogenic events

The stratigraphic succession and igneous units of the lower sequence, which includes the metabasites and the 'GOOV', can be correlated with the 'Scisti dei Laghi' in the 'Strona-Ceneri Zone'. This sequence includes the 'Strona-Ceneri Border Zone' and granodiorites that are equivalent to the 'GOOV' of the Orobic basement because structural, igneous and petrographic relationships are similar (Feijth, in prep. a). The 'Strona-Ceneri sequence' in the 'Strona-Ceneri Zone', corresponds with the upper sequence of the Orobic basement. This is a useful correlation, because for the 'Strona-Ceneri Zone' isotopic age data are available for the 'Scisti dei Laghi sequence', which enables indirect geochronological constraint of the metamorphic and igneous development in the Orobic basement.

There is strong evidence for an Ordovician metamorphic event that affected paragneisses in the 'Strona-Ceneri Zone' which are equivalent to the host rock of the Orobic 'GOOV'. The available isotopic results are following; 450 ± 10 Ma (U-Pb monazite; Köppel &-Grünenfelder, 1971), 450-500 Ma (U-Pb zircon; Köppel, 1974), 440-450 Ma (U-Pb monazite; Köppel & Grünenfelder, 1978, 1979), 473 Ma (Rb-Sr WR; Hunziker & Zingg, 1980) and 480 Ma (U-Pb staurolite; Romer & Franz, 1998), latter being the most unambiguous. It is therefore most likely that during this 'Sardic' metamorphic phase the first generation of folds developed in the lower sequence of the 'Orobic fold nappe'.

Granitoid intrusion of the 'GOOV' occurred at shallow levels after Pre-Variscan uplift, folding and metamorphism of the basement that forms lower sequence of the 'Orobic fold nappe' (Feijth, in prep. a). Similarly, in the 'Scisti dei Laghi sequence', at 'Monte Gambarogno', the host rock was metamorphosed and deformed before intrusion of the granodiorites (Boriani et al., 1990).

Eclogitic metamorphic grade of xenoliths/eclogitic pods in the 'Ceneri gneisses' (Zurbriggen et al., 1997), the western equivalent of the 'GOOV', indicate a tectonic environment of an

White Mica:
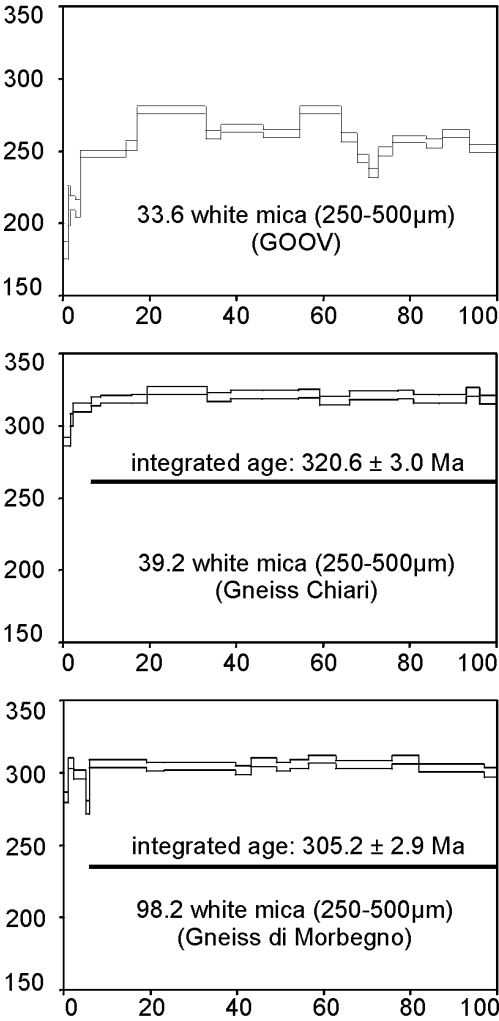
Fig. 8. [40]Ar-[39]Ar apparent age spectra of white mica and biotite from different lithologies of the Orobic basement, Southern Alps (locations shown in Fig. 2). Analytical uncertainties (Two sigma intralaboratory) are represented by the vertical width of the bars. Experimental temperatures increase from left to right. Plateau ages are listed. Plateau increments used for calculation of plateau ages are delineated.
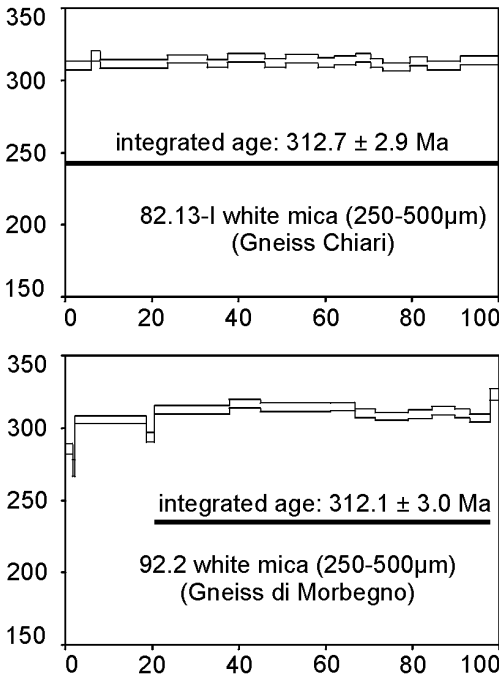
Biotite:
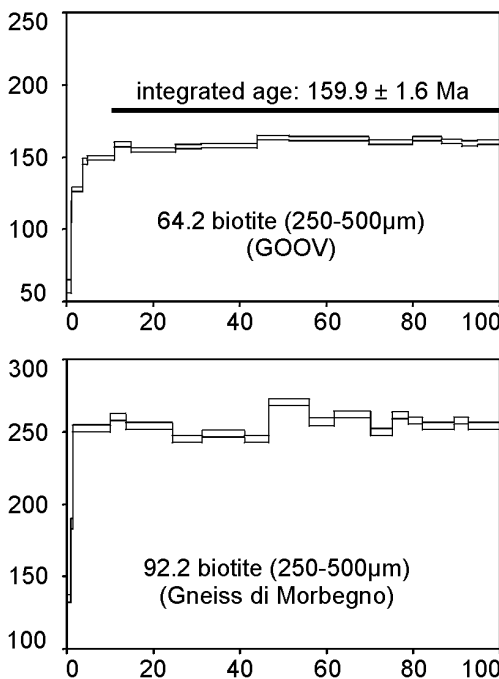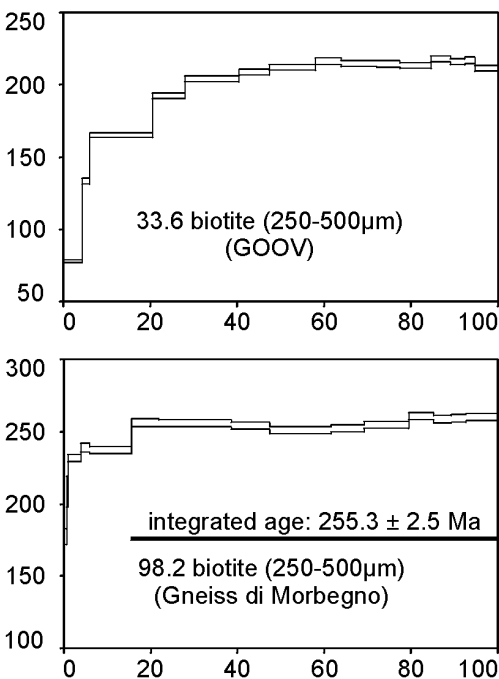
accretionary complex that previously affected the subcropping units. This 'Sardic' phase of accretion and underplating in the 'Strona-Ceneri Zone' was suggested by Handy et al. (1999) for the period between 440 and 480 Ma must have preceded the intrusion of the granodiorites. In plate-tectonic context this phase of collision of an island arc with northern Gondwana was suggested before by Stampfli (1987). The accreted sediments, the volcanics of the lower sequence and the protoliths of the eclogitic xenoliths of the 'Ceneri gneisses' might have originally belonged to the oceanic plate that subducted below the arc that approached Gondwana (Fig. 9, profile 1). The earliest phase of metamorphism and folding that affected the lower sequence before late-to post-orogenic igneous and magmatic phases is most likely related to the orogenic front of the frontal arc by which the sedimentary sequence of the accretionary complex were subsequently affected (Fig. 9, profile 2). After uplift and erosion these rocks formed the base of an active marginal basin behind the frontal arc, with the late-to post-orogenic plutonic activity related to the 'GOOV' and rhyolitic volcanism (Fig. 9, profile 3).
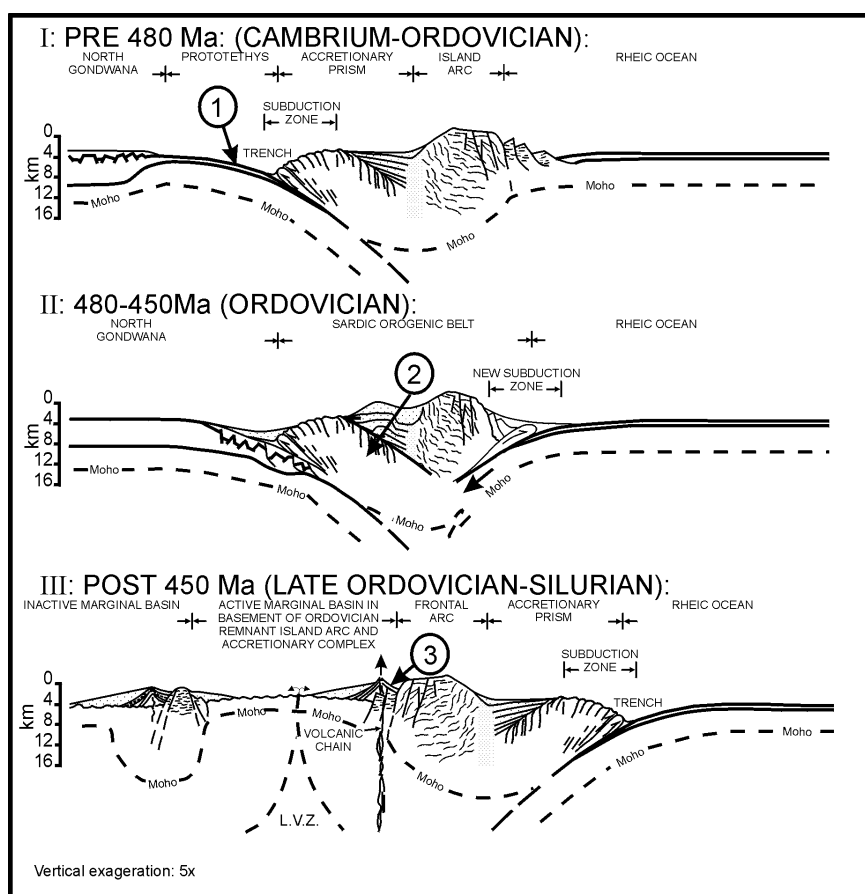
Fig. 9. Scenario for the Early Palaeozoic evolution indicated by the different positions of the Orobic protoliths at three progressive stages around the Sardic event, which are indicated by profiles I to III. At these three stages protoliths of the Orobic basement were respectively positioned at locations 1 to 3 (encircled numbers in profiles) during depositional, metamorphic, igneous and volcanic phases: (1) Sedimentation of the protoliths of the lower sequence, including the metabasitic intercalations, (2) Peak-metamorphism and (3) intrusion of 'GOOV' and rhyolitic volcanism (protoliths of 'Gneiss Chiari'). Stages I, and a somewhat later stage of III, might correspond respectively with the paleogeographic maps of the Early Ordovician (490 Ma) and Early Silurian (435 Ma) of Stampfli (1996).

The age of igneous emplacement of the 'GOOV' would be similar to isotopic ages from the 'Ceneri-granodiorites'; 466 Ma (Rb-Sr WR; Boriani et al., 1982/1983), 468 Ma (Rb-Sr WR; Boriani & Giobbi Origoni, 1992) and 430-500 Ma for related metasomatism (U-Pb zircon; Köppel & Grünenfelder, 1971). Köppel & Sommerauer (1974) Caironi (1986) later recognised a magmatic origin of the zircons dated by Köppel & Grünenfelder (1971).

It is an open question if Ordovician igneous activity of the granodiorites and the 'GOOV' was cogenetic with volcanic activity related to the 'Gneiss Chiari'. Such a relationship was already proposed by Heinisch & Schmidt (1982) for equivalent rocks of the Eastern Alps.

The 'Gneiss Chiari' is a possible Orobic counterpart of the 'Upper Ordovician Rhyolitic Plateau' (Feijth, in prep. a). When they represent a time marker in the 'Northern Greywacke Zone', they must have been extruded around or after the Caradocian-Ashgillian boundary (~450 Ma) (Feijth, in prep. a; with reference to Flajs & Schönlaub, 1976).

Biostratigraphic data of Sassi et al. (1984) allow earlier rhyolitic volcanism in the Eastern Southalpine basement, because their palynological assemblages from the Col di Foglia Formation suggest a late Early Cambrian to Early Ordovician (Tremadocian) age (520-475 Ma) for the sedimentation, the late Cambrian being more probable.

Recently Meli and Klötzli (2001) have dated zircons from Eastern Southalpine metavolcanics, the Comelico porphyroids, which yielded ages of 479 ± 8 Ma and 485 ± 8 Ma. These ages are older (30-35 Ma) than the 'Upper Ordovician Rhyolitic Plateau' in the 'Northern Greywacke Zone'. However, the age of rhyolitic volcanism of the protoliths of 'Gneiss Chiari' in the western part of the Italian Southern Alps, would have occurred earlier, because of the reliable U-Pb-age of 480 Ma of staurolite of the 'Strona Ceneri Zone' (Romer & Franz, 1998). The different ages for Ordovician rhyolitic volcanism might indicate a diachronous event, but all ages are still in the same range as the isotopic ages of the igneous phase of the 'Scisti dei Laghi sequence'. This would support a cogenetic origin of the 'GOOV'-intrusion and rhyolitic volcanic volcanism.

6.2 Variscan events

Syn-kinematic relationships of larger garnet porphyroblasts with weak relic prograde zonation are typical of early deformation in a zone of intense shearing identified at many locations around the contact between the lower and upper sequences of the 'Orobic fold nappe'. This prograde metamorphism and shearing preceded the phase of development of the 'Orobic fold nappe' and would be related to a phase of crustal thickening. Also in the lower sequence of the 'Orobic fold nappe' garnet grew during this phase, particularly in the halos around the 'GOOV'. This phase of tectonic burial is related to thrusting during a collisional phase that progressively affected deeper crustal levels. During this phase the main foliation that transposes bedding in the upper sequence of the 'Orobic fold nappe' developed and prograde garnet- and kyanite- porphyroblast-grew under prograde P- and T-conditions. Peak conditions, $\leq 1,3$ GPa and 750 °C (Feijth & Franz, in prep.), occurred at 330-320 Ma in the substructure, as determined by U-Th-Pb monazite-dating. During the following ductile to brittle-ductile collapse phase kinematic conditions were significantly different (Feijth, in prep. a). Diapirism by dehydration melting induced buoyancy and extrusion by superimposed tectonic strain occurred and the 'Orobic fold nappe' was formed, which was modified by gravitational collapse and wrenching (Feijth, in prep. b, c). The staurolite-porphyroblasts in

lithologic variety (a) of the 'Gneiss di Morbegno' grew during the earliest retrogression (Feijth & Franz, in prep.). Structural and metamorphic relationships indicate that the formation of the 'Orobic fold nappe' marks the start of processes of uplift, crustal thinning and retrogression (Feijth, in prep. a, b; Feijth & Franz, in prep.). Isotopic age-data show that related closure of the $^{40}Ar/^{39}Ar$-system in white mica occurred between 325 and 305 Ma. During this phase the main foliation and other related fabrics that formed under immediately preceding peak-conditions were folded and deformed due to the formation of the 'Orobic fold nappe'. Later stages of this event are represented by the closure of Biotite at 291 ± 6 (Bocchio et al., 1981) and 292 ± 9 Ma (Mottana et al., 1985).

The Variscan $^{40}Ar/^{39}Ar$-ages of white mica and biotite comply with conclusions drawn from the 'Manno conglomerates' (Graeter, 1951; Lehner, 1952; Reinhard, 1964) and further constrain the age, because it is now certain that the peak metamorphic phase affecting the rhyolitic 'Gneiss Chiari'-protoliths is not older than Early-Mid Carboniferous.

This main Variscan cooling event and the development of the 'Orobic fold nappe' corresponds to the 'Gambarogno Phase' in the 'Strona-Ceneri Zone' of Handy et al. (1999) and the 'Schlingen-phase' of Zurbriggen et al. (1998), which was determined by Boriani & Villa (1997) to have occurred at 290 Ma.

A conceptual model of Variscan tectonic development is illustrated in Fig. 10 of Feijth. (in prep. a). Orogenic belts, including the Variscan, consist of a metamorphic core with a lower grade suprastructure characterised by thin-skinned tectonics, which metamorphic grade reduces to the outer zones of the belt. Such a structural configuration of Variscan origin is still well-preserved in the 'Cantabrian mountains' and the 'Montagne Noire'. The suprastructure is connected with the foreland thrust-system. A similar configuration might exist in the relic Variscan structure of the Orobic chain. The greenschist metamorphic conditions attained by the 'Scisti di Edolo' (Gansser & Pantić, 1988), are substantially lower than metamorphism of the underlying sequence. A potential contact between core and suprastructure is exposed near San Antonio, east of Aprica, and can be eastwards followed in the 'Val di Corteno', east of 'Aprica'. The typical bedding-parallel shear of the suprastructure, which is present in the 'Scisti di Edolo', decreases upward. This style of deformation differs from the deformation structures of the sub-cropping 'Orobic fold nappe', that formed under ductile deformation at significantly higher metamorphic conditions.

The age of metamorphism in the 'Scisti di Edolo' is not yet exactly known, because isotopic age data are not available, but field relationships mentioned above and in Feijth (in prep. a) and its grade indicate that it is certainly Variscan and is possibly different to the metamorphic age of the substructure. Other units of similar metamorphic grade in the Austroalpine and Southalpine basement of the Eastern Alps that didn't reach high pressure conditions like those attained in the Orobic substructure could be potentially equivalent to the 'Scisti di Edolo'. The Southalpine 'Agordo- and -Bressanone phyllitic complexes' have much older protolith ages, Late Cambrian to Early Tremadocian (Sassi et al., 1995), which leaves the Eastern Alpine 'qaurtzphyllites', which have been deposited in the Late Ordovician and Silurian, as a potential equivalent. These, have a metamorphic age of 300-310 Ma (Personal comm., F. Neubauer). In the Kreuzeck mountains, just south of the Tauern window, metamorphism of an equivalent unit has been dated ca. 300 (+320?) Ma (Hoke, 1990, presenting previously unpublished data of Brewer). The 'Quartzphyllites' of the Austroalpine basement which

should be equivalent to the 'Scisti di Edolo' is a continuous fossil-bearing section reaching early Namurian, locally Westphalian A. Therefore the age of this relatively low grade metamorphic imprint of these units cannot be older than 310-320 Ma.

Gansser & Pantic, (1988) have already indicated that the oldest phase of metamorphism of the 'Scisti di Edolo' is of Variscan age. Another indication for a Variscan age of the metamorphism of the lower grade rocks of the suprastructure are the garnet-relics that indicate imprint of a metamorphic phase that exceeds the Alpine conditions.

The contact between the 'substructure' and suprastructure, across which the metamorphic grade changes abruptly, is thus at least a Variscan tectonic discontinuity between the metamorphic core and a suprastructure, represented by the 'Scisti di Edolo', in the Orobic basement. Because the hanging wall has a lower Variscan metamorphic grade than the footwall the contact is interpreted as a normal fault. This fault is rooted in the rootzone.

The 'Val Biandino plutonic complex' seals the structures formed by the event of fold nappe development. Furthermore the age of the emplacement of this plutonic complex (307-271 (±9) Ma) (De Capitani et al., 1988) predates the development of the 'Orobic Collio basin', which minimum age is indicated by zircon ages from samples from the Novazza Uranium mine. Rhyolite cooling units 3 and 4 of the lower member of the Collio formation were sampled and the ages of these zircons are respectively 287 (J. Hunziker, in Cadel, 1986) and 280 Ma (Philippe et al., 1987).

The geologically short time interval between peak metamorphism, dated by the U-Th-Pb method on monazite, and last closure of the $^{40}Ar/^{39}Ar$ isotopic systems in muscovite and biotite as well as the development of the 'Orobic Collio basin' soon after closure of these isotopic systems expresses high exhumation rates. The main retrograde phase-changes and reactions occurred in this period (Feijth & Franz, in prep.). This time-interval overlaps with the period of dextral shearing in the Variscan belt discussed by Arthaud & Matte (1977), that lasted from 290 to 250 Ma. However in Feijth & Neubauer (in prep. a) and in the above presented data a hydrothermalthermal phase imprint at 300-350 °C was identified for the period between 255 and 260 Ma, just before the deposition of the Upper Permian fluviatile conglomerates of the 'Verrucano Lombardo' formation started. This is a late stage of the Permian volcanic phase. In the field related ore-deposits, in the form of Fe-concretions, siderite- and barite veins, all concentrated in and along Late-Permian syn-diagenetic hydroplastic faults, have been identified. These faults affect the uppermost Lower Permian and do not continue into the 'Verrucano Lombardo formation'.

6.3 Mesozoic overprint

Structural, petrographic and geochronological data presented above, particularly the Y-contents of Monazite, and in Feijth (in prep. a) and Feijth & Franz (in prep) indicate that the late-Variscan to Mid-Permian development is of other nature than the Mesozoic. Thermal or hydrothermal overprint, related to the long period of (Permo-)Mesozoic (possibly intermittent) rifting is well pronounced in the 'Lario basement' (western Orobic Alps) (Bertotti et al., 1999; Hanson et al., 1966; Bocchio, 1981; Mottana et al., 1985). Monazite-xenotime- and two feldspar thermometry indicate a relatively low T hydrothermal overprint at least for a Mesozoic phase. Temperatures calculated by monazite-xenotime thermometry (Gratz & Heinrich, 1997) and two feldspar thermometry (Stormer & Whitney, 1985)

presented in (Feijth & Franz, in prep.) revealed temperatures of 322 °C and 339 ± 18 °C respectively. These temperatures fall exactly in the range between the closure temperatures of white mica and biotite, which is confirmed by the results of the $^{40}Ar/^{39}Ar$-isotopic data. Radiometric $^{40}Ar/^{39}Ar$-ages of white mica are dominantly Variscan, whereas the biotite ages are either Mesozoic (~160 Ma) and Middle Permian (~250-255 Ma). The Permian re-equilibration of biotite (samples 92.2 and 98.2) must be related to hydrothermal activity in connection with volcanism in the 'Collio Orobico basin', which was also identified in the detrital white mica of the Permian sediments (Feijth & Neubauer, in prep. a).

Early Mesozoic N-S striking extensional faults in the study area are not very obvious in the field. By reactivation during the Alpine phases as 'transverse structures', the 'Ballabio-Barzio'-, 'Bovegno-Valbondione'-, 'Brembana'- and 'Lower Seriana'- and 'Vedra' transverse zones their inheritance has become clear (Schönborn, 1992). Facies changes and asperities along the Mesozoic normal faults are the origin of the inheritance. Through comparison of a thermokinematic model, based on the sedimentary record with variable Ladinian to Late Liassic thicknesses, with isotopic age data in the 'Monte Generoso basin', Bertotti et al. (1999) has found evidence that at 223 Ma, the age of the start of rifting, there must have been a magmatic event that had increased the geothermal gradient. This volcanism occurred during deposition of the Ladinian 'Wengen-' and 'Buchenstein' formations, and was also identified in the Orobic Alps, but none of the $^{40}Ar/^{39}Ar$- age spectra points clearly to this volcanic event. The thermal effect of rifting would have been superposed on the magmatically induced geothermal gradient. Thermal gradients decreased from > 60 °C km^{-1} at the onset of extension to ~20 °C km^{-1} shortly after breakup. Cooling trough the closure temperatures of white mica and biotite is possibly identifiable in the apparent age spectra of few samples. Biotite of sample 33.6, shows a relatively poorly defined plateau around 210-220 Ma whereas Variscan muscovite of this sample shows a Mesozoic overprint. The integrated age of biotite of sample 64.2 is however much younger and possibly stronger related to the rifting itself. Separation of the magmatic and tectonic effects seems to be difficult with the available data from the central Orobic Alps.

The Jurassic ages obtained for investigated part of the Orobic basement are thus most probably connected to a combination of these volcanic/magmatic events and opening of the 'Lombardian basin'. Hydrothermal activity is likely, based on the re-equilibration of Variscan monazite under formation of xenotime at the edge of grains and mentioned ore-deposition. Presented data prove that these Mesozoic events would thus also have affected the study area, which forms the hanging wall of the oppositely dipping 'Lugano-Val Grande-' and the 'Sebino faults'. The geographic distribution of the 'Lombardian basin' is different (Fig. 2 in Bertotti et al., 1999) from the distribution of Upper Permian-Scythian formations. Subsidence, related to Permian-Scythian sagging, is expressed in thickness variation in the Upper Permian sequences. Marine influences progressively increase from west to east during deposition of the Upper Permian 'Verrucano'- and 'Bellerophon'- and Scythian 'Servino'- and 'Bovegno' Formations. The shallow shelf deposits of the 'Bellerophon formation' are not exposed in the Orobic Alps. These can be found in the provinces of Trentino and Alto Adige.

From the analytical data it seems obvious that the monazites of the 'Gneiss Chiari' were more vulnerable to hydrothermal overprint than those of the 'Gneiss di Morbegno', which might be related to the lithological characteristics that controlled diffusivity of hydrothermal fluids,

such as a relatively brittle rheological behaviour at the prevailing temperatures. However, unambigeous distinction of Middle Permian and Mesozoic overprint not possible for all analyses or samples. Separation of the effects of both phases is yet very difficult because the study area was overprinted by these to phases of comparable conditions.

APPENDIX 3.1

Ar-analytical data from multi-grain incremental heating analyses on white mica and biotite from the Orobic basement. Errors are 1-sigma inter-laboratory. Lithological units and sample locations, including co-ordinates, are indicated behind sample numbers. Short lithological descriptions are also given.

[a] measured
[b] corrected for post-irradiation decay of ^{37}Ar (35.1 days half-life)
[c] (^{40}Ar$_{tot}$ - ^{36}Ar$_{atmos}$ x 295.5) / ^{40}Ar$_{tot}$

Sample: JF-33.6 (white mica 250-500μm) Gneiss Occhiadini Orobico-Valtellinese (GOOV)
(Location: North of Alpe Cul, Co-ordinates: 1547798-5099712)
J-Value: 0.000396 ± 0.000004

step	^{36}Ar/^{39}Ar[a]	^{37}Ar/^{39}Ar[b]	^{40}Ar/^{39}Ar[a]	%39Ar	%40Ar[c]	age	+/-
1	0.59629	0.03735	443.52	1.2	60.3	181.5	6.1
2	0.68215	0.05133	516.77	0.4	61.0	212.2	13.9
3	0.31142	0.08805	409.92	1.3	77.6	213.9	4.8
4	0.43861	0.30713	442.03	1.1	70.7	210.5	6.1
5	0.09089	0.06778	398.76	10.5	93.3	247.9	2.4
6	0.19057	0.62004	437.23	2.7	87.1	253.6	3.3
7	0.04712	0.05945	435.11	15.8	96.8	278.3	2.6
8	0.10878	0.32034	425.29	3.4	92.4	261.1	2.8
9	0.05794	0.07391	417.86	9.9	95.9	265.7	2.6
10	0.02257	0.08956	401.64	8.3	98.3	262.2	2.6
11	0.02454	0.19475	428.20	9.5	98.3	278.2	2.7
12	0.05422	0.56200	406.17	3.9	96.1	259.3	2.8
13	0.07028	0.48764	387.43	2.6	94.6	244.7	2.9
14	0.08841	0.35014	377.30	2.2	93.1	235.0	3.3
15	0.08056	0.52603	398.25	3.3	94.0	249.5	2.9
16	0.05323	0.16395	404.39	7.7	96.1	258.3	2.5
17	0.08928	0.47188	410.17	3.7	93.6	255.3	2.9
18	0.08613	0.30765	420.08	6.2	93.9	262.0	2.6
19	0.15039	0.25408	422.78	6.4	89.5	251.9	2.6
total	0.08549	0.20653	416.22	100.0	93.9	259.7	2.4

Sample: JF-39.2 (white mica 250-500μm) Gneiss Chiari
(Location: Passo dei Lupi, Co-ordinates: 1557790-51018150)
J-Value: 0.000398 ± 0.000004

step	$^{36}Ar/^{39}Ar^a$	$^{37}Ar/^{39}Ar^b$	$^{40}Ar/^{39}Ar^a$	%39Ar	%40Ar[c]	age	+/-
1	0.10573	0.38398	467.44	1.7	93.3	288.9	2.9
2	0.05821	0.75149	478.32	0.6	96.4	304.1	4.1
3	0.05180	0.16454	490.66	4.2	96.9	312.6	2.9
4	0.03636	0.25255	492.86	2.2	97.8	316.7	3.1
5	0.04087	0.00526	496.93	7.0	97.6	318.3	3.0
6	0.01847	0.15435	490.58	3.6	98.9	318.5	3.0
7	0.01357	0.00201	498.82	14.0	99.2	324.3	3.0
8	0.01086	0.03044	490.49	5.4	99.3	319.8	3.0
9	0.00992	0.08502	493.46	7.4	99.4	321.7	3.0
10	0.00751	0.04102	492.19	8.1	99.5	321.4	3.0
11	0.01151	0.09148	494.77	5.1	99.3	322.3	3.0
12	0.00807	0.06416	485.92	6.8	99.5	317.5	3.0
13	0.00766	0.03832	491.46	11.2	99.5	320.9	3.0
14	0.00267	0.28853	491.33	3.5	99.8	321.8	3.1
15	0.00199	0.09798	486.08	6.0	99.9	318.7	3.0
16	0.00352	0.12791	486.60	6.1	99.8	318.8	3.0
17	0.00089	0.47824	493.51	3.1	99.9	323.5	3.2
18	0.00448	0.39801	485.70	3.9	99.7	318.1	3.0
total	0.01511	0.10358	491.52	100.0	99.1	319.7	2.9
steps 3-18				93.5		320.6	3.0

Sample: JF-82.13-I (white mica 250-500μm) Gneiss Chiari
(Location: Pizzo Zerna, Co-ordinates: 1564304-5100078)
J-Value: 0.000399 ± 0.000004

step	$^{36}Ar/^{39}Ar^a$	$^{37}Ar/^{39}Ar^b$	$^{40}Ar/^{39}Ar^a$	%39Ar	%40Ar^c	age	+/-
1	0.06361	0.05220	488.81	6.0	96.2	310.1	3.0
2	0.01067	0.14015	483.83	2.0	99.3	316.6	3.6
3	0.02009	0.01281	478.07	10.9	98.8	311.4	2.9
4	0.01365	0.25893	476.31	4.7	99.2	311.5	3.0
5	0.01714	0.13584	482.69	9.1	99.0	314.7	2.9
6	0.02008	0.33942	478.42	4.6	98.8	311.7	3.0
7	0.01257	0.11638	482.38	8.6	99.2	315.3	2.9
8	0.00977	0.32970	475.43	4.8	99.4	311.7	3.0
9	0.01168	0.16707	481.12	7.4	99.3	314.7	3.0
10	0.01687	0.49679	478.44	3.7	99.0	312.3	3.1
11	0.01433	0.34212	480.62	5.1	99.1	314.0	3.0
12	0.02055	0.57676	484.75	3.4	98.7	315.5	3.1
13	0.01576	0.12133	477.75	2.7	99.0	312.0	3.2
14	0.01096	0.14684	471.87	6.2	99.3	309.3	2.9
15	0.01168	0.00604	478.46	4.1	99.3	313.1	3.0
16	0.01820	0.01016	475.30	7.6	98.9	310.0	3.0
17	0.01356	0.15118	480.28	8.9	99.2	313.9	3.0
total	0.01802	0.16783	479.63	100.0	98.9	312.7	2.9

Sample: JF-98.2 (white mica 250-500μm) Lowest Gneiss di Morbegno
(Location: Val Lunga (Arale), Co-ordinates: 1553535-5105240)
J-Value: 0.000401 ± 0.000004

step	$^{36}Ar/^{39}Ar^a$	$^{37}Ar/^{39}Ar^b$	$^{40}Ar/^{39}Ar^a$	%39Ar	%40Ar^c	age	+/-
1	0.02084	0.99776	429.23	1.1	98.6	282.9	3.4
2	0.00240	0.61743	461.91	1.3	99.8	306.3	3.7
3	0.01767	0.44220	454.27	2.7	98.9	298.8	3.1
4	0.02937	1.23759	420.58	0.8	97.9	276.0	4.3
5	0.00875	0.11184	464.04	13.3	99.4	306.3	2.8
6	0.00538	0.37710	459.37	4.1	99.7	304.1	2.9
7	0.00513	0.05214	459.65	16.4	99.7	304.3	2.8
8	0.00479	0.16439	455.07	3.6	99.7	301.6	2.9
9	0.01190	0.13836	466.42	5.9	99.2	307.2	2.9
10	0.00338	0.48768	458.97	3.2	99.8	304.3	3.0
11	0.00345	0.32226	461.47	4.2	99.8	305.7	3.0
12	0.00504	0.24099	467.60	6.4	99.7	309.2	2.9
13	0.00495	0.03499	461.98	12.9	99.7	305.7	2.8
14	0.00139	0.12211	466.06	6.3	99.9	308.9	2.9
15	0.00294	0.20054	457.23	8.3	99.8	303.2	2.8
16	0.00542	0.13026	457.91	6.8	99.7	303.2	2.9
17	0.00925	0.35914	454.02	3.0	99.4	300.1	3.1
total	0.00624	0.18807	460.48	100.0	99.6	304.6	2.8
steps 5-17				94.1		305.2	2.9

Sample: JF-92.2 (white mica 250-500μm) Gneiss di Morbegno Lithological variety (b)
(Location: Bema, Co-ordinates: 1543675-5106350)
J-Value: 0.000400 ± 0.000004

step	$^{36}Ar/^{39}Ar^a$	$^{37}Ar/^{39}Ar^b$	$^{40}Ar/^{39}Ar^a$	%39Ar	%40Ar^c	age	+/-
1	0.06912	0.54849	448.27	1.6	95.4	285.1	3.6
2	0.02106	0.30939	413.13	0.6	98.5	272.1	5.7
3	0.01006	0.06142	464.69	16.4	99.4	305.8	2.8
4	0.00143	0.62579	442.09	1.9	99.9	293.6	3.5
5	0.01531	0.01401	477.57	17.3	99.1	312.6	2.9
6	0.00276	0.04313	480.74	7.1	99.8	316.8	3.0
7	0.00441	0.00897	476.96	16.3	99.7	314.2	2.9
8	0.00344	0.22623	477.35	5.6	99.8	314.7	3.0
9	0.00687	0.13927	470.76	4.7	99.6	310.0	3.0
10	0.00826	0.16639	467.74	7.5	99.5	308.0	2.9
11	0.00733	0.25458	469.87	5.5	99.5	309.4	3.0
12	0.00298	0.08811	472.66	5.3	99.8	311.9	3.0
13	0.00033	0.02316	469.15	3.3	100.0	310.2	3.1
14	0.00001	0.06538	463.40	4.7	100.0	306.8	3.0
15	0.00923	0.18468	492.85	2.2	99.4	323.0	3.7
total	0.00840	0.09780	471.71	100.0	99.5	310.3	2.9
steps 5-14				77.3		312.1	3.0

Sample: JF-33.6 (biotite 250-500μm) Gneiss Occhiadini Orobico-Valtellinese (GOOV)
(Location: North of Alpe Cul, Co-ordinates: 1547798-5099712)
J-Value: 0.000397 ± 0.000004

step	$^{36}Ar/^{39}Ar^a$	$^{37}Ar/^{39}Ar^b$	$^{40}Ar/^{39}Ar^a$	%39Ar	%40Ar^c	age	+/-
1	0.50259	0.03511	259.61	4.3	42.8	77.9	1.2
2	0.21877	0.55471	257.29	1.7	74.9	133.0	1.9
3	0.13973	0.03987	282.30	14.6	85.4	164.8	1.6
4	0.06963	0.06454	304.20	7.5	93.2	192.5	1.9
5	0.04753	0.03886	315.73	12.3	95.6	204.1	2.0
6	0.03601	0.01263	319.81	7.0	96.7	208.9	2.0
7	0.03139	0.01243	323.45	10.6	97.1	212.0	2.0
8	0.02210	0.01015	327.51	6.0	98.0	216.4	2.2
9	0.03311	0.11733	328.26	8.2	97.0	214.8	2.1
10	0.02277	0.04829	324.18	5.4	97.9	214.1	2.1
11	0.02573	0.13025	323.40	7.1	97.6	213.1	2.1
12	0.02910	0.09141	332.05	4.5	97.4	218.0	2.1
13	0.02435	0.15695	327.33	3.2	97.8	215.9	2.2
14	0.02486	0.26248	328.88	2.4	97.8	216.8	2.3
15	0.02570	0.14521	320.61	5.2	97.6	211.3	2.1
total	0.07366	0.07390	312.11	100.0	93.0	196.8	1.9

Sample: JF-64.2 (biotite 250-500μm) Gneiss Occhiadini Orobico-Valtellinese (GOOV)
(Location: Passo Pedesina, Co-ordinates: 1549418-5101755)
J-Value: 0.000399 ± 0.000004

step	$^{36}Ar/^{39}Ar^a$	$^{37}Ar/^{39}Ar^b$	$^{40}Ar/^{39}Ar^a$	%39Ar	%40Ar^c	age	+/-
1	1.12494	0.55718	417.97	1.1	20.5	60.6	4.3
2	0.23565	3.03380	229.98	0.2	69.7	112.2	7.4
3	0.14804	0.11466	227.30	2.4	80.8	127.5	1.6
4	0.08319	0.85597	236.90	1.1	89.6	146.8	2.2
5	0.06022	0.02507	234.07	6.2	92.4	149.3	1.5
6	0.02675	0.22876	238.23	3.9	96.7	158.6	1.7
7	0.02048	0.03780	230.87	10.2	97.4	155.0	1.5
8	0.01647	0.02694	232.90	5.9	97.9	157.1	1.6
9	0.01310	0.01170	232.66	13.0	98.3	157.6	1.5
10	0.01045	0.00622	240.43	7.3	98.7	163.2	1.6
11	0.01074	0.02310	239.63	11.6	98.7	162.6	1.6
12	0.01490	0.01237	240.81	6.7	98.2	162.6	1.6
13	0.01424	0.10552	237.07	10.1	98.2	160.3	1.6
14	0.01140	0.07695	239.57	6.7	98.6	162.5	1.6
15	0.01081	0.14199	236.94	4.7	98.7	160.9	1.6
16	0.00983	0.20441	234.56	3.6	98.8	159.5	1.7
17	0.00794	0.08657	235.12	5.1	99.0	160.2	1.6
total	0.03307	0.08122	237.91	100.0	95.9	157.2	1.5
steps 6-17				88.9		159.9	1.6

Sample: JF-98.2 (biotite 250-500µm) Lowest Gneiss di Morbegno
(Location: Val Lunga (Arale), Co-ordinates: 1553535-5105240)
J-Value: 0.000401 ± 0.000004

step	$^{36}Ar/^{39}Ar^a$	$^{37}Ar/^{39}Ar^b$	$^{40}Ar/^{39}Ar^a$	%39Ar	%40Ar^c	age	+/-
1	0.12554	1.77590	294.51	0.6	87.4	177.5	5.5
2	0.12740	5.81323	341.57	0.4	89.0	208.5	10.4
3	0.07013	1.17638	362.06	2.9	94.3	231.6	2.6
4	0.03682	1.15874	364.10	2.1	97.0	239.2	3.0
5	0.02426	0.11836	357.23	9.6	98.0	237.0	2.3
6	0.01669	0.27515	385.28	6.4	98.7	256.1	2.5
7	0.00603	0.10914	381.39	16.7	99.5	255.6	2.4
8	0.00630	0.19520	378.62	8.8	99.5	253.9	2.4
9	0.00479	0.21835	373.32	14.2	99.6	250.8	2.4
10	0.00281	0.26142	375.24	7.6	99.8	252.4	2.4
11	0.00499	0.22332	379.42	10.2	99.6	254.6	2.4
12	0.00447	0.22586	389.08	5.7	99.7	260.8	2.5
13	0.00014	0.30900	384.36	4.1	100.0	258.6	2.8
14	0.00840	0.75305	387.36	3.4	99.4	259.1	2.9
15	0.00464	0.22165	388.29	7.3	99.6	260.2	2.5
total	0.01123	0.29601	376.96	100.0	99.1	251.9	2.4
steps 6-15				84.5		255.3	2.5

Sample: JF-92.2 (biotite 250-500μm) Gneiss Occhiadini Orobico-Valtellinese (GOOV)
(Location: North of Alpe Cul, Co-ordinates: 1547798-5099712)
J-Value: 0.000400 ± 0.000004

step	$^{36}Ar/^{39}Ar^a$	$^{37}Ar/^{39}Ar^b$	$^{40}Ar/^{39}Ar^a$	%39Ar	%40Ar^c	age	+/-
1	0.27771	0.11096	275.79	0.9	70.2	134.7	2.6
2	0.11465	0.79257	305.54	0.6	88.9	186.2	3.6
3	0.08193	0.07410	399.53	8.6	93.9	252.3	2.4
4	0.01011	0.18174	390.63	3.6	99.2	260.1	2.6
5	0.02388	0.07389	385.48	10.7	98.2	254.3	2.4
6	0.01079	0.09332	366.70	6.9	99.1	244.9	2.3
7	0.00643	0.10547	371.05	9.8	99.5	248.5	2.3
8	0.00412	0.17753	364.73	5.5	99.7	244.9	2.4
9	0.00753	0.09893	406.33	9.4	99.5	270.3	2.5
10	0.00565	0.15543	384.07	5.7	99.6	256.8	2.5
11	0.00552	0.06239	392.26	8.4	99.6	261.9	2.5
12	0.00292	0.25776	372.16	5.0	99.8	249.9	2.4
13	0.00192	0.29019	390.39	3.7	99.9	261.5	2.6
14	0.00140	0.21858	384.16	3.3	99.9	257.7	2.6
15	0.00582	0.22223	379.30	7.3	99.5	253.8	2.4
16	0.00140	0.21858	384.16	3.3	99.9	257.7	2.6
17	0.00582	0.22223	379.30	7.3	99.5	253.8	2.4
total	0.01735	0.14654	382.57	100.0	98.7	253.7	2.4

Chapter 4

Geochronology of the Orobic Alps (Lombardy, Italy): (II) [40]Ar/[39]Ar-ages of detrital muscovite from the Collio basin, constraining tectono-thermal development

Abstract

The Early Permian 'Orobic Collio basin', located in the Central Southern Alps of Lombardy (Italy) contains a very low-grade metamorphic volcanoclastic sequence. Isotopic [40]Ar/[39]Ar-dating of single detrital white mica grains from this basin supplied information on: (1) their source areas (2) tectono-thermal characteristics of the exhumation history and (3) the geodynamic setting of basin formation. Three potential source units (a-c) in the Orobic basement are: The (a)'Orobic fold nappe', overlies a (b) parautochton forming the 'infrastructure', separated by a Variscan tectonic contact from the (c)'supra structure', consisting of 'Scisti di Edolo'. The 'Orobic fold nappe' is the source of the main population of detrital grains of 325-305 Ma, present throughout the sedimentary sequence. These grains represent a cooling event following peak conditions of uppermost amphibolite facies grade (750°C/ ≤1.3 Gpa) that jointly affected this nappe. The population of 338-350 Ma, however, identified in the 'basal conglomerates' and the 'base of the 'upper sedimentary member' of the 'Collio formation', is unlikely to be provenant from the 'Orobic fold nappe'. Possible source areas are is the parautochton, which micht correlate with the basement below the 'Collio Trumplino basin', with muscovite cooling ages of 364-340 Ma (Mottana, shown in Martin et al. (1996)), and the 'Brixen- and Agordo quartzphyllite complexes' with cooling ages around 350 Ma (Del Moro et al., 1980; Cavazzini et al., 1991). A population with ages of 300-290 Ma, found in a sample from the 'Ponteranica formation', might be derived from the Carboniferous late-orogenic 'Val Biandino Plutonic Complex' and its contactmetamorphic realm. Lag-time of Variscan white mica of the 'basal conglomerates', of 18 to 61 Ma indicates a contractional setting and most likely the deposition in a Molasse basin. The geodynamic setting might have changed before the following stage, the development of the 'Collio Orobico basin', which took place after a phase of erosion. The first phase of development of the 'Collio Orobico basin' was a caldera-stage, during which mainly volcanics were deposited. Variscan detrital grains from the overlying 'upper sedimentary member' of the Collio formation have lag-times of 31 to 70 Ma, slightly higher values than those of the 'basal conglomerates'. These, together with sedimentary, volcanic and structural relationships point to an intramontane basin, formed on a supradetachment with large transcurrent component. Some grains from this member contain detrital white mica of almost the same age (~270-255 Ma) as the age of deposition (~267-260 Ma). The [40]Ar/[39]Ar-isotopic system of these grains has been reset after deposition by Middle- to Late Permian hydrothermal activity, which is related to Permian volcanism during a phase of transtensional faulting. Permo-Mesozoic hydrothermal overprint (250-180 Ma) and Alpine overprint, both significantly younger than the age of deposition, have also been identified. The Alpine ages result from pressure solution and recrystallisation of white mica.

1 Introduction

Isotopic ^{40}Ar/^{39}Ar-dating has been carried out on single detrital white mica grains from Lower Permian very low grade metamorphic clastic sequences of the 'basal conglomerates', 'Collio Orobica'- and 'Ponteranica' formations, all exposed in the Orobic Chain (Fig. 1), in the Central part of the Italian Southern Alps. It was intended to identify (1) the source areas of individual detrital white mica grain populations, representing the exhumed tectonic basement units involved in this part of the Variscan belt, (2) the exhumation history and related important tectono-thermal characteristics of the geological history and (3) the tectonic setting of the deposition of sequences from which these samples of detrital grains were taken. The results contribute to an improved understanding of the Variscan-Permian structure- and orogenic evolution at the southern margin of this Alpine orogenic belt and reveal what strategy needs to be followed to solve questions concerning its Variscan-Permian and Permo-Mesozoic tectono-thermal evolution.
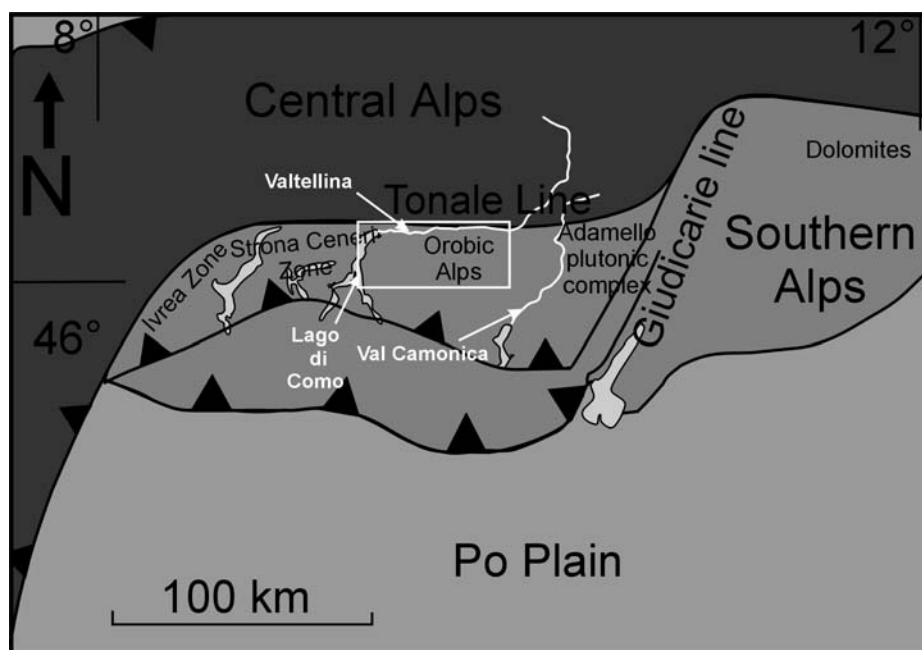
Fig. 1. Location of the Orobic Alps, inset shows the investigated area in Fig. 2.

Isotopic ^{40}Ar/^{39}Ar-age data of detrital white mica from unmetamorphosed and/or very low grade metamorphic clastic sequences, like the predominantly Early Permian 'Collio Orobico basin' (Feijth & Neubauer, in prep.; Schönborn, 1992 and references therein), provides important information regarding the tectonothermal history of source areas (e.g. Fitch et al., 1966; Mitchel & Taka, 1984; Kelly & Bluck, 1989, 1992; Dallmeyer & Nance, 1990; Renne et al., 1990; Welzel, 1991; Dallmeyer and Neubauer, 1994).

This method can resolve basement-cover relationships where these relationships are not clearly resolved by other means, and palinspastic correlations and tectonic derivations of tectonic units are uncertain. Additionally the time interval between cooling of the source rock through the argon retention temperature and the time of deposition is used to study exhumation history and classify various types of sedimentary basins (Copeland et al., 1990; Neubauer & Handler, 1997). All this is possible because of the resistance of detrital white mica to weathering (Clauer, 1981), sedimentation, diagenesis, and low-grade metamorphic

overprint (Dallmeyer & Takasu, 1992).

For the correlation of hinterland source areas with clastic deposits in sedimentary basins of varying tectonic setting it is of minor importance whether mica-bearing basement sources are of plutonic or metamorphic origin. However, to correlate isotopic ages of detrital minerals with tectonic activities in respective source areas, it must be anticipated that cooling trough temperatures required for retention of respective isotopic systems (e.g. of Ar in white mica) was associated with tectonic exhumation within the respective plutonic and/or metamorphic hinterland. However, geochronologic ages of the detrital grains can only be interpreted as minimum estimates for tectonothermal activities of the source areas.

Due to the weak Alpine and Mesozoic metamorphic overprint, compared to the Central Alps (Feijth, in prep. a and references therein), the Southern Alps are well suited to identify the Palaeozoic tectonothermal history of the source areas and are as well suitable for application of above introduced method on detrital white mica from the 'Orobic Collio basin'. Until recently ages of pre-Alpine metamorphism and structures in the Orobic Alps were poorly constrained, but Feijth et al. (in prep.) provided more isotopic age data for the Palaeozoic evolution of the central part of the Orobic basement. The Palaeozoic depositional, structural and metamorphic sequence of the basement of the Orobic Chain (Fig. 2) has been analysed and the tectono-metamorphic development of the various Orobic basement units identified (Feijth, in prep. a, b, c; Feijth & Franz, in prep.), which contributed to comprehension of the Palaeozoic geodynamic and structural development. This reconstruction of the basement of the southern margin of the Variscides includes analysis of the Pre-Variscan development. The results of these investigations enable identification of potential source areas of the exposed clastic sequences, required for the study presented here. An overview of all available geochronological data of the Orobic basement is given in Feijth et al. (in prep).

Mesozoic resetting of the isotopic systems had only local influence in the studied central Orobic Alps but has certainly occurred in the area of investigation, as indicated by a muscovite-age of 242 ± 7 Ma in a sample from 'Bema'/'Fumasi' (Mottana et al., 1985) and data presented here.

Pre-Variscan isotopic ages were not obtained so far for the Orobic basement, but an Ordovician igneous phase is likely (Colombo et al., 1994), who based this interpretation on the geochemistry of granodiorites of a particular sequence of the Orobic basement. This sequence could be structurally and lithologically correlated with the 'Scisti dei Laghi sequence' of the 'Strona Ceneri Zone' (Feijth, in prep. a; Feijth et al., in prep.). The available radiometric age data in that unit suggest Ordovician deformation, metamorphism and a related igneous phase in the corresponding Orobic sequence. This Ordovician phase was called the 'Sardic' phase in the Strona Ceneri Zone (Handy et al., 1999) and the Orobic basement (Feijth, in prep. a). Feijth (in prep. a) also identified that the Orobic basement contains at least one unit that was affected by only one Palaeozoic phase, the Variscan phase. This is the upper sequence of the 'Orobic fold nappe', a tectonic unit which is separated by a tectonically activated unconformity from the lower sequence (Feijth, in prep. a).

An interpretation of the Alpine ages of detrital white micas, that were obtained as a by-product of the here presented data, will be presented in the nearby future (Feijth & Neubauer, in prep.).
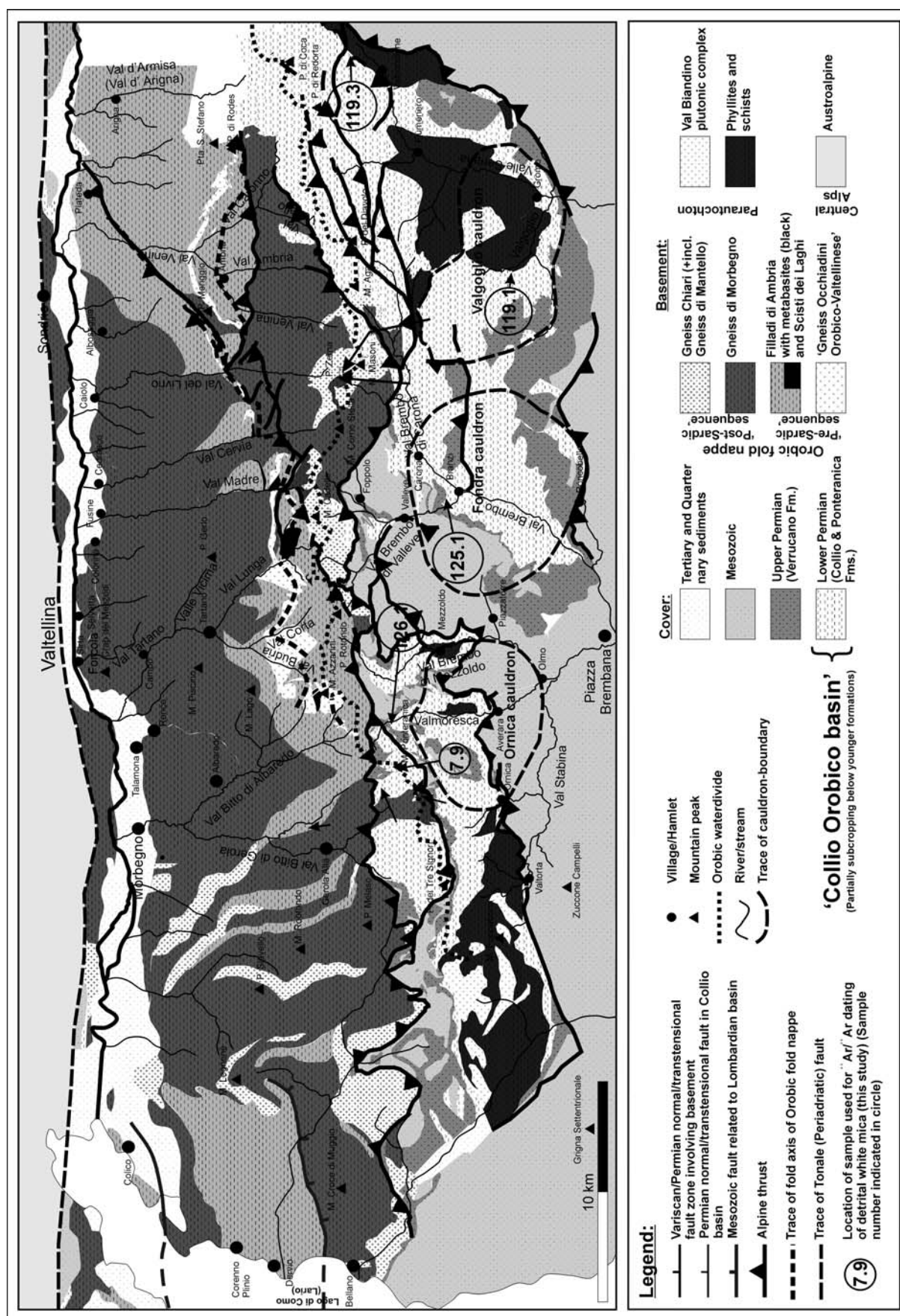
Fig. 2. Simplified geological map of the Orobic Alps with only the main Alpine faults shown. The area selected for the study is located East of the line 'Pizzo Slavello'-'Monte Rotondo'-'Pizzo Melasc'. The location of the 'Collio Orobico basin' is approximately the area where the Collio- and Ponteranica formations are exposed (see legend).

2 Geological setting, structure and stratigraphy

2.1 Geological setting and structure

The region and tectonic units discussed here form part of the southernmost margin of the Variscan belt (Fig. 1) and can be followed through Liguria, Tuscany, the Peloritani Mountains and Calabria into Sardinia (Vai & Cocozza, 1986). In eastern direction the trend of this zone can be traced approximately along the southern margin of the Alpine belt.

There is a close genetic relationship between the Variscan and Alpine structural trends. The present structure, although reactivation of Palaeozoic shearzones and faults took place, can be regarded as being inherited from the Variscan-Permian. A schematic tectono-stratigraphic section of the Permian configuration is shown in Fig. 3a.

The Orobic structure comprises of east-west trending zones (Fig. 2). The Variscan Southalpine basement is separated from the Austroalpine by the 'Periadriatic' or 'Tonale fault', that is located north of the investigated area (Fig. 2, 3a) along the northern slopes of the Valtellina. The root zone of a Variscan fold nappe, the 'Orobic fold nappe', is juxtaposed against and strikes parallel to the Alpine 'Tonale fault'. The 'Orobic fold nappe', consists of a
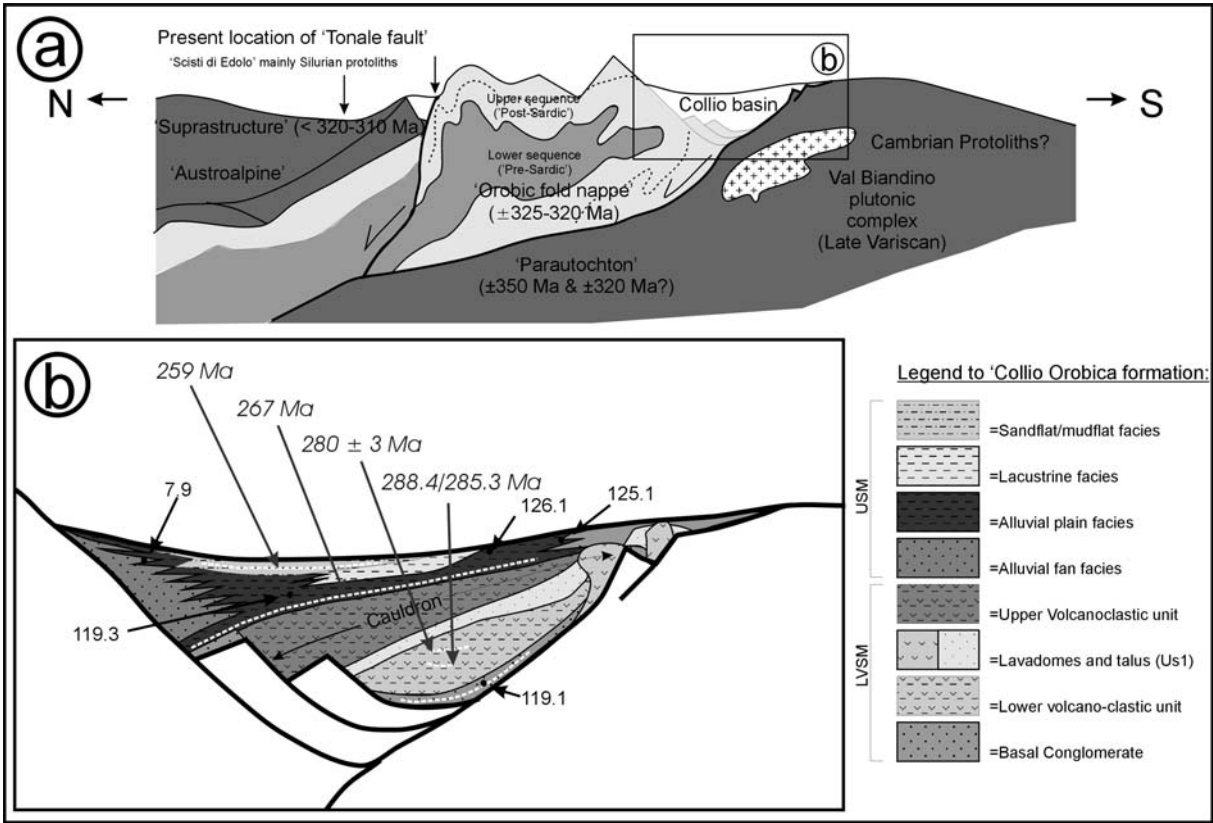
Fig.3

a. Schematic profile showing the Variscan structural configuration of the Orobic Chain and the stratigraphic relationships between the basement sequences. Within the 'Orobic fold nappe' the lower sequence is indicated in dark grey, whereas the upper sequence is indicated in light grey.

b. Schematic profile through the Collio-Orobico basin, illustrating the stratigraphic relationships of the Permian sedimentary and volcanic sequences. Numbers in Ma indicate ages of stratigraphic levels, the other numbers indicate samples (Compare Fig. 2, Table 2).

lower 'pre-Sardic'- and an upper 'post-Sardic' sequence, both jointly affected by Variscan metamorphism. The 'Orobic fold nappe' and parautochton respectively correspond approximately to the Alpine 'San Marco'- and 'Mezzoldo Units' of Schönborn (1990, 1992) and Schumacher et al. (1997) (Fig. 3a). Both Alpine units have also been called 'Upper'- and 'Lower Orobic nappe' by Schönborn (1994) and by Schumacher (1997).

In the present post-Alpine configuration the Early Permian 'Orobic Collio'- and 'Ponteranica' basins are exposed between the 'Orobic fold nappe' in the north and a thrust belt, consisting of mainly Mesozoic formations in the south (Fig. 2). The mainly rhyolitic volcanics and sediments of this basin are found in Alpine inversion-related large-scale gentle anticlines, the 'Orobic'-, 'Trabuchello'- and 'Cedegolo'- anticlines (de Sitter, 1963). The basement of the parautochton is exposed in inliers in these Permian volcano-sedimentary units. This parautochton extends northwards below the 'Orobic fold nappe' as footwall of the south-verging 'Orobic thrust'. The 'Porcile fault', which is found along the core of a Variscan fold nappe, crosses the Orobic basement north of the 'Orobic thrust' obliquely, from ENE to WSW. East of the junction of the 'Orobic thrust' and the 'Porcile fault' the importance of the 'Orobic thrust' is smaller than west of this point. Alpine deformation along the 'Orobic thrust' and the 'Porcile fault' is represented by black cataclasites with abundant dispersed pseudotachylytes.

The 'Orobic fold nappe' and parautochton together make up the infrastructure. The 'suprastructure' that consists of 'Scisti di Edolo' (Feijth, in prep. a) is in contact with the 'Orobic fold nappe' trough a Variscan roughly layering-parallel shearzone (Fig. 3a).

Alpine metamorphism of the Early Permian 'Orobic Collio basin' the overlying Upper Permian 'Verrucano Lombardo formation' and Mesozoic reached high anchimetamorphic conditions (Schönborn, 1992) and the Collio sediments were locally deformed by pressure solution- and recrystallisation processes during the activity of the 'Orobic thrust' (Feijth & Neubauer, in prep.).

2.2 The lithological units of the Orobic basement and protolith- and metamorphic ages

'Pre-Sardic' sequence of the 'Orobic fold nappe' (infrastructure)

The 'Filladi di Ambria', contain well-developed centimetre- to decimetre-scale layered schists, quartzitic-schists and chlorite-schists with subordinate thinner meta-greywackes and quartzites. Garnet is common and locally amphibole as well. The 'Filladi di Ambria' contains a discontinuous horizon metabasitic rocks. Individual bodies are km-scale in length and up to 200 metres, generally some tens of metres, thick. These metabasites are exposed in the core of the 'Orobic fold nappe' and consist of (1) foliated amphibolite schists and epidote-amphibolite-schists representing meta-ashes and -tuffs, likely deposited in an aquous environment and with cross bedding and lamination, and (2) amphibolite-sills with, locally at the base, mafic and ultramafic xenoliths.

Sills and stocks of slightly peraluminious and subalkaline (Colombo et al., 1994) meta-granodioritic 'augen gneisses', called 'Gneiss Occhiadini Orobico-Valtellinese' ('GOOV') (Feijth, in prep. a), are also exposed in the core of the 'Orobic fold nappe' within the 'Filladi di Ambria'.

This sequence correlates with the 'Scisti dei Laghi sequence' of the 'Strona Ceneri Zone'

(Feijth, in prep. a.; Feijth et al., in prep.). The 'Scisti dei Laghi' have been metamorphosed and folded during the Early- to Mid-Ordovician Sardic phase, at ~480 Ma (Romer & Franz, 1998). Therefore this must also be the case for the metabasites and metasediments of the lower sequence of the 'Orobic fold nappe'. When situated at shallow crustal levels latter sequence has, during the middle-Orodovician, been intruded by the 'GOOV' (Feijth, et al., and references therein). During the Variscan phase the Sardic folds were overprinted, causing type 2 and 3 fold-overprint relationships of Ramsay (1967).

'Post-Sardic' sequence of the 'Orobic fold nappe' (infrastructure)

In contrary to the lower sequence, that contains mainly basic volcanic components, the upper sequence contains felsic meta-volcanics, meta-rhyolites and derived metasediments. These belong to the psammo-pelitic 'Gneiss di Morbegno' and the included rhyolitic meta-volcanics, the 'Gneiss Chiari'. The basal unconformable contact with the 'Filladi di Ambria' has in many cases been developed as a Variscan shearzone. Brittle Alpine reactivation at this contact, leading to the formation of cataclasites, has also been identified. The 'Gneiss di Morbegno' and 'Gneiss Chiari' can be regarded as a meta-volcano-sedimentary system with massive rhyolitic complexes of up to 1000 m thick there where extrusion took place, for example the 'Monte Cadelle meta-rhyolitic complex'. The 'Monte Cadelle meta-rhyolitic complex' contains meta-rhyolite-domes along an Alpine reactivated fault juxtaposing the sequence with 'Gneiss Chiari' against the lower sequence. Also rhyolitic dykes and feeder pipes are locally still recogniseable in the 'Gneiss Chiari' (Feijth, in prep. a). Away from those rhyolitic complexes the proportion of meta-rhyolite in the upper sequence decreases and the meta-rhyolitic sheets of 'Gneiss Chiari' are situated between meta-volcano-sedimentary units of the 'Gneiss di Morbegno' with commonly a rust-brown weathering colour. Amongst the other less distinctive psammo-pellitic rocks lithology there are lithologic varieties (a) and (b) of the 'Gneiss di Morbegno' and which occurrence is predominantly below and above the meta-rhyolites for each variety respectively:

Lithologic variety (a) consitsts of garnet-staurolite-white mica schists containing kyanite and tourmaline. The protoliths are volcano-sedimentary sequences. The mineral paragenesis is largely a product of Variscan dehydration melting of white mica and following staurolite-formation during retrogression, just after the thermal peak was reached (Feijth & Franz, in prep.).

Lithologic variety (b) consists of biotite and albite-rich psammo-pelitic gneisses with garnet (seldom with staurolite and/or kyanite), called 'Albitknotengneise' by Cornelius & Cornelius-Furlani (1930), because of the typical albite-blasts. Compositionally these are meta-greywackes, which have undergone a short phase of Variscan dehydration melting of biotite (and white mica, where originally present), without much segregation beyond microscopic to mesoscopic scale, and retrograde back-reaction (Feijth & Franz, in prep.).

These metamorphosed volcanic and volcano-sedimentary rocks have been correlated with similar rocks of the Austroalpine (Feijth, in prep. a; Feijth et al, in prep.), which underlines that the pre-Variscan development of this part of the Southern Alps and the Austroalpine Alps are closely related.

Peak metamorphic conditions of 750 °C at ≤ 1.3 GPa (Feijth & Franz, in prep.), were reached in the both sequences now found in the Orobic fold nappe during the main Variscan phase and

must have reset all white mica, including the 'Sardic' grains, completely. Peak conditions were reached at 330-320 Ma, as revealed by applying the U-Th-Pb-isotopic with Monazite from 'Gneiss Chiari' and 'Gneiss di Morbegno' (Feijth et al., in prep.; Feijth & Franz, in prep.). The following decrease in temperature and pressure was synchronous with the nappe folding (Feijth & Franz, in prep.) and was dated by the ^{40}Ar/^{39}Ar step-heating method on white mica. The ^{40}Ar/^{39}Ar white mica ages indicate 325-305 Ma for this event. The ^{40}Ar/^{39}Ar age spectra are shown in Feijth et al. (in prep.). Biotite K-Ar-cooling ages of 291 ± 6 (Bocchio et al., 1981) and 292 ± 9 Ma (Mottana et al., 1985) were obtained for the lithologic variety of the 'Gneiss di Morbegno' called type (b). These ages represent later stages of the same Variscan regional cooling-event. This cooling is related to the event of nappe-folding and orogenic collapse, immediately preceding the development of the 'Collio Orobico basin'. Either due to a very short time interval between peak conditions and closure of the ^{40}Ar/^{39}Ar-system of white mica and/or the poorer defined U-Th-Pb data of monazite, or both, the time-interval between peak conditions and the muscovite-retention temperature is not as well resolved as desireable.

Biotite age spectra presented by Feijth et al. (in prep.) show Middle- to Late Permian and Mesozoic overprint. Monazite-xenotime thermometry and 2 feldspar thermometry indicate a temperature of ~335 °C for hydrothermal overprint being the cause of Middle- to Late Permian and Mesozoic plateaux in the biotite ^{40}Ar/^{39}Ar-spectra whereby most white mica was't affected (Feijth et al., in prep.). The Middle- to Late Permian hydrothermal phase was at approximately 255 Ma.The Mesozoic hydrothermal phase was dated by the U-Th-Pb-method on monazite at 178 ± 93 Ma and by white mica around 160 Ma.

Parautochton (infrastructure)

The parautochton, exposed in the inliers at 'Valmoresca', 'Mezzoldo', 'Lago Fregabolgia-Lago Rotondo' and 'Monte della Croce-Fiumenero-Valbondione' consists of intensely sheared phyllitic schists, schists, quartzitic phyllites and quartzites, with occasionally garnet. Not yet solved are (1) correlation of the parautochton with other tectonic units in the Southern Alps or Austroalpine (2) its tectonic and sedimentary origin. No isotopic age-data and biostratigraphic data are available for this unit of the Orobic basement.

Along the southwestern border of the study area, in the 'Val Sassina', 'Val Biandino' and 'Val Stabina', stocks and laccoliths of Variscan syn-late tectonic tonalites, granites, quartz-diorites and gabbro-diorites with a large contact metamorphic aureole, named 'Val Biandino plutonic complex', are exposed in the parautochton. These intrusions are syn-late tectonic stocks and laccoliths which emplacement age is determined by K-Ar Biotite-ages at 307 ± 9 to 271 ± 8 Ma (De Capitani et al., 1988). Intrusions are generally conformable to folded layering of the host rock of the parautochton, but at places discordant, especially at the apophyses. The contact metamorphic aureole consists of sillimanite-, cordierite- and andalusite- bearing hornfelses, indicating a depth of intrusion of at maximum 10-12 km (De Capitani et al., 1988), narrowed in by Al- in hornblende barometry to < 5 km by Feijth & Franz (in prep.). The results of K-Ar isotopic dating of these rocks by De Capitani et al. (1988), are indicated in Fig. 2.

'Suprastructure'

The 'Scisti di Edolo', that make up the 'supra structure', are characterised by finely laminated phyllites, micaschists and fine quartzitic layers that form the highest unit of the Orobic structure. In this study only the low-grade tectonic unit, a sequence mainly exposed on the N-side of Val Cortena are called 'Scisti di Edolo'. The original use of the name 'Scisti di Edolo' or 'Quartzlagenphyllite', was used for a low-grade metamorphic schistose complex west of the Adamello massif and of the Valle Camonica (Salomon, 1901). In later publications also the higher-grade sequence of the Orobic fold nappe of the Eastern Orobic Alps (Gansser & Pantić, 1988) was included, which is confusing. So did Liborio & Mottana (1969). At the base of the lower grade sequence these lithologies are intensely sheared parallel to layering, predominantly during Variscan phases (Feijth, in prep. a and references therein). Ductile folding is associated with this shear zone. These are the only basement-rocks of the Orobic Alps of which the age of deposition has been determined by micropalaeontological methods. The age of the identified spores and acritarchs is mainly Silurian and subordinate Ordovician (Gansser & Pantić, 1988).

Because, due to the 'Tonale fault', the top of the sequence of the 'Scisti di Edolo' is missing in this part of the Alps, the minimum age of the metamorphism that affected the complete sequence to which the 'Scisti di Edolo' belongs cannot be determined. To get an impression of the minimum possible age of metamorphism of the 'Scisti di Edolo' the equivalence with the 'Quartzphyllites' of the Austroalpine basement (Feijth, in prep. a) is very important. The 'Quartzphyllites' of the Austroalpine basement, also exposed along the 'Periadriatic fault'have similar structural and metamophic relationships. Also there a tectonic contact separates a higher-grade substrate from the lower grade phyllites. The 'Quartzphyllites' belong to a continuous fossil-bearing section reaching early Namurian, locally Westphalian A. Therefore the age of the relatively low grade metamorphic imprint, also of the 'Scisti di Edolo', cannot be older than 310-320 Ma. In the Kreuzeck Mountains, just south of the Tauern window, muscovite-ages are mostly around ca. 300 Ma, with very few samples 320 Ma (Hoke, 1990), presenting previously unpublished data of Brewer).

2.3 Stratigraphy of the low-grade sequence of the 'Collio Orobico basin'

The stratigraphic subdivision of Cadel et al. (1996) is based on excellent mapping of the Eastern part of the area of investigation, was applied and expanded for the areas not covered by their detailed work. In the areas newly investigated some new aspects of the basin have been recognised, which have strong implications for the interpretation of the sequences introduced by Cadel et al. (1996) and newly recognised and related units. A schematic cross section is presented as Fig. 3b.

The low-grade succession starts with the 'basal conglomerates', which is discordantly overlain by the Collio succession. The 'basal conglomerates' are exposed only in the eastern sector of the Bergamasc Alps, in the Valle Brembana di Carona and Valleve and Valle Seriana as well as around the E-W striking main mountain crest delineating the boundary of the Bergamasc valleys to the Valtellina. This distribution might represent the erosional remnants of a basin superposed by the younger 'Collio-Orobico basin'. The maximum thickness of this unit, deposited by braided rivers, debris flows and in lacustrine environments, is 120 m. The majority of these exposures show breccias with either micaceous components from schists

and phyllites or clasts of Gneiss Chiari, but locally also contain red quartz pebble conglomerates and sandstones interbedded with purplish-red, often burrowed siltstone and occasionally andesitic fragments. The depositional distribution of the 'basal conglomerates', with channels incised in the basement and a less fault-controlled distribution than the overlying Lower Permian sequences, is analogous with a molasse sequence. The 'Collio Orobica formation' constitutes of two members, the lower volcano-clastic member (LVCM) and the upper sedimentary member (USM). The LVCM is made up of two sequence units, the 'lower- and upper volcano-clastic units', both separated by an angular erosional unconformity. Successive Collio volcanics and reworked and redeposited volcanoclastic sediments of the LVCM are present in three E-W aligned circular-shaped depressions (Fig. 2) recognised in the Val Brembo di Mezzoldo/Valle Stabina, Valle Brembana and Valle Seriana obviously formed simultaneously with volcanism and sedimentation. These circular structures have not only been recognised by the distribution of their volcano-sedimentary succession itself, but also by well-defined Alpine inversion along some parts of the ring-fractures of the 'Ornica'-, 'Fondra'- and 'Valgoglio cauldrons'.

The unit of the LVCM in the 'Valgoglio cauldron', according to Cadel et al. (1996), consists of an andesitic tuff bed, 5 rhyolitic ash flow units and 3 interbedded sedimentary units, generally fining-up sequences of alluvial plain conglomerates, with or without sheetflood deposits. Each of these units has varying thicknesses, with variation partly due to palaeofaults. Maximum thickness, in the Novazza area, is ~250 m. Similar successions occur in all three intracalderic successions, whereby the developments in the 'Fondra'- and particularly the 'Valgoglio'-cauldrons are most extensive. The 'Banco dell' Abete', the third rhyolitic flow unit from the Novazza Uranium mine has been dated at 288,4 Ma (U-Pb, Zircon) and 285,3 Ma (Pb-Pb, Zircon; J. Hunziker in Cadel, 1986) and 280 ± 3 Ma (U-Pb, Zircon) (Philippe, 1984) has been obtained for the 'Banco di Novazza', the fourth rhyolitic cooling unit (Fig. 3b).

Massflow units, conglomerates and breccias of porphyritic pumice and clasts in a matrix of ash, and pyroclastic flows grade distally into finer grained turbidite facies. These reworked volcanics are provenant and drape from the top and flanks of sub-circular crystalline rhyolitic to dacitic domes and subvolcanic masses, that locally in the 'Fondra'- and 'Ornica'- cauldrons breached through the lower volcano-clastic unit.

The 'Monte della Croce basement high' in the 'Valgoglio cauldron' might be an example of a cryptodome, where the lavas did not extrude in large volumes as lavadomes, but caused subareal expansion of a subvolcanic body.

The sediments of the lower volcano-sedimentary unit, penetrated and flanked by the lavadomes, are present in all cauldrons, except where deep erosion occurred immediately before deposition of the USM, covered by deposits of the upper volcano-clastic unit. They also reach their maximum thickness of 950 m in the eastern part of the basin. The upper unit starts with a thick sedimentary unit (generally 120-150 m), consisting of very immature sandstones, pebbly sandstones and fine-conglomerates, with abundant predominantly andesitic lithic but also basement fragments, shows large lateral thickness variation caused by mentioned subvolcanic activity. It has some air-fall tuffs at its top.

Four northwards thinning depositional wedges of the upper unit follow in the 'Valgoglio cauldron'. In the other cauldrons these wedges are thinner and possibly of lesser abundance.

Each of these wedges consists of poorly welded more or less porphyritic rhyolitic tuffs and ash flows, covered by lacustrine thin-bedded sandstones and siltstones with large thickness changes due to synsedimentary faulting. Absence of individual units, due to Permian erosion, is widespread. In the western two cauldrons this unit is much reduced in thickness and number of wedges. Up to this stage the area of deposition of the Collio formation was restricted to the cauldrons. At least three upper rhyolitic units extend further toward the N and do not seem to be solely confined to a cauldron-structure. Their thickness is controlled by syn-depositional faults.

Starting with deposition of the USM the area of deposition extended to an even wider approximately E-W trending 50 km long and 15-20 km wide zone, the actual extension of the Collio basin. The USM consists of alluvial fan facies at the northern and locally at the southern margin of the basin, which grade into deltaic and braided river plain facies and lacustrine facies toward the center. Some extracalderic ignimbrites, possibly correlating with the upper units of the LVCM, are present at the base, along the northern margins of the cauldrons. The USM reaches thicknesses of up to 1500 m in the Pizzo Coca-Pizzo Redorta area. The alluvial fan facies is represented by several alluvial fans, each with clasts of a different range of compositions, some also with volcanic clasts, representing their individual source areas. One of these fans consists of the 'Ponteranica conglomerates'. These have been attributed to a separate formation (Casati & Gnaccolini, 1965) although other alluvial fan-conglomerates to the east all belong to the Collio formation, which can be considered more correct, since all grade laterally into the same continuous lacustrine facies of the Collio formation. The 'Ponteranica-fan' is the largest and was fed by east- to southeast-flowing palaeo-rivers that followed normal fault-controlled troughs. South-directed rivers, flowing through palaeo-valleys in the Orobic basement, fed the other fans in the north, whereas north-flowing streams deposited the 'Val Sanguigno' fan-sediments. Sedimentary facies point to mudflow and sheetflooding as the dominant depositional process on the fans. Streamchannel deposits are less abundant. Proximal facies of these fans are characterised by generally top-missing Bouma sequences, pointing to turbidites as depositional process. These turbidites and steamchannel deposits grade into lake-sediments.

These fans grade basinward into braided river plains with channels and erosional scours with depths of up to 1 m, particularly well developed in the 'Scisti di Carona' that are characterised by a well developed steeply north-dipping pressure solution foliation.

Incision, particularly by sublacustrine channels into the LVCM before and during deposition of the upper sedimentary member has left steep erosional channels, especially in the central and western regions of the basin. Most channels are incised into volcanics of the upper volcano-sedimentary unit only. Boulders of the upper volcanoclastic unit are found in some channels. Preservation of the LVCM in the east and south of the basin is better.

Toward the center of the basin fluviatile and alluvial fan facies sediments grade into the volumetrically important black and dark grey shales, siltstones and sandstones of the turbidite facies. Light coloured, grey, purplish red and greenish rocks of similar nature, derived from the LVCM, occur mostly close to the volcanic centres in the south of the basin. In distal direction and upward they grade into reddish sandflat and mudflat facies with wave-ripple marks, raindrop inprints and mudcracks. Tetrapod footprints (*Amphiosauropus latus,* HAUBOLD, *Amphiosaurus imminitus,* HAUBOLD, *Dromopus lacertoides,* GEINITZ *and*

Varanus curvidactilus, MOODIE (Nicosia et al., 1999) and Conifer species (*Cassinis Orobica* sp, *Walchia* sp.) (Casati & Gnaccolini, 1967, Kerp et al., 1996), 3-dimensionally well-preserved in stromatolites (Freytet et al., 1996), have been identified at the top of the Collio-succession, which contains soils in the uppermost 20 m. Massive fluviatile conglomerates of the 'Verrucano Lombardo formation' unconformibly overly the USM of the 'Collio Orobica formation'. This angular unconformity reaches angles of approximately 20° .

3 Sampling locations and sample description

Samples of detrital white mica were taken from locations shown in Fig. 2, from the 'basal conglomerates' (119.1), the base of the 'USM' of the 'Collio formation' (119.3), the top of the 'Collio Formation' (125.1, 126.1) and from the conglomerates of the 'Ponteranica formation' (7.9). Table I summarises co-ordinates and altitude of the sampled outcrops, a short description of the samples and outcrop. Fig. 3b shows the relative stratigraphic position of the sample locations in a schematic profile. Thin section photographs of each sample are shown in Fig 4. The assessed age of deposition of these samples is also listed in Table I.

Table I: Summary of sample-data, including sampling locations and lithological description of the rocks in outcop and assessed age of deposition.

Sample (measured sieve fractions)	Sample location	Co-ordinates (UTM)	Altitude (m)	Formation and position	Sample and outcrop description	Assessed age of deposition (explanation in text)
119.1 (125-250µm /250-500µm)	'Selva d'Agnone'	1568661-5092555	1280	Basal conglomerate	Conglomerate with dominantly subangular components of crystalline basement and a matrix rich in white mica. Directly overlying Orobic basement of the 'parautochton'	Carboniferous or Permian (301 ± 9 Ma – 288,4 Ma)
119.3 (125-250µm)	Above 'Maslana'	1578531-5099781	1170	Collio formation (USM) (Base)	Grey banded interlayered arenites silt and minor claystones, with occasionally relatively coarse white mica, overlying directly the Orobic basement ('Orobic fold nappe'?)	Lower Permian (280 ± 3 –259 Ma, most likely 267 Ma)
125.1 (125-250µm)	'Cornello'	1558405-5095362	935	Collio formation ('Scisti di Carona' = USM) (Top)	Dark grey finely laminated arenites and silt/claystone with well developed foliation developed by pressure solution. Verrucano Lombardo immediately underlies these sediments.	Lower Permian (~ 259 Ma)
126.1 (250-500µm/ 125-250µm)	'Lago di Valmora'	1548332-5097785	1550	Collio formation (USM) (Top)	Dark grey finely laminated silt/claystone of the upper sedimentary member. 10 m from synvolcanic fault.	Lower Permian (~ 259 Ma)
7.9 (250-500µm/ 125-250µm)	At N-flank of 'Monte Ponteranica'	1546240-5097680	2235	Ponteranica formation	Fine conglomerates with greenish and redish grey sedimentary and volcanic components derived from the underlying sequences in a matrix of arenite and silt.	Lower Permian (~ 259 Ma)

Deposition of the 'basal conglomerates' must have occurred at around 290 Ma, between Late Carboniferous igneous emplacement of the 'Val Biandino plutonic complex' (according to K-Ar Biotite-ages of 307 ± 9 to 271 ± 8 Ma of De Capitani et al. (1988)) and extrusion of the rhyolites of the Collio formation, starting at 288 Ma (see above). For dating the top of the 'Collio Trumplino' formation, in the province of Brescia, Visscher et al. (1999) used macrofloras. They suggest a Late Artinskian-?early Ufimian age. For the same sequence Cassinis & Doubinger (1991), applying palynomorph assemblages, suggested Artinskian-Ufimian ages. Nicosia et al. (1999) correlated the Orobic ichnofauna of 'Val Varrone' and suggested a deeper incision of the Collio Orobica sequence during deposition of the
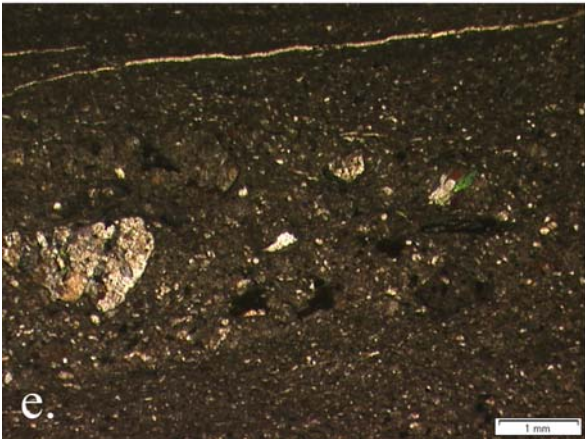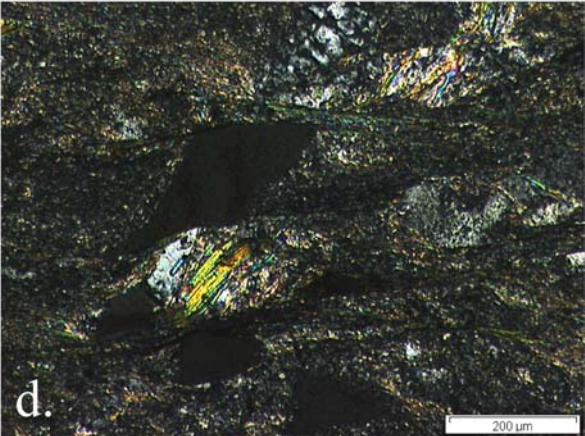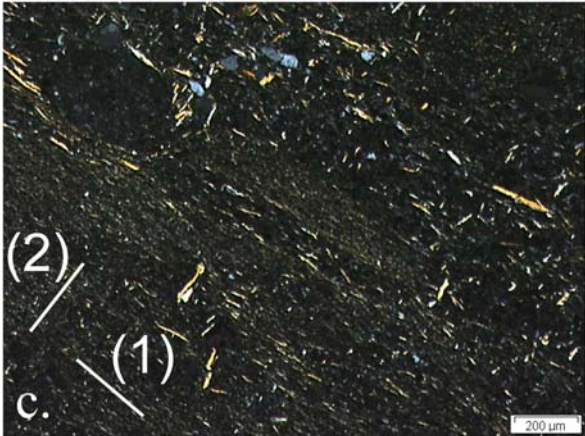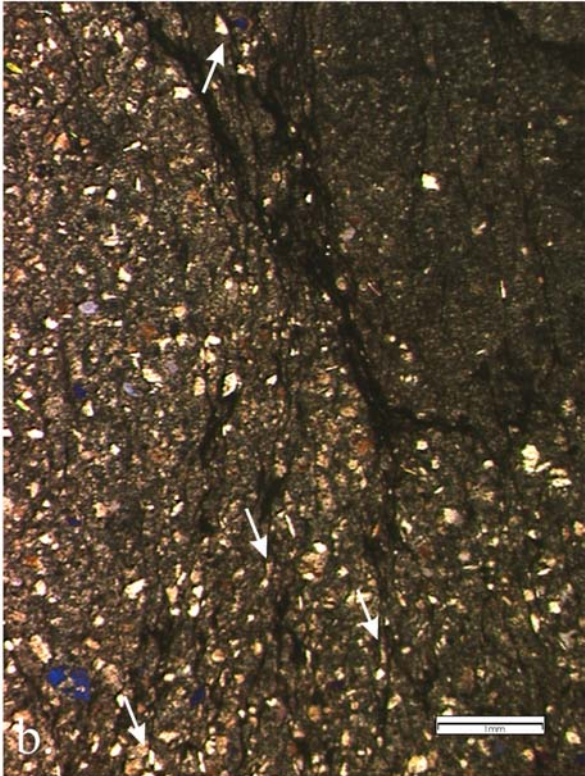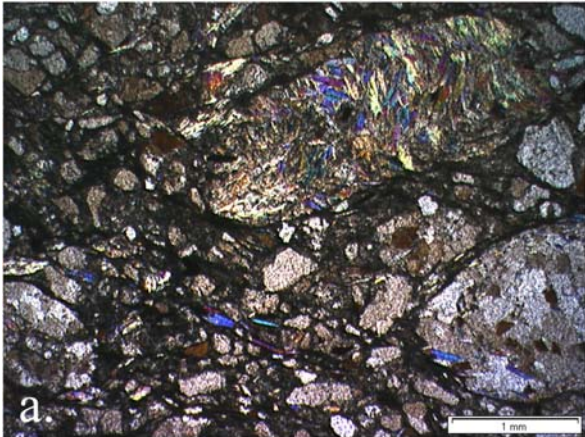
Fig.4 Microphotographs of the samples from which the detrital white mica-grains were separated. Crossed and oblique polars.

a. Sample 119.1: 'Basal conglomerate' with mica-bearing clasts and white mica in the matrix.

b. Sample 119.3 from the base of the upper sedimentary member of the 'Collio-Orobico formation', with weakly developed dark pressure solution seams, straight boundaries of some quartz grains. Arrows indicate partly dissolved grains. White mica is also present as isolated grains.

c. Sample 125.1: Microfabric of the fine-grained silt- and claystones of the upper part of the 'Collio-Orobico formation'. Very fine white mica crystals are oriented in two perpendicular orientations, indicated as (1) detritral white mica parallel to primary layering and (2) crystals formed by precipitation related to the Alpine pressure-solution-process.

d. Sample 126.1: Well-developed pressure-solution-precipitation fabric. The bright and inclusion-free white mica grains with oblique orientations to the dark pressure-solution seams are Variscan grains. 'Dirty' Alpine white mica formed by precipitation contains numerous inclusions is oriented parallel to the solution seams.

e. Sample 7.9: Photograph of very poorly sorted wacke of the 'Ponteranica formation', which contain clasts of the coarse sandstone fraction, including isolated white mica grains.

Verrucano Lombardo formation than in the Collio Trumplino and Tregiovo basins. Therefore the depositional age of the top of the 'Collio Orobica' and 'Ponteranica' formations is assumed at 259 Ma. Siderite- and barite ores, as well as silicic impregnations, are present in Permian syn-diagenetic extensional faults that reached up to the exposed top of the 'Collio Orobica' and 'Ponteranica' formations and could have been conduits during hydrothermal activity related to rhyolitic volcanism.

The base of the upper sedimentary member marks the end of rhyolitic volcanism in the 'Collio Orobico basin', possibly in the entire Southern Alps. In the area of investigation no radiometric age is available for the uppermost rhyolitic unit. Therefore an age of general cessation of the volcanism of 267 Ma for the central Southern Alps (Cassinis & Neri, 1992 and references therein) is also assumed for the Orobic Alps. The applied age of the base of the upper sedimentary member is therefore also estimated at approximately 267 Ma, a maximum age.

4 Geochronological method

Concentrates of white mica of sieve fractions 125-250 and 250-500 μm were prepared by breaking the rock-samples, dry sieving, washing first in tap water, finally in distilled water, using an ultrasonic bath and drying. Single grains to be measured were handpicked under a binocular microscope. 6 to 17 individual mica grains were selected from the two fractions of each sample. For irradiation in the central position of the MTA-KFKI-reactor in Budapest the minerals were packed into Al-foil packets and sealed in quartz vials. The samples were exposed to radiation for 8 hours at a flux of c. 1,7 x 10^{18} n/cm^{2}s. Correction factors for production of interfering isotopes have been reported by Handler & Neubauer (in review) and

are: ^{36}Ar/^{37}Ar$_{(Ca)}$ = 2.6025x10^{-4}, ^{39}Ar/^{37}Ar$_{(Ca)}$ = 6.5014x10^{-4}, and ^{40}Ar/^{39}Ar$_{(K)}$ = 1.5466x10^{-2}.

Variations in the flux of neutrons were monitored with B4M white mica standard (Flisch, 1982) for which a ^{40}Ar/^{39}Ar plateau age of 18.555 ± 0.395 Ma has been reported (Burghele, 1987).

^{40}Ar/^{39}Ar analyses have been carried out in the ARGONAUT Laboratory at the Institute of Geology and Palaeontology at the University of Salzburg using a UHV Ar-extraction line equipped with a combined MERCHANTEK^{TM} UV/IR laser ablation facility, and a VG ISOTECH^{TM} NG3600 Mass Spectrometer following procedures described in Handler & Neubauer (in review). Single grains were measured by total fusion, using a 25 W CO_2-IR laser operating in Tem$_{00}$ mode at wavelengths between 10.57 and 10.63 μm. The laser was defocused to a spot size of ca. 1.0 mm. The laser was controlled from a PC, and the position of the laser beam on the sample was monitored through a double-vacuum window on the sample chamber via a video camera in the optical axis of the laser beam on the computer screen. Gas clean-up was performed using one hot and one cold Zr-Al SAES getter. Measurement was performed on an axial electron multiplier in static mode, peak jumping and stability of the magnetic field was controlled by a Hall-probe. For each increment the intensities of ^{36}Ar, ^{37}Ar, ^{38}Ar, ^{39}Ar and ^{40}Ar were measured, the baseline readings on mass 33.5 were automatically subtracted. Intensities are corrected for system blanks, background, post-irradiation decay of ^{37}Ar, and interfering isotopes. Ages and errors were calculated following suggestions of McDougall & Harrison (1988) and decay factors reported by Steiger & Jäger (1977) using our own MICROSOFT EXCEL^{TM} worksheet.

5 Results and discussion

5. 1 Geochronological results
Results of total fusion measurements of detrital muscovite from the 'Collio formation' and the 'basal conglomerates' are shown in Table II and in Fig. 5.
Three Variscan age populations (A-C) two Permo-Mesozoic (D and E) and two Alpine (F and G) have been identified (See Table II and Fig 5). In the Orobic Alps three possible source units, with a different development exist, the parautochton, the 'Orobic fold nappe' and the 'suprastructure', consisting of 'Scisti di Edolo'. Source areas outside the Orobic basement were also held for possible, but at first it is assumed that all grains are derived from Southalpine units that are also exposed in the Orobic Alps. Given the proximal nature of the sediments, this is a realistic assumption.
The oldest population (A) represents an Early Carboniferous (early Variscan) cooling phase at 350-338 Ma (analyses 00s0421a in 119.1 and 00s0434a and 00s0435a in 119.3). This early phase is recognised only in the detrital grains of samples 119.1 and 119.3. Assuming that these grains are derived from a unit of the Orobic basement it is unlikely that population (A) is derived from the 'Orobic fold nappe', since the uppermost amphibolite facies imprint at 330-320 Ma should have reset and recrystallised all included white mica, including those of the 'pre-Sardic' sequence. Two potential source areas remain in the Orobic basement, the 'suprastructure' and the parautochton. As discussed in the lithological description of the

Table II: Ar-analytical data from single-grain total fusion analyses on detrital muscovite from the 'Collio'- and 'Ponteranica' formations and the 'Conglomerato Basale'. Errors are 1-sigma inter-laboratory. Lithological units and sample locations, including co-ordinates (UTM), are indicated behind sample numbers. Lithological descriptions of the samples are also given as well as the age population to which the result was assigned .

Sample:	119.1 (250-500μm) Conglomerato Basale (Location: Selva d'Agnone, Co-ordinates: 1568661-5092555, 1280 m) Conglomerate with dominantly subangular components of crystalline basement and a matrix rich in white mica. Directly overlying Orobic basement of the 'parautochton'						
J-Value:	0.000414 ± 0.000004						
analysis	^{36}Ar/^{39}Ar^a	^{37}Ar/^{39}Ar^b	^{40}Ar/^{39}Ar^a	%40Ar^c	age [Ma]	±	age population
00s0437a	0.01516	0.00132	355.87	98.7	245.0	2.2	E

	119.1 (125-250μm)						
J-Value:	0.000419 ± 0.000004						
analysis	^{36}Ar/^{39}Ar^a	^{37}Ar/^{39}Ar^b	^{40}Ar/^{39}Ar^a	%40Ar^c	age [Ma]	±	age population
00s0419a	0.05360	0.48108	485.26	96.7	324.0	4.3	B
00s0420a	0.03631	0.29899	481.12	97.8	324.6	3.4	B
00s0421a	0.15732	0.96962	543.75	91.5	341.7	8.4	A
00s0422a	0.00250	0.00706	456.55	99.8	315.3	3.4	B
00s0423a	0.00991	0.05467	446.69	99.3	307.7	4.9	B

Sample:	119.3 (125-250μm) Base of Collio formation (upper sedimentary member) (Location: Maslana, Co-ordinates: 1578531-5099781, 1170 m) Grey banded interlayered arenites silt and minor claystones, with occasionally relatively coarse white mica, overlying directly the Orobic basement ('Orobic fold nappe'?)						
J-Value:	0.000424 ± 0.000004						
analysis	^{36}Ar/^{39}Ar^a	^{37}Ar/^{39}Ar^b	^{40}Ar/^{39}Ar^a	%40Ar^c	age [Ma]	±	age population
00s0424a	0.00234	0.00639	462.78	99.9	322.8	3.5	B
00s0425a	0.06067	0.75688	267.79	93.3	181.8	12.0	E
00s0426a	0.01542	0.16222	428.67	98.9	298.4	4.7	C
00s0434a	0.06903	0.82211	506.24	96.0	338.1	5.7	A
00s0435a	0.10832	0.73602	537.60	94.0	350.6	5.4	A
00s0436a	0.04956	0.50587	486.52	97.0	329.1	3.9	B

Sample:	125.1 (125-250μm) Top of Collio formation (upper sedimentary member) (Location: Cornello; Co-ordinates: 1558405-5095362, 935 m) Dark grey finely laminated arenites and silt/claystone with well developed foliation developed by pressure solution. Verrucano Lombardo immediately underlies these sediments.						
J-Value:	0.000422 ± 0.000004						
analysis	^{36}Ar/^{39}Ar^a	^{37}Ar/^{39}Ar^b	^{40}Ar/^{39}Ar^a	%40Ar^c	age [Ma]	±	age population
00s0463a	0.03864	0.00000	96.53	88.2	63.7	3.0	F
00s0464a	0.03377	0.04869	111.21	91.0	75.5	3.1	F
00s0465a	0.00133	0.02345	90.52	99.6	67.3	3.0	F
00s0466a	0.04988	0.76278	79.17	81.4	48.5	3.0	F
00s0468a	0.09248	0.78715	99.99	72.7	54.5	2.7	F
00s0469a	0.05404	1.70016	84.47	81.1	51.6	4.7	F

Sample:	126.1 (250-500μm) Top of Collio formation (upper sedimentary member) (Location: Lago di Valmora, Co-ordinates: 1548332-5097785, 1550 m) Dark grey finely laminated silt/claystone of the upper sedimentary member.						
J-Value:	0.000421 ± 0.000004						
analysis	^{36}Ar/^{39}Ar^a	^{37}Ar/^{39}Ar^b	^{40}Ar/^{39}Ar^a	%40Ar^c	age [Ma]	±	age population
00s0470a	0.32197	1.53305	221.19	57.0	93.4	1.7	F
00s0471a	0.11846	0.98047	165.62	78.9	96.7	2.2	F
00s0473a	0.52373	0.06226	521.59	70.3	259.1	49.0	D
00s0474a	0.06447	0.45627	165.50	88.5	108.0	1.7	Mixed
00s0476a	0.07077	0.75023	162.33	87.1	104.4	2.0	F
00s0475a	0.03059	2.19242	202.89	95.5	141.8	9.3	Mixed
00s0477a	0.04168	0.35682	184.85	93.3	126.5	2.8	Mixed
00s0480a	0.14056	0.66016	175.79	76.4	99.3	2.0	F

Table II (continued)

Sample:	JF-126.1 (125-250μm)						
J-Value:	0.000420 ± 0.000004						
analysis	^{36}Ar/^{39}Ar[a]	^{37}Ar/^{39}Ar[b]	^{40}Ar/^{39}Ar[a]	%40Ar[c]	age [Ma]	±	age population
00s0427a	0.09465	0.00000	391.33	92.9	256.2	59.8	D
00s0431a	0.00890	0.22169	176.94	98.5	127.5	3.4	Mixed
00s0433a	0.15256	0.60124	105.73	57.4	45.4	12.8	G

Sample:	JF-7.9 (250-500μm) Top of Ponteranica formation (Location: Monte Ponteranica, Co-ordinates: 1546240-5097680, 2235 m) Fine conglomerates with greenish and redish grey sedimentary and volcanic components derived from the underlying sequences in a matrix of arenite and silt.						
J-Value:	0.000404 ± 0.000004						
analysis	^{36}Ar/^{39}Ar[a]	^{37}Ar/^{39}Ar[b]	^{40}Ar/^{39}Ar[a]	%40Ar[c]	age [Ma]	±	age population
00s0449a	0.01708	0.01353	442.78	98.9	293.8	2.9	C
00s0450a	0.02320	0.01288	439.19	98.4	290.4	2.8	C
00s0451a	0.01027	0.02833	382.55	99.2	257.3	2.4	D
00s0452a	0.02291	0.10545	370.48	98.2	247.3	2.8	E
00s0453a	0.16024	0.05547	228.89	79.3	127.7	3.2	Mixed
00s0454a	0.02627	0.06970	440.44	98.2	290.6	3.1	C
00s0455a	0.13484	0.06683	434.90	90.8	267.1	2.6	D
00s0456a	0.04413	0.03657	397.11	96.7	260.2	2.5	D
00s0457a	0.16345	0.01975	672.48	92.8	405.7	3.7	Pre-Variscan
00s0458a	0.01229	0.02295	178.24	98.0	123.0	1.3	Mixed
00s0459a	0.01006	0.00980	304.31	99.0	207.2	2.1	E
00s0460a	0.01355	0.00651	477.33	99.2	315.7	3.0	B

Sample:	JF-7.9 (125-250μm)						
J-Value:	0.000408 ± 0.000004						
analysis	^{36}Ar/^{39}Ar[a]	^{37}Ar/^{39}Ar[b]	^{40}Ar/^{39}Ar[a]	%40Ar[c]	age [Ma]	±	age population
00s0413a	0.04853	0.53944	502.34	97.1	327.7	4.4	?
00s0415a	0.02265	0.20391	438.49	98.5	292.8	2.9	C
00s0416a	0.07087	0.57904	466.65	95.5	301.6	4.2	B
00s0417a	0.14859	1.11956	487.15	91.0	300.1	6.1	B
00s0418a	0.06571	0.51140	478.15	95.9	309.6	4.2	B

[a] measured
[b] corrected for post-irradiation decay of ^{37}Ar (35.1 days half-life)
[c] (^{40}Ar$_{tot}$ - ^{36}Ar$_{atmos}$ x 295.5) / ^{40}Ar$_{tot}$

'Scisti di Edolo', the maximum age of metamorphism of the 'suprastructure' is 310-320 Ma most likely being 300 Ma. The parautochton then remains the only possible Orobic source. Muscovite ages of 364-340 Ma. (Mottana in Martin et al., 1996), from Southalpine basement with exactly the same structural position, underlying the 'Collio Trumplino basin', show that this assumption is very realistic.

Other units of the Southern Alps that have cooled in the same period are the 'Brixen quartzphyllite complex' and the 'Agordo- and Recaro quartzphyllite complexes'. A Rb-Sr-muscovite-garnet-whole rock isochron of 354 ± 10 Ma of the 'Brixen quartzphyllite complex' (Del Moro et al., 1980) indicates a similar cooling event, just like the Rb-Sr whole rock isochron of the 'Agordo quartzphyllite complex' of 347 ± 17 Ma (Cavazzini et al., 1991). Both these units have also been affected by a younger event dated by Rb-Sr on muscovite and biotite, for both minerals 314 ± 5, K-Ar on muscovite 316 ± 8 Ma and 319 ± 5,5 Ma (Hammerschmidt & Stöckhert, 1987) and with a Rb-Sr biotite-Kfs-WR isochron at 321 ± 5 Ma (Del Moro et al., 1984). Metamorphic imprint of these units is of lower grade than the 'Orobic fold nappe', 420-520 °C at 0.2-0.45 GPa (Ring & Richter (1994) or zoned from 350-
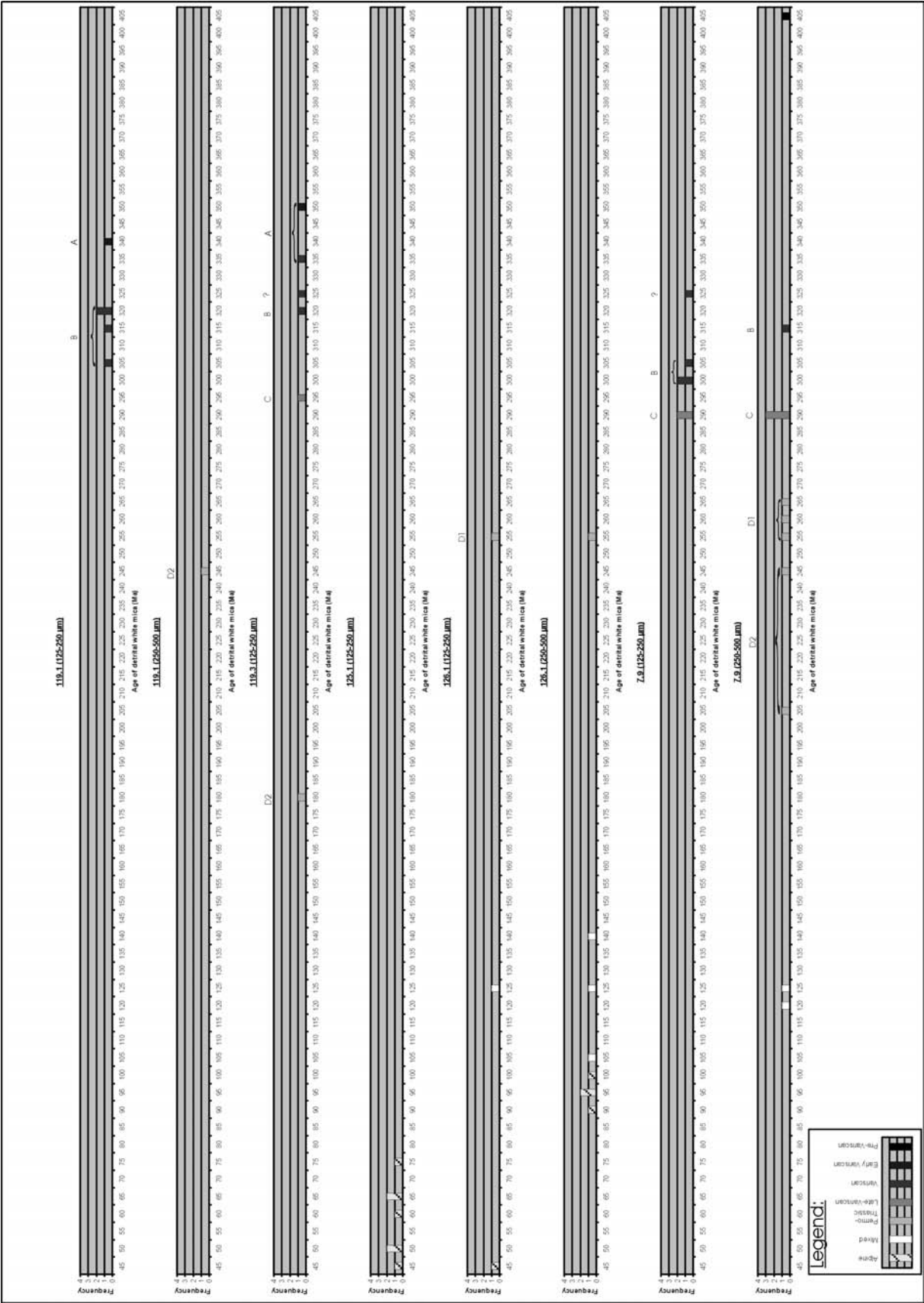
Fig. 5. Age-frequency plots of the individual samples, showing the ^{40}Ar/^{39}Ar-age distribution of the analysed white mica grains.

520 °C at 0.35-0.40 GPa (Mazzoli & Sassi, 1988) in the 'Brixen quartzphyllite complex' and of approximately 350 °C at 0,35 GPa in the 'Recaro quartzphyllite'. The 'Col di Foglia formation' of the 'Agordo-Ceredo phyllitic area' in the 'Agordo quartzphyllite complex', which has supplied the isotopic age data contains Cambrian acritarchs (Sassi et al., 1984) and according to Kalvacheva et al. (1986) contains acritarchs older than Arenig, and would therefore most likely be a Gondwana-derived crustal fragment. Acquisition of biostratigraphic data from the Orobic parautochton, if possible, and ^{40}Ar/^{39}Ar-dating of white mica from this unit would be necessary to ascertain the proposed correlation and interpretation.

A Variscan peak and cooling event between 325 and 305 Ma is represented by population (B) of detrital white mica (00s0419a, 00s0420a, 00s0422a and 00s0423a in sample 119.1, 00s0424a and 00s0436a in sample 119.3, 00s0460a, 00s0413a and 00s0418a in sample 7.9). In the age-spectra of white mica from the Orobic fold nappe a Variscan event of a similar age (~325-305 Ma) is very obvious, however the age of analyses 00s0413a and 00s0436a, 327.7 ± 4.4 and 329.1 ± 3.9 Ma do not fit very well with the basement data, because peak metamorphism of the 'Orobic fold nappe' was at around 330 Ma and cooling below muscovite retention temperature would have occurred earliest around 325 Ma. Detrital white mica derived from the 'Orobic fold nappe' is thus certainly present amongst the measured detrital grains of population (B).

Some total fusion ages of detrital mica (analyses 00s0426a in 119.3, and 00s0449a, 00s0450a, 00s0454a, 00s0415a, 00s0416a and 00s0417a in 7.9) of population (C) are younger, ~300-290 Ma and very probably represents cooling of late-Variscan plutonic bodies and their contact zones, like the 'Val Biandino plutonic complex'. The facies distribution of the alluvial fans of the Ponteranica formation, from where sample 7.9 was collected, indicates a provenance area in the direction where the 'Val Biandino plutonic complex' is situated. In this source area the Ponteranica formation directly overlies the 'Val Biandino plutonic complex' and its host rock, either with unconformable or with fault contacts. Another possible source unit, for reasons explained above in this section, is the 'suprastructure', which is likely for the analysis 00s0426a of sample 119.3.

Thermal activity related to Permo-Mesozoic events might have overprinted some grains of samples 7.9 (analyses 00s0451a, 00s0452a, 00s0455a, 00s0456a and 00s0459a), 119.1 (analysis 00s0437a), 119.3 (analysis 00s0425a) and 126.1 (00s0473a, 00s0427a, both with large errors) (Table II). This is population (D). It makes sense to subdivide this population in two sub-populations; a Middle- to Late Permian (D1) with ages of 270-255 Ma (analyses 00s0451a, 00s0455a, 00s0456a, 00s0473a and 00s0427a) and a Mesozoic (D2) with ages of 250-180 Ma (analyses 00s0452a, 00s0459a, 00s0437a and 00s0425a). Some of the isotopic ages are similar to the age of deposition of the sampled rock (population D1), and others can only be related to a younger Mesozoic overprint (population D2). The grains of analyses 00s0452a and 00s0437a, because they are too young for a single Middle- to Late Permian overprint and would have at least a dual-phase overprint, either Middle- to Late Permian and Mesozoic or Middle- to Late Permian and Alpine or both.

Middle- to Late Permian and Mesozoic events have also been identified in step heating analysis of some multigrain samples of biotite from the Orobic basement. (samples 33.6 and 64.2 from the 'GOOV' as well as 98.2 and 92.2 from the 'Gneiss di Morbegno' in Feijth et al., in prep.). A Mesozoic event was also identified in monazite data, in samples from the

'Gneiss Chiari', microprobe-analyes revealed U-Th-Pb ages of 178 ± 93 and 158 ± 59 Ma (Feijth et al., in prep.).

This population (D2) indicates a hydrothermal overprint related to Mesozoic phases. The Mesozoic phases are well pronounced in isotopic data from the 'Lario basement' (in the western Orobic Alps) (Bertotti et al., 1999; Hanson et al., 1966; Bocchio, 1981; Mottana et al., 1985).

Detrital micas of population (D1) with ^{40}Ar/^{39}Ar-ages of close to 260 Ma were exclusively found in the top of the USM of the 'Collio Orobica formation'. The white mica grains of population (D1) are a result of Middle- to Late Permian hydrothermal and volcanic activity. The possibility that this population represents fresh reworked grains of an exhumed basement can be ruled out, because this stage of basin development is characterised by sagging, and an overprint related to Permian volcanism has also been identified in biotite of the basement (sample 98.2 in Feijth et al., in prep.).

Among the results of the total fusion of detrital white mica (Table II) two Alpine age groups, 40-75 Ma and 90-105 Ma (populations F and G) are prominent, particularly in samples 125.1 and 126.1, representing young pressure-solution related recrystallisation phases (Fig. 4b, c and d) or growth of white mica between only recorded and recognised in the uppermost units of the Lower Permian Collio formation (Feijth & Neubauer, in prep. a). Cenomanian-Turonian ages of total fusion analyses 00s0470a, 00s0471a and 00s0480a of sample 126.1 are also considered Alpine, because in the Orobic basement a Cretaceous event at 100-80 Ma was determined trough relationships of faults with the 'Adamello plutons' by Schönborn & Schumacher (1994). This phase can possibly be related to the 'Trupchun phase' in the Australpine of Graubünden. The Truphun phase is related to the closure of the 'Meliata-Hallstatt Ocean' (Froitzheim, 1996). In contrast the Early Cretaceous ages (analyses 00s0474a, 00s0476a, 00s0475a, 00s0477a, 00s0431a, 00s0453a and 00s0458a) are mixed ages and fall in a period in which no cooling phase is known and might be related to recrystallisation of older grains in conjunction with contractional tectonics.

The growth and recrystallisation of the younger Alpine white micas (analyses 00s0463a, 00s0464a, 00s0465a, 00s0466a, 00s0468a, 00s0469a and 00s0433a), found in samples 125.1 and 126.1, is related to solution-precipitation processes (Fig. 4b,c and d).

5.2 Lag times and geodynamic setting of the deposition of basin sequences

In Fig. 6 the ^{40}Ar/^{39}Ar-isotopic ages of these muscovite-grains of all white mica grains that are Carboniferous-Permian in age or older are plotted against the depositional ages of the sediments from which these grains were separated. The calculated lag times for Variscan grains are also indicated. The Middle- to Late Permian white mica ages (population (D1)) are also plotted (white squares). The ages of population (D1), however are related to overprint by Permian hydrothermal activity that occurred after deposition and should therefore not be applied in evaluations that relate geodynamic setting to lag times. Detrital Variscan grains of the populations (B) and (C) show a general trend of progressive younging with depositional age (Fig. 6). The upward younging of these ^{40}Ar/^{39}Ar isotopic ages suggests provenance from a progressive unroofing of a metamorphic basement during a late-orogenic stage, during which the measured grains were uplifted through the temperature-window of closure of the ^{40}Ar/^{39}Ar isotopic system of white mica. Formation of the basins containing the 'basal

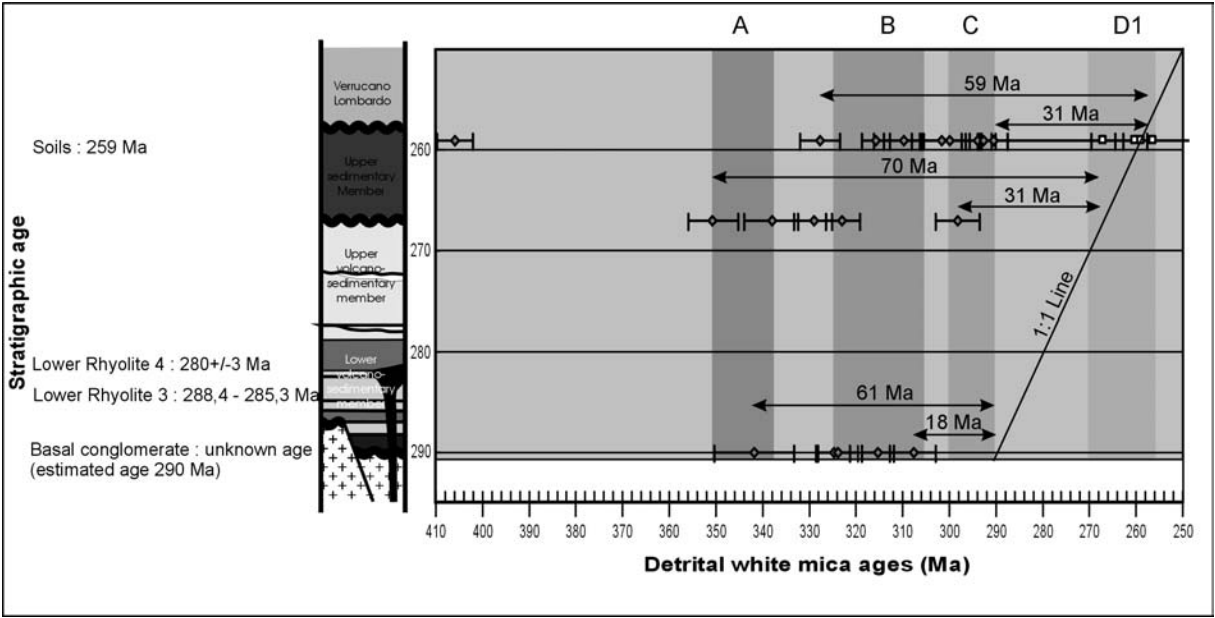*Fig. 6. Plot of ^{40}Ar-^{39}Ar-muscovite age versus approximate depositional age, showing a trend of progressive younging of detrital mica-ages with ongoing deposition. Only Variscan results are shown. Populations that can be linked to basement units and hydrothermal events (A, B, C, D1) are indicated by darker grey coloured bars. Lag-times are indicated for three stratigraphic levels, the basal conglomerate (estimated depositional age 290 Ma for sample 119.1), base of the upper sedimentary member of the Collio formation (estimated depositional age 267 Ma for sample 119.3) and the top of the upper sedimentary member (depositional age close to 259 Ma for samples 125.1 and 126.1). For the 'Ponteranica formation' (sample 7.9) also a depositional age of 259 Ma was assumed.*

conglomerates' and the 'Orobic Collio- and Ponteranica' is thus directly related to Variscan exhumation. For grains of population (A) and for the grains with ages that fall inbetween the ages of population (A) and (B), a younging is not obvious.

The minimum lag time between mica closure during uplift and deposition is 18 Ma for grains of the 'basal conglomerates'. This is a rather narrow time interval between cooling of the source rock and very typical for contractional settings. Such lag times have been found in accretionary wedge sequences according to Renne et al. (1990), Kelley & Bluck (1992) and Neubauer & Handler (1997). Detrital mica in syn-collisional flysch foredeep sequences might even contain white mica with ages identical, within uncertainty, to the cooling age (Turner et al., 1997). Peripheral molasse foreland and intramontane basins can also contain very young grains, but the youngest grains in these types of setting should be older than those in flysch foredeep sequences and accretionary wedge sequences. The most appropriate designation for the sequence of the 'basal conglomerates', based on the lithological characteristics, would be molasse. Because the range of the ages of Variscan detrital white mica reaches an upper limit of 61 Ma, not far from the avearge value for Molasse basins (~55 Ma), this interpretation seems appropriate.

This initial stage should possibly be seen as a separate stage, independent of the following stages of the development of the 'Collio Orobico basin' that took place after a phase of erosion. The initial phase of the Collio basin was a caldera-stage during which mainly

volcanics were deposited. No samples of white mica are availabe for this dominantly volcanic stage, because the sediments are almost completely derived from volcanic rocks.

Sample 119.3 was taken from the base of the fluvio-lacustrine Collio-sequence (USM), which was deposited early during the following stage and is characterised by syn-diagenetic transtensional faulting, whereas the siltstones and shales of samples 126.1 and 125.1 as well as the Ponteranica formation, represented by sample 7.9, were deposited during the end of that stage. Lag time of the measured grains of these samples varies from 31 to 70 Ma (Fig. 6), also characteristic for contractional settings. This range fits well with the average value for peripheral molasse foreland- and intramontane basins (~55 Ma). The minimum values, 31 and 31 Ma indicate a longer residence time interval of micas in the crust than determined for the micas from the 'basal conglomerates' and too high to be expected for syn-collisional flysch foredeep sequences and accretionary wedge sequences. Considering also the field-relationships, that include strong relationships between wrench tectonics and sedimentation, having caused enormous thickness and facies variation over short distance above a low-angle detachment, combined with rhyolitic calc-alkaline volcanism, the appropriate designation for this basin would be intramontane strike-slip supradetachment basin.

The detrital white mica ages of population (D1) (Fig. 6) are related to the next stage that had obviously already started in the region before and during deposition of the sandflat and mudflat facies of the 'USM'. For this population the application of lag-time, which would be close to 0 Ma, is not warranted. An overprint of these grains by Middle Permian volcanism related hydrothermal activity is likely and has possibly affected the ^{40}Ar/^{39}Ar isotopic system of white mica in the USM. Given the observations made nearby the location from where sample 126.1 was taken (see above), this should be considered.

The Mesozoic detrital white mica grains of population (D2) represent a complete tectonic reorganisation, the opening of the 'Lombardian basin' following a magmatic event at 223 Ma (Bertotti et al., 1999). N-S striking extensional detachments, like the 'Lago Maggiore fault', the 'Lugano Val Grande fault', the 'Sebino fault' and the 'Garda fault' (Bertotti et al., 1993, 1999) and the 'transverse zones' of (Schönborn, 1990; 1992; 1994) have been active after this magmatic event. Chronologically this phase succeeded deposition of a transgressional sequence in a sagging-phase, involving the 'Verrucano Lombardo formation' and eastwards the 'Bellerophon formation' onlapping the 'Valgardena Sandstone'.

5.3 Implications for the Variscan evolution

The basin, as formed during deposition of the 'Collio Orobica' and 'Ponteranica' formations, manifests itself as a supradetachment basin with superposed volcanic cauldrons. The detachment was identified at the base of the 'Collio-Orobico basin' and inbetween the 'Orobic fold nappe' and the parautochton (Feijth, in prep. a, b). Some important characteristics of the structural development of the development of this basin are derivable from the results of isotopic dating presented above and in Feijth et al. (in prep.) and the metamorphic development of hanging- and footwall (Feijth & Franz, in prep.). These are: (1) Lack of an abrupt change in Variscan T imprint across the detachment, opposite to expected for detachments with significant normal displacements. The 'Orobic fold nappe' is even affected by higher T regional metamorphism than the parautochton. (2) In case of low angle normal detachment the low-grade sequences of this basin would contain detrital white micas from the

exhumed footwall, of similar age as the age of basin formation (290-260 Ma), which is not the case. Instead, footwall-derived grains are much older, and include the populations (A) and (B) and the rocks that later supplied population (C) were probably not yet exhumed. Population (D1) is already related to a postorogenic hydrothermal stage.

Instead of a normal component, the detachment system would have had a large transcurrent component, which is confirmed by the structural configuration (Feijth, in prep. b, c). The 'Collio Orobico basin' strikes parallel to the orogenic structure, which is mainly delineated by the 'Orobic fold nappe' with its root zone. A precursor of the 'Orobic fold nappe', a diapiric ridge, formed by buoyancy and diapirism as a result of dehydration melting of muscovite and biotite at 750°C and ≤ 1.3 GPa. The development of the nappe fold-structure and further amplification occurred by superposed tectonic strain, chronologically partly overlapping with the melting-related petrographic- and structural changes. Following thinning of the 'Orobic fold nappe' is related to spreading-related collapse of the diapiric structure that extruded from a rootzone. Wrenching along this rootzone, located along the Orobic foothills in the Valtellina caused high magnitudes of additional thinning of the nappe and the formation of oblique structures, like NE-dipping transtensional shearzones. Details of this deformation are discussed in Feijth (in prep. b, c). This crustal thinning above the parautochton was penetrative and evenly distributed throughout the hangingwall, causing evenly distrubuted strain related to internal thinning of this unit (Feijth, in prep. c). This development, particularly the diapirism and extrusive nappe-folding, would be the cause of the 'Orobic fold nappe' of higher grade overlying a footwall of contrasting relatively low-grade, a configuration different to usually found at detachments which accomodated a large extensional component.

References:

Aerden, D.G.A.M., 1998. Tectonic evolution of the Montagne Noire and a possible orogenic model for syncollisional exhumation of deep rocks, Variscan belt, France. Tectonics, 17, 62-79.

Aerden, D.G.A.M., & Malavieille, J., 1999. Origin of a large-scale fold nappe in the Montagne Noire, Variscan belt, France. J. Struct. Geol., 21, 1321-1333.

Ahrendt, H., 1980. Die Bedeutung der Insubrischen Linie für den tektonischen Bau der Alpen. N. Jb. Geol. Paläont. Abh., 160/3, 336-362.

Albini, S., Battaglia, D., Bellini, G., Bigoni, C., Carminati, E., Ceriani, S., Forcella, F., Gosso, G., Guizetti, D., Oliva, A., Rebay, G., Siletto, G.B., & Spalla, M.I., 1994. Alpine deformations and pre-Alpine remnants in the north-eastern Orobic Alps, Southalpine belt. Proceedings of Symposium «CROP – Alpi Centrali» Sondrio, 20-22 October 1993: Montrasio, A. & Sciesa, E. (Editors), Quaderni di Geodynamica Alpina e Quaternaria (1994), vol. 2, 25-39.

Anderson, J.L. & Smith, D.R., 1995. The effects of temperature and f_{O2} on the Al-in-hornblende barometer. Am. Mineral., 80, 549-559.

Andrehs, G. & Heinrich, W., 1998. Experimental determination of REE distributions between monazite and xenotime: potential for temperature-calibrated geochronology. Chemical Geology, 149, 83-96.

Arthaud, F. & Matte, P., 1977. Late Paleozoic strike-slip faulting in southern Europe and northern Africa: Result of a right-lateral shear zone between the Appalachians and the Urals. Geol. Soc. Am. Bull., 88, 1305-1320.

Bailey, S.W., 1984. Crystal chemistry of the true micas. Reviews in Mineralogy, 13, 13-60.

Bea, F., 1996. Residence of REE, Y, Th and U in granites and crustal protoliths; Implications for the chemistry of crustal melts. Journal of Petrology, 37, 521-552.

Belieni, G. & Sassi, F.P. (1981). New chemical data and a review on the South-Alpine "pre Hercynian rhyolitic plateau" in the Eastern Alps. In: Karamata, S. & Sassi, F.P. (Eds.): IGCP No. 5 Newsletter, 3, 22-27, Beograd.

Bell, T.H. & Johnson, S.E., 1989. Porphyroblast inclusion trails: the key to orogenesis. J. Metam. Geol., 3, 109-118.

Bell, T.H., 1985. Deformation partitioning and porphyroblast rotation in metamorphic rocks: a radical reinterpretation. J: Metam. Geol., 3, 109-118.

Bellini, G. & Sassi, F.P. (1981). New chemical data and a review on the South-Alpine "pre Hercynian rhyolitic plateau" in the Eastern Alps. In: Karamata, S. & Sassi, F.P. (Eds.): IGCP No. 5 Newsletter, 3, 22-27, Beograd.

Bernouilli, D., Bertotti, G. & Froitzheim, N., 1990. Mesozoic faults and associated sediments in the Austroalpine-Southalpine continental margin. Mem. Soc. Geol. Ital., 45, 25-38.

Bertotti G., Ter Voorde, M., Cloetingh, S., & Picotti, V., 1997. Thermomechanical evolution of the South Alpine rifted margin (North Italy): constraints on the strenghth of passive continental margins. Earth and Planetary Science Letters, 146, 181-193.

Bertotti, G., Siletto, G.B. & Spalla, M.I., 1993. Deformation and metamorphism associated with crustal rifting: the Permian to Liassic evolution of the Lake Lugano-Lake Como area (Southern Alps). Tectonophysics, 226, 271-284.

Bertotti, G., Seward, D., Wijbrans, J., ter Voorde, M. & Hurford, A.J., 1999. Crustal thermal regime prior to, during and after rifting: A geochronological and modelling study of the Mesozoic South Alpine rifted margin. Tectonics, 18/2, 185-200.

Blundy, J.D. & Holland, T.J.B., 1990. 'Calcic amphibole equilibria and a new amphibole-plagioclase geothermometer' – reply to the comment of Poli and Schmidt. Contrib. Mineral. Petrol., 111, 278-282.

Blundy, J.D. & Holland, T.J.B., 1990. Calcic amphibole equilibria and a new amphibole-Plagioclase geothermometer. Contrib. Mineral. Petrol., 104, 208-224.

Bocchio, R., De Capitani, L, Liborio, G., Mottana, A., Nicoletti, M. & Petrucciani, C., 1981. K-Ar radiometric age determinations of the south-Alpine metamorphic complex, western Orobic Alps (Italy). N. Jb. Miner. Mh., 7, 289-307.

Bocchio, R., De Capitani, L., Liborio, G., Mottana, A, Nicoletti, M. & Petrucciani, C., 1981. K-Ar radiometric age determinations of the south-Alpine metamorphic complex, western Orobic Alps (Italy). N. Jb. Miner. Mh., 7, 289-307.

Bons, A.J., 1988. Intracrystalline deformation and slaty cleavage development in very low-grade slates from the central Pyrenees. Geologica Ultraiectina, 56.

Bonsignore, G., Casati, P., Crespi, R., Fagnani, G., Liborio, G., Montrasio, A., Mottana, A., Ragni, U., Schiavinato, G. & Venzo, S., 1971. Note ill. della Carta Geologica d'Italia. F.i 7-18, Pizzo Bernina e Sondrio, Serv. Geol. D'Italia, Roma.

Boriani A.C. & Villa, IM., 1997. Geochronology of regional metamorphism in the Ivrea-Verbano Zone and Serie dei Laghi, Italian Alps. Schweiz. mineral. petrogr. Mitt., 77, 381-401.

Boriani, A. & Colombo, A., 1979. Gli Gneiss Chiari tra la Val Sesia e il Lago di Como. Rend. Soc. Ital. Mineral. Petrol. 35/1, 299-312.

Boriani, A. & Giobbi Origoni, E., 1992. The geology of the Serie dei Laghi: A summary. In: Contributions to the Geology of Italy with special regard to the Palaeozoic basements. A volume dedicated to Tommaso Cocozza. Eds.: Carmignani, L. & Sassi, F.P., IGCP No. 276, Newsletter Vol. 5, Siena, 443-447.

Boriani, A., Origoni, E.G., Borghi, A. & Caironi, V., 1990. The evolution of the "Serie dei Laghi" (Strona-Ceneri and Scisti dei Laghi): the upper component of the Ivrea-Verbano crustal section; Southern Alps, north Italy and Ticino, Switzerland. Tectonophysics, 182, 103-118.

Boriani, A., Origono Giobbi, E. & Del Moro, A., 1982/1983. Composition, level of intrusion and age of the "Serie dei Laghi" orthogneisses (Northern Italy-Ticino, Switzerland). Rend. Soc. Ital. Mineral. Petrol., 38(1), 191-205.

Brunsmann, A., 2000. Strukturelle, Kristallchemische und phasenpetrologische Untersuchungen an synthetischen und natürlichen Zoisit und Klinozoisit Mischkristallen. PhD-thesis, Technische Universität Berlin.

Buletti, M., 1983. Zur Geochemie und Entstehungsgeschichte der Granat-Amphibolite des Gambarognogebietes, Ticino, südalpen. Schweiz. mineral. petrogr. Mitt., 63, 233-247.

Burghele, A., 1987. Propagation of error and choice of standard in the $^{40}Ar/^{39}Ar$ technique. Chem. Geol., 66, 17-19.

Cadel, G, 1986. Geology and Uranium mineralisation of the Collio basin (Central Southern Alps, Italy). Uranium, 2, 215-240.

Cadel, G., Cosi, M., Pennachioni, G. & Spalla, M.I., 1996. A new map of the Permo-Carboniferous cover and Variscan metamorphic basement in the central Orobic Alps, Southern Alps-Italy: Structural and stratigraphic data. Memorie di Scienze Geologiche, 48, 1-53.

Caironi, V., 1985. Characterization of different granitic facies in the Baveno-Mattarone pluton by means of the typologic study of zircon populations. Rend. Soc. Ital. Mineral. Petrol., 43(2), 429-444.

Carmignani, L., Oggiano, G. & Pertusati, P.C., 1994. Geological outline of the Hercynian basement of Sardinia. In: Carmignani, L. (Editor), Guidebook to the Field Excursion: Petrology, Geology and Ore Deposits of the Paleozoic Basement of Sardinia, 9-20, Int. Mineral. Assoc., Pisa.

Carminati, E. & Siletto, G.B., 1997. The effects of brittle-plastic transitions in basement-involved foreland belts: the Central Southern Alps case (N. Italy). Tectonophysics, 280, 107-123.

Carminati, E., 1992. Rapporti strutturali tra complessi metamorfici e coperture sedimentarie affioranti nelle testate delle Valli Belviso e Campovecchio (Alpi Orobiche). Laurea thesis, Univ. di Milano, Milano, Italy.

Carminati, E., Siletto, G.B. & Battaglia, D., 1997. Thrust kinematics and internal deformation in basement-involved fold and thrust belts: The eastern Orobic Alps case (Central Southern Alps, northern Italy). Tectonics, Vol. 16, 259-271.

Casati, P. & Gnaccolini, M., 1965. Una nuova formazione paleozoica dell' alta Val Brembana: la Formazione del Ponteranica. Riv. It. Pal. Strat., v. 70, 791-804, Milano.

Cassinis, G. & Doubinger, J., 1991. Artkinskian to Ufimian palynomorph assemblages from the central Southern Alps, Italy, and their regional stratigraphic implications. Contribution to Eurasian Geology, papers presented at the International Congress on the Permian System of the World, Perm, Russia, 1991 – Part 1, pp. 9-18. Occasional Publications ESRI, New Series No. 8B.

Cassinis, G. & Neri, C., 1992. Sedimentary and palaeotectonic evolution of some Permian continental basins in the central Southern Alps, Italy. Cuadernos de Geología Ibérica, 16, 145-176.

Cavazzini, G.C., Del Moro, A., Sassi, F.P. & Zipoli, G., 1991. New data on the radiometric age of the Southalpine basement of the Eastern Alps. Geologia del Basamento Italiano. Convegno in memoria di Tommaso Cocozza. Siena 21-22 marzo 1991. Abstr. Vol. (Siena).

Cello, G. & Mazzoli, S., 1996. Extensional processes driver by large scale duplexing in collisional regimes. J. Struct. Geol., 18, 1275-1279.

Clauer, N., 1981. Strontium and argon isotopes in naturally weathered biotites, muscovites and feldspars. Chem. Geol., 31, 325-334.

Clemens, J.D. & Mawer, C.K., 1992. Granite magma transport by fracture propagation. Tectonophysiscs, 204, 339-360.

Colombo, A., Siletto, G.B. & Tunesi, 1994. Pre-Variscan magmatism in the central Southern Alps: the Monte Fioraro magmatic complex. Schweiz. mineral. petrogr. Mitt., 74, 127-135.

Copeland, P, Parrisch, R. R. & Harrison, T.M., 1988. Identification of inherited radiogenic Pb in monazite and implications for U-Pb systematics. Nature (London), 333, 760-763.

Copeland, P.C., Harrison, T.M. & Heizler, M.T., 1990. ^{40}Ar/^{39}Ar single crystal dating of detrital muscovite and K-feldspar from Leg 116, southern Bengal Fan: Implications for the uplift and erosion of the Himalayas. Proc. of the ODP, Scientific results, 116, 93-114.

Cornelius, H.P. & Cornelius-Furlani, M., 1930. Die insubrische Linie vom Tessin bis zum Tonalepass. Denkschr. Akad. Wiss. Wien, v. 102, pp., 207-301.

Crespi, R., Liborio, G. & Mottana, A., 1980. L'isograda della Sillimanite negli Gneiss di Morbegno della bassa Valtellina (Complesso subalpino, Alpi Centrali, Italia). Memorie di Scienze Geologiche, Vol. XXXIV, 247-272.

Crespi, R., Liborio, G. & Mottana, A., 1980. L'isograda della Sillimanite negli Gneiss di Morbegno della bassa Valtellina (Complesso subalpino, Alpi Centrali, Italia). Memorie di Scienze Geologiche, Vol. XXXIV, 247-272.

Crespi, R., Liborio, G. & Mottana, A., 1981. Metamorphismo tardo-alpino di grado bassisimo nel basamento a sud della linea insubrica. Rendiconti Società Italiana di Mineralogia e Petrologia, 37/2, 813-824.

Crespi, R., Liborio, G. & Mottana, A., 1981. Metamorphismo tardo-alpino di grado bassisimo nel basamento a sud della linea insubrica. Rendiconti Società Italiana di Mineralogia e Petrologia, 37/2, 813-824.

Crespi, R., Liborio, G. & Mottana, A., 1982. On a widespread occurrence of stilpnomelane to the South of the Insubric line, Central Alps, Italy. N. Jb. Miner. Mh., 6, 265-271.

Dallmeyer, R.D. & Neubauer, F., 1994. Cadomian ^{40}Ar/^{39}Ar apparent age spectra of detrital muscovites from the Eastern Alps. J. Geol. Soc. London, 151, 591-598.

Dallmeyer, R.D. & Takasu, A., 1992. ^{40}Ar/^{39}Ar ages of detrital muscovite and whole-rock slate/phyllite, Narragansett Basin, RI-MA, USA: implications for rejuvenation during very low grade metamorphism. Contr. Mineral. Petrol., 110, 515-527.

Dallmeyer,R.D. & Nance, R.D., 1990. ^{40}Ar/^{39}Ar ages of detrital muscovite within early Palaeozoic overstep sequences, Avalon composite terrane, southern New Brunswick: implications for extent of late Palaeozoic tectonothermal overprint. Can. J. Earth Sci., 27, 1209-1214.

De Capitani, L., Delitala, M.C., Liborio, G., Mottana, A., Nicoletti, M. & Petrucciani, C., 1988. K-Ar Dating of the Val Biandino plutonic complex (Orobic Alps, Italy). Memorie di Scienze Geologiche, Vol. XL, 285-294.

De Sitter, L.U. & De Sitter-Koomans, C.M., 1949. Geology of the Bergamasc Alps, Lombardia, Italy., Leid. Geol. Meded., 14B, 1-257.

De Sitter, L.U., 1963. La Structure des Alpes Lombardes. In : Livre à la mémoire du Prof. P. Fallot, Tome II : Soc. Géol. France, 247-256, Paris.

De Sitter, L.U., 1963. La Structure des Alpes Lombardes. In : Livre à la mémoire du Prof. P. Fallot, Tome II : Soc. Géol. France, 247-256, Paris.

Del Moro, A., Pardini, G., Quercioli, C., Villa, I.M. & Callegari, E., 1983. Rb/Sr and K/Ar chronology of Adamello granitoids, Southern Alps. Mem. Soc. Geol. It., 26, 285-299.

Del Moro, A., Sassi, F.P. & Zipoli, G., 1980. Preliminary results on the radiometric age of the Hercynian metamorphism in the South-Alpine basement of the Eastern Alps. N. Jb. Geol. Paläont. Mh., 12, 707-718.

Del Moro, A., Sassi, F.P. & Zipoli, G., 1980. Preliminary results on the radiometric age of the Hercynian metamorphism in the South-Alpine basement of the Eastern Alps. N. Jb. Geol. Paläont. Mh., 12, 707-718.

Del Moro, A., Sassi, F.P. & Zipoli, G., 1984. Acidic gneisses from the Plan de Corones area, and chronological data on South-Alpine basement in Pusteria (Eastern Alps). Mem. Sci. Geol. Padova, 36, 403-412.

Del Moro, A., Sassi, F.P. & Zipoli, G., 1984. Acidic gneisses from Plan de Corones area, and chronological data on South-Alpine basement in Punteria (Eastern Alps). Mem. Sci. Geol. Padova, 36, 403-412.

Diella, V., Spalla, M.I. & Tunesi, A., 1992. Contrasted thermomechanical evolutions in the Southalpine metamorphic basement of the Orobic Alps, Italy. J. metamorphic geol., 10, 203-219.

Diella, V., Spalla, M.I. & Tunesi, A., 1992. Contrasted thermomechanical evolutions in the Southalpine metamorphic basement of the Orobic Alps, Italy. J. metamorphic geol., 10, 203-219.

Dirks, P.H.G.M., Zhang, J.S. & Passchier, C.W., 1997. Exhumation of high-pressure granulites and the role of lower crustal advection in the North China Craton near Datong. J. Str. Geol., 19, No. 10, 1343-1358.

Doessegger, R., 1974. Verrucano und "Buntsandstein" in den Unterengadiner Dolomiten. PhD-Thesis, ETH- Zürich.

El Tahlawi, M.R., 1965. Geologie und Petrographie des Nordöstlichen Comerseegebietes (Provinz Como, Italien). Thesis ETH Zürich.

Feijth, J. & Franz, G., (in prep.). P-T Conditions of Variscan and Mesozoic phases in the

Orobic chain (Southern Alps, Italy). Manuscript for submission to: Mineralogy and Petrology.

Feijth, J., Neubauer, F. & Finger, F., (in prep.). Geochronology of the Orobic Alps (Lombardy, Italy): (I) Evolution of the basement constrained by the U-Th-Pb-method on monazite and the ^{40}Ar/^{39}Ar-method on biotite and muscovite. Manuscript for submission to: Swiss Bulletin of Mineralogy and Petrology.

Feijth, J., Neubauer, F. & Handler, R. (in prep. a). Geochronology of the Orobic Alps (Lombardy, Italy): (II) ^{40}Ar/^{39}Ar-ages of detrital muscovite from the Collio basin, constraining Variscan-Permian and Mesozoic tectono-thermal development. Manuscript for submission to: Eclogae Geologicae Helvetiae.

Feijth, J., Neubauer, F. & Handler, R. (in prep. b). Variscan and Alpine ^{40}Ar/^{39}Ar mica ages from detrital mica of the Permian 'Orobic Collio basin' (Lombardian Alps, N. Italy): Evidence for Alpine pressure solution in relation to activity of the Orobic thrust. Manuscript for submission to: Eclogae geol. Helvetiae.

Feijth, J., (in prep. a). Palaeozoic structure and evolution of the Orobic chain (Southern Alps, Lombardy, Italy). Manuscript for submission to: Swiss Bulletin of Mineralogy and Petrology.

Feijth, J., (in prep. b). The Variscan 'Orobic fold nappe' (Southern Alps, Lombardy, Italy): Structure and evolution. Manuscript for submission to: Tectonophysics.

Feijth, J., (in prep. c). The Variscan 'Orobic fold nappe' (Southern Alps, Lombardy, Italy): Kinematic conditions of related orogenic collapse. Manuscript for submission to: Tectonophysics.

Feijth, J., (in prep. d). Permian development of the Orobic Collio supradetachment basin (Lombardian Alps, N. Italy): a final phase of Variscan exhumation. Manuscript for submission to: Eclogae geol. Helvetiae.

Finger, F., Broksa, I., Roberts, M.P. & Schermaier, A., 1998. Replacement of primary monazite by apatite-allanite-epidote coronas in an amphibolite facies granite gneiss from the eastern Alps. Am. Mineral., 83, 248-258.

Fitch, F.J., Miller, J.A. & Tomson, D.B., 1966. The palaeogeographic significance of isotopic age determinations on detrital micas from the Triassic of the Stockport-Macclesfield District, Chesire, England. Palaeogeogr. Palaeoclim. Palaeoecol., 2, 281-312.

Flajs, G. & Schönlaub, H.P., 1976. Die biostratigraphische Gliederung des Altpaläozoikums am Polster bei Eisenerz (Nördliche Grauwackenzone, Österreich). Verh. Geol. B.-A., 1976, 257-303, Wien.

Flisch, M., 1982. Potassium-argon analysis. In: Odin, G.S. (Editor): Numerical dating in

stratigraphy, Wiley & Sons, Chickester-New York-Brisbane, 151-158.

Franz, G., Andrehs, G. & Rhede, D., 1996. Crystal chemistry of monazite and xenotime from Saxothuringian-Moldanubian metapelites, NE Bavaria, Germany. Eur. J. Mineral., 8, 1097-1118.

Franz, G., Andrehs, G. & Rhede, D., 1996. Crystal chemistry of monazite and xenotime from Saxothuringian-Moldanubian metapelites, NE Bavaria, Germany. Eur. J. Mineral., 8, 1097-1118.

Freytet, P., Kerp, H. & Broutin, J., 1996. Permian freshwater stromatolites associated with the conifer shoots Cassinisia orobica Kerp et al. – a very peculiar type of fossilisation. Rev. Palaeobot. Palynol., 91, 63-84.

Froitzheim N., Schmid, S.M. & Frey, M, 1996. Mesozoic paleogeography and the timing of eclogite facies metamorphism in the Alps: A working hypothesis. Eclogae geol. Helv., 89/1, 81-110.

Gansser, A. & Pantić, C., 1988. Prealpine events along the eastern Insubric Line (Tonale Line northern Italy). Eclogae Geol. Helv., 81/3, 567-578.

Gansser, A., 1968. The Insubric Line, a major geotectonic problem. Schweiz. mineral. petrogr. Mitt., 48/1, 123-143.

Giobbi-Origoni, E., Zappone, A., Boriani, A., Bocchio, R. & Morten, L., 1997. Relics of pre-Alpine ophiolites in the Serie dei Laghi (Western Southern Alps). Schweiz. mineral. Petrogr. Mitt., 77, 187-207.

Gosso, G., Siletto, G.B. & Spalla, M.I., 1997. First day: H-T/L-P metamorphism and structures in the South-alpine basement near lake Como, Orobic Alps; intracontinental imprints of the Permo-Triassic rifting. Ofioliti, 22 (1), 133-145.

Graeter, P., 1951. Geologie und Petrographie des Malcantone (südliches Tessin). Schweiz. mineral. petrogr. Mitt., 31, 361-483.

Graham, C.M. & Powell, R., 1984. A garnet-hornblende geothermometer: calibration, testing, and application to the Pelona Schist, Southern California. J. metamorphic Geol., 2, 13-31.

Gratz, R. & Heinrich, W., 1997. Monazite-xenotime thermobarometry: Experimental calibration of the miscibility gap in the binary system $CePO_4$-YPO_4. Am. Mineral., 82, 772-780.

Gratz, R. & Heinrich, W., 1998. Monazite-xenotime thermometry. III. Experimental calibration of the partitioning of gadolinium between monazite and xenotime. Eur. J. Mineral.,

10, 579-588.

Guidotti, C.V. & Sassi, F.P., 1986. Classification and correlation of metamorphic facies series by means of muscovite *b* data from low-grade metapelites. Neues Jahrb. Miner. Abh., 153, 363-380.

Guidotti, C.V., Cheney, J.T. & Conatore, P.D., 1975. Interrelationships between Mg/Fe and octahedral Al content in biotite. American Mineralogist, 60, 849-853.

Hammarstrom, M. & Zen, E., 1986. Aluminium in hornblende: An empirical igneous geobarometer. Am. Mineral., 71, 1297-1313.

Hammerschmidt, K. & Stöckhert, B., 1987. A K-Ar and ^{40}Ar/^{39}Ar study on white micas from Brixen quartzphyllite, Southern Alps. Evidence for argon loss at low temperatures. Contrib. Mineral. Petrol., 95, 393-406.

Handler, R. & Neubauer, F. (in review): Formation of Veins in the Tauern Window related to Continental Escape in the Eastern Alps: Constraints from ^{40}Ar/^{39}Ar Dating of White Mica and Adularia. - submitted to Tectonophysics

Handy, M.R., 1986. The structure and rheological evolution of the Pogallo fault Zone, a deep crustal dislocation in the Southern Alps of northwestern Italy. Ph. D. Dissertation, Univ. Basel, 327 pp.

Handy, M.R., 1987. The structure, age and kinematics of the Pogallo fault line, Southern Alps, northwestern Italy. Eclogae geol. Helv., 80, 593-632.

Handy, M.R., Franz, L., Heller, F., Janott, B. & Zurbriggen, R., 1999. Multistage accretion and exhumation of the continental crust (Ivrea crustal section, Italy and Switzerland). Tectonics, 18, 1154-1177.

Hanson, G.N., El Tahlawi, M.R., & Weber, W., 1966. K-Ar and Rb-Sr ages of pegmatites in the south-central Alps. Earth Planet Sci. Lett. 1, 407-413.

Heinisch, H. & Schmidt, K., 1976. Zur kaledonischen Orognese in den Ostalpen. Geol. Rundsch., 65, 459-482.

Heinisch, H.& Schmidt, K., 1982. Zur Genese der Augengneise im Altkristallin der Ostalpen. N. Jb. Geol. Paläont. Mh., 1982(4), 211-239.

Heinisch, H., 1986. Die Geologie der Nördlichen Grauwackenzone zwischen Kitzbühel und Zell am See und ihre Bedeutung für die Rekonstruktion der altpaläozoischen Geodynamik des Ostalpenraumes. Habilitationsschrift, Univ. München.

Heinisch, H., 1988. Hinweise auf die Existenz eines passiven Kontinentalrandes im Altpaläozoikum der Nördlichen Grauwackenzone – Ostalpen. Schweiz. Mineral. Pertogr. Mitt., 68/3, 407-418.

Heinrich, W., Andrehs, G. & Franz, G., 1997. Monazite-xenotime miscibility gap thermometry. I. An empirical calibration. J. metamorphic Geol., 15, 3-17.

Hess, W., 1953. Beiträge zur Geologie der südöstlichen Engadiner Dolomiten zwischen dem oberen Münstertal und der Valle di Fraéle (Graubünden). Ecl. Geol. Helv., 46, 39-142.

Hodges, K.V. & Crowley, P.D., 1985. Error estimation and emperical geothermobarometry for pelitic systems. Am. Mineral., 70, 702-709.

Hoisch, T.D., 1989. A muscovite-biotite geothermometer. Am. Mineral., 74, 565-572.

Hoisch, T.D., 1990. Empirical calibration of six geobarometers for the mineral assemblage quartz + muscovite + biotite + plagioclase + garnet. Contrib. Mineral. Petrol., 104, 225-234.

Hoke, L., 1990. The Altkristallin of the Kreuzeck Mountains, SE Tauern Window, Eastern Alps – Basement Crust in a Convergent Plate Boundary Zone. Jahrbuch der Geologischen Bundesanstalt, 133-1, 5-87.

Holland, T.J.B. & Blundy, J., 1994. Non-ideal interactions in calcic amphiboles and their bearing on amphibole-plagioclase thermometry. Contrib. Mineral. Petrol., 116, 433-447.

Holland, T.J.B. & Powell, R., 1985. An internally consistant dataset with uncertainties and correlations: 2. Data and results. J. metramorphic Geol., 3, 343-370.

Holland, T.J.B. & Powell, R., 1990. An enlarged and updated internally consistent thermodynamic dataset with uncertainties and correlations: the system K_2O-Na_2O-CaO-MgO-MnO-FeO-Fe_2O_3-Al_2O_3-TiO_2-SiO_2-C-H_2-O_2. J. metamorphic Geol., 8, 89-124.

Hollister, L.S., Grissom, G.C., Peters, E.K., Stowell, H.H. & Sisson, V.B., 1987. Confirmation of the empirical confirmation of Al in hornblende with pressure of solidification of calc-alkaline plutons. Am. Mineral. 72, 231-239.

Hunzicker, J.C. & Zingg, A., 1980. Lower Palaeozoic amphibolite to granulite facies metamorphism in the Ivrea zone (Southern Alps, Northern Italy). Schweiz. mineral. petrogr. Mitt., 60, 181-213.

Johnson, M.C. & Rutherford, M.J., 1989. Experimental calibration of an aluminium-in-hornblende geobarometer with application to Long Valley caldera (California) volcanic rocks. Geology, 17, 837-841.

Johnson, S.E. (1993a) Unravelling the spirals: a serial thin section study and three-dimensional computer-aided reconstruction of spiral-shaped inclusion trails in garnet-porphyroblasts. J. Metam Geol., 1, 621-634.

Johnson, S.E., 1993b). Testing models for the development of spiral-shaped inclusion trails in garnet-porphyroblasts: to rotate or not to rotate, that is the question. J. Metam. Geol., 11, 635-659.

Kalvacheva, R., Sassi, F.P. & Zanferrari, A., 1986. Acritarch evidence for the Cambrian age of phyllites in the Agordo area (South Alpine basement of Eastern Alps, Italy). Rev. Palaeobot. Palynol., 48, 311-326.

Keller, P., 1986. Die Geologie des Passo San Simone. Diploma thesis, Univ. Basel, 103 pp., unpubl., Basel.

Kelley, S.P. & Bluck, B.J., 1992. Detrital mineral ages from the Southern Uplands using $^{40}Ar/^{39}Ar$ laser probe. J. Geol. Soc. London, 146, 401-403.

Kleemann, U. & Reinhardt, J., 1994. Garnet-biotite thermometry revisited: The effect of Al^{VI} and Ti in Biotite. Eur. J. Mineral., 6, 925-941.

Koch-Müller, M., 1997. Experimentally determined Fe-Mg exchange between synthetic staurolite and garnet in the system $MgO-FeO-Al_2O_3-SiO_2-H_2O$. Lithos, 41, 185-212.

Kohn, M.J. & Spear, F.S., 1990. Two new geobarometers for garnet amphibolites, with applications to southeastern Vermont. Am. Mineral., 75, 89-96.

Köppel, V. & Grünenfelder, M., 1971. A Study of Inherited and Newly Formed Zircons from Paragneisses and Granitised Sediments of the Strona-Ceneri-Zone. Schweiz. mineral. petrogr. Mitt., 51, 385-409.

Köppel, V. & Grünenfelder, M., 1978/1979. Monazite and zircon U-Pb ages from the Ivrea and Ceneri Zones. Abstr. 2nd Symp. Ivrea-Verbano, Varallo. Mem. Sci. Geol., Padova, 33, 257.

Köppel, V. & Sommerauer, J., 1974. Trace elements and the behaviour of the U-Pb system in inherited and newly formed zircons. Contrib. Mineral. Petrol., 43, 71-82.

Köppel, V., 1974. Isotopic U-Pb ages of monazites and zircons from the crust-mantle transitino and adjacent units of the Ivrea and Ceneri Zones (Southern Alps, Italy). Contrib. Mineral. Petrol., 43, 55-70.

Koziol, A.M. & Newton, R.C., 1988. Redetermination of the anorthite breakdown reaction and improvement of the plagioclase-garnet-Al_2SiO_5-quartz barometer. Am. Mineral., 73, 216-223.

Koziol, A.M., 1989. Recalibration of the garnet-plagioclase-Al_2SiO_5-quartz (GASP) geobarometer and applications to natural paragenesis. EOS, 70, no. 15, 493.

Krainer, K., 1993. Late- and Post-Variscan Sediments of the Eastern and Southern Alps. In: Von Raumer, J.F. & Neubauer, F., (Editors), Pre-Mesozoic Geology in the Alps. Springer Verlag, 537-564.

Lanzirotti, A. & Hanson, G.N., 1996. Geochronology and geochemistry of multiple generations of monazite from the Wepawaug Schist, Connecticut, USA: Implications for monazite stability in metamorphic rocks. Contributions to Mineralogy and Petrology, 125, 332-340.

Lardelli, T., 1981. Die Tonalelinie im unteren Veltlin. Ph.D. thesis, Univ. Zürich.

Laubscher, H.P., 1971. Das Alpen-Dinariden-Problem und die Palinspastik der südlichen Tethys. Geologische Rundschau, 60, 813-833.

Le Breton, N. & Thomson, A.B., 1988. Fluid-absent (dehydration) melting of biotite in metapelites in the early stages of crustal anatexis. Contrib. Mineral. Petrol., 99, 226-237.

Leake, B.E., 1978. Nomenclature of amphiboles. Am. Min., 63, 1023-1052.
Lehner, P., 1952. Zur Geologie des Gebietes der Denti della Vecchia, des M. Boglia, des M. Brè und des M. San Salvatore bei Lugano. Ecl. Geol. Helv., 45, 85-159.

Liborio, G. & Mottana, A., 1969. Lineamenti geologico-petrografici del complesso metamorfico subalpino nelle Alpi Orobie orientali. Rendiconti della Società Italiana di Mineralogia e Petrologia, Vol. XXV, 475-519.

Liborio, G. & Mottana, A., 1971. Gneiss Chiari del Corno Stella. Boll. Serv. Geol. It., 43-51.

Liborio, G. & Mottana, A., 1971. Gneiss del Pizzo Meriggio. Boll. Serv. Geol. It., 35-42.

Loeschke, J. & Heinisch, H., 1993. Palaeozoic Volcanism of the Eastern Alps and its Palaeotectonic significance. In: Von Raumer, J.F. & Neubauer, F., (Editors), Pre-Mesozoic Geology in the Alps. Springer Verlag, 441-455.

Mader, D., Neubauer, F. & Handler, R., submitted. Geochemistry, detrital mode and $^{40}Ar/^{39}Ar$ dating of Palaeozoic sandstones in the Carnic Alps (Austria): Implications for the geodynamic environment of the Southalpine basement. Int. J. Earth Sci.

Martin, S., Zattin, M., Del Moro, A. & Macera, P., 1996. Chronologic constraints for the evolution of the Guidicarie belt (Eastern Alps, NE Italy). Annales Tectonicae, Vol. X, No. 1-2, 60-79.

Martina, E., 1958. Osservazioni geologiche nella zona dell'Alpe Trela (Alpe Retiche, Bormio). Boll. Del Serv. Geol. d'It., Vol. LXXX, 479-495.

Martínez, F.J., Carreras, J., Arboleya, M.L. & Dietsch, C., 1996. Structural and metamorphic evidence of local extension along the Vivero fault coeval with bulk crustal shortening in the Variscan chain (NW Spain). J. Struct. Geol., 18, 61-73.

Massone & Schreyer, 1987. Phengite geobarometry based on the limiting assemblage with K-feldspar, phlogopite, and quartz. Contrib. Mineral. Petrol., 96, 212-224.

Mawer, C.K., Rubie, D.C. & Brearly, A.J., 1988. A model for rapid melting in crustal shear zones: Implications for mechanisms of melt migration. Eos, Trans. Am Geophys. Union, 69, 1411.

Mazzoli, C. & Sassi, R., 1988. Carrateri del metamorphismo ercinico nella fillade sudalpina ad ovest di Bressanone. Mem. Sci. Geol. , Univ. Padova, XL, 295-314.

McClay, K.R., 1992. Glossary of thrust tectonics terms. In: McClay, K.R. (Editor), Thrust Tectonics. Chapman & Hall, 419-433.

McDougall, I. & Harrison, T.M., 1988. Geochronology and Thermochronology by the ^{40}Ar/^{39}Ar Method. Oxford Monographs on Geology and Geophysics, No. 9, Oxford University Press, Oxford, pp 212.

McDowell, F.W., 1968a. Potassium-argon ages from the Ceneri Zone of southern Switzerland. Schweiz. mineral. petrogr. Mitt., 48/1, 211-212.

McDowell, F.W., 1968b. Potassium-argon ages from the Valle d'Ossola section of the Ivrea Verbano Zone (northern Italy). Schweiz. mineral. petrogr. Mitt., 48/1, 205-210.

McDowell, F.W., 1970. Potassium-Argon-Ages from the Ceneri Zone, Southern Swiss Alps. Contib. Mineral. Petrol., 28, 165-182.

Meli, S. & Klözli, U.S., 2001. Evidence for Lower Palaeozoic magmatism in the Eastern Southalpine basement: zircon geochronology from Comelico porphyroids. Schweiz. mineral. petrogr. Mitt., 81, 147-157.

Mitchel, J.K. & Taka, A.S., 1984. Potassium and argon loss patterns in weathered micas, implications for detrital mica studies, with particular reference to the Triassic paleography of the British Isles. Soc. Geol., 39, 261-278.

Montel, J-M., Foret, S, Veschambre, M, Nicollet, C. & Provost, A., 1996. Electron microprobe dating of monazite. Chem. Geol., 131, 37-53.

Montrasio, A., Biggioggero, B., Brigo, L., Casati, P., Cremaschi, M., Ferrario, A., Gaetani, M., Gelati, R., Gregnanin, A., Jadoul, F., Orombelli, G., Rossi, P.M. & Zuffardi, P., 1990. Carta Geologica della Lombardia (Servizio Geologico Nazionale, Dipartimento degli Studi di Milano (Dipartimento di Scienza della Terra), Regione Lombardia, Consiglio Nazionale delle Richerche), Roma, Istituto Poligrafico e Zecca dello Stato.

Mostler, H., 1984. Erfassung basischer Massengesteine im Raum Mittersill-Zell am See - Salzburg. Arch Lagerstättenforsch (Ostalpen) 5, 105-115.

Mottana, A. 1963. Il basamento cristallino subalpino nelle valli di Arigna e di Scais (Alpi Orobie centrali). Estratto dagli *Atti della Società Italiana di Scienze Naturali e del Museo Civico di Storia Naturale in Milano*, Vol., CII, Fasc. IV.

Mottana, A., Nicoletti, M., Petrucciani, C., Liborio, G., De Capitani, L. & Bocchio, R., 1985. Pre-alpine and alpine evolution of the South-alpine basement of the Orobic Alps. Geologische Rundschau, 74/2, 353-366.

Neubauer, F. & Frisch, W., 1988. Ordovician-Silurian geodynamic evolution of the Alps- the orogeny back-arc basin model. Schweiz. Min. Petr. Mitt., 68, 351-357.

Neubauer, F. & Handler, R., 1997. Mica tectonics. Terra Nostra, Abstract, Jahrestagung Geologische Vereinigung.

Neubauer, F. & Handler, R., 1999. Variscan orogeny in the Eastern Alps and Bohemian Massif: How do these units correlate? Mitt. Österr. Geol. Ges., 92, 35-59.

Neubauer, F. & Sassi, F.P., 1993. The Austro-Alpine Quartzphyllites and Related Palaeozoic Formations. In: Von Raumer, J.F. & Neubauer, F., (Editors), Pre-Mesozoic Geology in the Alps. Springer Verlag, 423-439.

Nicosia, U. Ronchi, A. & Santi, G., 1999. Permian tetrapod footprints from the western Orobic basin (N. Italy), with correlations. International Congress on "The Continental Permian of the Southern Alps and Sardinia (Italy). Regional Reports and General Correlations", 15-25 September, 1999, Brescia, Italy, Abstract vol. (Earth Science Department, Pavia University), 28-30.

Overstreet, W.C., 1967. The geological occurrence of monazite. U.S. Geological Survey Professional Paper, 530.

Parrisch, R.R., 1990. U-Pb dating of monazite and ist application to geological problems. Canadian Journal of Earth Sciences, 27, 1431-1450.

Pasquarè, G., 1967. Analisi geologico-strutturale del complesso intrusivo di Val Biandino (alpi Orobie Occidentali). Mem. Soc. Geol. It., 6, 343-357.

Passchier, C.W., Trouw, R.A.J., Zwart, H.J. & Vissers, R.L.M., 1992. Porphyroblast rotation: eppur si muove? J. Metam. Geol., 10, 283-294.

Perchuk & Geyra,1998. PT-paths as MIRROR of dynamics of granulite complexes. Experiment in Geosciences, mineralogy, petrology, geochemistry, crystallography, geophysics, Vol. 7, No.1, 26-27.

Perchuk, L.L., 1969. The staurolite-garnet thermometer. Dokl. Akad. Nauk, SSSR, Vol. 186, 189-191.

Perchuk, L.L., 1991. Derivation of a thermodynamically consistent set of geothermometers and geobarometers for metamorphic and magmatic rocks. In: Perchuk, L.L., Progress in Metamorphic and Magmatic Petrology, A Memorial Volume in Honor of D.S. Korzhinsky. Cambridge Univ. Press, Cambridge, 93-112.

Perchuk, L.L., Podlachikov, Y.YU. & Polyakov, N., 1992. Hydrodynamic modelling of some metamorphic processes. J. metamorphic Geol., 10, 311-319.

Pérez-Estaún, A., Martínez-Catalán, J.R. & Bastida, F., 1991. Crustal thickening and deformation sequence in the footwall to the suture of the Variscan belt of northwest Spain. Tectonophysics, 191, 243-253.

Petö, P., 1976. An experimental investigation of melting relations involving muscovite and paragonite in the silica-saturated portion of the system K_2O-Na_2O-Al_2O_3-SiO_2-H_2O to 15 kbar total pressure. Prog. in Exper. Petrol. NERC London, 3rd Report, 41-45.

Philippe, S., Villemaire, C., Lancelot, J.R., Girod, M. & Mercadier, H., 1987. Données minéralogiques et isotopiques sur deux gîtes hydrothermeaux uranifères du bassin volcano-sédimentaire permien de Collio Orobico (Alpes Bergamasques) : mise en évidence d'une phase de remobilisation crétacée. Bull. Minéral., 110, 283-303.

Pidgeon, R.T., Köppel, V. & Grünenfelder, M., 1970. U-Pb isotopic relationships in zircon suites from a para- and orthogneiss from the Ceneri zone, Southern Switzerland. Contrib. Mineral. Petrol., 26, 1-11.

Powell, R. & Holland, T.J.B., 1985. An internally consistant dataset with uncertainties and correlations: 1. Methods and a worked example. J. metamorphic Geol., 327-342.

Powell, R. & Holland, T.J.B., 1988. An internally consistant dataset with uncertainties and correlations: 3. Applications to geobarometry, worked examples and a computer program. J. metamorphic Geol., 6, 173-204)

Ramsay, J.G., 1967. Folding and Fracturing of Rocks. McGraw-Hill-New York, 568 pp., New York.

Reinhard, M., 1953. Über das Grundgebirge des Sottoceneri im südlichen Tessin. Ecl. Geol. Helv., 46, 214-222.

Reinhard, M., 1964. Über das Grundgebirge des Sottoceneri in Süd-Tessin und die darin auftretenden Ganggesteine. Mat. Carta Geol. Svizz., 117, x-89.

Renne, P.R., Becker, T.A. & Swapp, S.M., 1990. ^{40}Ar/^{39}Ar laser-probe dating of detrital micas from the Montgomery Creek Formation, northern California; Clues to provenance, tectonics and weathering processes. Geology, 18, 563-566.

Riklin, K., 1983. Kontaktmetamorphose permischer Sandsteine im Adamello-Massiv (Nord-Italien). Mitt. Geol. Inst. ETH u. Univ. Zürich, v. 3715, Zürich.

Ring, U. & Richter, C., 1994. the Variscan structural and metamorphic evolution of the Eastern Southalpine basemnt. J. Geol. Soc. London, 151, 755-766.

Roeder, D., 1985. Geodynamics of Southern Alps. Semin. Paper, Milano Nov. 85, The Anschutz Company, Exploration Research Division, 22 pp., Denver.

Roeder, D., 1989. South-Alpine thrusting and trans-Alpine convergence. In: Coward, M.P., Dietrich, D. & Park, R.G. (Editors), Alpine Tectonics: Geological Society Special Publication No. 45, 211-227.

Roeder, D., 1992. Thrusting and wedge growth, Southern Alps of Lombardia (Italy). Tectonophysics, 207, 199-243.

Romer, R.L. & Franz, L., 1998. Ordovician Barrow-type metamorphism in the Strona-Ceneri Zone (northern Italy) dated by U-Pb on staurolite. Schweiz. mineral. petrogr. Mitt., 78, 383-395.

Rubie, D.C., 1998. Disequilibrium during metamorphism: the role of nucleation kinetics. In: Treloar, P.J. & O'Brien, P.J.O., What Drives Metamorphism and Metamorphic Reactions? Geological Society Special Publication No. 138.

Salomon, W., 1901. Ueber neue geologische Aufnahmen in der östlichen Hälfte der Adamellogruppe. Sitzungen. k. preus. Akad. Wiss., Berlin, I, 170-185.

Sanders, C.A.E., Bertotti, G., Tommasini, S., Davies, G.R. & Wijbrans, J.R., 1996. Triassic pegmatites in the Mesozoic middle crust of the Southern Alps (Italy): fluid inclusions, radiometric dating and tectonic implications. Ecl. Geol. Helv., 89, 505-525.

Sassi, F.P. & Spiess, R., 1992. Further data on the pre-Alpine metamorphic pressure conditions of the Austridic phyllitic complexes in the Eastern Alps. In: Carmignani, L. &

Sassi, F.P. (Editors), Contribtions to the Geology of Italy with special regard to the Palaeozoic basements. IGCP No. 276 Newsletter 5, 297-307, Siena.

Sassi, F.P. & Zanferrari, A., 1972. Il significato geologico del Complesso del Turntaler (Punteria), con particolare riguardo alla successione di eventi metamorfici prealpini nel basamento austridico delle Alpi Orientali. Boll. Soc. Geol. It., 91, 533-557.

Sassi, F.P. & Zipoli, G., 1968. Il basamento cristallino di Recoaro: Studio petrografico. Mem. Soc. Geol. Ital., 7, 227-245.

Sassi, F.P., 1972. The petrological and geological significance of the b values of potassic white micas in low-grade metamorphic rocks: an application to the Eastern Alps. Tschermaks Mineral. Petrogr. Mitt., 18, 105-113.

Sassi, F.P., Kalvacheva, R. & Zanferrari, A., 1984. New data on the age of deposition of the South-Alpine phyllitic basement in the Eastern Alps. N. Jb. Geol. Paläont. Mh., 1984.

Sassi, F.P., Neubauer, F., Mazzoli, C., Sassi, R., Spiess, R. & Zipoli, G., 1995. A tentative comparison of the palaeozoic evolution of the Austroalpine and Southalpine quartzphyllites in the Eastern Alps. Per. Miner., 63, 35-62.

Sassi, F.P.,Kalvacheva, R. & Zanferrari, A., 1984. New data on the age of the South-Alpine phyllitic basement in the Eastern Alps. N. Jb. Geol. Paläont. Mh., 47, 741-751.

Schitter, F., 1997. Spurenelementkonzentration in den gesteinsbildenden Mineralien des Gebhartser Diorits und des Eisgarner Granits, bestimmt mittels des Instrumentellen Neutronenaktivierungsanalyse. 75p, Diplomarbeit thesis, Universität Salzburg, Salzburg.

Schmid, S.M., Aebli, H.R., Heller, F. & Zingg, A., 1989. The role of the Periadriatic Line in the tectonic evolution of the Alps. In: Coward, M.P., Dietrich, D. & Park, R.G. (Editors), Alpine Tectonics: Geological Society Special Publication No. 45, 113-134.

Schmid, S.M., Zingg, A. & Handy, M., 1987. The kinematics of movements along the Insubric line and the emplacement of the Ivrea zone. Tectonophysics, 135, 47-66.

Schönborn, G., 1990. A kinematic model of the western Bergamasc Alps, Southern Alps, Italy. Eclogae geol. Helv. 83/3, 665-682.

Schönborn, G., 1992. Alpine tectonics and kinematic models of the Central Southern Alps. Memorie di Scienze Geologiche, Vol. XLIV, 229-393.

Schönborn, G., 1994. Evolution and Deep Structure of Val Brembana based on surface data (Southern Alps, Italy). Proceedings of Smposium «CROP – Alpi Centrali» Sondrio, 20-22 October 1993: Montrasio, A. & Sciesa, E. (Editors), Quaderni di Geodynamica Alpina e

Quaternaria (1994), vol. 2, 197-212.

Schönlaub, H.P. & Heinisch, H., 1993. The Classic Fossiliferous Palaeozoic Units of the Eastern and Southern Alps. In: Von Raumer, J.F. & Neubauer, F., (Editors), Pre-Mesozoic Geology in the Alps. Springer Verlag, 395-422.

Schumacher, M.E., 1997. Geological interpretation of the seismic profiles through the southern Alps (lines S1-S7 and C3 south). In: In: Pfiffner, O.A., Lehner, P., Heitzmann, P., Mueller, St., Steck, A. (Editors), Deep Structure of the Swiss Alps, Results of NRP 20, 101-114.

Schumacher, M.E., Schönborn, G., Bernoulli, D. & Laubscher, 1997. Rifting and collision in the Southern Alps. In: In: Pfiffner, O.A., Lehner, P., Heitzmann, P., Mueller, St., Steck, A. (Editors), Deep Structure of the Swiss Alps, Results of NRP 20, 186-204.

Seydoux-Guillaume A.M., Wirth R., Heinrich W. and Montel J.M. (2002). Experimental determination of the Th partitioning between monazite and xenotime using Analytical Electron Microscopy and X-Ray Diffraction Rietveld analysis. In press in Eur. J. Mineral., Vol. 14.

Siletto, G.B., Spalla, M.I., Tunesi, A., Lardeaux, J.M. & Colombo, A., 1993. Pre-Alpine Structural and Metamorphic Histories in the Orobic Southern Alps, Italy. In: Von Raumer, J.F. & Neubauer, F., (Editors), Pre-Mesozoic Geology in the Alps. Springer Verlag, 585-598.

Siletto, G.B., Spalla, M.I., Tunesi, A., Lardeaux, J.M. & Soldo, L., 1990. Structural analysis in the Lario basement (Central Southern Alps, Italy). Mem. Soc. Geol. It., 45, 93-100.

Smith, H.A. & Barreiro, B., 1990. Monazite U-Pb dating of staurolite grade metamorphism in pelitic schists. Contrib. Mineral. Petrol., 105, 602-615.

Spalla, M.I., Carminati, E., Ceriani, A., Oliva, A. & Battaglia, D., 1999. Influence of deformation partitioning and metamorphic re-equilibration on P-T path reconstruction in the pre-Alpine basement of central Southern Alps (Northern Italy). J. metamorphic Geol., 17, 319-336.

Spear, F.S. & Cheney, J.T., 1989. A petrogenetic grid for pelitic schists in the system SiO_2-Al_2O_3-FeO-MgO-K_2O-H_2O. Contrib. Mineral. Petrol., 101, 149-164.

Stampfli, 1996. The Intra-Alpine terrain: A Paleotethyan remnant in the Alpine Variscides. Eclogae geol. Helv., 89/1, 13-42.

Steiger, R.H. & Jäger, E., 1977. Subcommision on Geochronology: Convention on the use of decay constants in geo- and cosmochronology. Earth & Planet. Sci. Lett., 36, 359-362.

Stormer, J.C. & Whitney, J.A., 1985. Two-feldspar and iron-titanium oxide equilibria in silicic magmas and the depth of origin of large volume ash-flow tuffs. Am. Mineral., 70/1-2, 52-64.

Thomson, B., 1982. Dehydration melting of pelitic rocks and the generation of H_2O-undersaturated granitic liquids. Am. J. Sc., 282, 1567-1595.

Thöni, M., Mottana, A., Delitala, M.C., De Capitani, L. & Liborio, G., 1992. The Val Biandino composite pluton: A late Hercynian intrusion into the South-Alpine metamorphic basement of the Alps (Italy). N. Jb. Miner. Mh., 12, 545-554.

Trümpy, R., 1980. Geology of Switzerland, part A: An outline of the geology of Switzerland. Part B: Geological Excursions. Schweiz. Geol. Komm. (Editor), Wepf and Co. Publishers, basel New York, pp. 1-104.

Turner, S.P., Kelley, S.P., VandenBerg, A.H.M., Foden, J.D., Sandiford, M., Flöttmann, T., 1996. Source of the Lachlan fold belt flysch linked to convective removal of the lithospheric mantle and rapid exhumation of the Delamarian-Ross fold belt. Geology, 24, 941-944.

Vai, G. B. & Cocozza, T., 1986. Tentative schematic zonation of the Hercynian chain in Italy. Bull. Soc. Géol. France, 1986, 8 (t. II, no. 1), 95-114.

Vielzeuf, D. & Montel, J.M.,1994. Partial melting of metagrauwackes. Part I. Fluid-absent experiments and phase relationships. Contrib. Mineral. Petrol., 117, 375-393.

Vielzeuf, D. & Schmidt, M.W., 2001. Melting relations in hydrous systems revisited: application to metapelites, metagrauwackes and metabasalts. Contrib. Mineral. Petrol., 141, 251-267.

Viskupic, K. & Hodges, K.V., 2001. Monazite-xenotime thermochronometry: methodolgy and an example from the Nepalese Himalaya. Contrib. Mineral. Petrol., 141, 233-247.

Visscher, H., Kerp, H., Clement-Westerhof, J.A. & Looy, C.V., 1999. Permian floras of the Southern Alps. International Congress on "The Continental Permian of the Southern Alps and Sardinia (Italy). Regional Reports and General Correlations", 15-25 September, 1999, Brescia, Italy, Abstract vol. (Earth Science Department, Pavia University), 13-21.

Von Raumer, 1998. The Palaeozoic evolution in the Alps: From Gondwana to Pangea. Geol. Rundsch., 87, 407-435.

Ward, C.D., McArtur, J.M. & Walsh, J.N., 1991. Rare earth element behaviour during evolution and alteration of the Dartmoor granite, SW England. Journal of Petrology, 33, 785-815.

Wayte, G.J., Worden, R.H., Rubie, D.C. & Droop, G.T.R. (1989) A TEM study of

disequilibrium plagioclase breakdown at high pressure: the role of infiltrating fluid. Contrib. Mineral. Petrol., 101, 426-437.

Weber, K., 1986. Metamorphism and crustal rheology – implications for the structural development of the continental crust during prograde metamorphism. In: Dawson, J.B., Carswell, D.A., Hall, J. & Wedepohl, K.H. (Editors), The Nature of the lower Continental Crust, Geological Society Special Publication, No. 24, 95-106.

Welzel, B., 1991. Die Bedeutung von K/Ar-Datierungen an detritischen Muskoviten für die Rekonstruktion tektonometamorpher Einheiten im Liefergebiet – ein Beitrag zur Frage der varistischen Krustenentwicklung in der Böhmischen Masse. Göttinger Arb. Geol. Paläont., 49, 1-61.

Werner, D., Koppel, V., Hänny, R. & Rybach, L., 1977. Cooling models for the Lepontine area (central Swiss Alps). Schweiz. mineral. petrogr. Mitt., 56/3, 661-668.

Wiedenbeck, M., 1986. Structural and isotopic age profile across the Insubric Line, Mello, Valtellina, N. Italy. Schweiz. mineral. Petrogr. Mitt, 66, 211-227.

Zanchi, A., Chiesa, S. & Gillot, P-Y., 1990. Tectonic evolution of the Southern Alps in the Orobic chain: Structural and Geochronological indications for Pre-Tertiary compressive Tectonics. Mem. Soc. Geol. It., 45, 77-82.

Zurbriggen, R., Franz, L. & Handy, M.R., 1997. Pre-Variscan deformation, metamorphism and magmatism in the Strona-Ceneri Zone (southern Alps of northern Italy and southern Switzerland). Schweiz. mineral. petrogr. Mitt., 77, 361-380.

Zurbriggen, R., Kamber, B.S., Handy, M.R. & Nägler, T.F., 1998. Dating synmagmatic folds: a case study of Schlingen structures in the Strona-Ceneri Zone (Southern Alps, northern Italy). J. metamorphic Geol., 16, 403-414.

Acknowledgements

Curriculum Vitae

Name	Jurriaan Feijth
Anschrift	Lieselotte-Herrmann Straße 4
	10407 Berlin
Geburtsdatum/Ort	07.03.1964, Tripolis (Libyen)

Schulbildung:
1968-1974   Panaga School, Seria, Brunei Darussalam
1974-1976   Piassau School, Lutong (Sarawak), Malaysia
1976-1983   Rijnlands Lyceum, Wassenaar, Niederlande, ‚Voorbereidend Wetenschappelijk Onderwijs' (Niederländischer
                      Gymnasialzweig, Hochschulreife)

Hochschulstudium:
09.1983-05.1989   Geologie an der Rijksuniversiteit Utrecht, Niederlande
                                Hauptfach: Strukturgeologie
                                Nebenfach: Materialkunde (auf Strukturgeologie bezogen)
                                Judicium: Cum Laude.

Diplomarbeit (bei Prof. Dr. C.W. Passchier):
Strukturgeologische Geländearbeit in den Orobisch-Bergamasker Alpen (Provinzen Sondrio und Bergamo, Italien)
Titel: ‚The geology of the Val Brembo di Valleve, upper Valle di Lemma, upper Val Lunga and Upper Val Madre,
Orobic-Bergamasc Alps (Bergamo, Sondrio), N. Italy'.

Studienarbeit (bei Dr. W. Nijman und Prof- P. Ypma)
Geländearbeiten im Rahmen des ‚Mount Isa Regional Tectonic History Project' des Bureau of Mineral Resources
(BMR), Canberra, Australia.
Titel des Berichts: ‚Structural analysis and interpretation of D_2-thrusts in the Leichhardt River Fault Trough, Mount
Isa, Queensland, Australia'.

Praktika: Structural Geology Group des ‚Koninklijke/Shell Exploratie en Produktie Laboratorium' (Shell Research),
Rijswijk,   Niederlande. (im Rahmen des Nebenfachs)
                                Titel des Berichts: ‚Spacing of normal faults and displacement distribution development along normal faults in
                                sandbox experiments'.

01.02.1989-30.04.1989   Grundbauberatung AG, St. Gallen, Schweiz

Militärdienstpflicht
08.05.1989-13.02.1990   Geometer bei der Artillerie
                                Enddienstrang: Unteroffizier

Berufserfahrung: Shell Internationale Petroleum Maatschappij B.V.
19.03.1990-19.08.1990   ‚Junior Geologist' in der Abteilung ‚prospect evaluation & forecasting' der ‚Shell Internationale Petroleum
                                Maatschappij B.V.' (Exploration & Production), Den Haag, Niederlande
20.08.1990-10.01.1991   Basic Exploration Training
11.01.1991- 31.05.1995   ‚Geologist/Interpreter' in der Explorationsabteilung der ‚Nederlandse Aardolie Maatschappij B.V.',
                                Assen, Niederlande (Eine Shell operation company)

Technische Universität Berlin
01.06.1995-31.03.2000   Befristet beschäftigter wissenschaftlicher Mitarbeiter mit Lehraufgaben (38,5 Wochenstunden, BAT IIa)
                                Fachgebiet: Explorationsgeologie, speziell Tektonik/Strukturgeologie aber auch ‚Exploration der
                                Kohlenwasserstoffe' und ‚Beckenanalyse'.
                                Doktorand

Freier wissenschaftlicher Mitarbeiter
10.04.2000-22.07.2000   Technische Universität Berlin, Fachgebiet Explorationsgeologie (prof. D. Walde) Lehrauftrag: ‚Exploration der
                                Kohlenwasserstoffe'

Weiterbildung: - Basic exploration training bei der 'Shell Internationale petroleum Maatschappij' (20.08.1990-10.01.1991)
                                - Southern North Sea Structural Geological Workshop (Shell)
                                - 3D Seismic Interpretation (Alistair R. Brown)
                                - Sequence Stratigraphy Workshop (Prof. Dr. P.R. Vail, Prof. Dr. J.E. van Hinte)
                                - Formation Evaluation, Basic and Intermediate Concepts (OGCI, Dr. Donald P. Helander)
                                - Zmap$^+$ (Grid, Contour und T/Z-Conversions Software)(Landmark, A.L. Young)
                                - Advanced Seismic Stratigraphy, a Sequence and Wavelet Analysis Workshop (OGCI, Dr. John D. Pigott)
                                - Borehole Seismic Seminar (Schlumberger)
                                - Effektive Presentation (R.O.C., H. Kockx)

Sprachen: Niederländisch, English, Deutsch, Italienisch, Französisch

Berlin, im Januar 2002